The Understanding of Norrin's Role in Angiogenesis

Dissertation

zur

Erlangung der naturwissenschaftlichen Doktorwürde
(Dr. sc. nat.)

vorgelegt der

Mathematisch-naturwissenschaftlichen Fakultät
der
Universität Zürich

von
Lucas Raphael Mohn

von
Märstetten TG

Promotionskomitee

Prof. Dr. Wolfgang Berger (Vorsitz und Leitung der Dissertation)
Prof. Dr. Thierry Hennet
Prof. Dr. Christian Grimm

Zürich, 2013

Declaration

I declare that the present thesis was composed by myself and the enclosed experimental work was performed on my own as indicated. Contributions performed by coworkers are specified in Appendix E.

This dissertation has not been submitted for any other degree or professional qualification except as specified.

Lucas Mohn, Zurich 2012

To my family

Abbreviations

∞	forever
µ	micro (10^{-6})
°C	degree Celsius
A	adenine
aa	amino acid
AB	anti body
ABD	actin binding domain
ad	autosomal dominant
al.	alia (others)
AMD	age related macula degeneration
APS	ammonium persulfate
ar	autosomal recessive
ATOH7	atonal homolog 7
β-ME	β -mercaptoethanol
BBB	blood brain barrier
BCA	bicinchoninic acid
BLAST	Basic Local Alignment Search Tool
BLAT	BLAST-Like Alignment Tool
Bmp4	bone morphogenetic protein 4
bp	basepair/s
BRB	blood retina barrier
BSA	bovine serum albumin
C2H2	cysteine 2 Histidine 2-type domain
C	cytosine
Ch.	chromosome
CD	Coat's disease
CDS	coding sequence
cDNA	complementary DNA
CHV	choroidal vasculature
CNS	central nervous system
Ct	cycle threshold
ddH_2O	double destilled water
ddNTP	dideoxy nucleotide-triphosphate
DAPI	4',6-diamidino-2-phenylinole
DEPC	diethylpyrocarbonate
DMEM	Dulbecco's modified eagle medium
DMSO	dimethylsulfoxide
DNA	deoxyribonucleic acid
Dnase	deoxyribonuclease
dNTP	deoxy nucleotide-triphosphate
DTT	dithiothreitol
DVP	deeper vascular plexus
E	embryonic day
EC	endothelial cell
ECM	extracellular matrix

EDTA	ethylenediaminetetraacetic acid
EGTA	ethylene glycol tetraacetic acid
ELM	external limiting membrane
ER	endoplasmatic reticulum
ERG	electroretinography
ESE	exonic splice enhancer
EtBr	ethidium bromide
EtOH	ethanol
EVR	exudative vitreoretinopathy
FA	focal adhesion
FCS	fetal calf serum
FEVR	familial exudative vitreoretinopathy
FITC	fluorescein isothiocyanate
FPLC	fast protein liquid chromatography
fwd	forward
FZD4	frizzled homolog 4
g	gram
G	guanine
GCL	ganglion cell layer
Glu	glutamine
Gapdh	glyceraldehyde-3-phosphate dehydrogenase
gDNA	genomic deoxyribonucleic acid
HA	hyaloid artery
HBM	high bone mass
HCl	hydrogen chloride
HMEC-1	human microvascular endothelial cells
HEK	human embryonic kidney cells
Hepes	2-[4-(2-hydroxyethyl)piperazin-1-yl]ethanesulfonic acid
HRP	horseradish peroxidase
HUVEC	human umbilical vein endothelial cells
ICC	immunocytochemistry
IgG	immunoglobulin G
IHC	immunohistochemistry
ILK	intergrin-linked kinase
ILM	inner limiting membrane
IMAC	immobilized metal affinity chromatography
INL	inner nuclear layer
IP	immuno precipitation
IPL	inner plexiform layer
IPP	ILK PINCH parvin complex
ITGB3	Integrin-β 3
IVL	intermediate vascular layer
kb	kilobasepair/s
KCl	potassium chloride
kDa	kilo Dalton
KO	knockout
l	litre

LB	Lysogeny Broth, bacterial growth medium
LEF/TCF	lymphoid enhancer factor/T-cell
LRP5	low-density lipoprotein receptor related protein 5
m	milli (10^{-3})
M	methionine or molar
MAOA/B	mono amine oxidase A/B
MAPK	mitogen - activated protein kinase
$MgCl_2$	magnesium chloride
MIM	mendelian inheritance in man
MKL1	megakaryoblastic leukemia (translocation) 1
MKL2	myocardin-like 2
NINJ1	nerve injury induced protein 1
MR	mental retardation
mRNA	messenger RNA
MW	molecular weight
n	nano (10^{-9})
NaCl	sodium chloride
NCBI	National Center of Biotechnology Information
ND	Norrie Disease
NDP	Norrie Disease Pseudoglioma
NEUROD1	neurogenic differentiation 1
NFL	nerve fiber layer
NMD	nonsense-mediated mRNA decay
OIR	oxygen induced retinopathy
OMIM	Online Mendelian Inheritance in Man
o/n	over night
ONL	outer nuclear layer
OPL	outer plexiform layer
OPPG	osteoporosis pseudoglioma syndrome
ORF	open reading frame
P/S	penicillin / streptomycin
PAGE	polyacrylamide gel electrophoresis
PARVA	α-parvin
PBS	phospate buffered saline
PBST	phospate buffered saline with Tween® 20
PCR	polymerase chain reaction
PEI	polyethylene imine
PM	pupillary mambrane
PMSF	phenylmethanesulfoyl fluoride
PND	post natal day
PolyPhen	polymorphism phenotyping
Pro	proline
pDNA	plasimd deoxyribonucleic acid
PFA	paraformaldehyde
Pfu	Pyrococcus furiosus
PFV	persistent fetal vasculature

PHPV	persistent hyperplastic primary vitreous
PLVAP	plasmalemma vesicle associated protein
PRDX	primary retinal dysplasia, X-linked
PVDF	polyvinyliden difluoride
qRT-PCR	quantitative reverse transcription polymerase chain reaction
RB	retinoblastoma
rev	reverse
RGC	retinal ganglion cell
RIN	RNA integrity number
RIPA	radioimmunoprecipitation assay buffer
RLU	relative light units
RNA	ribonucleic acid
RNase	ribonuclease
ROP	retinopathy of prematurity
RPE	retinal pigment epithelium
rpm	revolutions per minute
rRNA	ribosomal RNA
RT	room temperature
RT-PCR	reverse transcription polymerase chain reaction
SDS	sodium dodecyl sulfate
SEM	standard error of mean
SFM	serum free medium
SIFT	Sort Intolerant From Tolerant amino acid substitutions
SNP	single nucleotide polymorphism
SRE	serum response element binding domain
SRF	serum response factor
SVP	superficial vascular plexus
T	thymine or threonine
TAE	tris - actetae/EDTA
Taq	Thermus aquaticus
TE	tris - EDTA
TEMED	N.N,N',N'-tetramethylethylenediamine
TGF-β	transforming growth factor β
Tris	2-amino-2-hydroxymethyl-propane-1,3-diol
TSPAN12	tetraspanin 12
TVL	tunica vasculosa lentis
U	unit or uracil
UTR	untranslated region
VEGF	vascular endothelial growth factor
VHP	vasa hyaloidea propria
VPA	valproic acid
WB	western blot
WGA	whole genome amplification
Wnt	wingless Int-1
WST-1	water soluble tetrazolium 1
wt	wild type
ZNF408	zinc-finger protein 408

Summary

Norrie disease is a rare X-linked recessive neurodevelopmental disorder. Patients are often born blind and develop deafness during life, some patients also have cognitive impairments. The causative gene (*NDP*) is very small but crucial for proper vascularization during embryonic development and adult homeostasis. Norrin is an unconventional Wnt ligand, which only binds one single Wnt receptor, but in addition, Norrin can directly inhibit another important signaling pathway, the TGF-β pathway. This Wnt-receptor selectivity on the one hand and the pathway plurality on the other hand are of special interest. Recombinant human Norrin could help to elucidate structural properties of Norrin's interaction with other proteins and also to develop pharmaceutical agents affecting these pathways. Therefore, I am especially interested in establishing a system to produce and purify recombinant human Norrin (wild type and mutant isoforms) in an unlimited amount to investigate its functional and structural properties.

My second interest is the identification of new genes involved in retinal diseases, to elucidate their function, and pathophysiological mechanisms leading to the disease. We screened 10 genes in more then 200 patients and identified 79 potentially disease relevant DNA sequence variations in patients with different forms of retinal diseases. In one gene (*ATOH7*) we could identify the disease causing molecular mechanism. The deletion of the major part of the basic DNA – binding domain of ATOH7 leads to an underrepresentation of the protein in the nucleus. Further, we could show that ATOH7 is a target of proteasomal degradation in the cytoplasm and that the mutant ATOH7 is degraded faster compared to the wild type ATOH7. In another case (*ZNF408*) we could identify a new gene involved in retinal vascularization for the first time in collaboration with Prof. Frans Cremers from the Department of Human Genetics at the Radboud University in Nijmegen (Holland). Other candidate gene projects are still ongoing, but revealed interesting results already. This will help to better understand molecular mechanisms in the pathophysiologie of retinal dysplasias and is a prerequisite to develop novel therapeutic interventions.

Zusammenfassung

Die Norrie Krankheit ist eine seltene, rezessive Form einer geschlechtsgebundenen neuronalen Entwicklungsstörung. Patienten werden häufig blind geboren und entwickeln eine Taubheit, manche Patienten haben auch kognitive Einschränkungen. Das krankheitsverursachende Gen (*NDP*) ist sehr klein, aber äusserst wichtig für die korrekte Entwicklung des Blutgefässsystems während der embryonalen Entwicklung und der adulten Homeostase. Norrin ist ein ungewöhnlicher Wnt Ligand, welcher nur einen einzelnen Wnt Rezeptor bindet. Zusätzlich aber kann Norrin einen anderen Signalweg, den TGF-β Signalweg, direkt inhibieren. Diese Wnt Rezeptor Selektivität einerseits und die Signalweg Pluralität andererseits sind von speziellem Interesse. Rekombinantes humanes Norrin könnte helfen die strukturellen Eigenschaften von Norrin's Interaktionen mit anderen Proteinen aufzuklären und pharmakologische Wirkstoffe, welche diese Signalwege beeinflussen, zu entwickeln. Deshalb bin ich besonders daran interessiert, ein System zur Produktion und Aufreinigung von unlimitierten Mengen an rekombinantem humanem Norrin (wildtyp und mutante Isoformen) zu entwickeln, um seine Funktion und Struktur aufzuklären.

Mein zweites Interesse gilt der Identifikation von neuen Genen, welche Fehlentwicklungen der Netzhaut verursachen, der Aufklärung von deren Funktion und der pathophysiologischen Mechanismen, welche zur Krankheit führen. Wir untersuchten 10 Gene in mehr als 200 Patienten und identifizierten 79 potentiell krankheitsrelevante DNA Sequenzevariationen in Patienten mit verschiedenen Fehlentwicklungen der Netzhaut. In einem Gen (*ATOH7*) konnten wir den krankheitsverursachenden molekularen Mechanismus identifizieren. Die Deletion des grössten Teils der DNA bindenden Domaine von ATOH7 führt zu einer Unterrepresentation des Proteins im Zellkern. Des Weiteren konnten wir zeigen, dass ATOH7 vom cytoplasmatischen Proteasom abgebaut wird und dass das mutante ATOH7 schneller abbgebaut wird als das normale Protein. In einem anderen Fall (*ZNF408*) konnten wir, in Zusammenarbeit mit Prof. Frans Cremers vom Department of Human Genetics an der Radboud Universität in Nijmegen (Holland), ein neues Gen identifizieren, welches in der retinalen Blutgefässbildung involviert ist. Andere Kandiadatengenprojekte sind noch laufend, haben aber bereits interessante Resultate gezeigt. Diese werden helfen die molekularen Mechanismen in Netzhautfehlentwicklungen besser zu verstehen und sind eine Vorraussetzung für die Entwicklung von neuen therapeutischen Interventionen.

Table of Contents

Abbreviations 7
Summary 11
Zusammenfassung 12
1. Introduction 15
1.1 The eye 15
1.2 The retina 16
1.3 The retinal vasculature 18
1.4 Retinal vascular diseases 20
1.4.1 Diabetic retinopathy (DR) 20
1.4.2 Retinopathy of prematurity (ROP) 20
1.4.3 Age-related macula degeneration (AMD) 21
1.5 Exudative vitreoretinopathies (EVRs) 21
1.5.1 Genetic basis of EVR 21
1.5.1.1 Norrie Disease (ND) 22
1.5.1.2 Allelic disorders 23
1.6 The Norrie disease pseudoglioma (*NDP*) gene 24
1.6.1 Expression of the *NDP* gene 25
1.6.2 The Norrin protein 25
1.6.3 Norrin's pleiotropic properties 28
1.6.4 Norrin signaling 31
1.7 Candidate genes for retinal dysplasia 33
1.7.1 ATOH7 – a transcription factor, required for proper retinogenesis 33
1.7.2 NINJ1 – a myeloid cell adhesion molecule 33
1.7.3 ZNF408 – a transcription factor, involved in retinal vascular development 34
1.7.4 ILK – Focal adhesion and actin-dependent cytoskeletal organisation 34
1.7.4 MAPK signaling, required for retinal vascular development 35
1.8 Aims of the Thesis 36
2. Material and Methods 37
2.1 Material 37
2.1.1 Cloning 37
2.1.2 DNA isolation 37
2.1.3 DNA electrophoresis 37
2.1.4 RNA techniques 38

2.1.5 PCR and Sequencing 38
2.1.6 Cell culture – routine work 38
2.1.7 Cell culture – assays 39
2.1.8 Protein techniques 39
2.1.9 Additional reagents and equipment/instruments 40
2.2 Methods 42
2.2.1 DNA techniques 42
2.2.2 RNA techniques 53
2.2.3 Protein techniques 54
2.2.4 Mammalian cell culture technology 63
2.2.5 *In vitro* assays 65
3. Results 67
3.1 Candidate gene screening 67
3.1.1 New sequence variations in candidate genes 67
3.2 New sequence variations in known disease causing genes 103
3.3 Recombinant human Norrin – production, purification 106
3.4 Functional assays with rhNorrin 113
3.5 Ligand Receptor Capturing on living cells 119
4. Discussion 121
4.1 Variability of the human genome and potential consequences 121
4.2 Pathogenicity prediction - a combinatory approach of multiple methods 122
4.3 Basic helix-loop-helix transcription factors and retinogenesis 122
4.4 Adhesion of macrophages and endothelial cells 123
4.5 Extracellular signal transduction and cellular response to the ILK pathway 123
4.6 Vascular integrity might be altered by mutations in SRF, MKL1, and MKL2 125
4.7 Differential diagnosis of ND 125
4.8 Non-endothelial retinal cells and retinal vascular disesaes 125
4.9 Recombinant human Norrin (rhNorrin) 126
Acknowledgements 129
References 130
Appendix A – Electropherograms 146
Appendix B – Multiple sequence alignments 156
Appendix C – Primer- and Vectorcollection 171
Appendix D – Co-author publication 181
Appendix E – Contributions 193
Curriculum vitae 194

1. Introduction

1.1 The eye

The eye is probably the most important sensory organ of human beings, and the initial organ for visual perception. The eye is a highly complex and unique organ, hence visual acuity is a precious gift we should not take as guaranteed. First, I would like to explain the amazing biology of the eye in more detail.

The capsule of the eye consists of three layers (Figure 1). The first and outermost layer, the tunica oculi externa, is stick and tough and consists of connective tissue, which gives the eye its integrity as a globe and protects its structures inside. The front part of the connective tissue is specialized in terms of collagen fiber orientation and called cornea. The collagen fibers in the cornea are orientated perfectly orthogonally, so that light can pass trough. Hence the cornea appears transparent and functions as a window where reflected light can enter the eye. The rest of the connective tissue layer appears white and is called sclera.

The second layer of the eye is the tunica oculi media or uvea. More precisely, the uvea consists of three different parts. In the front the iris can be found, which is the colored part of the eye, and encompasses a round and central opening, the pupil. The function of this part of the eye is adjusting to different levels of light, so that under different light conditions always the appropriate amount of light can enter the eye. The second part of the uvea is the ciliary body, which produces aqueous humor and contains ciliary muscles. The aqueous humor is a clear gelatinous fluid, secreted into the posterior and anterior chamber between lens and cornea. It also nourishes the lens. The ciliary muscles can alter the shape of the lens by contraction and thus light gets focused onto the retina. This process is called accommodation. The third part of the uvea is the choroid, which is located at the back of the eye. It is a vascular tissue, that provides oxygen and nutrients to the photoreceptors at the outer part of the retina.

The retina is the third layer of the eye capsule, which is called tunica oculi interna. The retina consists of neural and glial cells and contains blood vessels. It is the most important and complex structure in the eye and will be described in more detail later.

The eyeball (Bulbus oculi) is anatomically subdivided into two parts, the anterior and the posterior segment. The anterior segment includes the lens and everything distal to the lens. Everything proximal belongs to the posterior segment. To finish the gross anatomy of the eye I would like to introduce one additional structure of the posterior segment, the vitreous, a transparent, and gelatinous mass that fills-out the space between the lens and the retina. It pushes the retina against the choroid and helps to keep the light-sensitive retina in place. Unlike the fluid in the anterior segment (aqueous humor), which is constantly replenished, the vitreous humor is stagnant. Hence any problems concerning the vitreous can have direct effects on the integrity of the retina, and might result in retinal traction that might lead to retinal detachment and blindness.

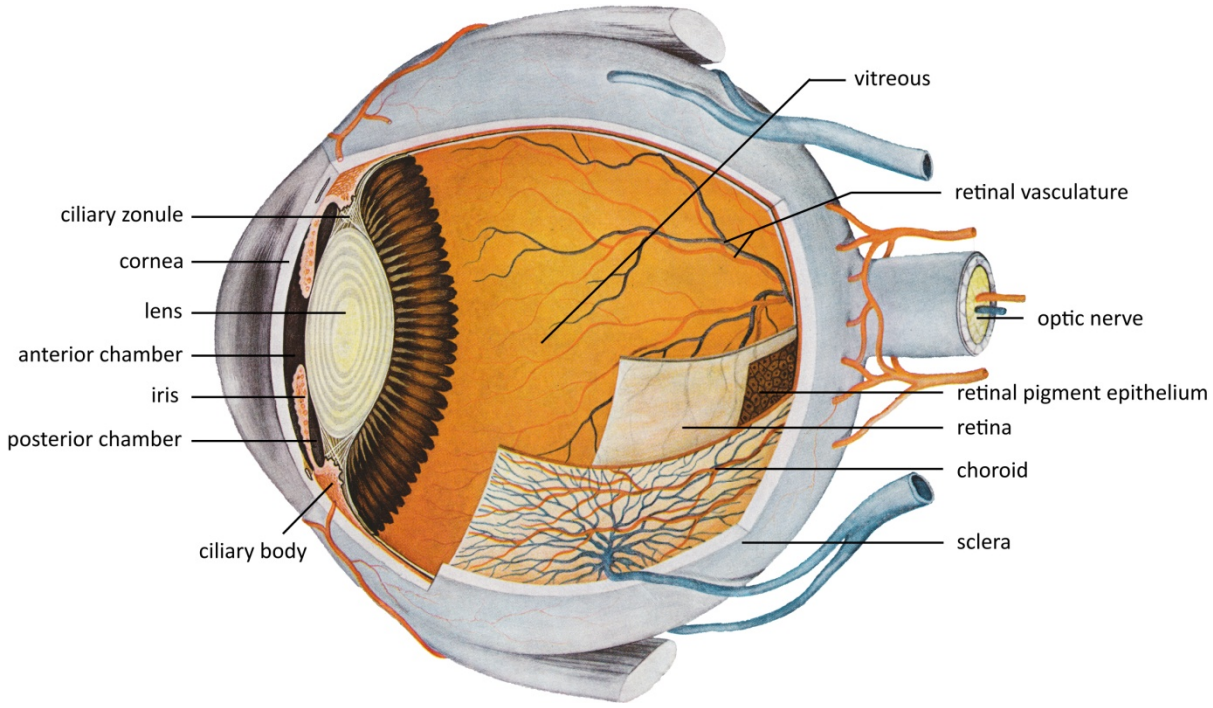

Figure 1: Structure of the Bulbus oculi. The eye is fenestrated from lateral. Single layers and other important structures are indicated. (Adapted from: Rohen 1971)

1.2 The retina

The retina is a thin (approximately 0.5mm) but highly complex structure of the eye and is a part of the central nervous system (CNS). The vertebrate retina develops in a highly conserved manner, from the uniform neuroepithelium towards a complex laminar structure with seven major cell types, six neuronal and one glial (Holt et al. 1988, Turner et al. 1987, Wetts et al. 1988). The first-born neurons in the retina are the retinal ganglion cells (RGC). Then amacrine, horizontal, and cone photoreceptor cells develop in an overlapping phase, followed by rod photoreceptors, bipolar and Müller glia cells, which are established last (Carterdawson and Lavail 1979, Livesey et al. 2001, Young 1985). To form the highly organized laminar structure of these different cell types, retinal progenitor cells have to differentiate and migrate in a distinct manner which is guided by both intrinsic and extrinsic factors (Cepko et al. 1996). In the end a structure with ten distinct layers is build up (Figure 2).

Adjacent to the vitreous, the inner limiting membrane (ILM) is the first layer of the retina and functions as a physical boundary between vitreous and retina. The second layer is the nerve fiber layer (NFL), which is formed by RGC axons. The ganglion cell layer (GCL) consists of RGC nuclei. RGCs are the first-born neurons in the retina of all vertebrates. Their axons assemble the optic nerve, and convey light signals from the retina to the lateral geniculate nucleus from where visual information is processed to the visual cortex. In addition a subset of RGC axons projects directly to the suprachiasmatic nucleus, which controls circadian rhythm. In the inner plexiform layer (IPL) bipolar cells are connected to the RGCs. The inner nuclear layer (INL) is formed by bipolar cell nuclei. In the outer plexiform layer (OPL) photoreceptors are connected to the bipolar cells. In the transmission between photoreceptors and bipolar cells the visual

information gets processed on a synaptic level. These synapses are laterally connected by horizontal and amacrine cells. The outer nuclear layer (ONL) is formed by rod and cone photoreceptor nuclei. The external limiting membrane (ELM) separates the inner and the outer segments of the photoreceptors from their nuclei. In the photoreceptor layer the photosensitive cells are located, the rods and cones. The human retina consists of about 120 million rods, which are responsible for dim light vision, while about 7 million cones are important for daylight and color vision. Interestingly, the photosensitive cells are located at the outer edge of the vertebrate retina, so that the light has to pass through all neurons of the retina to reach the photosensitive cells, therefore it is also called inverted retina. The photoreceptors are in contact with the light absorbing retinal pigment epithelium (RPE), which is the last layer of the retina and restores the photopigment retinal. Retinal is a carotinoid and can absorb light in its 11-cis conformation and therefore is the key molecule to convert electromagnetic radiation (light) into neuronal impulses. The pigments in the RPE further prevent photoreceptors from radiation damage by absorbing light energy.

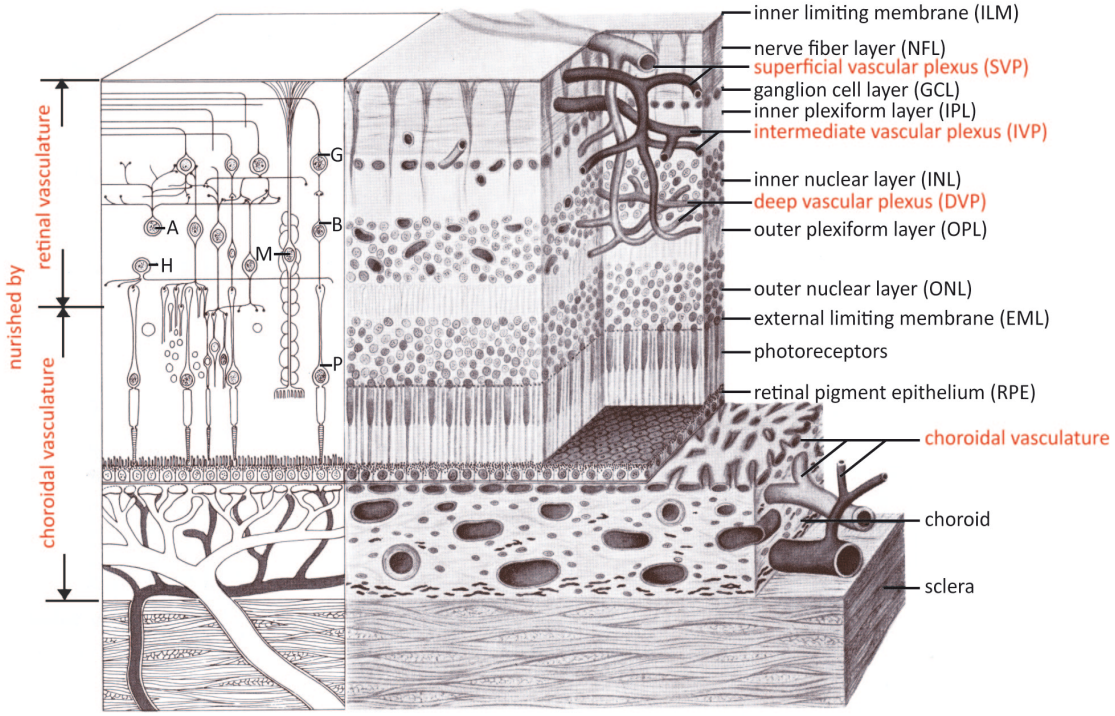

Figure 2: Structure of the layers in the posterior bulbus. A= amacrine cell, H= horizontal cell, M= Müller glia cell, G= ganglion cell, B= bipolar cell, P= photoreceptor cell. (Adapted from: Rohen, 1971)

To complete the anatomy of the retina I would like to introduce the three glial cell types present in the retina. The Müller glias are the principle glial cells of the retina and extend radial from the ILM to the ELM. They perform several functions including structural support and nourishment. It has also been shown that Müller glia cells can dedifferentiate after retinal injury and differentiate into multiple retinal cell types (Ooto et al. 2004, Osakada et al. 2007). The second glial cells in the retina are the astrocytes. Astrocytes are not glial cells of the retinal neuroepithelium, they enter the developing retina from the brain along the optic nerve (Stone and Dreher 1987, Watanabe and Raff 1988). Astrocytes establish a cellular network in the NFL

and function as a scaffold for the subsequent invasion of blood vessels. The may also have metabolic function in the retina. Microglia are the third glial cell type present in the retina and are the macrophages of the CNS. Retinal microglia comprise a heterogeneous population of cells. Some have a mesodermal origin and invade the retina during early gestation (Diazaraya et al. 1995, Ling et al. 1993, Streit 2001). Others might be of myeloid origin and enter the retina through the blood vessel system. However, the developmental origin of microglia cells is still debated. Microglia cells are in every layer of the retina, function as innate immune system and have phagocygotic function. Retinal microglia play an important role in blood vessel pruning and remodeling (Checchin et al. 2006, Feng et al. 2011, Unoki et al. 2010). All three glial cell types have distinct functions during retinal vascularization, the development of the blood vessel system, and therefore, these cells might be implicated in different vascular eye diseases.

1.3 The retinal vasculature

The retina has the highest oxygen consumption rate per gram of any other tissue in the human body (Warburg 1928). Since oxygen cannot be stored, a continuous supply is essential. To meet the requirements of the high metabolic rate of the retina, several blood vessel systems are present in the eye. During development the immature mammalian eye is nourished by the transient hyaloid vasculature, including the pupillary mambrane (PM), tunica vasculosa lentis (TVL), as well as the vasa hyaloidea propria (VHP) and the hyaloid artery (HA). The HA enters the eye at the optic disc and extends through the vitreous towards the lens. The VHP are small branches extending from the main trunk of the HA throughout the vitreous. The TVL is a capillary envelope of the posterior lens; the PM is arising from the TVL and covers the anterior lens. In humans, these vessel systems normally regress before birth coeval to the development of the retinal blood vessel system. The regression of the hyaloid vessel system is macrophage – dependent. In some pathological conditions these vessels persist and can cause developmental defects, which may lead to loss of vision (Fruttiger 2007).

The mature retina is nourished by two different vascular systems, the retinal and the choroidal vasculature (Figures 2 and 3). The retinal vasculature nourishes the inner part of the retina and consists of three parallel and interconnected layers. The retinal blood vessel system develops in a highly stereotypic manner. Blood vessels enter the eye through the optic nerve head and spread radially along a pre-established astrocytic network in the NFL towards the periphery. In humans the retinal vasculature of the primary superficial vascular plexus (SVP) reaches the periphery just before birth, in mice about eight days postnatally (Figure 3).

When the primary SVP is established, blood vessels start to remodel into a mature SVP and sprout from the NFL into deeper regions of the retina along the processes of Müller glia cells. First, the deeper vascular plexus (DVP) is formed at the boundary between OPL and INL, a third retinal blood vessel layer, the intermediate vascular layer (IVL) at the border between INL and IPL, is established last.

The retinal vasculature is similar to the cerebral vasculature in respect to its barrier function, retinal endothelial cells are non-fenestrated, tightly interconnected by tight-junctions, and covered by pericytes or mural cells. This barrier function, also known as the blood-retina barrier (BRB), prevents passive passage of plasma proteins and other macromolecules in or out of the capillary system. The second vasculature, the choroidal vasculature (CHV), nourishes the outer

part of the retina and the RPE but has no BRB. Therefore, posterior to the retina, the RPE fulfills epithelial barrier functions to ensure the maintenance of the specialized environment of the neural retina.

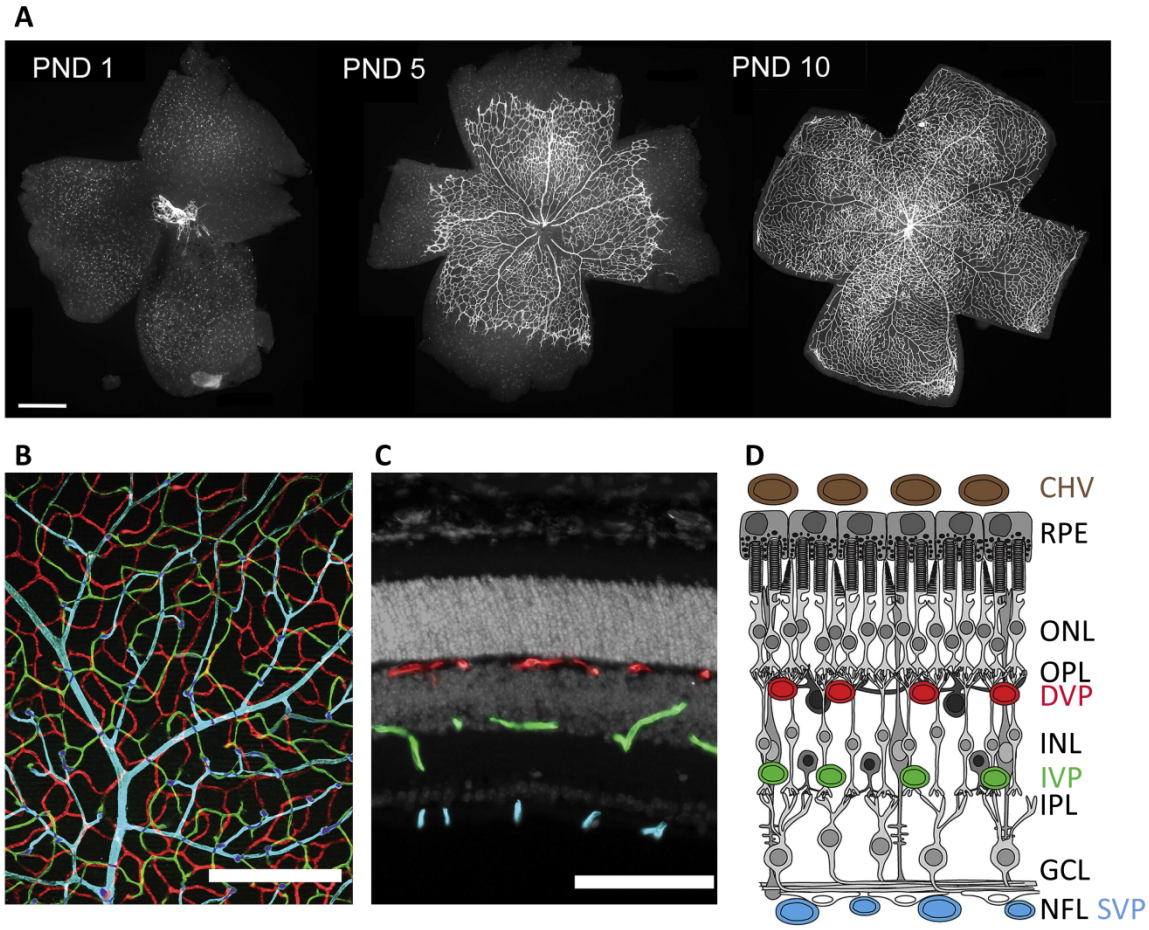

Figure 3: Development of the retinal vasculature in mouse under normoxic conditions. (A) Flat mount preparation of mouse retinas at PND 1, 5, and 10, stained for endothelial cells with isolectin B_4. (B) Retinal vascular plexi of mouse, stained with isolectin B_4 on a retinal flat mount (B) and cryosection (C) of the adult mouse. Vessels are highlighted with artificial coloring (superficial plexus: blue; intermediate plexus: green; deep plexus: red). (D) Schematic illustration of vascular plexi location within the neural retina. Scale bars: 500µm (A), 200µm (B), 100µm (C). (Adapted from: Caprara and Grimm 2012).

The retinal vasculature undergoes drastic changes during development. Vessel regression, vascular remodeling, sprouting angiogenesis, vessel differentiation and maturation are crucial during this process and depend on different cell types and proper signaling pathways among these cells. The understanding of normal and disease-specific vascular development and remodeling have been constantly expanded during the last decades, and are the key to understand retinal vascular diseases, including diabetic retinopathy (DR), retinopathy of prematurity (ROP), and age-related macula degeneration (AMD), which belong to the leading causes of blindness in western populations.

1.4 Retinal vascular diseases

As explained, the retinal vasculature is a three dimensional network of blood vessels penetrating the retina in three different but interconnected layers. Failures in this diminutive structure with complex architecture lead to retinal dysfunction and are the major cause of blindness in the western world. The absence of only one of these three retinal blood vessel layers leads to hypoxia and results in neuronal degeneration. On the other hand, excessive and abnormal growth of new blood vessels, called neovascularization, can disturb proper visual function as well. Overall, the development of the retinal vasculature is highly tuned and any mis-regulation of this process may lead to visual impairment. Over the last years, enormous progress has been achieved in the understanding of the molecular basis of retinal vascularization and associated pathophysiological mechanisms. This might lead to the development of new treatments leading to the prevention of retinal vascular diseases in the future. The three most common retinal vascular diseases today are diabetic retinopathy (DR), retinopathy of prematurity (ROP) and age-related macula degeneration (AMD).

1.4.1 Diabetic retinopathy (DR)

DR (MIM# 603933) is the leading cause of vision loss in working-age adults. As the term suggests, it is a microvascular complication in the retina of patients with diabetes (Antonetti et al. 2012). It is characterized by the loss of pericytes, formation of microaneurysms as well as hyperpermeability of the retinal vasculature and therefore often leads to macular edema and exudates. But also retinal capillary blockage can occur and cause ischemia. Beside the non-proliferative form of DR without neovascularization, another form, which is called proliferative DR, is known. Proliferative DR also shows neovascular proliferation and is the most severe form of DR. In very severe cases retinal detachment can occur due to the formation of fibrotic tissue, which causes traction of the retina. It is thought that genetic predispositions influence the development of DR.

1.4.2 Retinopathy of prematurity (ROP)

ROP (MIM# 133780), previously known as retrolental fibroplasia, effects preterm babies, who are born before completion of the 31st week of gestation with low birth weight (≤1250g, mean: 700g) (Gilbert 2008, Terry 1946). ROP is the major cause of childhood blindness in the western world and is increasingly prevalent in the developing world. The retinal vasculature of these babies is not fully developed when they are born. In normal development, hypoxia in the inner retina present at this stage triggers the formation of the retinal blood vessel system. These premature infants are supplemented with oxygen to alleviate respiratory distress. Under hyperoxic condition the retinal blood vessel system stops to develop. After the infants are back in normoxic environment, the retina senses hypoxia and abnormal retinal vascularization might result. But the etiology of ROP is not yet fully understood. Recent reports suggest a relationship between hyperglycemia and ROP (Blanco et al. 2006, Ertl et al. 2006). ROP has different clinical manifestations and is categorized into five stages. Stage I is the mildest form with only minor vascular changes, stage V is the most severe form with excessive blood vessel growth, fibrous bands and complete retinal detachment.

1.4.3 Age-related macula degeneration (AMD)

AMD (MIM# 603075) is the major cause of vision loss in age group older then 65. There are two forms, the dry and the wet AMD (Rattner and Nathans 2006). Dry AMD or geographic AMD is the most common form of AMD in its early and intermediate stages and is non-neovascular. In the dry AMD, macula degeneration is due to aging and thinning of the retina and depositing of material in the macular region seen as yellow spots, also called drusen. The wet form is less common but more severe, new choroidal blood vessels grow (choroidal neovascularization) under the retina and leakage of these vessels can cause damage of the macula.

All three retinal vascular diseases described above (DR, ROP, AMD) lead to a vascular damage in the retina, which then initiates fibrotic tissue to grow and destroy the fragile structures of the retina. Laser photocoagulation and anti-VEGF therapies are the most commonly used treatments at the moment for all of these diseases. There is another group of eye diseases, called exudative vitreoretinopaties (EVRs), from which we might learn how pathological vascularization processes in the eye lead to blindness. The understanding of this group of eye diseases might help to develop new treatment strategies for different retinal vascular diseases, including DR, ROP, and AMD.

1.5 Exudative vitreoretinopathies (EVRs)

Exudative vitreoretinopaties (EVRs) is a group of eye disorders characterized by incomplete retinal vascularization and the formation of fibrovascular masses in the eye (Figure 4A, B, C). The symptoms range from mild forms with completely asymptomatic patients to very severe forms with bilateral congenital retinal non-attachment that causes blindness (Berger et al. 2010). Its clinical appearance shows highly variable phenotypes, even within a family or between the two eyes of an affected patient. In mild cases, an avascular periphery of the retina can only be seen with fluorescein angiography and these patients may not suffer from visual problems at all. Severe forms are often diagnosed early in life but the milder forms can also be recognized at any age and might lead to sight-threatening manifestations later in life.

1.5.1 Genetic basis of EVR

To date, mutations in four genes have been associated with the pathogenesis of EVR, all involved in the same signaling pathway, the so called Norrin/Wnt signaling pathway. Norrin/Wnt signaling has been shown to be important for proper eye development and retinal vascularization (Xu et al. 2004, Ye et al. 2009).

The first EVR associated gene identified was the Norrie disease pseudoglioma ((*NDP*) gene, located on Xp11.4-p11.3; MIM# 300658) (Berger et al. 1992a, Chen et al. 1992). Approximately one decade later two Wnt receptors were identified, frizzled 4 (FZD4), located on chromosome 11q14.2 (MIM# 604579) and low-density lipoprotein receptor-related protein 5 (LRP5), located on 11q13.2 (MIM# 603506), both were shown to bind the *NDP* gene product (Norrin) with high affinity and, upon binding, trigger canonical Wnt signaling (Xu et al. 2004). Shortly after the discovery of Norrin's Wnt receptors FZD4 and LRP5 a third molecule, tetraspanin 12 (TSPAN12), located on 7q31.31 (MIM# 613138) was identified in a comprehensive reverse genetic approach

(Junge et al. 2009). TSPAN12 might be important to assemble the receptors in the cell membrane to ensure proper Norrin/Wnt signaling. Mutations in all of these four genes (*NDP, FZD4, LRP5* and *TSPAN12*) lead to similar ocular phenotypes (Berger et al. 1992b, Nikopoulos et al. 2010, Poulter et al. 2010, Robitaille et al. 2002, Toomes et al. 2004). EVR is a genetically heterogeneous group of diseases with different patterns of inheritance (autosomal dominant (adFEVR; MIM# 133780), autosomal recessive (arFEVR; MIM# 601813), and X-linked recessive (FEVRX; MIM# 305390 and ND; MIM# 310600). The most prevalent pattern of inheritance in FEVR is autosomal dominant, which can be caused by mutations in either of two genes *FZD4* and *TSPAN12*. Mutations in *LRP5* have also been linked to arFEVR (Jiao et al. 2004). Mutations in *NDP* lead to FEVRX or Norrie disease (ND; MIM# 310600).

1.5.1.1 Norrie Disease (ND)

ND is a severe and syndromic form of EVR. Beside the severe ocular phenotype, the disease is characterized by progressive sensorineural hearing loss and cognitive impairment. ND is a rare X-linked recessive neurodevelopmental disorder. The *NDP* gene is the only gene in which mutations have been found leading to this severe syndromic form with ocular, acoustic and cerebral involvement. First, I would like to explain the disease in more detail, I will come back to the genetic basis later.

ND is named after Dr. Gordon Norrie, a Danish ophthalmologist who investigated familial cases with the disease and described the ocular phenotype in the early 19th century (Norrie 1927). The name was given by Dr. Mette Warburg who expanded the clinical description of the disease and noted the X-linked inheritance and the high variability of the phenotype (Andersen and Warburg 1961, Warburg 1963, Warburg 1966). The ocular phenotype, which is characterized by fibrous and vascular changes, is usually bilateral and symmetric, present at birth and progressive. At birth the eyes might appear normal but usually the first sign in ND gets evident in infancy, which is leukocoria (Figure 4C). Leukocoria is a reflection of light by retrolental fibrotic masses (pseodoglioma) (Figure 4E) appearing as a yellowish-white dot in the pupil of an infant. Clinical manifestations in the eye include opacification of the lens (cataract), posterior synechiae (iris to lens), anterior synechiae (iris to cornea), iris atrophy, shallowing of anterior chamber with occlusion of the outflow tracts which may result in increased intraocular pressure and pain, corneal opacification, band keratopathy, reduction of intraocular pressure, and shrinking of the globe (phthisis bulbi) (Figure 4F). Overall, the phenotype can vary even within a family (Berger and Ropers 2001, Allen et al 2006, Zaremba et al. 1998). The ocular phenotype of ND can be similar to EVR, PFVS, ROP and Coats' disease. Beside the ocular phenotype, most of the affected patients suffer from a progressive hearing loss (Halpin et al. 2005, Halpin and Sims 2008, Smith et al. 2012). In the literature, it is often written that about 30% suffer from hearing loss, but recent data suggest an almost complete penetrance of hearing loss in ND patients (Smith et al. 2012). Further, systemic neurological signs were described in approximately 30% - 50% of ND patients, including developmental delay/mental retardation, psychotic-like features, behavioral abnormalities, seizures, and autism spectrum disorders. Several patients with very complex phenotypes were described including hypogonadism, epileptic seizures, microcephaly, immunodeficiency, and growth retardation (de La Chapelle et al. 1985, Donnai et al. 1988, Gal et al. 1986). A very severe neurological phenotype was described recently with infantile spasm and

profound developmental impairment (Lev et al. 2007). Further, peripheral vascular insufficiency was reported including lower leg ulceration and varicose veins (Michaelides et al. 2004, Rehm et al. 1997).

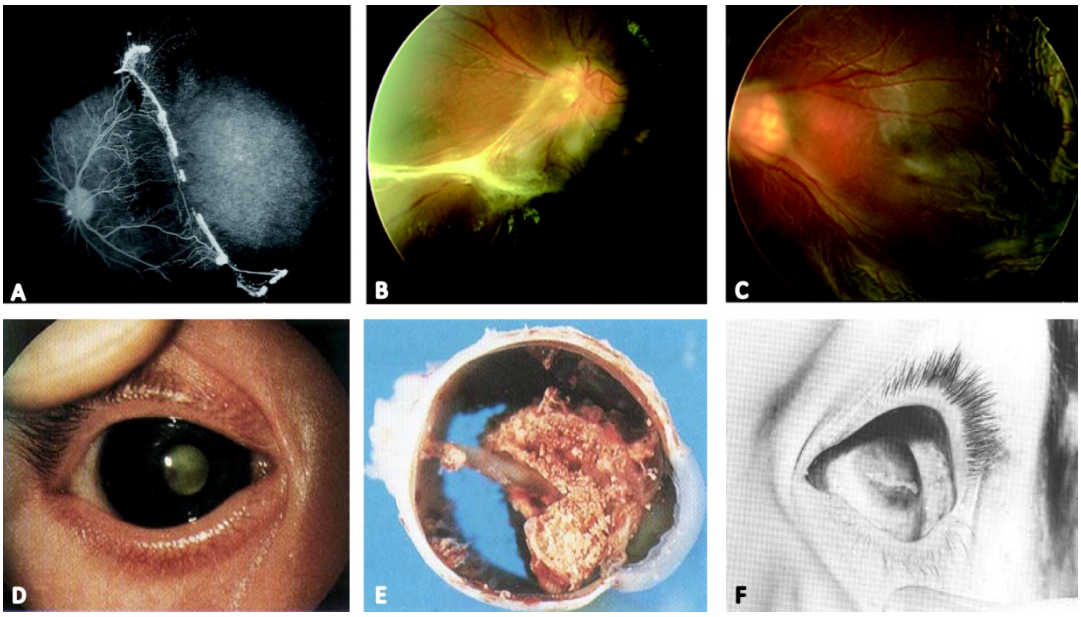

Figure 4: Characteristic clinical manifestation of the ocular ND phenotype. (A) Fluorescein angiogram showing severe retinal avascularization typical of FEVR (Kondo et al. 2007). (B) Fundus photograph showing a dragged macula with persistent hyaloid remnants (Kondo et al. 2007). (C) Fundus photograph showing total retinal detachment (Kondo et al. 2007). (D) Leukocoria of a one month old ND infant (Chynn et al. 1996). (E) Enucleated eye of the same patient as in (D) at the age of two months. (F) Shrinked eye bulb (phthisis bulbi) of a ten year old ND patient (Bergen et al. 1993).

1.5.1.2 Allelic disorders

Since the clinical spectrum of symptoms in ND patients can vary enormously, it is difficult to be diagnosed correctly without genetic testing. Therefore, different distinct diseases are described in the literature, which ultimately were then associated with *NDP* mutations. Three different traits, which have all been associated with mutations in the *NDP* gene and show similar but also slightly different clinical pictures, are the following.

Persistent fetal vasculature syndrome (PFVS)

PFVS, also known as persistent hyperplastic primary vitreous (PHPV) (Goldberg 1997, Reese 1955), is a congenital malformation of the eye which can be inherited in an autosomal recessive (MIM# 611311) or autosomal dominant fashion (MIM# 611308). As the term suggests, the fetal vasculature (TVL and hyaloid vessels) persists in the vitreous of these patients and a fibrotic stalk spans from the optic disk to the temporal posterior lens capsule. PFVS is also associated with microphthalmos, cataract, and glaucoma (Haddad et al. 1978). PFVS is usually unilateral, but also bilateral cases have been described. If bilateral, ND should be considered and genetic testing for *NDP* mutations is indicated.

Retinopathy of prematurity (ROP)

ROP is clinically similar to EVR and three of the four causative EVR genes (*NDP, FZD4, LRP5*) are mutated in a small percentage (3-11%) of severe ROP patients (Dickinson et al. 2006, Ells et al. 2010, Gregory-Evans et al. 2001, Hiraoka et al. 2001, MacDonald et al. 2005, Shastry et al. 1997). This indicates the involvement of Norrin/Wnt signaling in advanced cases of ROP.

Coats' disease (CD)

CD (MIM# 300216) is also called retinal telangiectasia, which is often unilateral and associated with retinal vessel leakage, subretinal exudation, and retinal detachment (Coats 1908). It is suggested that CD might be secondary to somatic *NDP* gene mutations (Black et al. 1999). Overall, CD etiology is unknown and lots of different reports describe additional syndromic manifestations including neurological symptoms (reviewed by Muletarow et al. 2004).

1.6 The Norrie disease pseudoglioma (NDP) gene

The Norrie disease pseudoglioma (*NDP*) gene (NM_000266) has been genetically linked (Bleeker-Wagemakers et al. 1985), physically mapped (Sims et al. 1992) and positional cloned on the proximal short arm of the X chromosome (Xp11.4-p11.3) (Berger et al. 1992a, Chen et al. 1992). The human gene spans 24729 bp of genomic DNA and consists of three exons and two introns (Figure 5). Exon 1 is untranslated and suggested to contain an expression regulatory sequence (Kenyon et al. 1999, Meindl et al. 1992), exon 2 codes for the first 58 amino acids, and the remaining residues (59 – 133) of the open reading frame (ORF) are encoded by exon 3.

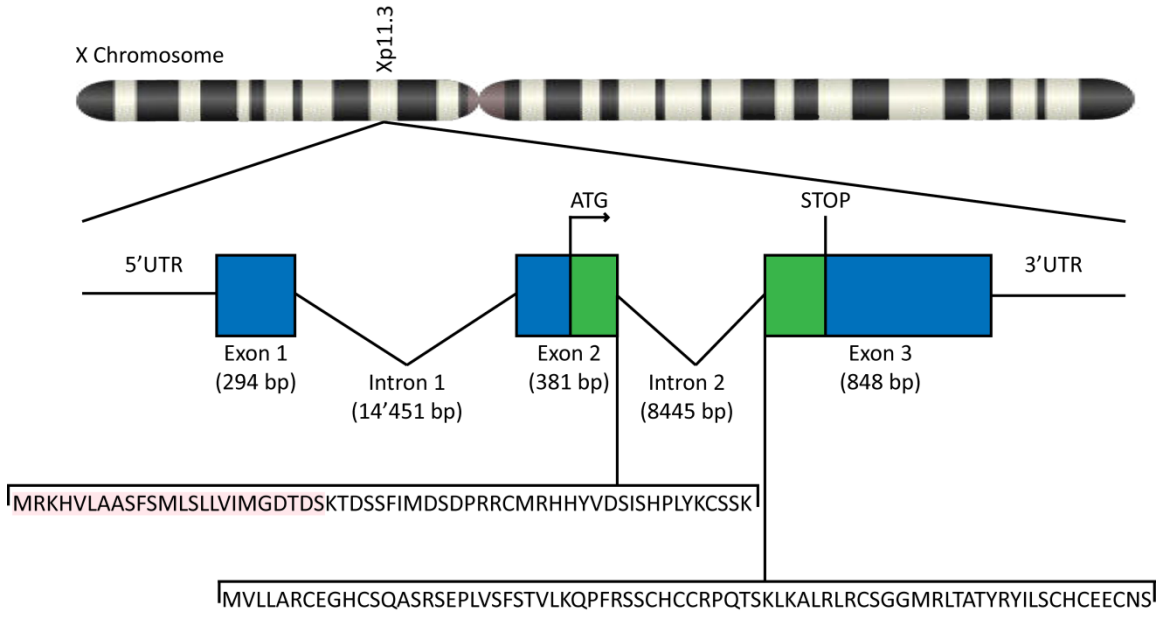

Figure 5: *NDP* gene and protein. *NDP* locus (Xp11.4-p11.3) on the X chromosome. Genomic structure of the *NDP* gene (blue) is shown and the open reading frame (ORF) is indicated (green). Amino acid sequence is indicated, including the signal peptide (red).

1.6.1 Expression of the *NDP* gene

Two reports describe the localization of Norrin mRNA by *in situ* hybridization (Berger et al. 1996, Hartzer et al. 1999). In one report, Norrin was found to be expressed in almost all tissues of mouse embryos from 12.5 to 18.5 days post conception (dpc), including the eye, ear and brain (Berger et al. 1996). Norrin expression was detected in the INL and the GCL of the retina as well as in Purkinje cells of the cerebellum of 2 weeks old mice. Strong expression was also seen in the olfactory bulb at 14.5 dpc. In the second report, Norrin was shown to be expressed in the ONL, INL, and GCL of the retina in three different species (mice, rabbit, and human) (Hartzer et al. 1999). Further high expression levels were detected in the cerebellar granular layer, hippocampus, olfactory bulb, cortex, and epithelium of the rabbit brain. Ye et al. reported that Norrin is expressed in Müller glia cells in all ages postnatally using a knock-in mouse, which carries the coding sequence of human placental alkaline phosphatase (AP) at the *NDP* locus (Ndp^{AP}) (Ye et al. 2009). The same group published recently a comprehensive report about the expression of the Ndp^{AP} allele (Ye et al. 2011). They found Norrin to be expressed at E 10.5 at the optic stalk of the developing retina, and between E 15.5 and PND 0 Norrin expression is apparent at the optic disc. From PND 0 to PND 3 Ndp^{AP} expression is detectable across the whole retina without a spatial gradient. At E 10.5 Norrin is also expressed in dorsal and mid-dorsal regions of the neural tube and the hindbrain. At E 15.5 Norrin expression can be seen in several brain regions: the olfactory bulb and along the lateral olfactory tract, the amygdala, the inferior region of the subventricular zone (SVZ) of the lateral ventricles, the territories flanking the medial ganglionic eminence, the hypothalamus, within the posterior thalamus, and the cerebellar primordium. In adult brain tissue Norrin expression can be seen extensively in astrocytes of the forebrain and the whole diencephalon, and in Bergman glia of the cerebellum. At PND 2 Norrin expression was found in the inner ear in highly vascularized tissue including the lateral wall adjacent to the stria vascularis and between the organ of Corti and the spiral ganglion. This expression pattern in the inner ear is maintained in adult stages. Further, Norrin mRNA expression was detected by RT-PCR in different mouse tissues, including kidney, lung, and ovary (Luhmann et al. 2005b). High expression was detected in brain, epididymus and uterus, weak expression in spleen, testis and thymus (Hsieh et al. 2005). In addition, Norrin has been shown to be expressed in the human placenta (Luhmann et al. 2005b). Taken together, Norrin expression seems to be broad, dynamic and complex.

1.6.2 The Norrin protein

The human *NDP* gene encodes a 133 amino acids protein including an N-terminal signal peptide of 24 amino acids (Figure 5) and was designated Norrin (NP_000257). Norrin is highly conserved through evolution (Figure 6).

Figure 6: Multiple protein sequence alignment of Norrin. Norrin is a highly conserved protein. Colors indicate the residues according to their physicochemical properties. For an explanation of the color-coding see Appendix B.

Norrin is a small, secreted signaling molecule with similarities to the cystine-knot growth factor superfamily with the characteristic feature of a cystine-knot motif (Figure 7) (Meindl et al. 1992). Sequence pattern searches and three dimensional modeling of Norrin suggested a tertiary structure that is similar to the transforming growth factor β (TGF-β) (Meitinger et al. 1993). TGF-β belongs also to the cystine-knot growth factor superfamily as well as nerve growth factor (NGF), platelet-derived growth factor (PDGF), human chorionic gonadotropin (hCG), and vascular endothelial growth factor (VEGF). All these molecules are extracellular ligands and are involved in cell growth, differentiation, and cell-cell communication, are structurally related and share a common overall topology (Mcdonald et al. 1993). Although the members of the cystine-knot growth factor superfamily do not show significant sequence homology they share a common pattern of a cysteine-rich domain (CRD) in which the number and spacing of the cysteine residues is highly conserved. The cysteine residues form disulfide bridges between each other and build a knot – the cystine-knot. More precisely, two disulfide bridges, one between C2 and C5 and another between C3 and C6 form a ring and a third disulfide bridge between C1 and C4 penetrates this ring (Figure 7). A glycine between the second and the third cysteine is highly conserved, and when substituted by another amino acid, severe steric hindrance to the formation of the knot is induced (Isaacs 1995, Sun et al. 1995).

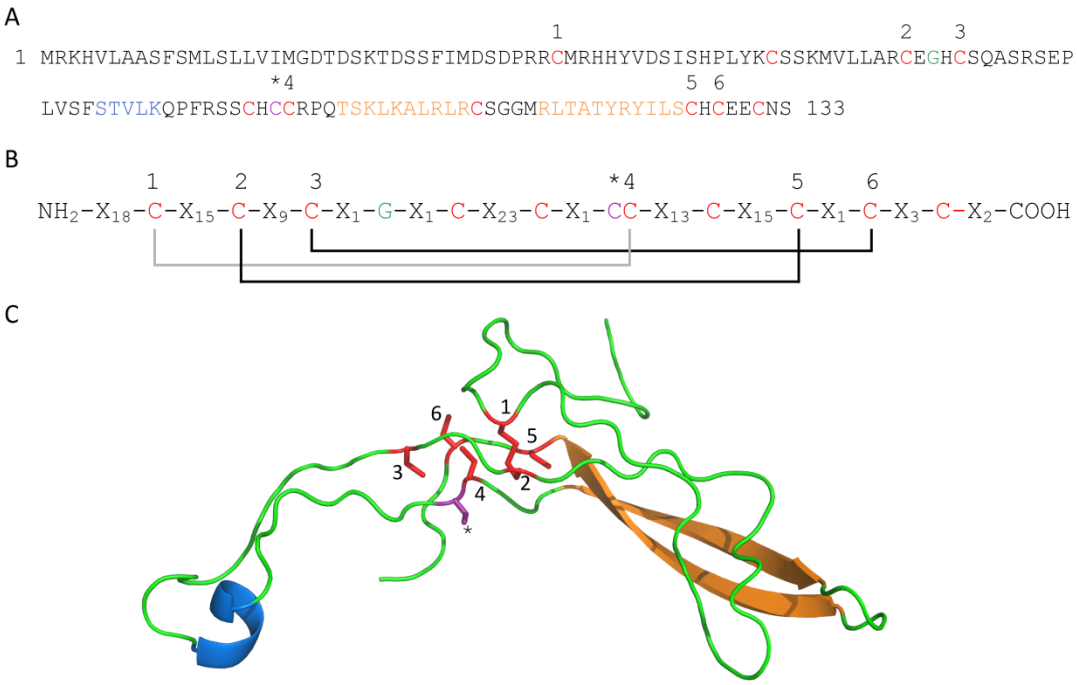

Figure 7: The predicted structure of Norrin. (A) Amino acid sequence of human wild type Norrin. (B) All cysteine residues are labeled red and the cysteine residues that are important for the cystine-knot are numbered. The asterisk marks the cysteine at position 95 which might be important for dimerization or oligomerization. (C) Human Norrin modeled using iTASSER and visualized with PyMol, predicted α-helix (blue) and β-sheets (orange).

Dimerization of Norrin

All cystine-knot proteins function in a dimeric form, and sometimes both hetero- and homodimers can be formed. Norrin has been described as a 200 kDa oligomeric protein in the extracellular matrix (Perez-Vilar and Hill 1997). Structural similarity between Norrin and TGF-β as well as the presence of the cysteine residue at the respective position in Norrin (cysteine at position 95), which is important for dimerization of TGF-β, suggests a similar dimerization mechanism of these two proteins (Meitinger et al. 1993). However, there are conflicting data regarding the functional role of the cysteine at position 95 in Norrin. One report used a p.Cys95Ala mutant and showed that oligomerization is disrupted but dimerization occurred (Perez-Vilar and Hill 1997). Another report, using a p.Cys95Arg substitution, predominantly detected this mutant Norrin in a monomieric form (Junge et al. 2009). But also small fractions of dimers were detected and the authors suggest that these dimers might have formed by alternative disulfide bonding. Interestingly, the p.Cys95Arg mutant could bind FZD4 but was not able to trigger canonical Wnt signaling in the TOPflash reporter assay. In the presence of TSPAN12 this mutant had comparable signaling activity as the wild type Norrin, but only in the highest concentration tested. The authors conclude that TSPAN12 can compensate the inability of the monomeric p.Cys95Arg Norrin to promote receptor multimerization (Junge et al. 2009).

1.6.3 Norrin's pleiotropic properties

Norrin plays an important role in the development of the retinal vasculature and the maintenance of the vasculature in the inner ear. Especially its function in the retina has been studied extensively (Berger et al. 1996, Luhmann et al. 2005a, Ohlmann et al. 2005, Ohlmann et al. 2010, Richter et al. 1998, Schaefer et al. 2009, Xu et al. 2004, Zuercher et al. 2012), less is known about Norrin's function in the ear (Rehm et al. 2002), the brain (Luhmann et al. 2008, Ye et al. 2009) and other organs including organs of the reproductive tract (Kaloglu et al. 2011, Luhmann et al. 2005b, Mintz-Hittner et al. 1996).

Norrin dependent development of the retinal vasculature

Norrin and its high affinity receptor FZD4 and co-receptor LRP5 are crucial for retinal vascularization. Upon binding of this complex β-catenin is stabilized in the cell and LEF/TCF-mediated transcription is activated (Xu et al. 2004). FZD4 is the only Norrin receptor among the ten known mammalian frizzleds (Smallwood et al. 2007) but FZD4 also mediates signals from other Wnt ligands (Lobov et al. 2005). TSPAN12 was identified as a third receptor of Norrin. It is exclusively expressed in the retinal vasculature and required for the Norrin/β-catenin but not for Wnt/β-catenin signaling during retinal vascular development (Junge et al. 2009). Further, it was shown that Norrin is expressed in Müller glia cells and activates FZD4 on retinal endothelial cells (Ye et al. 2009). Extensive mutational analysis of Norrin-FZD4 recognition was conducted (Smallwood et al. 2007), but so far no crystal structure of this complex is available. However, these studies revealed that Norrin-FZD4-LRP5-TSPAN12 complex is important for the proper formation of the retinal blood vessel system.

In addition, several publications exist which describe the retinal vasculature in the *Ndp*$^{y/-}$ mice in detail (Luhmann et al. 2005a, Richter et al. 1998, Schaefer et al. 2009, Zuercher et al. 2012). The *Ndp*$^{y/-}$ mice have a delayed outgrowth of the superficial retinal plexus. In addition, the hyaloid vessels persist and do not regress. Sometimes the hyaloid vessels even penetrate the ILM and enter the retina (Richter et al. 1998). The persistence of the hyaloid vessel system might be secondary due to hypoxic condition in the retina, and remains intact to nourish the avascular retina with oxygen, or it is a primary effect of Norrin. Wnt7b/Fzd4 signaling has been shown to be involved in the microglia dependent regression of the hyaloid vessels and Norrin might have a similar function (Lobov et al. 2005). Also *Fzd4*$^{-/-}$, *Lrp*5$^{-/-}$, and *Tspan12*$^{-/-}$ mice have a delayed regression of the hyaloid vessels, whereas the degrees of delay in *Ndp*$^{y/-}$ and *Tspan12*$^{-/-}$ is less severe than in *Fzd4*$^{-/-}$ and *Lrp5*$^{-/-}$ mice, which might be due to Wnt7b activity (Lobov et al. 2005, Xu et al. 2004). In addition, the retinal vasculature is leaky and hemorrhages are common in the *Ndp*$^{y/-}$ mice. Electromicrographs indicate that the capillary endothelial cells of the retinal blood vessels in the *Ndp*$^{y/-}$ mice are fenestrated (Richter et al. 1998). This fenestration and leakiness might be due to the upregulation of *Plvap* (plasmalemma vesicle associated protein), also called MECA-32, in the *Ndp*$^{y/-}$ model (Schaefer et al. 2009). PLVAP is a membrane glycoprotein important for blood vessel fenestration which is normally not expressed in the retinal vasculature to maintain the BRB (Hallmann et al. 1995). Further, *Plvap* is strongly upregulated in a mouse model with conditional β-catenin loss of function in endothelial cells which leads to immature BBB (Liebner et al. 2008). *Plvap* is also upregulated in retinal endothelial cells of *Lrp5*$^{-/-}$

and *Tspan12*$^{-/-}$ mice (Junge et al. 2009) and in pathological conditions such as Alzheimer's disease, brain tumors, and stroke (Carson-Walter et al. 2005, Sparks et al. 2000). PLVAP upregulation is also triggered by activation of the Erk1/2 MAPK pathway (Stan et al. 2004). Further, *Claudin5* is downregulated in *Ndp*$^{y/-}$ mice which is a major protein of tight junctions of endothelial cells and is involved in barrier function (Amasheh et al. 2005, Schaefer et al. 2009). *Claudin5* is also downregulated in *Lrp5*$^{-/-}$ mice (Chen et al. 2012). Additionally the leakiness of the blood vessels could also be due to diminished mural cell coverage of the retinal vasculature in the *Ndp*$^{y/-}$ mice (Ye et al. 2009, Zuercher et al. 2012). Further, *Fzd4* is expressed in mural cells, and therefore Norrin-FZD4-LRP5 might play an important role in endothelial cell – mural cell interactions. Whether the Norrin dependend leakiness is restricted to brain derived vessels has to be investigated, there is increasing evidence that Norrin is also involved in the vascular stabilization of non CNS vessels (Michaelides et al. 2004, Rehm et al. 1997, Smith 2012).

The maintenance of inner ear homeostasis

Beside the development of the retinal blood vessel system, Norrin is important for the maintenance of the stria vascularis and spiral ganglion of the chochlea. The stria vascularis develops properly in the *Ndp*$^{y/-}$ mice but progressively degenerates over time. In severe cases, this blood vessel system is almost completely degenerated (Rehm et al. 2002). *Ndp*$^{y/-}$ mice show progressive hearing loss and in advanced stages, a loss of inner hair cells. This is consistent with the human ear phenotype, since almost every Norrie disease patient suffers from progressive hearing loss, sometimes earlier and sometimes later in life with the median age of onset of 12 years of age (Smith et al. 2012). Also the *Fzd4*$^{-/-}$ mice show progressive hearing loss but the mechanism of this hearing loss is not well investigated (Wang et al. 2001). No hearing loss in the *Lrp5*$^{-/-}$ mice has been described so far (Xia et al. 2008). In humans, no *FZD4* or *LRP5* mutations have been shown to cause an ear phenotype.

Norrin dependent development of the vasculature in the cerebellum

Norrin and FZD4 play also an important role in the vascularization of the cerebellum. In both *Ndp*$^{y/-}$ and *Fzd4*$^{-/-}$ mice, progressive reduction of the vascular density and integrity in the cerebellum was described similar to the retinal vasculature (Luhmann et al. 2008, Xu et al. 2004). But no alterations were detected in the amount of Purkinje and granular cells in *Ndp*$^{y/-}$ mice, whereas in *Fzd4*$^{-/-}$ mice neuronal degeneration of Purkinje and granular cells was observed. Interestingly, in humans cognitive impairment has only been detected in patients with a mutation in *NDP* but not in *FZD4*. Therefore mouse and human data are to some extend contradictory regarding the involvement of Norrin/FZD4 signaling in the development of the vasculature in the cerebellum. Further it is not clear whether Norrin is involved in BBB formation of cerebral or cerebellar capillaries which is also controlled by the canonical Wnt signaling (Liebner et al. 2008).

Norrin dependent development of the embryonic vasculature

Norrin is also important for the development of the embryonic vasculature. When Norrin is ubiquitous overexpressed in early embryogenesis, a severe disruption in angiogenesis and mid-gastational lethality was observed, which was fully suppressed in a *Fzd4*$^{-/-}$ background and

partially supressed in *LRP5*$^{-/-}$ background (Ye et al. 2009). FZD4 seems to be the major receptor for Norrin not only in the retina but also during embryonic vascularization. LRP5 might be, at least partially, compensated by LRP6.

Norrin's function in the reproductive tract

Norrin is expressed in the human placenta and the mouse and rat endometrium. Further, female mice homozygous for the *Ndp* knockout allele are almost completely infertile (Kaloglu et al. 2011, Luhmann et al. 2005b). Pregnant *Ndp*$^{-/-}$ females show defects in the vascularization of the decidua and in decidualization, leading to embryo resorption and an increased bleeding tendency starting at E 7 (Luhmann et al. 2005b). Infertility has also been reported for *Fzd4*$^{-/-}$ mice, which show an insufficiency of their ovaries (Hsieh et al. 2005). Thus Norrin is suggested to play a role in the vascular development of the female reproductive tract, but whether FZD4 is involved in the same mechanism or other receptors are important in this setting is not known.

Norrin's proangiogenic function has also been demonstrated *in vitro*. Recombinant human Norrin induced proliferation, migration and tube formation of human retinal and dermal microvascular endothelial cells which could be blocked with Dickkopf (Dkk)-1, an inhibitor of the canonical Wnt signaling (Ohlmann et al. 2010).

Norrin's neuro-protective function

Beside the vascular function, a neuro-protective function was described for Norrin. In *Ndp*$^{y/-}$ mice, a loss of RGCs was observed (Richter et al. 1998). This might be a direct effect of Norrin, rather than a secondary effect due to the defective retinal vasculature. Norrin protects RGC death in a RGC degeneration model induced by N-methyl-D-aspartate (NMDA) (Seitz et al. 2010). In eyes treated with Norrin and NMDA, an increased retinal expression of leukemia inducible factor (Lif), endothelin-2 (Edn2), fibroblast growth factor-2 (Fgf2), brain-derived neurotrophic factor (Bdnf), lens epithelium-derived growth factor (Ledgf) and ciliary neurotrophic factor (Cntf) was detected compared to NMDA treated eyes (Seitz et al. 2010). Further, cultured Müller glia cells release neurotrophic factors upon Norrin treatment and a direct and indirect neuro-protective effect of Norrin on RGC-5 survival was shown (Seitz et al. 2010). RGC-5 cells have recently been shown to be of mouse instead of rat origin and do not express RGC markers, RGC-5 cells rather represent a lineage of mouse neuronal precursor cells than rat RGCs (Van Bergen et al. 2009). Another study showed a neuro-protective effect of Norrin on RGC-5 cells by attenuating tissue plasminogen activator (tPA) and urokinase plasminogen activator (uPA)-mediated cell death (Lin et al. 2009). This neuro-protective function of Norrin is mediated through the regulation of Wnt signaling and the phosphorylation status of low-density lipoprotein-related receptor-1 (Lrp1), which is a cell surface receptor for both tPA and uPA.

Transplacental effect of maternal Norrin

One report describes abnormalities in the retinal periphery in four genetically healthy children of a *NDP* mutation carrier mother (Mintz-Hittner et al. 1996). Another report describes maternal xNorrin's function during early neuroectodermal specification in Xenopus (Xu et al. 2012). Both suggest a transplacental effect of Norrin on the embryo. In Xenopus, maternal xNorrin is

upstream of neuronal inducers like *Chordin*, *Noggin*, and *Xnr3* and promotes anterior neural tissue formation in the embryo. Therefore, maternal xNorrin is required for early neuroectoderm specification, from which the CNS derives.

1.6.4 Norrin signaling

So far two signaling pathways were described in which Norrin plays a direct role, the canonical Wnt/ β-catenin signaling and the TGF-β signaling pathways (Xu et al. 2004, Xu et al. 2012).

Wnt signaling

Wnt signaling is a very well known signaling pathway involved in many processes during embryonic development, adult homeostasis and diseases. In particular, Wnt signaling is crucial in early embryonic patterning by the regulation of cell fate decisions, tissue polarity and cell movements (McMahon and Moon 1989). Aberrant Wnt singaling has been implicated in various human diseases (Moon et al. 2004, Logan and Nusse 2004, Clevers et al. 2006, Clevers and Nusse 2012). Beside Norrin, Wnt7a and Wnt7b were shown to be involved in CNS angiogenesis, thus canonical Wnt signaling is a major component for proper vascular development in the CNS (Stenman et al. 2008). Canonical Wnt signaling regulates transcription of target genes through a β-catenin dependent mechanism and is also called Wnt/β-catenin pathway. Other, non-canonical Wnt signaling pathways, like the Planar Cell Polarity (PCP) and Wnt/Calcium pathways regulate cell polarity and intracellular calcium levels respectively, both independent of β-catenin (Veeman et al. 2003).

So far 19 Wnt proteins and 10 Frizzled (FZD) receptors are known in humans. Wnt proteins are secreted glycoproteins, which bind to the extracellular cysteine-rich domain of the seven transmembrane domain cell surface receptors of the FZD receptor family. In canonical Wnt signaling, Wnt ligands bind not only FZD receptors but also single-pass transmembrane co-receptors called LDL-receptor-related proteins 5 or 6 (LRP5 and LRP6) (Bhanot et al. 1996, Yang-Snyder et al. 1996, Tamai et al. 2000). Norrin is not related to other Wnt family proteins but acts as a Wnt ligand and triggers canonical Wnt signaling (Xu et al. 2004).

In the absence of Wnt ligands, a large cytoplasmic complex that includes Axin, adenomatous polyposis coli (APC), casein kinase 1 (CK1) and GSK-3 (glycogen synthase kinase 3) phosphorylates β-catenin, which is recognized by the E3 ubiquitin ligase β-Trcp and degraded by the proteasome. In the absence of canonical Wnt signaling, Wnt target genes are repressed by TCF-TLE/Groucho and histone deacetylases (HDAC) (Figure 8A). Upon binding of Wnt ligands to its FZD receptors, Dishevelled (Dvl) is recruited to the membrane and LRP5/6 is phosphorylated. Subsequently, Axin binds to LRP5/6 leading to dissociation of the Axin/APC/CK1/GSK-3 complex and inhibition of β-catenin phosphorylation. Therefore β-catenin accumulates in the cytoplasm and translocates into the nucleus where it interacts with TCF/LEF family transcription factors and triggers transcriptional activation of target genes (Figure 8B).

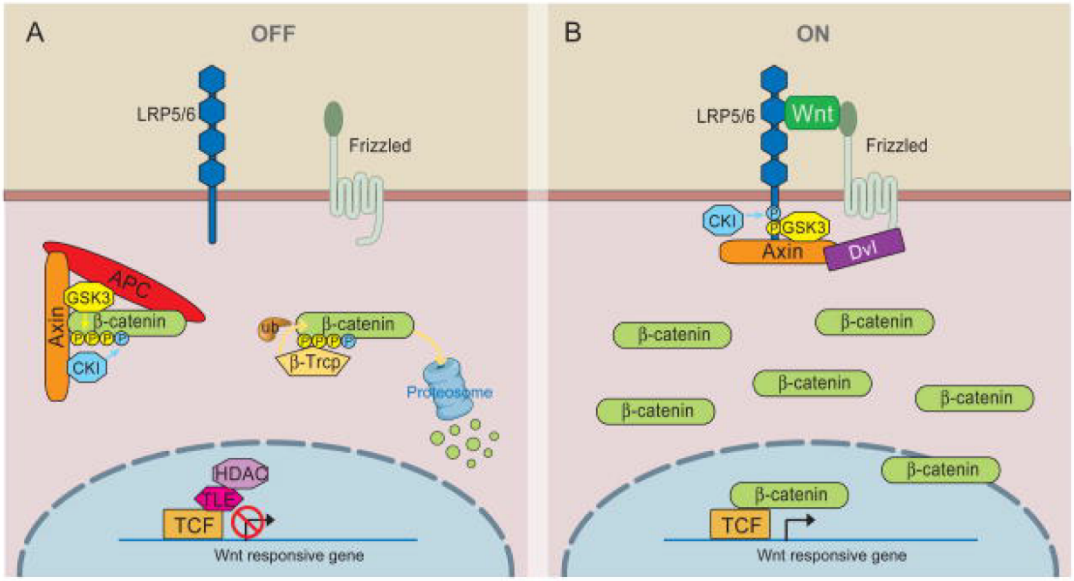

Figure 8: Canonical Wnt signaling. (A) No ligand is bound to the receptor on the cell membrane. The canonical Wnt signaling is in its OFF sate, and target gene expression is inhibited. (B) A ligand is bound to the receptors and initiates canonical Wnt signaling leading to inhibition of β-catenin phosphorylation, its translocation to the nucleus, and the activation of target gene transcription. (McDonald et al. 2009)

TGF-β signaling

Norrin is an inhibitor of TGF-β signaling in Xenopus (Xu et al. 2012). In particular, xNorrin directly binds bone morphogenic protein 4 (Bmp4) and inhibits the activity of Bmp4 and vice versa. Therefore, xNorrin and Bmp4 are reciprocal inhibitors. xNorrin inhibits Activin/Nodal activity and Bmp4 induced Smad1 phosphorylation and antagonizes Bmp4. BMPs control dorsal–ventral patterning, are potent inhibitors of neural differentiation in vertebrate embryos, and play a role in the maintenance of neural stem cells. The *Bmp4*$^{-/+}$ mice have persistent hyaloid vessels and and optic nerve dysplasia (Chang et al. 2001). In humans, mutations in *BMP4* are associated with SHORT syndrome and anophthalmia-microphthalmia, retinal dystrophy, myopia, poly- and/or syndactyly, and brain anomalies (Bakrania et al. 2008, Reis et al. 2011). Inhibition of BMP4 signaling has also been asocciated with primary open-angle glaucoma (POAG) (Wordinger et al. 2007).

The effect on Wnt and TGF-β signaling of three known Norrin mutations (p.Arg40Lys, p.Leu60Pro, and p.Lys57Asn) associated with human phenotypes was investigated and revealed interesting results (Xu et al. 2012). Two mutations (p.Arg40Lys, p.Leu60Pro) showed reduced and one mutation (p.Lys57Asn) strong increased activation of Wnt target gene expression, which is consistent with previous findings (Smallwood et al. 2007). The same mutations had different effects on the TGF-β target gene Xbrachyury (*Xbra*), a mesoderm marker. The xNorrin p.Arg40Lys mutant largely inhibited *Xbra* expression, while the xNorrin p.Leu60Pro mutant showed only slight inhibitory activity. But the xNorrin p.Lys57Asn mutant completely failed to suppress *Xbra* expression. Norrin is a very small protein but it is capable of inducing and inhibiting two different pathways at the same time. How this is achieved is not known. The three-dimensional structure of Norrin and its binding partners, in the wild type and mutant

form, will be needed to answer this question. Such a multifunctional activity on different signaling pathways has also been shown for other proteins like Cerberus (Piccolo et al. 1999).

MAPK signaling

We have evidence that also MAPK signaling is implicated in Norrie disease pathogenesis and similar disorders. In a microarray experiment, retinal transcripts of wild type and *Ndp*$^{y/-}$ mice were compared and MAPK signaling was the top-ranking signaling pathway to be affected by the knockout mutation, whereas Wnt signaling showed up only on rank five (Schaefer et al. 2009). Norrin has also an effect in an *in vitro* reporter assay using a pSRF luciferase reporter. HEK293T cells stably expressing wild type rhNorrin showed an 1.9-fold increase in pSRF luciferase activity compared to cells expressing a mutant (p.Cys95Arg) rhNorrin variant (Zuercher et al. 2012). Further, several mouse models with a defective MAPK signaling pathway have similar retinal vascularization phenotypes as it can be seen in the *Ndp*$^{y/-}$ mice (personal communication, Prof. A. Nordheim). One of these MAPK signaling components is the serum response factor (SRF), which is a transcription factor that controls the expression of cytoskeletal proteins and immediate early genes in different cell types (Knoell and Nordheim 2009). SRF is expressed in endothelial cells (ECs) of capillaries in the mouse embryo and lead in an endothelial-specific knockout model to reduced capillary density, aneurysms, and heamorrhages (Franco et al. 2008). SRF is important for sprouting angiogenesis and small vessel integrity in the mouse embryo. In humans SRF and other molecules involved in MAPK signaling might be implicated in human diseases with a similar phenotype as observed in humans with *NDP* mutations.

1.7 Candidate genes for retinal dysplasia

The genes, which were screened for mutations in patients with severe retinal dysplasia, were selected due to different reasons. I would like to introduce these genes and the reasons why they were selected for mutation screening briefly.

1.7.1 ATOH7 – a transcription factor, required for proper retinogenesis

A deletion in a remote enhancer of *ATOH7* was reported in patients with a similar eye phenotype like Norrie disease (Ghiasvand et al. 2011). Thus we screened *ATOH7* in our cohort. This deletion was suggested, to result in a null allele. ATOH7 is a basic helix-loop-helix (bHLH) transcription factor important for retinogenesis. More detailed information about ATOH7 can be found in the manuscript, which is enclosed in the results chapter.

1.7.2 NINJ1 – a myeloid cell adhesion molecule

The nerve injury induced protein 1 (NINJ1, Ninjurin1) is an adhesion molecule on the cell surface, which plays a role in vascular remodeling (Lee et al. 2009). Its name derives from its role in the peripheral nervous system where it is induced by nerve injury and promotes axonal growth (Araki et al. 1997, Araki and Milbrandt 1996). *NINJ1* is ubiquitously expressed in all tissues with epithelial origin. In addition, *NINJ1* is strongly expressed in myeloid cells and partially expressed in endothelial cells. Its role in vascular remodeling and the central nervous system is not fully understood. But during hyaloid vessel regression *NINJ1* is transiently expressed in macrophages, which migrate and adhere on vascular endothelial cells and activate

WNT7b-Ang pathway to initiate hyaloid vessel regression (Lee et al. 2009). NINJ1 is involved in cell-cell communication and enhances the entry, migration, and activity of leukocytes during development and inflammation through the vascular wall to the site of injury (Ahn et al. 2009, Lee et al. 2010). Especially its role in the interaction between macrophages and endothelial cells is interesting regarding retinal vascular diseases. *NINJ1* expression eventually leads to apoptosis of the vascular endothelial cells and non-functional NINJ1 therefore might be implicated in the progression of retinal vascular diseases.

1.7.3 ZNF408 – a transcription factor, involved in retinal vascular development

The group of Prof. Frans Cremers (Department of Human Genetics, Radboud University Nijmegen Medical Centre) performed linkage analysis, exome sequencing, and segregation analysis of DNA variants in one Dutch FEVR family and identified two putative disease-causing DNA variants in *PASK* (c.791dup; p.Ser265ValfsX64) and *ZNF408* (c.1363C>T; p.His455Tyr). The second sequence variant was also present in an additional Dutch FEVR family that subsequently appeared to share a common ancestor with the original family. ZNF408 is a transcription factor and is involved in the development of the retinal vasculature, at least in zebrafish. Prof. Frans Cremers asked us to screen our patient cohort for mutations in this gene. The manuscript has recently been submitted to the Proceedings of the National Academy of Sciences of the United States of America.

1.7.4 ILK – Focal adhesion and actin-dependent cytoskeletal organisation

Integrin linked kinase *(ILK)*, integrin beta 3 (*ITGB3*) and α-parvin (*PARVA*) were screened due to a similar retinal phenotype of a mouse model with conditional *ILK* KO in endothelial cells and the *Ndp*$^{y/-}$ mouse model. Prof. Ralf Adams (Max-Planck Institute for Molecular Biomedicine, Münster, Germany) contacted us regarding this project. We screened our patient cohort for mutations in these genes. This collaboration is still ongoing and already revealed very interesting results.

ILK is a multifunctional intracellular effector of cell-matrix interactions. It is localized at focal adhesion (FA) complexes and is a serine/threonine protein kinase that regulates cell proliferation, migration, and survival (Fielding et al. 2008, McDonald et al. 2008). ILK mediates extracellular signals over membrane bound integrins to the actin cytoskeleton. We think that there might be a link between ILK, Norrin, and planar cell polarity (PCP) signaling. Besides canonical Wnt signaling, Norrin might also be implicated in the PCP pathway. The PCP pathway mediates asymmetric cytoskeleton organization and the polarization of cells by inducing modifications to the actin cytoskeleton. ILK is implicated in vascular development and leukocyte recruitment (Friedrich et al. 2002, Friedrich et al. 2004, Vouret-Craviari et al. 2004). It is also involved in the vascular smooth muscle cell coverage and vascular wall formation, regulated by the Rho/ROCK signaling (Ho and Bendeck 2009, Kogata et al. 2009).

Integrins are transmembrane proteins and the main cell adhesion receptors involved in focal adhesion. They mediate attachment to the actin cytoskeleton and are involved in transmitting signals from the extracellular space inside of the cell. Integrins are heterodimeric receptors composed of an alpha and a beta subunit. Different combination of alpha and beta subunits can bind different extracellular molecules and attach cells to the extracellular matrix through

integrin-fibronectin, integrin-vitronectin, integrin-collagen and integrin–laminin interactions. ITGB3 was shown to be involved in endothelial cell adhesion and migration (Hayashi et al. 2008, Pula et al. 2010) and is upregulated in the *Ndp*$^{y/-}$ mouse model at PND 15 and PND 20 (Luhmann et al. 2005a). Therefore this integrin was selected for a mutation screening.
PARVA plays a role in the regulation of cell adhesion and cytoskeleton organization and is part of the ILK-PINCH-PARVIN (IPP) complex that localizes to focal adhesions. Since PARVA is a binding partner of ILK, we also screened this gene for mutations in patients with Norrin- or EVR-like symptoms.

1.7.4 MAPK signaling, required for retinal vascular development

Three other candidate genes were derived from a collaboration with the group of Prof. Alfred Nordheim (Tübingen, Germany). The group of Prof. Alfred Nordheim has an inducible and endothelial cell-specific KO mouse model for *Srf*, and a double KO for *Mkl1* (*Mrtf-A*) and *Mkl2* (*Mrtf-B*), which all have retinal vascularization defects similar to the *Ndp*$^{y/-}$ mouse model. Thus, and due to our observations in the expression analysis experiment (Schaefer et al. 2009) and *in vitro* reporter assays (Zuercher et al. 2012), we suggested that mutations in these genes might lead to a similar retinal vascular phenotype like EVR in humans. Therefore we screened our cohort for mutations in *SRF*, *MKL1* and *MKL2*.
SRF is a member of the MADS (MCM1 agamous deficiens SRF) box family of transcription factors and regulates gene expression (Miano et al. 2007). SRF binds different cofactors including myocardin family of transcription factors (MKL1 and MKL2), which were shown to be invovled in cytosekeleton gene regulation and smooth muscle cell differentiation (Mack and Hinson 2005, Pipes et al. 2006). SRF is also regulated by VEGF in endothelial cells and is required for sprouting angiogenesis and vascular integrity (Chai et al. 2004, Franco et al. 2008). SRF links nuclear transcription and actin cytoskeleton dynamics in endothelial cells, neurons and macrophages (Sullivan et al. 2011).
MKL1 and MKL2 are cofactors of SRF, activate serum response element (SRE) dependent genes and are regulated by MAPK or Rho-dependent pathways (Cen et al. 2003, Gineitis and Treisman 2001, Pipes et al. 2006). MKL1 and MKL2 have an N-terminal RPEL domain, which binds these molecules to the monomeric G-actin in the cytoplasm. Upon serum induced actin polymerization, MKL1 and MKL2 accumulate in the nucleus (Vartiainen et al. 2007). Mice with endothelial-specific ablation of serum response factor develop normally until E 10.5 but then, cerebrovascular hemorrhages and severely disrupted vascular networks within the yolk sac appear and the embryos die (Holtz and Misra 2008). It seems that endothelial cell-cell contacts are affected and that vascular remodeling does not occur appropriately.

1.8 Aims of the Thesis

(1) Expression and purification of wild type Norrin and mutant isoforms produced in human embryonic kidney cells (HEK293T) and *Pichia pastoris*

(2) Analysis of protein function (proliferation, migration, and 3D-angiogenesis assay)

(3) To investigate if Norrin is associated with the extracellular matrix (ECM) and if glycolysation of the protein occurs

(4) Structural analysis of Norrin by X-ray crystallography

(5) Isolation of retinal endothelial cells (RECs) from wild type and *Ndp*$^{y/-}$ mouse retinae to stimulate them with recombinant Norrin and VEGF

(6) Identification of mutations in novel genes, not yet implicated in Norrin- or EVR-like human retinal diseases

2. Material and Methods

2.1 Material

2.1.1 Cloning

Reagents and equipment/instruments	Company
Kanamycin	Sigma-Aldrich, Buchs, Switzerland
Ampicillin	Sigma-Aldrich, Buchs, Switzerland
Bacto Agar	Brunschwig, Basel, Switzerland
Bacto Tryptone	Brunschwig, Basel, Switzerland
Bacto Yeast Extract	Brunschwig, Basel, Switzerland
Culture tubes / Snap-cap 12ml	Sarstedt, Nümbrecht, Germany
Disposable inoculation loops	Nunc, Langenselbold, Germany
EcoRI	Fermentas, St. Leon-Rot, Germany
NotI	Fermentas, St. Leon-Rot, Germany
SgsI	Fermentas, St. Leon-Rot, Germany
Innova™ 4400 incubator shaker	New Brunswick Scientific, Edison, NJ, USA
One Shot® TOP10 competent cells	Life Technologies, Zug, Switzerland
One Shot®ccdB Survival™ 2 T1	Life Technologies, Zug, Switzerland
TOPO TA Cloning® Kit	Life Technologies, Zug, Switzerland
pEntry/D-TOPO Cloning Kit	Life Technologies, Zug, Switzerland
LR Clonase Enzyme Mix	Life Technologies, Zug, Switzerland
Heraeus Incubator	Kendro Laboratory Products AG, Zürich, Switzerland

2.1.2 DNA isolation

Equipment/Kits	Company
NucleoSpin® Plasmid Kit	Macherey-Nagel, Düren, Germany
NucleoSpin® Extract II	Macherey-Nagel, Düren, Germany
NucleoBond® Xtra Maxi	Macherey-Nagel, Düren, Germany
NucleoSpin® Robot-8-Plasmid	Macherey-Nagel, Düren, Germany

2.1.3 DNA electrophoresis

Reagents and equipment/instruments	Company
Agarose	Eurobentech, Seraing, Belgium
1kb Plus Ladder	Life Technologies, Zug, Switzerland
Ethidium bromide (10 mg/ml)	Fluka/Sigma-Aldrich, Buchs, Switzerland
Plus Ladder™	Life Technologies, Zug, Switzerland
Acetic acid	Merck, Darmstadt, Germany
Agarose	Eurogentech, Seraing, Belgium
EDTA	Brunschwig, Basel, Switzerland
Ethidium bromide (EtBr)	Fluka/Sigma-Aldrich, Buchs, Switzerland
Ficoll® 400	Pharmacia Biotech, Vienna, Austria
Glacial acetic acid	Merck, Darmstadt, Germany
Glycerol 87%	Fluka/Sigma-Aldrich, Buchs, Switzerland
Horizon® 11-14 gel electrophoresis chamber	Life Technologies, Zug, Switzerland
Horizon® 20-25 gel electrophoresis chamber	Life Technologies, Zug, Switzerland
Horizon® 58 gel electrophoresis chamber	Life Technologies, Zug, Switzerland
Standard Power Pack P25 Power Adapter	Biometra, Göttingen, Germany

Tris-Base	Merck, Darmstadt, Germany

2.1.4 RNA techniques

Reagents and equipment/instruments	Company
RNeasy Kit	Qiagen, Hilden, Germany
NucleoSpin® RNA II	Macherey-Nagel, Düren, Germany
RNA Nano Chips	Agilent Technologies, Santa Clara, CA, USA
Agilent Bioanalyzer 2100	Agilent Technologies, Santa Clara, CA, USA
Superscript III RT	Life Technologies, Zug, Switzerland

2.1.5 PCR and Sequencing

Reagents and equipment/instruments	Company
PTC-200 Peltier Thermal Cycler	MJ Research, Oldendorf, Germany
PTC-225 Peltier Thermal Cycler	MJ Research, Oldendorf, Germany
2720 Thermal Cycler	Life Technologies, Zug, Switzerland
Buffer B	Solis Biodyne, Tartu, Estland
$MgCl_2$ (25 mM)	Solis Biodyne, Tartu, Estland
dNTP mix (20 mM)	Solis Biodyne, Tartu, Estland
10x Solution S	Solis Biodyne, Tartu, Estland
ExoSAP-IT	Qiagen, Hilden, Germany
HotFire™ polymerase	Solis BioDyne, Tartu, Estonia
Pfu DNA polymerase	Promega, Madison, WI, USA
AmpliTaq Gold	Life Technologies, Zug, Switzerland
Primer	Microsynth, Balgach, Switzerland
ABI Prism 3100 DNA-sequencer	Life Technologies, Zug, Switzerland
ABI 3730 DNA-sequencer	Life Technologies, Zug, Switzerland
Sephadex G-50	Sigma-Aldrich, Steinheim, Germany
5x Sequencing Buffer	Life Technologies, Zug, Switzerland
BigDye™ Terminator v.3.1 Cycle Sequencing kit	Life Technologies, Zug, Switzerland
Pfu 10x Buffer (w/ 20 mM $MgSO_4$)	Promega, Madison, USA

2.1.6 Cell culture – routine work

Reagents and equipment/instruments	Company
Dulbecco's Modified Eagle Medium (DMEM)	Sigma-Aldrich, Buchs, Switzerland
Minimal Essential Medium Eagle (MEM)	PAA, Pasching, Austria
M199	Sigma-Aldrich, Buchs, Switzerland
Opti-MEM	Life Technologies, Zug, Switzerland
EBM-2	Lonza, Walkerville, MD, USA
ExCell293	Sigma-Aldrich, Buchs, Switzerland
Fetal Bovine Serum (FBS)	PAA, Pasching, Austria
L-Glutamin	PAA, Pasching, Austria
Zeocin	Life Technologies, Zug, Switzerland
Penicillin-Streptomycin	PAA, Pasching, Austria
Phosphate Buffered Saline (PBS)	PAA, Pasching, Austria
Trypsin/EDTA (0,05 %)	PAA, Pasching, Austria
DMSO	Sigma-Aldrich, Buchs, Switzerland
Supplement Mix für Endothelmedium	PromoCell, Heidelberg, Germany
PureCol (purified collagen)	Inamed Biomaterials, Fremont, USA

Gelatine	Sigma-Aldrich, Buchs, Switzerland
EGF	Sigma-Aldrich, Buchs, Switzerland
Hydrocortisone	Sigma-Aldrich, Buchs, Switzerland
Sodium Chlorate	Sigma-Aldrich, Buchs, Switzerland
Heparin	Bichsel Apotheke, Interlaken, Switzerland
HEBES	Sigma-Aldrich, Buchs, Switzerland
Valproic acid	Sigma-Aldrich, Buchs, Switzerland
Barrycidal 36	Interchem Hygiene, Zürich, Switzerland
Standard tissue culture flask (75 cm2, 150cm2)	TechnoPlasticProducts, Trasadingen, Switzerland
6-/ 12-/ 24-/ 48-/ 96-well cell culture plate	TechnoPlasticProducts, Trasadingen, Switzerland
Casy®, Cell counter	Roche, Basel, Switzerland
Gelaire TC-60 LaminarFlow	Skan, Basel, Switzerland
HEPA CELL 100, Incubator	Thermo Scientific, Wilmington, DE, USA
Serological Pipett	Sarstedt, Nürnbrecht, Germany
Axiovert 40 CFL, Inverted Microscope	Carl Zeiss MicroImaging, Jena, Germany
HEK 293T (Human Embryonic Kidney cell line)	in-house (Institute of Medical Molecular Genetics)
COS-7 (Monkey Kidney Fibroblast cell line)	in-house (Institute of Medical Molecular Genetics)
HMEC-1 (Human Microvasular Endothelial cell line)	CDC, Atlanta, GA, USA
HUVEC (Human Umbilical Vein Endothelial cells)	Lonza, Walkerville, MD, USA
Trypan blue	Sigma-Aldrich, Buchs, Switzerland
Steri-cycle CO_2 incubator	Fisher Scientific, Wohlen, Switzerland

2.1.7 Cell culture – assays

Reagent	**Company**
Heparin	Bichsel Apotheke, Interlaken, Switzerland
Heparitinase	Seikagaku Corporation, Tokyo, Japan
Heparitinase II	Seikagaku Corporation, Tokyo, Japan
Chondoitinase ABC Protease Free	Seikagaku Corporation, Tokyo, Japan
WST-1	Roche Diagnostics, Mannheim, Germany
BD Matrigel® (Growth Factor Reduced)	BD Biosceince, Bedford, USA
Poly-L-Lysine	Sigma-Aldrich, Buchs, Switzerland
Cell Culture Water Pxrogen Free	LabForce, Nunningen, Switzerland
Ethanol absolute	Sigma-Aldrich, Buchs, Switzerland
Cytodex 3	GE Healthcare, Uppsala, Sweden
Polyethylenimine (PEI, 1 ng/µl)	Sigma-Aldrich, Buchs, Switzerland
Dual-Glo Luciferase Assay System	Promega, Madison, USA

2.1.8 Protein techniques

Reagents and equipment/instruments	**Company**
Amicon® Ultra centrifugal device	Merck Millipore AG, Darmstadt, Germany
Float-A-Lyzer 3.5 MWCO	Pierce / Thermo Scientific, Rockford, IL, USA
Float-A-Lyzer 8-10 MWCO	Pierce / Thermo Scientific, Rockford, IL, USA
Slide-A-Lyzer 10 MWCO	Pierce / Thermo Scientific, Rockford, IL, USA
PD-10	GE Healthcare, Otelfingen, Switzerland
β-mercaptoethanol	Merck, Darmstadt, Germany
Ammonium persulfate	Carl Roth, Karlsruhe, Germany
BCA Protein Assay Kit	Sigma-Aldrich, Buchs, Switzerland
Bovine serum albumine (BSA)	Sigma-Aldrich, Buchs, Switzerland
Bromphenol blue	Serva, Heidelberg, Germany

Complete Protease Inhibitor Cocktail tablets	Roche Diagnostics, Rotkreuz, Switzerland
EDTA	Brunschwig, Basel, Switzerland
ELx808™ absorbance microplate reader	Bio-Tek, Bad Friedrichshall, Germany
Gel dryer model 543	BIO-RAD Laboratories AG, Reinach, Switzerland
Glacial acetic acid	Merck, Darmstadt, Germany
Glycerol	Sigma-Aldrich, Buchs, Switzerland
Imperial™ protein stain	Pierce / Thermo Scientific, Rockford, IL, USA
Laboratory shaker	GFL, Burgwedel, Germany
Mini-PROTEAN® 3 electrophoresis system	BIO-RAD Laboratories AG, Reinach, Switzerland
Nonidet P40	Roche Diagnostics, Rotkreuz, Switzerland
Powerpack 200	BIO-RAD Laboratories AG, Reinach, Switzerland
PVDF Western blotting membrane	Roche Diagnostics, Rotkreuz, Switzerland
Rotiphorese® Gel 30 acrylamide gel mix	Carl Roth, Karlsruhe, Germany
Roto-Torque® Heavy Duty rotator	Cole-Parmer instruments, London, England
Silver nitrate ($AgNO_3$)	Merck, Darmstadt, Germany
TEMED	Sigma-Aldrich, Buchs, Switzerland
Trans-Blot® SD Semi-Dry Transfer Cell	BIO-RAD Laboratories AG, Reinach, Switzerland
Tris-HCl	Merck, Darmstadt, Germany
Western Lightning™ ECL Reagent Plus	Perkin Elmer, Boston, MA, USA
Whatman® Chromatography Paper 3mm	GE Healthcare, Otelfingen, Switzerland
PMSF	Fluka/Sigma-Aldrich, Buchs, Switzerland
Imidazole	Fluka/Sigma-Aldrich, Buchs, Switzerland
$NiSO_4$	Fluka/Sigma-Aldrich, Buchs, Switzerland
Sodium thiosulfate	Fluka/Sigma-Aldrich, Buchs, Switzerland
Sodium chlorate	Fluka/Sigma-Aldrich, Buchs, Switzerland

2.1.9 Additional reagents and equipment/instruments

Reagents	**Company**
Sodium chloride	Merck, Darmstadt, Germany
Potassium chloride	Merck, Darmstadt, Germany
Glycine	Merck, Darmstadt, Germany
Hepes	Merck, Darmstadt, Germany
Sodium deoxycholate	Merck, Darmstadt, Germany
Sodium dodecyl sulphate	Merck, Darmstadt, Germany
Guanidine hydrochloride	Qiagen, Hombrechtikon, Switzerland
Ethanol	Merck, Darmstadt, Germany
Methanol	Merck, Darmstadt, Germany
Isopropanol	Merck, Darmstadt, Germany
Tween®20	Carl Roth GmbH, Karlsruhe, Germany
Triton X-100	Sigma-Aldrich, Buchs, Switzerland
Triton X-114	Sigma-Aldrich, Buchs, Switzerland
Bovine Serum Albumin (BSA)	Sigma-Aldrich, Buchs, Switzerland
VECTASHIELD mounting medium with DAPI	Vector Laboratories, Burlingame, USA
Formaldehyde	Fluka/Sigma-Aldrich, Buchs, Switzerland
Glutaraldehyde	Fluka/Sigma-Aldrich, Buchs, Switzerland
Acetic acid	Merck, Darmstadt, Germany
Sodium butyrate	Sigma-Aldrich, Buchs, Switzerland
Roti®- Phenol	Carl Roth GmbH, Karlsruhe, Germany

Instruments	Company
UV-transilluminator (TFX-20.M)	Vilber Lourmat, Eberhardzell, Germany
Molecular Imager ChemiDoc XRS+	BIO-RAD Laboratories AG, Reinach, Switzerland
Thermomixer comfort 0.5 ml	Eppendorf, Hamburg, Germany
NanoDrop® spectrophotometer ND-1000	Thermo Scientific, Wilmington, DE, USA
Luminoskan Ascent	ThermoLabsystems, Helsinki, Finnland
Axioplan 2 microscope	Carl Zeiss, Jena, Germany
GelAirDryer	BIO-RAD Laboratories AG, Reinach, Switzerland
ISMATEC ecoline ISM1089C (peistaltic pump)	IDEX Health & Science GmbH. Glattbrugg, Switzerland
Bio-Tek EL 808	Witec, Littau, Switzerland
pH-Meter 766 Calimatic	Knick, Berlin, Germany
ÄKTA purifier	GE Healthcare, Otelfingen, Switzerland
Centrifuge 5417R centrifuge	Eppendorf, Hamburg, Germany
Centrifuge 5810R centrifuge	Eppendorf, Hamburg, Germany
Axioplan 2 microscope	Carl Zeiss MicroImaging, Jena, Germany

Other Material	Company
Miscroscope slide	Carl Roth GmbH, Karlsruhe, Germany
Glass plate (15 mm)	Carl Roth GmbH, Karlsruhe, Germany
Petri dishes (9 cm)	Sterilin, Newport, England
96-well plate read-out plate	TechnoPlasticProducts, Trasadingen, Switzerland
Microtest Plate 96-Well	SARSTEDT, Sevelen, Switzerland
96-well PCR Plate, non skirted	Axonlab, Baden-Dättwil, Switzerland
Bacterial culturing tubes (12 ml)	Greiner bio-one, St.Gallen, Switzerland
PP testtube (15 ml / 50 ml)	Greiner bio-one, St.Gallen, Switzerland
PCR Strip tubes (0.2 ml)	Axygen, Basel, Switzerland
Eppendorf tubes (1.5 ml, 2 ml)	Carl Roth GmbH, Karlsruhe, Germany

Software	Company
Image Lab 4.0.1 software	BIO-RAD Laboratories AG, Reinach, Switzerland
Alamut® version 2.2	Interactive Biosoftware, Rouen, France
Sequencing Analysis 5.2	Life Technologies, Zug, Switzerland
SeqScape version 2.5	Life Technologies, Zug, Switzerland
Sequence Pilot 3.1	JSI Medical System GmbH, Kippenheim, Germany
SDS 2.4 software	Life Technologies, Zug, Switzerland
Photoshop CS4 Extended Edition	Adobe Systems, Inc., San Jose, USA
ImageJ 1.43m	Rasband, W.S., Bethesda, USA

2.2 Methods

2.2.1 DNA techniques

DNA isolation from patient's blood or saliva

All patients were referred either to the Institute of Medical Molecular Genetics at the University of Zurich or to the Developmental Neurogenetics Clinic at Massachusetts General Hospital at Harvard University in Boston for diagnostic purposes. Informed consent according to the declaration of Helsinki or applicable Swiss/US law was obtained from all subjects involved in genetic testing. DNA samples were extracted from EDTA blood or saliva samples. Saliva samples were collected with OraGene™ Kit (DNA Genotek, Ottawa, Canada). DNA extraction was performed in the diagnostic division of the Institute of Medical Molecular Genetics by semi-automated DNA extraction robot (chemagic MSMI, Chemagen, Baeseiler, Germany) or approved foreign diagnostic laboratories sent purified DNA to us. All samples obtained an identification (ID) number in order to anonymize personal data. Patients in this cohort are from all over the world. Therefore, as a control database, the 1000 Genome Database and HGMD Professional Database were used. At this point I would like to thank Esther Glaus, she extracted most of the patients DNAs.

DNA isolation from agarose gels

A DNA band with the expected size of the DNA fragment of interest was excised with a scalpel on a UV-transiluminator (TFX-20.M; Vilber Lourmat, Eberhardzell, Germany) and transferred into a microcentrifuge tube. DNA was isolated with the column-based kit (NucleoSpin®Extract II, Macherey-Nagel, Düren, Germany) according to manufacturer's instruction.

Plasmid DNA (pDNA) isolation from bacterial cells

Plasmid DNA was isolated according to manufacturer's instruction with a column-based kit by hand or with a robot (BioRobot 9600, Quiagen) if more than 16 samples had to be isolated at the same time. Depending on the amount of pDNA to be isolated, different kits were used (NucleoBond® Xtra Midi/Maxi kit or NucleoSpin® Plasmid, Macherey-Nagel, Düren, Germany).

Genomic DNA isolation from mammalian cell lines

Mammalian cells were harvested in RIPA buffer (Table 1) and disrupted with three repeating cycles of freezing and thawing. Genomic DNA of mammalian cells was isolated with a column-based kit (NucleoSpin® Tissue, Macherey-Nagel, Düren, Germany) according to manufacturer's instruction.

RIPA-buffer			**stock**
Tris, pH 7.5	50mM	5ml	1M
NaCl	150mM	3ml	5M
sodium deoxycholate	0.50%	0.5g	
SDS (sodium dodecyl sulphate)	0.10%	0.1g	
Trition X-100	1.00%	1ml	
complete protease inhibitors	1 tablette		
ddH_2O		add 100ml	

Table 1: RIPA buffer recipe.

Phenol Chloroform extraction

Phenol Chloroform extraction was used to obtain highly pure DNA without protein contaminations. This technique was also used to isolate DNA, RNA and protein from the same sample. The working space was cleaned to work in RNase free environment. Gloves were exchanged frequently.

- transfer 20µg DNA in a fresh microcentifuge tube
- add 392µl DEPC water
- add 400µl Roti®- Phenol (Carl Roth GmbH, Karlsruhe, Germany)
- vortex 30s
- zentrifuge at 14000rpm for 5min
- collect upper phase in a new tube
- add 400µl Roti®- Phenol/Chloroform/Isoamylalkohol (25:24:1) to upper phase
- vortex 30s
- zentrifuge at 14000rpm for 5min
- collect upper phase in a new tube
- add 400µl Chloroform to upper phase
- vortex 30s
- zentrifuge at 14000rpm for 5min
- collect upper phase in a new tube
- add 1ml 100% EtOH
- add 150µl 5M sodium acetate pH 5,6 (10% 3M NaAc) or ad 150µl 5M NH_4AcO pH 5,6
- mix shortly, let it rest for 5min
- zentrifuge at 14000 rpm for 20min at 4°C
- wash with 200µl 70 – 80% EtOH (use DEPC water)
- air dry pellet
- resuspend in 20µl DEPC – water

DNA quantification

DNA concentration was quantified with a photo-spectrometer NanoDrop® ND-1000 (NanoDrop Technologies/Thermo Scientific, Wilmington, DE, USA).

Polymerase chain reaction

Different polymerases were used for different purposes. Usually HotFire™ polymerase (Solis BioDyne, Tartu, Estonia) was used for sequence amplification prior to sequencing (Mullis et al., 1986, Saiki et al. 1988). Polymerase chain reaction was established for each PCR-product (amplicon) using a control DNA with an average integrity quality. Whenever proofreading activity was essential (eg. for molecular cloning of expression constructs), Pfu DNA polymerase (Promega, Madison, WI, USA) was used. For sequences with high GC content, which were difficult to amplify with HotFire™, AmpliTaq Gold (Life Technologies, Zug, Switzerland) was used. PCR products were analyzed with agarose gel electrophoresis to determine whether the reaction yielded in a specific amplicon of the expected size.

PCR clean-up

To remove unused primers in a sample after a PCR, a column-based kit (NucleoSpin®Extract II, Macherey-Nagel, Düren, Germany) according to manufacturer's instruction was used.

Primer design

Primers were designed using the web-based program Primer3 (v0.4.0). Primer specificity was checked by BLAT search using the UCSC Genome browser. Primer pairs were designed in the way that the difference in the annealing temperature (T_A) between primers of a primer pair was not more than 1.5°C. Primers longer than 30bp and primers for molecular cloning purposes were HPLC purified by Microsynth (Balgach, Switzerland). All primers were obtained from Microsynth (Balgach, Switzerland)

Gel electrophoresis

The PCR products (amplicons) were separated by size using agarose gel electrophoresis. Depending on the expected size of the amplicon, gels with different agarose concentrations were used (Table 2).

agarose (%)	Linear range of separation (bp)
2.5	50 - 100
2	100 - 200
1.5	200 - 300
1.2	400 - 600
0.9	500 - 700
0.7	800 - 1000
0.6	1000 - 20 000

Table 2: Effective Range of separation of agarose gels.

TAE-buffer (Table 3) was used to dissolve different amounts of agarose and was also used as running buffer. DNA was stained with ethidium bromide (EtBr; 0.5µg/ml) and was visualized on a UV transilluminator using ChemiDoc XRS+ system (BioRad, Reinach, Switzerland) pictures were analysed using Image Lab 4.0.1 software (BioRad, Reinach, Switzerland).

TAE-buffer 50x	
Tris-base	242g
Glacial acetic acid	57.1ml
EDTA 0.25M pH 8.0	200ml
ddH_2O	add 1000ml

10x Loading-buffer (agarose gel)	
Ficoll® 400	7.5g
Bromphenol blue	0.25g
EDTA 0.5M pH 8.0	1ml
Glycerol	12.5ml
ddH_2O	add 50ml

Table 3: TAE buffer and agarose gel loading dye recipes

Mutation analysis

The exons and flanking intronic regions of eleven different genes were amplified from patients DNA and sequenced afterwards. An overview of all genes is listed in Table 4, primers in Appendix C. The PCR conditions for each amplicon were established by using a control DNA. Here I would like to thank Silke Feil, Mariana Wittmer and Lea Sollfrank, all of them helped in several projects regarding candidate gene screening. Established PCR conditions for each gene are listed in the following section.

Gene	Gene ID	Strand	Transcript ID (Ensemble)	Lenght (bp)	Lenght (aa)	Ch.
ATOH7	ENSG00000179774	reverse	ENST00000373673	1486	152	10
NEUROD1	ENSG00000162992	reverse	ENST00000295108	2852	356	2
ZNF408	ENSG00000175213	forward	ENST00000311764	2442	720	11
ILK	ENSG00000166333	forward	ENST00000299421	1802	452	11

PARVA	ENSG00000197702	forward	ENST00000334956	4458	412	11
ITGB3	ENSG00000259207	forward	ENST00000262017	4894	788	17
SRF	ENSG00000112658	forward	ENST00000265354	4200	508	6
MKL1	ENSG00000196588	reverse	ENST00000355630	4496	931	22
MKL2	ENSG00000186260	forward	ENST00000318282	8608	1049	16
NDP	ENSG00000124479	reverse	ENST00000378062	1833	133	X
TSPAN12	ENSG00000106025	reverse	ENST00000222747	2796	305	7

Table 4: Candidate genes screened for mutations.

Candidate gene screening – PCR and cycling conditions

ATOH7

***ATOH7* Exon1_1**	**Stock conc.**	**Vol.**	**Final conc.**
360 Master Mix		12.5µl	
360 GC Enhancer		5µl	
Primer fwd	10µM	1µl	500nM
Primer rev	10µM	1µl	500nM
DNA template	50ng/ul	1µl	2.5ng/µl
ddH_2O		4.5µl	
Total		**25µl**	

ATOH7 Exon1_1

Cycling conditions		
95°C	10min	
95°C	1min	
60°C	1min	35x
72°C	2min	
72°C	10min	
10°C	∞	

***ATOH7* Exon1_2**	**Stock conc.**	**Vol.**	**Final conc.**
Buffer B	10x	2.5µl	1x
$MgCl_2$	25mM	1.5µl	1.8mM
dNTPs	20mM	0.25µl	200µM
Primer fwd	10µM	1µl	500nM
Primer rev	10µM	1µl	500nM
HotFire™ Polymerase	5U/µl	0.3µl	0.05U/µl
DNA template	50ng/ul	1.3µl	2.5ng/µl
ddH_2O		14.65µl	
S-Solution	10x	2.5µl	1x
Total		**25µl**	

ATOH7 Exon1_2

Cycling conditions		
95°C	15min	
95°C	1min	
60°C	1min	35x
72°C	2min	
72°C	10min	
10°C	∞	

Table 5: PCR and cycling conditions for amplification of exon 1 of the *ATOH7* gene.

NEUROD1

NEUROD1	**Stock conc.**	**Vol.**	**Final conc.**
Buffer B	10x	2.5µl	1x
$MgCl_2$	25mM	1.5µl	1.8mM
dNTPs	20mM	0.25µl	200µM
Primer fwd	10µM	1µl	500nM
Primer rev	10µM	1µl	500nM
HotFire™ Polymerase	5U/µl	0.3µl	0.05U/µl
DNA template	50ng/ul	1.3µl	2.5ng/µl
ddH_2O		14.65µl	
S-Solution	10x	2.5µl	1x
Total		**25µl**	

NEUROD1 Exon2

Cycling conditions		
95°C	15min	
95°C	1min	
60°C	1min	35x
72°C	2min	
72°C	10min	
10°C	∞	

Table 6: PCR and cycling condition for amplification of exon 2 of the *NEUROD1* gene.

ZNF408

ZNF408 Exon 1

***ZNF408* Exon 1**	**Stock conc.**	**Vol.**	**Final conc.**
Buffer B	10x	2µl	1x
$MgCl_2$	25mM	1.2µl	1.5mM
dNTPs	20mM	0.2µl	200µM
Primer fwd	10µM	1µl	500nM
Primer rev	10µM	1µl	500nM
HotFire™ Polymerase	5U/µl	0.1µl	0.025U/µl
DNA template	50ng/ul	1µl	2.5ng/µl
ddH_2O		13.5µl	
Total		**20µl**	

Cycling conditions		
95°C	15min	
95°C	1min	
61°C	1min	35x
72°C	2min	
72°C	10min	
10°C	∞	

ZNF408 Exon 2, 5B, 5C, 5D

***ZNF408* Exons 2, 5B**	**Stock conc.**	**Vol.**	**Final conc.**
Buffer B	10x	2µl	1x
$MgCl_2$	25mM	2µl	2.5mM
dNTPs	20mM	0.2µl	200µM
Primer fwd	10µM	1µl	500nM
Primer rev	10µM	1µl	500nM
HotFire™ Polymerase	5U/µl	0.2µl	0.05U/µl
DNA template	50ng/ul	1µl	2.5ng/µl
ddH_2O		12.6µl	
Total		**20µl**	

Cycling conditions		
95°C	15min	
95°C	45s	
60°C	1min	40x
72°C	1.5min	
72°C	10min	
10°C	∞	

ZNF408 Exon 3, 4, 5A

***ZNF408* Exons 3, 5A, 5C, 5D**	**Stock conc.**	**Vol.**	**Final conc.**
Buffer B	10x	2µl	1x
$MgCl_2$	25mM	1.2µl	1.5mM
dNTPs	20mM	0.2µl	200µM
Primer fwd	10µM	1µl	500nM
Primer rev	10µM	1µl	500nM
HotFire™ Polymerase	5U/µl	0.2µl	0.05U/µl
DNA template	50ng/ul	1µl	2.5ng/µl
ddH_2O		13.4µl	
Total		**20µl**	

Cycling conditions		
95°C	15min	
95°C	1min	
60°C	1min	35x
72°C	2min	
72°C	10min	
10°C	∞	

***ZNF408* Exon 4**	**Stock conc.**	**Vol.**	**Final conc.**
Buffer B	10x	2µl	1x
$MgCl_2$	25mM	2µl	2.5mM
dNTPs	20mM	0.2µl	200µM
Primer fwd	10µM	1µl	500nM
Primer rev	10µM	1µl	500nM
HotFire™ Polymerase	5U/µl	0.1µl	0.025U/µl
DNA template	50ng/ul	1µl	2.5ng/µl
ddH_2O		12.7µl	
Total		**20µl**	

Table 7: PCR and cycling conditions for amplification of exon 1-5 of the *ZNF408* gene.

ILK

ILK Exon 2-13

ILK	**Stock conc.**	**Vol.**	**Final conc.**
Buffer B	10x	2.5µl	1x
$MgCl_2$	25mM	1.5µl	1.5mM
dNTPs	20mM	0.25µl	200µM
Primer fwd	10µM	1µl	500nM
Primer rev	10µM	1µl	500nM
HotFire™ Polymerase	5U/µl	0.3µl	0.05U/µl
DNA template	50ng/ul	1µl	2.5ng/µl
ddH_2O		17.45µl	
Total		**25µl**	

Cycling conditions		
95°C	15min	
95°C	1min	
58°C	1min	35x
72°C	2min	
72°C	10min	
10°C	∞	

Table 8: PCR and cycling conditions for amplification of exons 2-13 of the *ILK* gene.

PARVA

PARVA Exon 1-10, 12, 13

***PARVA* Exon 1-10, 12, 13**	**Stock conc.**	**Vol.**	**Final conc.**
Buffer B	10x	2µl	1x
$MgCl_2$	25mM	1.2µl	1.5mM
dNTPs	20mM	0.2µl	200µM
Primer fwd	10µM	1µl	500nM
Primer rev	10µM	1µl	500nM
HotFire™ Polymerase	5U/µl	0.2µl	0.05U/µl
DNA template	50ng/ul	1µl	2.5ng/µl
ddH_2O		13.4µl	
Total		**20µl**	

Cycling conditions		
95°C	15min	
95°C	45s	
52°C	1min	35x
72°C	1.5min	
72°C	10min	
10°C	∞	

PARVA Exon 11

***PARVA* Exon 11**	**Stock conc.**	**Vol.**	**Final conc.**
Buffer B	10x	2µl	1x
$MgCl_2$	25mM	1.6µl	2.0mM
dNTPs	20mM	0.2µl	200µM
Primer fwd	10µM	1µl	500nM
Primer rev	10µM	1µl	500nM
HotFire™ Polymerase	5U/µl	0.2µl	0.05U/µl
DNA template	50ng/ul	1µl	2.5ng/µl
ddH_2O		13.2µl	
Total		**20µl**	

Cycling conditions		
95°C	15min	
95°C	45s	
64°C	1min	35x
72°C	1.5min	
72°C	10min	
10°C	∞	

Table: 9 PCR and cycling conditions for amplification of exon 1-13 of the *PARVA* gene.

ITGB3

***ITGB3* Exon 2-15**	**Stock conc.**	**Vol.**	**Final conc.**
Buffer B	10x	2µl	1x
$MgCl_2$	25mM	1.2µl	1.5mM
dNTPs	20mM	0.2µl	200µM
Primer fwd	10µM	1µl	500nM
Primer rev	10µM	1µl	500nM
HotFire™ Polymerase	5U/µl	0.2µl	0.05U/µl
DNA template	50ng/ul	1µl	2.5ng/µl
ddH_2O		11.4µl	
S-Solution	10x	2µl	1x
Total		**20µl**	

ITGB3 Exon 2-15

Cycling conditions		
95°C	15min	
95°C	1min	
60°C	1min	35x
72°C	2min	
72°C	10min	
10°C	∞	

Table 10: PCR and cycling conditions for amplification of exon 2-15 of the *ITGB3* gene.

SRF

SRF	**Stock conc.**	**Vol.**	**Final conc.**
Buffer B	10x	2.5µl	1x
$MgCl_2$	25mM	1.5µl	1.5mM
dNTPs	20mM	0.25µl	200µM
Primer fwd	10µM	1µl	500nM
Primer rev	10µM	1µl	500nM
HotFire™ Polymerase	5U/µl	0.3µl	0.05U/µl
DNA template	50ng/ul	1µl	2.5ng/µl
ddH_2O		17.45µl	
Total		**25µl**	

SRF Exon 2-7

Cycling conditions		
95°C	15min	
95°C	1min	
58°C	1min	35x
72°C	2min	
72°C	10min	
10°C	∞	

Table 11: PCR and cycling conditions for amplification of exon 2-7 of the *SRF* gene.

MKL1

MKL1	**Stock conc.**	**Vol.**	**Final conc.**
Buffer B	10x	2µl	1x
$MgCl_2$	25mM	1.2µl	1.5mM
dNTPs	20mM	0.2µl	200µM
Primer fwd	10µM	1µl	500nM
Primer rev	10µM	1µl	500nM
HotFire™ Polymerase	5U/µl	0.2µl	0.05U/µl
DNA template	50ng/ul	1µl	2.5ng/µl
ddH_2O		13.4µl	
Total		**20µl**	

MKL1 Exon 1-9, 12-15

Cycling conditions		
95°C	15min	
95°C	1min	
58°C	1min	35x
72°C	2min	
72°C	10min	
10°C	∞	

MKL1 Exon 10

Cycling conditions		
95°C	15min	
95°C	1min	
60°C	1min	35x
72°C	2min	
72°C	10min	
10°C	∞	

Table 12: PCR and cycling conditions for amplification of exon 1-15 of the *MKL1* gene.

MKL2

***MKL2* Exon 2-5, 7-16**	**Stock conc.**	**Vol.**	**Final conc.**
Buffer B	10x	2µl	1x
$MgCl_2$	25mM	1.2µl	1.5mM
dNTPs	20mM	0.2µl	200µM
Primer fwd	10µM	1µl	500nM
Primer rev	10µM	1µl	500nM
HotFire™ Polymerase	5U/µl	0.2µl	0.05U/µl
DNA template	50ng/ul	1µl	2.5ng/µl
ddH_2O		13.4µl	
Total		**20µl**	

MKL2 Exon 1-16

Cycling conditions		
95°C	15min	
95°C	1min	
58°C	1min	35x
72°C	2min	
72°C	10min	
10°C	∞	

***MKL2* Exon 1, 6**	**Stock conc.**	**Vol.**	**Final conc.**
Buffer B	10x	2µl	1x
$MgCl_2$	25mM	1.6µl	2mM
dNTPs	20mM	0.2µl	200µM
Primer fwd	10µM	1µl	500nM
Primer rev	10µM	1µl	500nM
HotFire™ Polymerase	5U/µl	0.2µl	0.05U/µl
DNA template	50ng/ul	1µl	2.5ng/µl
ddH_2O		13.4µl	
Total		**20µl**	

Table 13: PCR and cycling conditions for amplification of exon 1-16 of the *MKL2* gene.

Screening of known disease-associated genes – PCR and cycle conditions

NDP

***NDP* Exon 1, 2, 3**	**Stock conc.**	**Vol.**	**Final conc.**
Buffer B	10x	2µl	1x
$MgCl_2$	25mM	1.2µl	1.5mM
dNTPs	20mM	0.25µl	250µM
Primer fwd	10µM	1µl	500nM
Primer rev	10µM	1µl	500nM
HotFire™ Polymerase	5U/µl	0.2µl	0.05U/µl
DNA template	50ng/ul	1µl	2.5ng/µl
ddH_2O		13.35µl	
Total		**20µl**	

NDP Exon 1-3

Cycling conditions		
95°C	15min	
95°C	1min	
58°C	1min	35x
72°C	1.5min	
72°C	10min	
10°C	∞	

Table 14: PCR and cycling conditions for amplification of exon 1, 2 and 3 of the *NDP* gene.

TSPAN12

TSPAN12	**Stock conc.**	**Vol.**	**Final conc.**
Buffer B	10x	2.5µl	1x
$MgCl_2$	25mM	1.5µl	1.8mM
dNTPs	20mM	0.25µl	200µM
Primer fwd	10µM	1µl	500nM
Primer rev	10µM	1µl	500nM
HotFire™ Polymerase	5U/µl	0.3µl	0.05U/µl
DNA template	50ng/ul	1µl	2.5ng/µl
ddH_2O		17.45µl	
Total		**25µl**	

TAPAN12 Exon1-7,8.1,8.2

Cycling conditions		
95°C	15min	
95°C	1min	
58°C	1min	35x
72°C	2min	
72°C	10min	
10°C	∞	

Table: 15 PCR and cycling conditions for amplification of exon 1-8 of the *TSPAN12* gene.

ExoSAP-IT® treatment

Unincorporated dNTPs and primers, which could interfere with the sequencing reaction, were removed by the ExoSAP-IT® PCR clean up method (USB, Cleveland, OH, USA) whenever required. It is based on Exonuclease I (Exo) and Shrimp Alkaline Phosphatase (SAP), Exo digests residual single-stranded primers or any other single stranded DNA fragments, and SAP removes phosphate groups of dNTPs to prevent their incorporation. 5µl of ExoSAP-IT® (diluted 1:50 in ddH_2O) were mixed with 0.8µl of PCR product and incubated as described in table 16. This solution was subsequently used in the cycle sequencing reaction.

ExpSAP-IT® treatment	
37°C	15min
80°C	15min
10°C	∞

Table 16: ExoSAP-IT® PCR clean up protocol.

DNA-Sequencing, Sanger method

The amplicons generated by PCR were sequenced using the Sanger chain-termination method (Sanger et a. 1977). By random incorporation of fluorescently labeled dideoxynucleotides (ddNTPs) into the DNA strand during amplification further elongation is inhibited. When ddNTPs are mixed with an excess of dNTPs, a heterogenous population of fragments of all possible lengths is generated, all ending with a fluorescently labeled nucleotide. Each of the four different nucleotides is labeled with a unique dye, so that a laser can distinguish the last nucleotide of each fragment after size separation by capillary gel electrophoresis. Same primers were used for sequencing as were used for amplicon generation. Cycle sequencing reaction was run according to table 17. When an amplicon was to long for one sequencing reaction (>600bp), additional internal sequencing primers were used, as indicated in the primer-collection (Appendix C). The sequencing reaction was purified with Sephadex G-50 (Sigma-Aldrich, Buchs, Switzerland) in a 96 well format according to manufacturer's instruction. The sequencing reaction was performed with the ABI PRISM BigDye Terminator v.3.1 Cycle Sequencing kit and the capillary gel electrophoresis and laser detection was done with an ABI PRISM 3100 or ABI PRISM 3730 Genetic Analyser (Life Technologies, Zug, Switzerland).

Cycle sequencing	Vol.
Sequencing buffer 5x	1.6µl
PCR Product	1µl
Primer	1µl
BigDye™	0.8µl
ddH_2O	5.6µl
Total	10µl

Cycling conditions		
96°C	1min	
96°C	20s	
50-58°C	10s	25x
60°C	2min	
10°C	∞	

Table 17: Cycle sequencing mix and reaction.

The results were analyzed using the softwares Sequencing Analysis 5.2, SeqScape version 2.5 (both Life Technologies, Zug, Switzerland) and Sequence Pilot 3.1 (JSI Medical System GmbH, Kippenheim, Germany). Reference sequences were downloaded from Ensembl (http://www.ensembl.org) (Table 4).

***In vitro* mutagenesis**

To analyze the effect of a specific mutation on the function of the particular protein, an expression construct for each mutation was generated. The wild type ORF of the gene of interest had to be present in any kind of vector. The wild type sequence of each ORF was verified by direct sequencing in the respective expression vector. When the wild type sequence was confirmed, two PCRs were performed using the wild type sequence as a template (Figure 9). The first PCR with a forward primer at the start codon of the gene (with an addition of the sequence CACC, for Gateway cloning using pENTR™/D-TOPO® cloning kit) and the reverse primer was at the position where the mutation had to be inserted. For the second PCR, the forward primer was at the position of the mutation and the reverse primer at the stop codon. After the naturally occurring stop codon, two additional stop codons were integrated to ensure proper termination of translation. Or no stop codon for C-terminaly tagged expression constructs was present in the primer. The two primers at the mutation site were both 30-45bp long and had an overlapping sequence of about 20bp. The mutation was present in the center of both. If necessary, the amplicon with the expect size was cut out of the agarose gel and purified. When a single distinct band with the expected size was detected in the agarose gel, a simple removal of primers by PCR clean-up (NucleoSpin® Extract II kit of Machery-Nagel) was sufficient for further use of the generated amplicon. The two long primers at the mutation site had an overlapping sequence of 20bp to link the two amplicons together in third PCR. Depending on the size of the two amplicons, the amplicon amount was adjusted, so that similar amounts of each amplicon were present in the third PCR. A total amount of 500ng DNA, the forward Primer of the first amplicon and the reverse primer of the second amplicon were used in the third PCR to get the full-length construct with a mutation incorporated. This amplicon was then used for cloning.

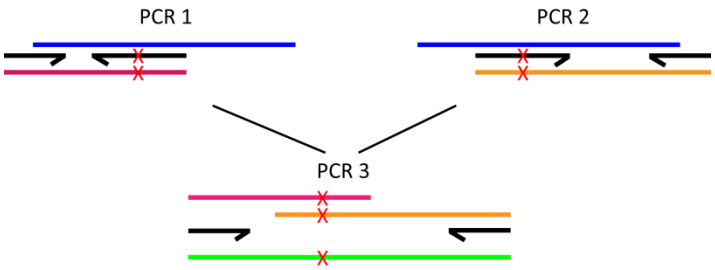

Figure 9: Illustration of the *in vitro* mutagenesis approach. ORF of interest (blue), generated amplicons in PCR 1 & 2 (red and orange), final amplicon after PCR 3 (green), and the red crosses indicate a mutation.

Mutagenesis PCR 1 & 2	Stock conc.	Vol.
Pfu Buffer 10x	10x	5µl
dNTPs	20mM	0.4µl
Primer fwd	10µM	1µl
Primer rev	10µM	1µl
Pfu™ Polymerase	3U/µl	1µl
DNA template (vector)	100ng/ul	1µl
ddH_2O		40.6µl
Total		**50µl**

Cycling conditions (PCR1&PCR2)		
95°C	2min	
95°C	45s	
42°C	30s	
72°C	3.5min	
95°C	45s	
46°C	30s	
72°C	3.5min	
95°C	45s	
58°C	30s	35x
72°C	3.5min	
72°C	10min	
10°C	∞	

Table 18: Mutagenesis PCR and cycling conditions for amplicons 1 & 2.

Mutagenesis PCR 3	Stock conc.	Vol.
Pfu Buffer 10x	10x	5µl
dNTPs	20mM	0.4µl
Primer fwd	10µM	1µl
Primer rev	10µM	1µl
Pfu™ Polymerase	3U/µl	1µl
DNA of PCR1&PCR2 (500ng)	100ng/ul	5µl
ddH_2O		36.6µl
Total		**50µl**

Cycling conditions (PCR3)		
95°C	2min	
95°C	45s	
62°C	30s	4x
72°C	3.5min	
95°C	45s	
58°C	30s	29x
72°C	3.5min	
72°C	10min	
10°C	∞	

Table 19: Mutagenesis PCR and cycling condition for amplicon 3.

The *ATOH7* constructs were generated directly from patients DNA. This was possible since *ATOH7* is a single-exon gene.

Cloning of DNA fragments

Cloning was performed using different approaches. When ever possible the Gateway cloning system (Life Technologies, Zug, Switzerland) was used. This system allows directional blunt-end cloning. I used the pENTR™/D-TOPO® cloning kit with OneShot TOP10 chemically competent cells (Life Technologies, Zug, Switzerland). With the pENTR™/D-TOPO® vector it is possible to go into different destination vectors by a very efficient LR-clonase reaction within 5min. Cloning was done according to manufacturer's instruction. Transformed TOP10 E. coli cells were grown on LB/Agar plates (Table 20) with the appropriate antibiotic at 37°C o/n. Clones were picked and grown in 3ml liquid culture medium with the appropriate antibiotic at 37°C o/n at 220rpm in a lab incubator shaker (Innova™ 4400; New Brunswick Scientific, Edison, NJ, USA). Plasmid DNA was extracted from each culture with NucleoSpin® Plasmid Kit from Machery-Nagel. A glycerole stock was made for storage (-80°C) by mixing 300µl glycerol (87.6%) with 300µl of the LB-culture.

LB Medium	
Bacto Tryptone	10g
Bacto Yeast extract	5g
NaCl	10g
ddH_2O	add 1000ml
autoclave	

LB/Agar plates	
Bacto Tryptone	10g
Bacto Yeast extract	5g
NaCl	10g
Bacto Agar	15g
ddH_2O	add 1000ml
autoclave	

Table 20: LB Medium and LB/Agar for E.coli cultivation

To identify pENTR™/D-TOPO clones with an insert of the correct size, 2µl vector DNA was digested in a 10µl approach with Tango buffer using NotI and SgsI restriction enzymes (Fermentas, St.Leon-Rot, Germany) for 2h at 37°C. Reaction was loaded on an agarose gel. Clones with insert of correct size were sequenced.

Dependent on the further usage of the expression vector, different destination vectors were used – with or without tags. Usually a vector with a CMV (cytomegalievirus) promoter was used for expression in mammalian systems. All vectors used in this work are listed in the Appendix C.

2.2.2 RNA techniques

RNA isolation
RNA was isolated according to manufacturer's instruction with a column-based kit (NucleoSpin® RNA II, Macherey-Nagel, Düren, Germany). RNA was stored at -80°C.

RNA quantification
RNA concentration was quantified with a photo-spectrometer NanoDrop® ND-1000 (NanoDrop Technologies/Thermo Scientific, Wilmington, DE, USA).

RNA quality determination
RNA quality was monitored according to manufacturer's instructions using Agilent Bioanalyzer 2100 (Agilent Technologies, Santa Clara, CA, USA). RNA quality was considered as adequate when RNA integrity number (RIN) was higher than 9.0.

cDNA synthesis
Only RNA with RIN higher than 9.0 was used for cDNA synthesis. 1000ng RNA was used in a 20µl reaction volume (50ng/µl). Using random hexamer primers (250ng) and Superscript III RT (Life Technologies, Zug, Switzerland) according to manufacturer's instructions.

RT-PCR
To verify whether a gene is transcribed in a certain tissue or cell line, RNA was isolated and reverse transcribed as described before. For each gene of interest, two exon spanning primers were designed to generate an amplicon of 150-250bp, specific for the gene of interest. Alternatively, primers were also designed in a way that large introns were between the two primers. Thus amplicons could not be generated with genomic DNA as a template. As a negative control a „-RT" reaction without reverse transcriptase was used.

qRT-PCR - TaqMan® analysis
To investigate transcript level differences between two samples TaqMan® analysis was performed. RNA was isolated and transcribed into cDNA, equal amounts of cDNA were used.

TaqMan® probes were all ordered from Life Technologies (Zug, Switzerland) and are listed in table 21. Reactions with a volume of 20µl were performed in 96-well plates. GAPDH was used as endogenous control. SDS 2.4 software (Life Technologies, Zug, Switzerland) was used to analyze TaqMan® results.

TaqMan probes		
Gene	**Probe**	**RNA**
Atoh7 mouse	Mm00844064_s1	60ng
Stmn1 mouse	Mm01185262_m1	60ng
Ndp mouse	Mm00477754_m1	60ng
Gapdh mouse	Mm99999915_g1	10ng
NDP human	Hs00181129_m1	60ng
GAPDH Human	Hs02758991_g1	10ng

Table 21: TaqMan® probes used in this work.

TaqMan reaction	
ddH_2O	5µl
Template	4µl
Primer/Probe (20x)	1µl
TaqMan® mastermix	10µl
Total:	20µl

Table 22: TaqMan® reaction recipes

Quantitative analysis was carried out in three to five replicates in an ABI PRISM® 7900HT system (Life Technologies, Zug, Switzerland) using standard cycling conditions: 45 cycles of denaturation (15s/95°C), annealing/extension (1min/60°C).

2.2.3 Protein techniques

Recombinant human Norrin – construct design

A major goal during this thesis was to get hands on recombinant human Norrin for use in functional assays. For this, stably Norrin (either wild type or disease-associated mutant isoforms) expressing cell lines were established. This was done during my Master thesis 2006-2007. A schematic representation of the constructs used for the generation of these sable cell lines is indicated in figure 10. The pBud CE4.1 vector (Life Technologies, Zug, Switzerland) with a CMV promoter was used to transfect HEK293T cells. Stable gene expression technology was used in a mammalian expression system to allow proper posttranslational modification of recombinant Norrin.

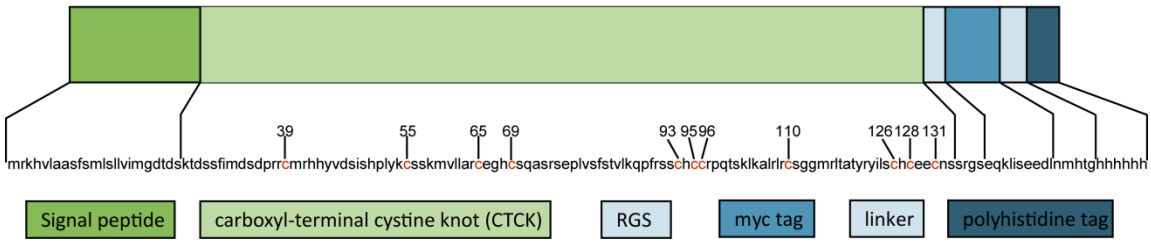

Figure 10: Schematic representation of Norrin constructs. *hNDP* sequence (light green), signal peptide (dark green), RGS (light blue), myc tag (blue), linker (light blue), polyhistidine tag (dark blue). The *hNDP* sequence and the signal peptide have been cloned site directed into a pBud CE4.1 vector (Life Technologies), myc and polyhistidine (6xHis) tags derive from vector sequence.

Beside the wild type human Norrin, four disease-associated mutant isoforms were used to generate stable cell lines. The mutations were selected according to the phenotype that is associated with the different mutations, including classical Norrie disase, FEVR, Coats' disease, mild ND and ROP. All human Norrin variants used in this work are listed in table 23.

Phenotype	Protein variant	Location
-	wild type	
ND	p.Cys95Arg	Exon 3
ND, EVR (sporadic), Coats' disease	p.Cys96Trp	Exon 3
FEVR	p.Arg121Leu	Exon 3
mild ND, FEVR, ROP	p.Arg121Trp	Exon 3

Table 23: Human Norrin isoforms used in this work.

Suspension adapted HEK293T cells - generation and maintenance

Suspension adapted stably Norrin (wild type and disease associated mutant isoforms) expressing cell lines were generated and used for the production of secreted recombinant human Norrin. Suspension adapted HEK293T cells were generated by a stepwise reduction of FCS concentration in the cell culture medium. This was done over a time frame of six month and cell viability was monitored carefully. Suspension-adapted HEK293T cells were routinely grown in 75cm^2 T-flasks stand upright in 100 mL of DMEM containing 2-5% FCS and supplemented with L-glutamine.

Recombinant protein production

Suspension culture allows a cultivation of cells with higher density compared to adherent cells (Wurm 2004). Further, by reducing FCS in the cell culture medium, the major contaminants are reduced in an early stage, which simplifies the whole downstream purification processe. Additionally the protein production costs are diminished significantly. To minimize clumping of the suspension cells, heparin was added to the cell culture medium, which also increases the solubility of Norrin. Suspension-adapted HEK293T cells were routinely grown in 75cm^2 T-flasks stand upright in 100 mL of serum-free DMEM supplemented with L-glutamine, 5000E Heparin and 50mM sodium chlorate. Stably Norrin expressing cells were grown to high densities by carefully monitoring cell viability using trypan blue staining. Suspension cells with viability higher than approximately 90% were used to inoculate the production medium. 3-5 x10^5 cells/mL were used for the inoculation of the production medium and recombinant protein was secreted for four days into the culture medium.

Protein purification

Purification of native Norrin was either performed using immobilized metal affinity chromatography (IMAC) or heparin chromatography (Porath et al. 1975, Hochuli et al. 1987, Farooqui 1980). For the IMAC approach a C-terminal polyhistidine (6x His) tag was used for protein capturing. For the heparin approach other protein characteristics, in particularly the high content of basic amino acids in Norrin, was taken in advantage. Also a combinatory approach was tried. During my master thesis I established stably Norrin expression cell lines and showed that recombinant human Norrin can be purified with IMAC in a batch setup. During my PhD thesis I established the purification on an ÄKTA purifier system using UNICRON™ 5.11 control software (both Amersham Biosciences/GE Healthcare Europe, Otelfingen, Switzerland). During my PhD thesis I further selected high expressing clones to get higher recombinant protein amounts. I also optimized growth conditions and purification strategy. Therefore I used different additives in the growth and production medium respectively and tried different purification strategies.

Recombinant human Norrin (rhNorrin) purification protocol (short)

- grow rhNorrin expressing HEK293T cells in production medium for 3-4 days to a density of 2 x10^6 cells/ml
- harvest, centrifuge, and filter medium – seed cells in fresh maintenance medium to recover
- load medium with peristaltic pump on equilibrated Heparin or IMAC column
- wash with 20 CV of wash buffer
- elute protein by increasing salt or imidazole concentration respectively
- detection of rhNorrin by western blot using anti-myc antibody
- desalting and concentrationof purified protein

Recombinant human Norrin (rhNorrin) purification protocol

Preparation of medium prior to purification is important to minimize backpressure on purification columns and maximize lifetime of the columns. To minimize backpressure on the purification columns the cell culture medium was centrifuged and filtered prior to column loading. Cell culture medium was harvested and centrifuged at 4000rpm for 10min, and filtrated with a bottle top filter Filtropur BT50 0.45µm (Sarstedt) to prevent column cogging by cell debris or other solid material. Columns were loaded using 4°C cold medium, which was cooled during centrifugation and while loading put on ice. Loading flow rate was according to manufacturers' instructions for each column. Columns were stored at 4°C in 20% EtOH.

IMAC purification

Before medium was loaded on HisTrap™ FF column (GE Healthcare) it was diluted 1:1 with 2x binding buffer to add 10-40mM imidazole that prevents unspecific binding of proteins to Ni^{2+} ions. Prior sample loading column was equilibrated using 5-10 column volumes (CV) of ddH_2O followed by 5-10 CV of 1x IMAC binding buffer. 1mL or 5mL HisTrap™ FF crude column was loaded with up to 100mL or 500mL cell culture medium/binding buffer using a peristaltic pump. The column was then connected to the ÄKTA purifier system and washed with wash buffer for approximately 20 CV or till A_{280} baseline was reached again, which indicates that no more protein impurities can be washed from the column. Different purification protocols were tested, including different imidazole and NaCl concentrations in the binding, wash and elution buffer. Further different wash and elution protocols were tested. The best results using IMAC columns were generated with the buffers in table 24.

2x IMAC binding buffer	
sodium phosphate buffer	20mM
NaCl	500mM
Imidazole	20mM

1x IMAC wash buffer	
sodium phosphate buffer	20mM
NaCl	500mM
Imidazole	20mM

1x IMAC elution buffer	
sodium phosphate buffer	20mM
NaCl	300mM
Imidazole	500mM

Table 24: IMAC binding (2x), wash (1x), and elution (1x) buffer recipes.

Since elution fractions contain high concentration of NaCl and imidazole, the recombinant protein containing fractions were desalted using two PD-10 (GE Healthcare) columns in series. Other desalting techniques were tried as well, including dialysis and ultracentrifugation. PD-10 group separation had the highest recovery rate and could be performed in less time then dialysis. To further concentrate purified recombinant Norrin Amicon® ultracentrifugation devices with a 3.5 molecular weight cut off (MWCO) were used. A diagram of the purification workflow can be seen in figure 11.

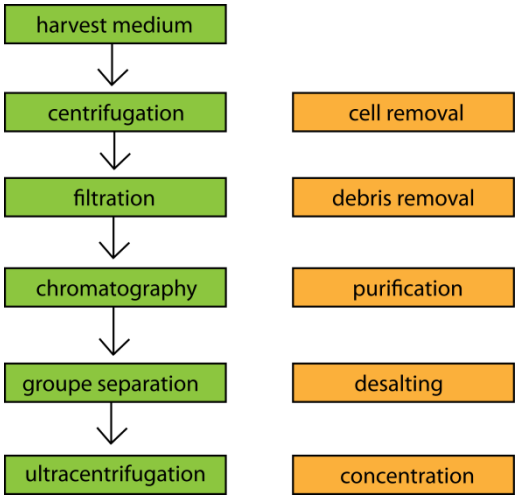

Figure 11: Illustration of purification workflow. Applied methods are indicated in green, while the effects of the applied methods are indicated in orange.

IMAC column stripping and regeneration

HisTrap™ FF crude columns are prepacked with Ni Sepharose™ 6 Fast Flow (GE Healthcare). Each column was stripped after four purification runs and recharged with fresh Nickel ions. Therefore column was stripped using 5-10 CV stripping buffer (Table 25). Then column was washed using 5-10 CV binding buffer and 5-10 CV ddH_2O. Column was recharged with 0.5mL of 0.1M $NiSO_4$ and washed again with 5 CV ddH_2O and 5 CV binding buffer. Regenerated column was stored in 20% EtOH at 4°C.

IMAC column stripping buffer	
sodium phosphate buffer	20mM
NaCl	500mM
EDTA	50mM
pH 7.4	

0.1M IMAC column recharge buffer		
$NiSO_4$ (Stock 650mM)	0.1M	77.375µl
ddH_2O		422.625µl

$NiSO_4$ (Stock 650mM)	
Ni(II) sulfate, anhydrous (154.8g/mol)	10g
ddH_2O	add 100ml

Table 25: IMAC stripping and recharge reagents.

Heparin purification

Another possibility to purify rhNorrin is using Heparin affinity chromatography (Farooqui 1980). We saw that Norrin is more soluble when heparin is present in the cell culture medium, thus we tried Heparin chromatography as an approach to purify rhNorrin. rhNorrin has a predicted pI of 9.5 and is positively charged when the pH of the medium is significantly lower then the pI of rhNorrin. Therefore, heparin can be used as a cation exchanger resin to purify Norrin in a certain pH range. HiTrap Heprain HP columns (GE Healthcare) were used, and 4°C cold medium with a pH of 7 was loaded directly on the equilibrated column after centrifugation and filtration. pH of the cell culture medium was adjusted using glacial acetic acid. Column was washed with Heparin wash buffer for 20 CV. By increasing the NaCl concentration the recombinant Norrin was eluted from the Heparin column. The concentration of the elution buffer was increased to 30% in a first step to further release unspecific proteins. In a second elution step recombinant Norrin was eluted from the Heparin column using 70% elution buffer.

Heparin wash buffer	
sodium phosphate pH 7.00	10mM

Heparin elution buffer	
sodium phosphate pH 7.00	10mM
NaCl	2M

Table 26: IEC wash (1x) and elution (1x) buffer recipes.

Tangential flow filtration – to concentrate conditional medium

Tangential flow filtration (TFF) was used to concentrate rhNorrin in the conditional medium. Medium was filtrated first with a bottle top filter and than filtered through a 500kDa membrane. Filtrate of this step was than concentrated on a 5kDa membrane. With this approach high volumes of cell culture supernatant have been concentrated prior to purification column loading.

BCA

Protein concentration was determined by bicinchoninic acid (BCA) assay (Sigma-Aldrich, Steinheim, Germany). The BCA assay is based on the generation of protein Cu^{2+}-Complex under alkaline conditions whereas Cu^{2+} gets reduced to Cu^{+}. The amount of reduced Cu^{+} is proportional to the amount of protein present in the sample. Bicinchoninic acid forms purple complexes with Cu^{+} and optical density was measured using light with a wavelength of 560nm. As an internal calibration curve BSA dilution series was used. Therefore a stock solution of 1mg/ml BSA was diluted with the accordant buffer into solutions with 1000, 800, 600, 400, 200 and 100µg/µl.

SDS-PAGE

Proteins were separated by size with SDS-PAGE. 20-200µg protein was mixed with appropriate amount of 6x SDS-loading buffer and heated for 5min at 95°C. For native SDS-PAGE, loading buffer without reducing agents (DTT; β-mercaptoethanol) was used. To break up disulfide bonds β-mercaptoethanol was used. Protein samples were centrifuged at 12'000rpm for 2min and protein samples were loaded on a SDS gel. Either precast gels (BioRad, Reinach, Switzerland) or home made polyacrylamid gels were used (Sambrook et al. 1989). Dependent on the size of the protein of interest, different acrylamid concentrations in the resolving gel were chosen. Proteins were separated by SDS-PAGE with 200V for app. 40 – 60min until loading dye reached the bottom of the gel. Since protein mass can only be determined relatively by this method, a molecular weight marker was loaded on each gel. For western blot either prestained PageRuler™ Protein Ladder #1811, #1841 or #0671 (Fermentas, St.Leon – Rot, Germany) was used. For silver stainings, preferably Silver Stain SDS-PAGE standard low range (BioRad, Reinach, Switzerland) was used.

5x SDS running buffer		
Tris/HCl, pH 8.3	125mM	15.1g
glycin	200mM	72g
SDS	0.05%	5g
ddH_2O		add 1000ml

5x SDS loading buffer	
Tris-HCl pH 6.8	250mM
SDS (electrophoresis grade)	10%
glycerol	50%
DDT	200mM
bromophenol blue	0.50%
ddH_2O	add 10ml
add DTT just before use from 1 M stock	

Table 27: SDS running and loading buffer recipes.

Western Blot

Proteins separated by SDS-PAGE were electrotransferred in a semi-dry system (BioRad, Reinach, Switzerland) onto a polyvinylidine difluoride (PVDF) membrane (Roche Diagnostics, Rotkreuz, Switzerland). The PVDF membrane was soaked shortly in methanol and washed for 5min in ddH_2O. The wet PVDF membrane and the SDS gel were incubated for 15min in blotting buffer (Table 28). Three chromatography filter papers (Whatman®, GE Healthcare, Otelfingen, Switzerland) were moistened with blotting buffer and stacked – avoiding air bubbles between – on the anode of the blotting system. The PVDF membrane was put on the top of the three filter papers and covered with the SDS gel. Three additional wet filter papers were stacked on top. The cathode was put on top and proteins were transferred for 21min at 15V. Used antibody dilutions can be seen in table 30.

1x Blot buffer	
5x blot buffer	20ml
methanol	20ml
ddH_2O	add 100ml

5x Blot buffer	
Tris	29.1g
glycin	14.65g
SDS	1.88g
ddH_2O	add 1000ml

Table 28: Blot-buffer recipes.

Immunoblotting

After blotting the proteins on the PVDF membrane, unspecific antibody binding was blocked with 5% milk powder in PBST for 2h at RT shaking on a laboratory rocker or o/n at 4°C on a rotator (Roto – Torque® Heavy Duty rotator, Cole-Parmer instruments, London, UK). PVDF

membrane was rinsed in PBST at RT and incubated with diluted primary antibody in 5% milk powder in PBST for 2h at RT or over night at 4°C. After washing four times for 10min with PBST at RT a horse radish peroxidase (HRP) secondary antibody was incubated for 30min – 1h at RT. The PVDF membrane was washed six times for 10 min with PBST. The membrane was placed between two plastic sheets and enhanced chemiluminescence (ECL) substrate (Western Lightning™ ECL plus system, NEL103; Perkin Elmer, Boston, MA, USA) was prepared according to the manufacturer's instructions and added on the membrane for 1min. The substrate was removed from the membrane, and the membrane was placed on a UV-transilluminated screen (ChemiDoc XRS+, BioRad, Reinach, Switzerland). Densitometric analysis of immunoblotted proteins was done using Image Lab software IL 4.0.1 (BioRad, Reinach, Switzerland).

WB blocking solution		
milk powder	5%	5g
PBST		100ml

Table 29: Western blot blocking solution.

Primary antibody	Host	Manufacturer	Dilution
anti-c-myc	mouse	Roche	1:500
anti-V5	rabbit	Sigma	1:500
anti-TBP	mouse	Abcam	1:1000
anti-tubulin	rabbit	Abcam	1:500
anti-MKL1	rabbit	Sigma	1:500
anti-GFP	rabbit	SantaCruz	1:500
anti-Histon H3	rabbit	Abcam	1:1000

Secondary antibody	Host	Manufacturer	Dilution
anti-mouse HRP	goat	Dianova	1:2000
anti-rabbit HRP	goat	GE Healthcare	1:2000

Table 30: Antibodies used for immunoblotting.

Western blot stripping and reprobing

To ensure, that equal protein amounts were loaded in the different lanes, a loading control antibody was used. Therefore PVDF membranes were stripped and reprobed using the following protocol. Stripping describes the removal of primary and secondary antibodies from a western blot membrane.

Preheat harsh stripping buffer to 60°C (Table 31). Incubate PVDF membrane for 1h at 60°C in harsh stripping buffer in a heated rotator (Mini Hybridisation Oven, Appligene Watford, UK). Rinse the membrane under running tab water for 15min, wash with PBST for 15min. Block PVDF membrane with 5% milk powder in PBST for 2h at RT. PVDF membrane is now ready to be reprobed.

WB stripping-buffer (harsh)	
10% SDS	20ml
1M Tris HCl pH 6.8	6.25ml
β-mercaptoethanol	0.8ml
ddH_2O	add 100ml

Table 31: Harsh stripping buffer recipe.

The stripping efficiency was checked by incubating the membrane with ECL detection reagent.

Silverstaing of SDS-PA gels

To visualize small amounts of protein (in low ng range) silver staining was used. It is a rapid, cheap and simple method, which is compatible with downstream processing like MS. Proteins were separated by SDS-PAGE as described before. All steps were performed at RT.

- fix the proteins on the SDS-PAGE by incubating the gel for 2-4h at RT with gentle shaking in at least 5 gel volumes of a solution of ethanol:glacial acetic acid: water (30:10:60) (Solution 1; Fixation)
- discard the fixing solution and ad at least 5 gel volumes of 30% ethanol; 30min; RT; gentle shaking (Solution 2; Incubation)
- repeat step 2
- discard the ethanol and add 10 gel volumes of deionized water; 10min; RT; gentle shaking
- repeat step 4
- discard the last of water washes, and wash with 0.01% NaS_2O_3 for 1min; RT (to reduce background) (Solution 3; sodium thiosulfate - background reduction)
- wash with deionized water 1min
- and ad 5 gel volumes of a fresh 0.1% solution of $AgNO_3$; 30min; RT; gentle shaking (Solution 4; Staining)
- wash with deionized water 30s
- ad 5 gel volumes of a freshly made 2.5% Na_2CO_3, 0.02% formaldehyde; RT; gentle shaking. Watch the gel carefully: Stained bands of protein should appear within a few minutes (Solution 5: Developer)
- quench the reaction by washing the gel in 1% acetic acid for a few minutes (Solution 6, Stop). Then wash the gel several times with deionized water (10min per wash)
- make a picture
- preserve the gel by drying

silver fixation (Solution 1)	
EtOH	300ml
Glacial acetic acid	100ml
ddH_2O	600ml

silver incubation (Solution 2)	
EtOH	300ml
ddH_2O	700ml

sodium thiosulfate - background reduction (Solution 3)	
$NaS_2O_3.5H_2O$	0.01g
ddH_2O	100ml

silver staining (Solution 4)	
$AgNO_3$	0.1g
ddH_2O	100ml

silver developer (Solution 5)	
Na_2CO_3	2.5g
formaldehyde	40µl
ddH_2O	100ml

silver stop (Solution 6)	
acetic acid	10ml
ddH_2O	990ml

Table 32: Sivler staining buffer recipes

Comassie staining of SDS-PA gels

To visualize whole protein fractions Imperial™ Protein Stain (Pierce Biotechnology Inc.) was used according to the manufacturer's instructions. SDS-PAG was washed three times for 5min with 100-200ml ddH_2O. Proteins were stained with 20ml Imperial™ Protein Stain solution for 1h with gently shaking on an orbital shaker. Gel was destained with ddH_2O for 1-2h. Frequent water changes decrease the time required to destain the gel.

Immunocytochemistry
Cells were transfected as described (Transient transfection of HEK293T section) and proceeded as following when transfection efficentcy was higher than 80%. All steps are performed at RT.

- wash cells with PBS
- fixation with 4% PFA (10 min)
- wash cells with PBS (3x 5min)
- permeabilize cells with 0.1% Trition X-100 in PBS (15min)
- wash cells with PBS (5min)
- block unspecific antigens with 1% BSA in PBS (30min)
- anti-V5 antibody 1:100 in 1% BSA in PBS (1h)
- wash cells with PBS (3x 5min)
- anti rabbit Alexa Fluor 488 1:200 in 1% BSA in PBS (40min) (or our secondary AB of choice)
- wash cells with PBS (3x 5min)
- mount cover slips on 10µl of Vectashield® mounting medium with DAPI (Reactolab S.A., Servion, CH)

Mass spectrometric analysis
To identify proteins, Mass spectrometric (MS) analysis was conducted. Protein bands of interest were cut out of silver stained SDS-PAGE and analyzed by Alphalyse (Odense, SØ, Denmark) or the Funcional Genomics Center Zürich (FGCZ, ETH and University of Zurich). Andres Frei did the MS analysis at the ETH campus for the receptor identification project.

Nuclear fractionation
10x 75cm^2 80%-100% confluent cell culture flasks were pooled per sample. For this purpose, the cell monolayer was rinsed first with 2ml of ice-cold PBS, and then 300µl (per flask) of ice-cold lysis buffer (NLB: 0.01M Tris-Cl pH 7.4, 0.01M NaCl, 0.003M $MgCl_2$, 0.5% triton X-100) was added. Flasks were scraped and cells were collected in a total volume of 5ml ice-cold NLB, and homogenized in a tissue glass Teflon dounce homogenizer, on ice. A "whole cell" aliquote was taken and the rest of the homogenate was centrifuged for 10min at 3'000rpm in a Sorvall HB4 rotor at 4°C. The supernatant (cytoplasmic fraction) was collected and the pellet was vortexed for 30s and then resuspended in 5ml of ice-cold NLB. The homogenate was layered over a 5ml cushion of 30% sucrose prepared in NLB and centrifuged for 10min at 3'000rpm in a Sorvall HB4 rotor at 4°C. The pellet (nuclear fraction) was resuspended in the appropriate volume (5ml or less) of NSB (40% glycerol, 0.05M Tris-Cl pH 7.4, 0.005M $MgCl_2$, 0.1mM EDTA) or a buffer of your choice for protein analysis (eg. RIPA).

NLB-buffer		
Tris-Cl pH 7.4	0.01M	1ml of 1M Tris
NaCl	0.01M	1ml of 1M NaCl
$MgCl_2$	0.003M	0.3ml of 1M $MgCl_2$
Triton X-100		500µl
ddH_2O		add 100ml

NSB-buffer		
Tris-Cl pH 7.4	0.05M	1ml of 1M Tris
glycerol 87%	40%	45.97ml glycerol
$MgCl_2$	0.005M	0.3ml of 1M $MgCl_2$
EDTA	0.1mM	0.1ml of 100mM EDTA
ddH_2O		add 100ml

Table 33: NLB and NSB buffer recipes.

Determination of protein palmitylation state

To predict a potential palmitoylation state, the CSS-Palm2.0 online prediction program was used (Jian et al. 2008). As an experimental approach, a Triton X-114 phase separation assay (Willert et al. 2003) was used. Norrin-conditioned medium was mixed 1:1 with ice cold 4.5% Triton X-114, 150mM NaCl, 10mM Tris-HCl, pH 7.5, incubated on ice for 5min, then at 31°C for 5min, and centrifuged at 2000g at 31°C for 5min. The top, aqueous phase was separated from the bottom Triton X-114 phase and equal volumes were immunoblotted with the anti-myc antibody.

2.2.4 Mammalian cell culture technology

Cultivation of all cell-lines was conducted under sterile conditions. All handling was done in a laminar flow hood (biosafety level II), material was either packed steril or cleaned with Barizidal or autoclaved before use. Cells were cultivated in an incubator with constant CO_2 level of 5% and 37°C.

Subcultivation of cells from a monolayer (splitting)

- aspirate spent medium
- wash cell monolayer with PBS, aspirate PBS
- add 1ml of 0,05 % Trypsin/EDTA and incubate at 37°C for 2-5min
- check detachment of cells with inverted microscope
- as soon as the cells get detached and get a round morphology, stop the trypsination reaction by adding cell culture medium containing FCS
- transfer the cellsuspension into a 15ml falcon
- seed appropriate amount of cells in a new cell culture flask
- incubate in a humidified 37°C, 5% CO_2 incubator
- if necessary, feed subconfluent cultures after 3 or 4 days by removing old medium and adding fresh medium

HEK 293T growth medium	
DMEM	500ml
FCS	50ml
L-glutamine	6ml

HUVEC growth medium
EBM-2,complete
10% FCS
10 ng/ml EGF
1 µg/ml Hydrocortisone

HMEC-1 growth medium
M199, complete
1ml L-glutamin
1ml Pen/Strep
1.5ml Hepes 1M
20ml FCS
75ml M199 (Sigma)

Table 34: Cell culture media recipes.

Cell freezing for long term storage

- aspirate old medium
- wash cells twice with PBS
- add 1ml of 0,05 % Trypsin/EDTA and incubate at 37°C for 2-5min
- check detachment of cells with microscope
- as soon as the cells get detached and get a round morphology, stop the trypsination reaction by adding cell culture medium containing FBS
- transfer the cell suspension into a 15ml falcon
- centrifuge cell to pellet at 2000rpm for 10min
- aspirate medium
- resuspend cell pellet with precold cell freezing medium (10% FCS, 10%DMSO in DMEM)
- aliquot cells in cryo tube and store cryo tubes for 48h at -80°C in Isopropanol
- transfer cryotubes into -196°C liquid nitrogen long for long term storage

Thawing and recovering cell from long term storage

- thaw cell at 37°C in a waterbath
- transfer cells into 15ml Falcon with 10ml fresh medium
- centrifuge cells cell to pellet at 2000rpm for 10min
- aspirate DMSO containg medium
- resuspend cells in standard growth medium and incubate in a humidified 37°C, 5% CO_2 incubator

Viable cell counts using trypan blue

The reactivity of trypan blue is based on the fact that the chromophore is negatively charged and does not interact with the cell unless the membrane is damaged. Therefore, all viable cells exclude the dye and non-viable cells are stained blue.

Dilute suspension cells in complete medium with an approximate concentration of 1x 10^5 to 2x 10^5 cells per ml were added on a coverslip. 0.4% trypan blue was mixed thoroughly with the cell suspension and incubated for 5min at RT. Staining was checked visually with an inverted microscope.

Transient transfection of HEK293T

75cm^2 were seeded with 6-7x 10^6 cells per flask in 10ml DMEM. 24h later, when the cells reached approximately 50% confluence, 30µg DNA was mixed with 525µl serum-free DMEM (w/o FCS) in a 15ml falcon. 37.5µl PEI (1mg/ml) and 487.5µl of serum-free DMEM (w/o FCS) was mixed in a microcentrifuge tube. PEI-Mix was added to DNA-Mix and incubated for 30min at RT. 3950µl of DMEM (w/FCS) was added to DNA-PEI-Mix. The old medium in cell culture flask was removed and replaced by 5ml of DMEM-DNA-PEI-Mix and incubated for 24h at 37°C and 5% CO_2. After 24h cell viability and transfection rate (cotransfected GFP) was checked visually with an inverted microscope. When cells reached app. 80% confluence and transfection efficiency was higher than 80% cells were used for further experiments. When convluence and transfection efficiency was not achieved, 10ml DMEM (w/FCS) was added to the cell culture flask and incubated for another 24h.

Poly-L- Lysin coating

Coverslips were washed with 100% EtOH for 5min and with sterile tissue culture grade water. Coverslip surface was coated with 1ml poly-L-Lysin per 25 cm^2 and rocked gently to ensure even coating of the surface. After 5min, the solution was removed by aspiration and the coverslips were thoroughly rinsed with sterile tissue culture grade water. Coverslips were allowed to dry at least 2h at 60°C before introducing cells and medium.

Coating of cell culture flask for endothelial cell cultivation

Cell culture fasks were either coated with 2% gelatin or bovine collagen.

Gelatin coating

- Gelatin was heated to 37°C to liquidate
- 1ml of 2% gelatine was added to cell culture flask and distributed evenly on the surface
- flask cap was left open and gelatine was dried in laminar flow hood for two hours

Collagen coating

- 8 parts of chilled PureCol collagen was mixed with 1 part of 10x PBS solution

- pH or the solution was adjusted to 7.4 ± 0.2 by the addition of 0.1M NaOH or 0.01N HCl. (pH was monitored by pH paper)
- adjust final volume to a total of 10 parts with sterile water
- temperature was maintained at 4-6°C to prevent gelation
- to gel, the PureCol solution was warmed to 37°C, gelation was allowed to occur for one hour
- 1ml of PureCol solution was added to cell culture flask and distributed evenly on the surface
- gel was dried for two hours under the laminar flow hood

2.2.5 *In vitro* assays

Different *in vitro* assays were established during this PhD thesis in order to have functional tests for wild type and mutant protein analyses. These assays include a viability or cell proliferation assay (WST-1, Roche). Further, three angiogenesis assays have been established: The scratch assay (a migration assay), a tube formation and the 3D sprouting assay.

Cell proliferation assay (WST-1)

WST-1 is a colorimetric assay for the nonradioactive quantification of cell proliferation, cell viability and cytotoxicity. The soluble and orange tetrazolium salts WST-1 (4-[3-(4-Iodophenyl)-2-(4-nitrophenyl)-2H-5-tetrazolio]-1,3-benzene disulfonate) are cleaved to red formazan by mitochondrial dehydrogenases. An augmentation in enzyme activity leads to an increase in the amount of formazan dye formed, which directly correlates to the number of metabolically active cells in the culture. Quantification of the formazan dye was done by a scanning multiwell spectrophotometer. The absorbance of the dye was measured at a wavelength of 450nm against 690nm reference wavelength. This assay was established for two different cell lines, HMEC-1 (human microvascular endothelial cells) and HUVEC (human umbilical vein endothelial cells).

- seed 1-2 x10^4 HMEC-1 or HUVEC per well (96-well), incubate over night
- aspirate medium
- add serum starve medium over night
- add medium with growth factor of interest, change medium every day, incubate for 72h
- add 10µl WST-1 reagent to 100µl medium, incubate 0.5-4 hours at 37°C
- shake thoroughly for 1min on a shaker
- measure the absorbance against background (without cells) using microplate reader at 420-480nm
- reference wavelength >600nm

Migration assay (Scratch assay or wound healing assay)

The *in vitro* scratch assay is a straightforward and cheap method to measure cell migration. In a monolayer of endothelial cells an artificial gap is induced by scratching a wound into the monolayer – therefore the assay is also called wound healing assay (Liang et al. 2007). The cells on the edge will start to migrate into the newly created gap to close it until new cell-cell contacts are established again. By capturing images at the beginning (time point 0) and at regular intervals during cell migration and comparison of the images allow determining the rate of the migration. One of the major disadvantages of this simple method is the fact that it is difficult to quantify. Different approaches were tested to quantify the migration rate of the endothelial cells: i) Counting the cells present in the scratched area, ii) distance measurement

between the two borders, iii) and overgrown area calculation by pixel measurement. In methods ii) and iii) the size of the scratch at time point 0 was set to 100%. For all three methods Photoshop software (Adobe, Version CS5) was used. To better distinguish between area overgrown by cells and uncovered area, the endothelial cells were stained with Calcein AM fluorescent dye.

- coate 6-well plate with collagen
- seed 5x 10^5 cell per well
- let cells grow to confluence
- scratch a scare with a sterile 200µl pipette tip, make a picture and mark location where the picture was taken
- add protein every day
- take picture every day at the same location

Tube formation assay

The tube formation assay allows assessing different aspects of angiogenesis at the same time *in vitro*. Endothelial cells are grown on a matrix so that cell attachment, migration, invasion and the modulation of these events by anti- or proangiogenic agents can be investigated. I established this assay using HMEC-1 cells.

- thaw the appropriate amount of Matrigel at 4°C o/n
- apply 50µl of Matrigel per well in a 96-well plate
- incubate at 37°C for 1h to allow the solution to solidify into a homogenous gel
- harvest endothelial cells (HMEC-1) and resuspend them in culture medium with or without proteins to be tested
- seed 100µl of endothelial cell suspension at 0.5 – 2x 10^5 cells/ml into each well
- culture the cells for the desired period of time (6-24h)
- take pictures with the inverted phase-contrast microscope

As positive control epidermal growth factor (EGF) and fibroblast growth factor (FGF) were used. To quantify the angiogenic effect of added substances, the tube length and branching points can be determined.

3D sprouting assay

The 3D sprouting assay is used to determine angiogenic properties in a three-dimensional assay, which better mimics the *in vivo* situation then the two-dimensional assays. Cytodex3 beads were washed with EBM-2 complete medium. 2500 beads were incubated with 1x 10^6 HMEC-1 cells in 1.5ml EBM-2 complete medium in a 15ml falcon at 37°C and 5% CO_2. Every 20min for 4h the falcon was shaked. Cell coating of beads was checked visually using the inverted phase-contrast microscope. When beads are coated with endothelial cells, transfer beads in round bottom 96-well and incubate o/n at 37°C and 5% CO_2. Coat 96-well plate with collagen I and add 20µl of covered beads per well. Add protein to test its effect on 3D cultured endothelial cells. After 48h cells were stained with Calcein AM according to manufacturer's instruction and pictures were taken to assess the length and number of sprouts. This assay was established using VEGF as positive control but no recombinant Norrin has been tested with this assay so far.

3. Results

3.1 Candidate gene screening

3.1.1 New sequence variations in candidate genes

Ten candidate genes were sequenced in 208 subjects with severe retinal developmental disorders. All exonic and 50-100bp flanking intronic regions of the candidate genes were bi-directionally Sanger-sequenced. All together, 79 new sequence variations, including 23 missense mutations and two in-frame deletions, were identified. The missense mutations and in-frame deletions might directly affect protein function. The remaining sequence variants are either intronic, and might affect splicing, or they are located in the 3'UTR or 5'UTR and potentially affect either splicing, transcript stability, or might have an effect on promoter activity. An overview of all sequence variations is listed in table 35. A complete list of all new sequence variants in the ten candidate genes can be found in table 36. Most of theses sequence alterations were not annotated in both the 1000 Genome project database and the Human Gene Mutation Database (HGMD® Professional) with two exceptions: p.Arg65Gly in *ATOH7* and p.Ala569Thr in *MKL1*. These are two known sequence variations but were included in the list of interesting sequence variations in this work, due to some reasons, which I would like to discuss later. Some of these sequence variations have been described in the master thesis of Lea Sollfrank, who was involved in several projects under my supervision, regarding candidate gene screening and functional characterization. *NINJ1* was her main project, but she also helped in sequencing and analyzing the *ZNF408* and *PARVA* data, and analyzing sequence data from *TSPAN12*, *ILK*, *ITGB3* and *SRF* genes. In this thesis, a complete overview of all sequence variations (including intronic and synonymous substitutions), which were found in the ten candidate genes for retinal dysplasias, are listed and described in detail (Tabel 36). The electropherograms of each new sequence variation can be found in the Appendix B, of this thesis.

	Exon	Intron	5'UTR	3'UTR
ATOH7	2	0	0	1
NEUROD1	1	0	0	0
NINJ1	1	0	2	0
ZNF408	6	0	0	2
ILK	5	4	0	0
ITGB3	3	6	0	0
PARVA	4	3	0	2
SRF	4	0	0	0
MKL1	10	5	4	1
MKL2	6	6	1	0
Total	42	24	7	6

Table 35: Summary of candidate gene sequence variations. Numbers of detected sequence variations in exons & introns of 10 candidate genes.

ATOH7								
Patient	**DNA variant**	**Protein variant**	**Location**	**PolyPhen**	**SIFT**	**A-GVGD**	**Effect**	**Zygosity**
70186	c.121_144del	p.Arg42_Arg48del	Exon 1	-	-	-	Deletion (in-frame)	homozygous
70187	c.121_144del	p.Arg42_Arg48del	Exon 1	-	-	-	Deletion (in-frame)	heterozygous
70100	c.193A>G	p.Arg65Gly	Exon 1	possibly damaging (0.897)	not tolerated	Class C45	Missense mutation	heterozygous
70102	c.193A>G	p.Arg65Gly	Exon 1	possibly damaging (0.897)	not tolerated	Class C45	Missense mutation	heterozygous
70217	c.193A>G	p.Arg65Gly	Exon 1	possibly damaging (0.897)	not tolerated	Class C45	Missense mutation	heterozygous
70163	c.*35C>T	p.?	3'UTR	-	-	-	Splicing, transcript stability	heterozygous

NEUROD1								
Patient	**DNA variant**	**Protein variant**	**Location**	**PolyPhen**	**SIFT**	**A-GVGD**	**Effect**	**Zygosity**
70086	c.463_465del	p.Glu155del	Exon 2	-	-	-	Deletion (in-frame)	heterozygous

NINJ1								
Patient	**DNA variant**	**Protein variant**	**Location**	**PolyPhen**	**SIFT**	**A-GVGD**	**Effect**	**Zygosity**
70221	c.-71-27G>A	p.?	5'UTR	-	-	-	Promotor region affected	heterozygous
70221	c.-71-14G>A	p.?	5'UTR	-	-	-	Promotor region affected	heterozygous
70135	c.124G>A	p.Ala42Thr	Exon 2	probably damaging (1.000)	not tolerated	Class C55	Missense mutation	heterozygous

ZNF408								
Patient	**DNA variant**	**Protein variant**	**Location**	**PolyPhen**	**SIFT**	**A-GVGD**	**Effect**	**Zygosity**
70182	c.35A>G	p.Lys12Arg	Exon 1	benign (0.002)	tolerated	Class C0	Missense mutation	heterozygous
70205	c.1574G>A	p.Arg525His	Exon 5	benign (0.081)	tolerated	Class C0	Missense mutation	heterozygous
70110	c.240C>T	p.=	Exon 2	-	-	-	Synonymous mutation	heterozygous
70128	c.1497G>A	p.=	Exon 5	-	-	-	Synonymous mutation	heterozygous
70116	c.1755C>T	p.=	Exon 5	-	-	-	Synonymous mutation	heterozygous
70139	c.1755C>T	p.=	Exon 5	-	-	-	Synonymous mutation	heterozygous
70215	c.*48+95G>C	p.?	3'UTR	-	-	-	Splicing, transcript stability	heterozygous
70216	c.*48+95G>C	p.?	3'UTR	-	-	-	Splicing, transcript stability	heterozygous

ILK								
Patient	**DNA variant**	**Protein variant**	**Location**	**PolyPhen**	**SIFT**	**A-GVGD**	**Effect**	**Zygosity**
25649	c.157T>A	p.Leu53Met	Exon 3	probably damaging (1.000)	not tolerated	Class C0	Missense mutation	heterozygous
70160	c.279C>A	p.=	Exon 4	-	-	-	Synonymous mutation	heterozygous
70159	c.631C>T	p.Arg211Cys	Exon 8	possibly damaging (0.856)	not tolerated	Class C25	Missense mutation	heterozygous
70231	c.631C>T	p.Arg211Cys	Exon 8	possibly damaging (0.856)	not tolerated	Class C25	Missense mutation	heterozygous
70147	c.950G>A	p.Arg317Gln	Exon 10	possibly damaging (0.615)	tolerated	Class C0	Missense mutation	heterozygous
70217	c.979-37A>C	p.?	Intron 10	-	-	-	Splicing	heterozygous
70151	c.1079-18C>T	p.?	Intron 11	-	-	-	Splicing	heterozygous
70231	c.1079-18C>T	p.?	Intron 11	-	-	-	Splicing	heterozygous
70246	c.1209+52A>C	p.?	Intron 12	-	-	-	Splicing	heterozygous

ITGB3								
Patient	**DNA variant**	**Protein variant**	**Location**	**PolyPhen**	**SIFT**	**A-GVGD**	**Effect**	**Zygosity**
70223	c.72C>T	p.=	Exon 1	-	-	-	Synonymous mutation	heterozygous
70211	c.79+15G>A	p.?	Intron 1	-	-	-	Splicing	heterozygous
70099	c.165+28C>G	p.?	Intron 2	-	-	-	Splicing	heterozygous
70113	c.847G>A	p.Ala283Thr	Exon 6	probably damaging (1.000)	not tolerated	Class C55	Missense mutation	heterozygous
70128	c.1035+25G>A	p.?	Intron 7	-	-	-	Splicing	heterozygous
70182	c.1125+31G>A	p.?	Intron 8	-	-	-	Extra branchpoint	heterozygous
70217	c.1125+31G>A	p.?	Intron 8	-	-	-	Extra branchpoint	heterozygous
70224	c.1530C>T	p.=	Exon 10	-	-	-	Synonymous mutation	heterozygous
70159	c.1913+25C>T	p.?	Intron 11	-	-	-	Splicing	heterozygous

PARVA								
Patient	**DNA variant**	**Protein variant**	**Location**	**PolyPhen**	**SIFT**	**A-GVGD**	**Effect**	**Zygosity**
70110	c.137-154C>T	p.?	Intron 1	-	-	-	new splice donor site	heterozygous
70198	c.657+18A>G	p.?	Intron 6	-	-	-	Splicing	heterozygous
27095	c.762C>T	p.=	Exon 9	-	-	-	Synonymous mutation	heterozygous
70151	c.798+15C>T	p.?	Intron 9	-	-	-	Splicing	heterozygous
70160	c.828G>A	p.=	Exon 10	-	-	-	Synonymous mutation	heterozygous
70228	c.891G>A	p.=	Exon 11	-	-	-	Synonymous mutation	heterozygous
70240	c.951G>A	p.=	Exon 11	-	-	-	New splice acceptor site	homozygous
27118	c.*4G>A	p.?	3'UTR	-	-	-	Transcript stability	heterozygous
70108	c.*4G>A	p.?	3'UTR	-	-	-	Transcript stability	heterozygous

SRF								
Patient	**DNA variant**	**Protein variant**	**Location**	**PolyPhen**	**SIFT**	**A-GVGD**	**Effect**	**Zygosity**
29833	c.147G>T	p.=	Exon 1	-	-	-	Synonymous mutation	homozygous
70098	c.534G>A	p.=	Exon 2	-	-	-	Synonymous mutation	heterozygous
70234	c.715A>T	p.Thr239Ser	Exon 2	possibly damaging (0.853)	tolerated	Class C0	Missense mutation	heterozygous
70226	c.1236G>T	p.=	Exon 5	-	-	-	Synonymous mutation	heterozygous

MKL1								
Patient	**DNA variant**	**Protein variant**	**Location**	**PolyPhen**	**SIFT**	**A-GVGD**	**Effect**	**Zygosity**
70223	c.-496C>T	p.?	5'UTR, Exon 1	-	-	-	Translation regulation	heterozygous
70092	c.-333A>G	p.?	5'UTR, Exon 2	-	-	-	Translation regulation	heterozygous
70245	c.-260T>C	p.?	5'UTR, Exon 3	-	-	-	Translation regulation	heterozygous
70176	c.-260T>C	p.?	5'UTR, Exon 3	-	-	-	Translation regulation	heterozygous
70213	c.301+12C>G	p.?	Intron 7	-	-	-	Splicing	heterozygous
70229	c.478-125C>T	p.?	Intron 8	-	-	-	Splicing	heterozygous
70196	c.627+79G>C	p.?	Intron 9	-	-	-	Splicing	heterozygous
70213	c.627+113C>T	p.?	Intron 9	-	-	-	Splicing	heterozygous
70136	c.726C>T	p.=	Exon 10	-	-	-	Synonymous mutation	heterozygous
70239	c.753G>C	p.=	Exon 10	-	-	-	Synonymous mutation	heterozygous
70246	c.1408T>C	p.Ser470Pro	Exon 12	probably damaging (0.998)	not tolerated	Class C0	Missense mutation	heterozygous
70214	c.1695C>A	p.=	Exon 12	-	-	-	Synonymous mutation	heterozygous
70116	c.1699G>A	p.Ala567Thr	Exon 12	benign (0.016)	tolerated	Class C0	Missense mutation	heterozygous
70148	c.1699G>A	p.Ala567Thr	Exon 12	benign (0.016)	tolerated	Class C0	Missense mutation	homozygous
70135	c.1705G>A	p.Ala569Thr	Exon 12	benign (0.001)	tolerated	Class C0	Missense mutation (rs144888766)	heterozygous
70147	c.1720C>T	p.Pro574Ser	Exon 12	benign (0.000)	tolerated	Class C0	Missense mutation	heterozygous
70111	c.1723G>A	p.Val575Met	Exon 12	probably damaging (0.996)	tolerated	Class C0	Missense mutation	heterozygous
70190	c.1909G>A	p.Ala637Thr	Exon 12	benign (0.002)	not tolerated	Class C55	Missense mutation	heterozygous
70226	c.1909G>A	p.Ala637Thr	Exon 12	benign (0.002)	not tolerated	Class C55	Missense mutation	heterozygous
70243	c.2003T>C	p.Val668Ala	Exon 12	possibly damaging (0.712)	not tolerated	Class C0	Missense mutation	heterozygous
70236	c.*55C>T	p.?	3'UTR	-	-	-	Splicing, transcript stability	heterozygous

MKL2								
Patient	**DNA variant**	**Protein variant**	**Location**	**PolyPhen**	**SIFT**	**A-GVGD**	**Effect**	**Zygosity**
70225	c.-63-1G>C	p.?	Intron 2	-	-	-	Splicing	heterozygous
70221	c.221-34A>G	p.?	Intron 4	-	-	-	Splicing	heterozygous
70206	c.300G>A	p.=	Exon 6	-	-	-	Synonymous mutation	heterozygous
70243	c.761C>G	p.Pro254Arg	Exon 9	Benign (0.002)	tolerated	Class C0	Missense mutation	heterozygous
70227	c.983G>A	p.Arg328His	Exon 10	probably damaging (1.000)	not tolerated	Class C25	Missense mutation	heterozygous
70244	c.1317C>T	p.=	Exon 12	-	-	-	Synonymous mutation	heterozygous
70189	c.2097+94A>G	p.?	Intron 12	-	-	-	Splicing	heterozygous
70189	c.2098-30A>C	p.?	Intron 12	-	-	-	Splicing	heterozygous
70189	c.2253+25G>A	p.?	Intron 13	-	-	-	Splicing	heterozygous
70189	c.2253+51C>T	p.?	Intron 13	-	-	-	Splicing	heterozygous
70189	c.2449G>A	p.Val817Ile	Exon 15	Benign (0.048)	tolerated	Class C0	Missense mutation	heterozygous
27116	c.2548C>A	p.Pro850Thr	Exon 15	Benign (0.084)	tolerated	Class C0	Missense mutation	heterozygous
27117	c.2548C>A	p.Pro850Thr	Exon 15	Benign (0.084)	tolerated	Class C0	Missense mutation	heterozygous

Table 36: Complete list of new sequence variations found in candidate genes.

***ATOH7* - Sequence variants and their predicted effect on the function**

In *ATOH7*, one in-frame deletion (c.121_144del, p.Arg42_Arg48del), one previously reported amino acid substitution (c.193A>G, p.Arg65Gly, rs111699024), and one variation in the 3'UTR (c.*35C>T, p.?) were found. For the in-frame deletion I refer to the manuscript enclosed here after. The known SNP was found three times, always heterozygous. The variation in the 3'UTR was found only once and might influence transcript stability.
Beside the experiments described in the manuscript additional experiments were performed, which are described in the following section.

ATOH7 is a transcription factor, which specifically binds to specific E-box motifs to regulate the expression of downstream target genes (Del Bene et al. 2007, Massari and Murre 2000). In an *in silico* analysis approach such E-boxes were searched upstream of the *NDP* gene and several of these were found and seemed to be evolutionary conserved (Figure 12).

The E-boxes between the mouse and human gene are conserved. To investigate whether the human ATOH7 is capable to regulate *Ndp* transcription, TaqMan analysis was used. Relative transcript levels of *Ndp* in mouse retinas were quantified after electroporation of the human wild type ATOH7 construct and compared to mouse retinas which were not electroporated. Jean-Marc Matter and Tania Rodriguez (University of Geneva, Switzerland) conducted the electroporation. After RNA isolation transcript levels of *Ndp* and *Gapdh* were analysed in these samples. As a positive control, *Stathmin1* (NM_019641) was used. *Stathmin1* was shown to be target of ATOH7, in particular it was 20 times higher expressed in wild type mice compared to ATOH7 KO mice (Mu et al. 2005). No difference of *Ndp* and *Stathmin1* transcript levels between wild type ATOH7 electroporated and unelectroporated mouse retinae were observed in our experiment (data not shown).

In addition to the *ex vivo* mouse experiment, RT-PCR on HEK293T cells transfected with wild type and mutant ATOH7 was performed. In this *in vitro* experiment transcript levels of *NDP*, *ATOH7*, and *18S* as an internal control were analyzed. No differences in transcript levels of *NDP* and *ATOH7* between samples transfected with either wild type or mutant ATOH7 were observed.

The deletion in the basic DNA binding domain of ATOH7 very likely affects the binding of the mutant protein to DNA. To investigate the interaction of ATOH7 and DNA, a fluorescence-based electromobility shift assay (EMSA) was performed. The ATOH7 wt construct was not able to induce a band shift in this assay. This might be due to the fact that ATOH7 needs its binding partner E47 to do so. Parsov et al. conducted the same experiment where ATOH7 wt only cotransfected with E47 induced a band shift (Parsov et al. 2012).

To investigate the transcriptional activity of ATOH7, a luciferase reporter assay was performed using a construct with seven E-box binding sites and a beta-actin minimal promoter in front of the luciferase gene (pE7-BA-PGV). As a negative control, the same vector without the E-boxes (pBA-PGV) was used. Prof. Ryoichiro Kageyama provided these constructs (Institute for Virus Research, Kyoto University). ATOH7 wt did not induce luciferase reporter. This might be due to the fact that the E-boxes in pE7-BA-PGV are CANNAG and not CANNTG.

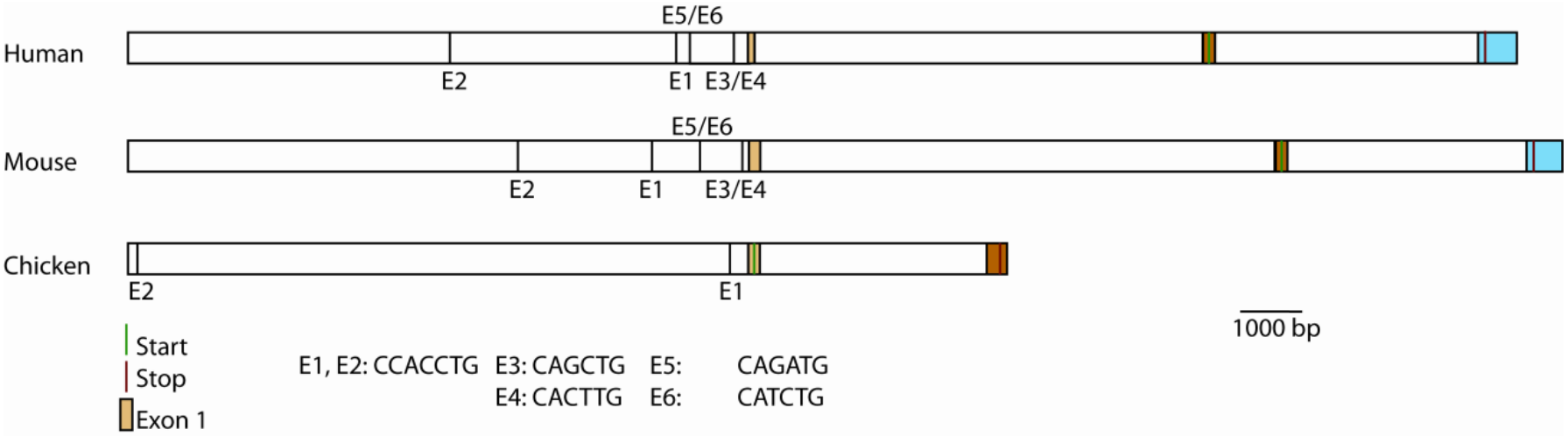

Figure 12: Illustration of the *NDP* genomic region from orthologous genes from human (*Homo sapiens*), mouse (*Mus musculus*), and chicken (*Gallus gallus*). *In silico* analysis of *NDP* upstream genomic regions from the three species revealed several conserved E-box motifs.

Pathogenic Mechanism of a Deletion in the Basic Domain of ATOH7 Responsible for Retinal Dysplasia.

Lucas Mohn[1, 2], Britta Seebauer[1, 2], Silke Feil[1], Katherine B. Sims[3], Wolfgang Berger[1, 2, 4]

[1]Institute of Medical Molecular Genetics, University of Zurich, Schwerzenbach, Switzerland
[2]Neuroscience Center Zurich (ZNZ), University of Zurich/ETH Zurich, Zurich, Switzerland
[3]Center for Human Genetic Research and Department of Neurology, Massachusetts General Hospital, Harvard Medical School, Boston, MA, USA
[4]Zurich Center for Integrative Human Physiology (ZIHP), University of Zurich, Zurich, Switzerland

* Author for correspondence: Wolfgang Berger, Institute of Medical Molecular Genetics, University of Zurich, Schorenstrasse 16, CH-8603 Schwerzenbach. Tel: +41 446557031; Fax: +41 446557213;
Email: berger@medmolgen.uzh.ch

Abstract

The gene *atonal homolog 7* (*ATOH7*) encodes a basic helix-loop-helix (bHLH) transcription factor, which is involved in neuronal cell fate determination and retinal development. ATOH7 is one of the earliest expressed transcriptional activators of neurogenesis in eye development and initiates retinal ganglion cell (RGC) fate determination in vertebrates. Depletion of *Atoh7* in mice results in the loss of RGCs, abnormal retinal vascular development and persistence of the hyaloid vasculature. A similar phenotype, with respect to abnormal vascular development in the eye, can be observed in Norrin knockout ($Ndp^{y/-}$) mice, a model for Norrie disease. In humans, loss of RGCs often leads to retinal detachment and blindness. Retinal vascular defects and persistence of hyaloid vessels occur in several human congenital eye diseases including exudative vitreoretinopathy (EVR), Norrie disease (ND), retinopathy of prematurity (ROP), Coat's disease and persistent hyperplastic primary vitreous (PHPV).

By direct sequencing of *ATOH7* we found a homozygous deletion of eight amino acids in the basic domain of ATOH7 in a patient with severe bilateral retinal dysplasia similar to ND. Functional analysis of the mutant ATOH7 revealed that the protein is mislocalized and rapidly degraded in the presence of cycloheximide. Further, we show that ATOH7 is a target of proteasomal degradation in the cytoplasm and that the presence of a SV-40 nuclear localization signal (NLS) in ATOH7 decreases its proteasomal accessibility. Thus, our data provide functional evidence that mutations in *ATOH7* are implicated in severe congenital human eye diseases and add novel information about the molecular mechanisms of ATOH7 regulation.

Introduction

The vertebrate retina develops in a highly conserved manner, from the uniform neuroepithelium towards a complex laminar structure with seven major cell types, six neuronal and one glial [1]– [3]. The first born neurons in the retina are the ganglion cells. Then, amacrine, horizontal, and cone photorezeptor cells develop in an overlapping phase, followed by rod photoreceptors, bipolar and müller glial cells, which are established last [4]– [6]. To form the highly organized laminar structure of these different cell types, retinal progenitor cells have to differentiate and migrate in a distinct manner which is guided by both intrinsic and extrinsic factors [7]. During retinogenesis, bHLH transcription factors like ATOH7 (also known as MATH5 or ATH5), MASH1, MATH3, NGN2, and NEUROD1 are activated in a subpopulation of progenitor cells and determine cell fate decisions of retinal progenitor cells [8]– [13]. *Atoh7* is one of the best characterized bHLH transcription factor genes involved in retinal development in different species and is thought to initiate neurogenesis in vertebrate and invertebrate eyes [9], [14]– [19]. The human ATOH7 is encoded by a single exon and consists of 152 amino acids [20]. Amino acid residues 41 – 52 form the basic domain, which is important for DNA-binding. Residues 53 – 93 form the helix-loop-helix motif which is important for hetero- or homo-dimerization [21], [22].

The expression pattern of *Atoh7* in retinal progenitor cells of *Mus musculus* (Mouse atonal homolog 7, *Atoh7* also known as *Math5*), *Xenopus laevis* (Xenopus laevis atonal homolog 7, *atoh7* also known as *Xath5*), *Danio rerio* (zebrafish atonal homolog 7, *atoh7* also known as *Zath5*), and Gallus gallus (Chicken atonal homolog 7, *Atoh7* also known as *Cath5*) coincides with the differentiation of RGCs [9], [16], [17], [19], [23]. Notably, *Atoh7* is not expressed exclusively in RGC lineages and hence might be involved in cell fate determination of other retinal cells [24], [25]. Depletion of *atonal* in *Drosophila melanogaster*, in zebrafish, and in mouse results in loss of initial neurons in the eyes of these organisms [14], [15], [17], [18], [26], [27]. *Atonal* mutant flies are almost eyeless, whereas zebrafish and mouse mutants have eyes but lack RGCs and the optic nerve. Axons of RGCs assemble the optic nerve and dispatch signals from the retina to the lateral geniculate nucleus from where information is processed to the visual cortex. In addition, a subset of RGC axons projects directly to the suprachiasmatic nucleus, which controls circadian rhythm. Since these neurons are also lacking in $Atoh7^{-/-}$ mice, they have abnormalities in circadian photoentrainment [28]. Proper RGC development is also crucial for the establishment of the retinal vasculature. $Atoh7^{-/-}$ mice show abnormal retinal vascularization and persistence of the hyaloid vessels, similar to Norrin knockout ($Ndp^{y/-}$) mice, a model for Norrie disease [29]– [31]. *Atoh7* overexpression experiments in chicken and frog eyes lead to a promoted RGC neurogenesis and photoreceptor abundance [16], [19], [32], [33], and ectopic expression of *atonal* during *Drosophila* eye development induces extra R8 cells [34], [35]. Thus, several lines of evidence, including expression, depletion, and overexpression of *Atoh7* in different species, suggest a role of this transcription factor during retinal development in vertebrates as well as invertebrates. Recently, a deletion of a remote enhancer in a large consanguineous family with nonsyndromic congenital retinal nonattachment (NCRNA, MIM # 221900) has been described and the authors suggested for the first time that *ATOH7* is implicated in severe human eye diseases [36]. The ocular symptoms of the patients are reminiscent of the ocular phenotype seen in some Norrie disease patients. Norrie disease is a severe X-linked recessive disorder with

retinal dysplasia and shows highly variable syndromic symptoms including progressive sensorineural hearing loss and cognitive impairment [37]– [42]. Therefore we screened for mutations in *ATOH7* in more than 200 human patients with the clinical diagnoses EVR, PHPV, or ND which were negative for disease-causing sequence alterations in one of the known genes.
Here we report a novel mutation in *ATOH7* and describe functional consequences of this mutation. Our findings strongly indicate that ATOH7 is a target of proteasomal degradation. Further we found that the proteasomal-dependent turnover of ATOH7 occurs in the cytoplasm and provide evidence that the mutation leads to reduced amounts of protein in the nucleus and causes severe human retinal dysplasia.

Results

In frame deletion in the basic domain of ATOH7 in a patient with severe retinal dysplasia

We screened genomic DNA of 208 unrelated patients with severe retinal diseases, and identified a deletion in the bHLH transcription factor gene *ATOH7* in a Korean patient. The proband is a 7 year-old boy who was examined at the age of 9 months with bilateral retinal detachment and no evidence for retained vision. The proband was considered as a typical Norrie disease patient, but no mutation was detected in the coding region of the *NDP* gene and no extra ocular symptoms were evident at that time. However, syndromic symptoms in Norrie disease can develop during childhood, adolescence or later in life. Six years after the initial clinical examination it was not possible to perform additional clinical examinations.
The patient is homozygous for an in frame deletion in the basic domain of *ATOH7* (c.121_144del, p.Arg41_Arg48del). His unaffected mother is heterozygous for the same deletion and we assume that the father, who was not available for genetic testing, is also a carrier of this or a larger deletion in *ATOH7* (Figure I). This sequence alteration was not annotated in both the 1000 Genome project database and the Human Gene Mutation Database (HGMD® Professional) [43].

Deletion of eight highly conserved amino acids in the basic DNA-binding domain of ATOH7

We first evaluated the evolutionary conservation of ATOH7 by aligning the bHLH domains of five different ATOH7 orthologous genes with a multiple sequence alignment (MSA) by using ClustalW2 (Figure II, A). The deletion described herein encompasses eight highly conserved amino acids of the basic, DNA-binding domain of ATOH7. To illustrate the binding of ATOH7 to DNA, we modeled the wild type protein structure based on experimentally determined structures of an E47/NeuroD1 heterodimer from mouse, bound to DNA (PDB code 2ql2) (Figure II, B) [44]. The deleted amino acids (blue) are in close contact to the major groove of the DNA.

Mutant ATOH7 predominantly localizes in the cytoplasm

For functional analyses we transfected COS-7 (African green monkey kidney fibroblast-like) cells with V5-tagged wild type (ATOH7 wt) or mutant (ATOH7 del) *ATOH7* expression constructs and visualized the protein localization by immunofluorescence microscopy (Figure III, A). The wild type protein was found predominately in the nucleus, while the mutant ATOH7 was observed significantly less frequent in nuclei (Figure III, B). We repeated this experiment in HEK293T (Human embryonic kidney) cells and obtained the same result (data not shown). In addition to immunofluorescence stainings, we performed a fractionation of cytoplasmic and nuclear

proteins of transfected HEK293T cells. Western blot analysis of whole cell, nuclear and cytoplasmic fractions confirmed the immunocytochemical data (Figure IV). In particular, Western blot analysis revealed that mutant ATOH7 in general is less abundant compared to the wild type construct. Only very little amounts of mutant ATOH7 protein were detected in nuclear fractions. But also in whole cell and cytoplasmic fractions less mutant ATOH7 was present compared to wild type ATOH7. The relative nuclear abundance of mutant ATOH7 was significantly lower compared to wild type ATOH7 (Figure IV, B). In contrast, the wild type ATOH7 was more abundant in the nucleus compared to the cytoplasm. Since the wild type ATOH7 was more abundant in the whole cell lysate than the mutant protein, we examined transfection efficiencies between the constructs. We repeated the transfection of wild type and mutant *ATOH7* plasmid DNAs and also cotransfected GFP. Cotransfected and fractionated cell lysates were subjected to immunoblotting using anti-V5-tag and anti-GFP antibodies. Western blot analysis of V5-tagged ATOH7 always revealed the same pattern (Figure IV, A). GFP expression levels were comparable when cotransfected together with different *ATOH7* expression constructs, suggesting equal transfection efficencies. As a loading control for whole cell and cytoplasmic fractions β-tubulin was used, for nuclear fractions Histone H3. Taken together, less mutant ATOH7 protein was found in whole cell lysate and its relative nuclear abundance was significantly lower compared to wilde type ATOH7 protein. These results suggest that the mutant ATOH7 protein is either less stable or less efficiently transcribed and/or translated compared to the wild type mRNA or ATOH7 protein. Further it indicates that the deleted amino acids in the mutant ATOH7 have an effect on the sub-cellular localization of the protein.

Sub-cellular localization of ATOH7 has an effect on protein stability

To test whether the sub-cellular localization of ATOH7 has an effect on its stability we cloned an artificial nuclear localization signal (NLS) from the SV-40 large T-antigen (PKKKRKV) downstream of the start codon of the wild type (NLS_wt) and mutant (NLS_del) *ATOH7* expression constructs. Immunofluorescence stainings and Western blot analyses showed that the artificial NLS is capable of forcing the protein into the nucleus, even when the deletion is present (Figure III and IV). Further Western blot analyses revealed higher levels of NLS_wt ATOH7 and NLS_del ATOH7 in the whole cell fraction compared to constructs lacking the artifical NLS (Figure IV). In addition to the total amount of ATOH7, the relative nuclear abundance of the NLS_del ATOH7 protein could be increased to a similar level as it has been observed with the wild type ATOH7 (Figure IV, B). This experiment suggests that the nuclear localization of ATOH7 has a protective effect against protein degradation or that the expression constructs with the artificial NLS are more efficiently transcribed or translated.

ATOH7 is a target of proteasomal degradation in the cytoplasm

Proteasomal degradation affects a wide range of proteins and regulates protein levels of many transcription factors [45]. To investigate whether ATOH7 is a target of proteasomal degradation, we treated HEK293T cells 24 hours after transfection with the different ATOH7 expression constructs by using the proteasome inhibitor MG-132 for 0, 1, 2, 4, and 8 hours, or DMSO as a vehicle control. Subsequently, cell lysates were harvested and subjected to immunoblotting (Figure V, A). Western blot analyses revealed an increase of protein levels upon proteasome

inhibition over time for wt, del, and NLS_del constructs. The protein level of NLS_wt ATOH7 was not affcted by proteasomal inhibition, which further supports the assumption that the nuclear localization of ATOH7 prevents proteasomal degradation. In addition, we used a second proteasome inhibitor (epoxomicin) with the same results (Figure V, B). However, ATOH7 protein accumulation could not be achieved with an inhibitor of lysosomal protein degradation (NH_4Cl, ammonium chloride) (Figure V, B). These results strongly indicate that ATOH7 is a target of proteasomal degradation and that this degradation of ATOH7 occurs in the cytoplasm.

The mutant ATOH7 protein has an increased turnover rate

To further investigate the mechanism of ATOH7 degradation, we examined the stability of ATOH7 in HEK293T cells. We incubated transfected HEK293T cells for 4 hours with MG-132 to stabilize ATOH7 and then added the protein synthesis inhibitor cycloheximide (CHX). Cells were lysed 0, 1, 2, 4, and 8 hours after incubation with CHX. The decay of ATOH7 over time was assessed by Western blot analyses (Figure VI). This experiment revealed that the half-life ($t_{½}$) of wild type ATOH7 is ~ 4 hours, wherease the mutant ATOH7 had a reduced half-life ($t_{½}$) of ~ 2 hours. Therefore we show an increased turnover rate of the mutant ATOH7 compared to the wild type protein. Further, the NLS_wt ATOH7 variant showed significant increased stability compared to the wild type ATOH7 without artifical NLS, suggesting a stabilizing effect due to its predominant nuclear localization. The NLS_del ATOH7 showed a similar decay as the del ATOH7 after the protein levels have been stabilized with MG-132.

Stabilization of the mutant ATOH7 does not compensate its nuclear mislocalization

To see whether mutant ATOH7 is present in higher amounts in the nucleus after stabilization with the proteasome inhibitor, we fractionated transfected HEK293T cells after 4 hours of MG-132 treatment and examined the whole cell, nuclear and cytoplasmic fractions by immunoblotting (Figure VII). This experiment revelad that a larger amount of mutant ATOH7 is still localized in the cytoplasm, even after protein stabilization. This further supports the assumption that the deleted amino acids in the basic domain of ATOH7 are important for the sub-cellular localization of ATOH7.

Discussion

We report the identification of a novel mutation (c.121_144del, p.Arg41_Arg48del) in the bHLH transcription factor gene *ATOH7* in a patient with severe retinal dysplasia, reminiscent of Norrie disease. The in frame deletion of 24 nucleotides is flanked by two identical DNA sequences of 6 nucleotides (Figure I). We suggest a microhomology-mediated end joining mechanism which gives rise to the in frame deletion. The deletion comprises eight highly conserved amino acids of the basic domain of ATOH7 (Figure II), which leads to a significant underrepresentation of the protein in the nucleus (Figure III and IV) and an increased turnover of the mutant ATOH7 protein (Figure VI). We show that ATOH7 stability is dependent on its nuclear localization and that the protein is degraded by the proteasome in the cytoplasm (Figure V). Further, we show that the basic domain of ATOH7 is important for the sub-cellular localization of ATOH7 even after stabilization through proteasomal inhibition (Figure VII). The low amount of ATOH7 in whole cell

lysates, even after proteasomal inhibition, may also indicate a less efficient gene transcription or mRNA translation due to the mutation. However, this explanation seems to be less likely.

Crystallographic and functional data for E47 and other bHLH proteins indicate that the highly conserved basic domains play an important role for interaction with DNA [21], [22], [46], [47]. Further, it has been shown that p.Asn46His mutant ATOH7 is neither able to bind DNA nor initiate transcription of a specific reporter [48]. Since almost the entire basic domain is deleted in the mutant ATOH7 protein, it can be expected that the mutant protein, which is present in the nucleus, in very small amounts, does not bind to the DNA. Most likely, the mutation identified in this patient leads to a severely reduced transcriptional activation of ATOH7 target genes, which are essential for normal ocular development.

Our data further support previous findings describing a 6,523-bp deletion that spans a remote *cis* regulatory element, 20 kb upstream of *ATOH7*, as disease causing in humans with nonsyndromic congenital retinal nonattachment [36]. The authors suggest that this deletion reduces or entirely silences *ATOH7* expression. Our findings are also consistent with recent observations, which provide functional evidence for the first time that a missense mutation (p.Asn46His) in the DNA-binding domain of ATOH7 is implicated in PHPV [48]. The mutation p.Asn46His affects DNA-binding and transcriptional activation of target gene expression. We now present functional evidence that a mislocalization and increased turnover of the p.Arg41_Arg48del ATOH7 causes severe retinal dysplasia. The deletion in our patient as well as the two previously reported cases most likely result in ATOH7 deficiency in the nucleus and therefore leads to similar eye phenotypes in humans.

The striking similarities between *Atoh7*$^{-/-}$ and *Ndp*$^{y/-}$ mice as well as human patients with mutations in the respective genes might result from the close interaction between the development of RGCs and the retinal vasculature. Atoh7 is crucial for RGC development and when this is disrupted, vascular defects can be observed within the eye. Norrin, the *NDP* gene product on the other hand, is important for the development of the retinal vasculature, and when this process fails, RGCs start to degenarate, at least in the mouse model [49]– [51]. Mutations in these two genes (*ATOH7* and *NDP*) lead to similar eye phenotypes but whether a direct molecular interaction of the respective proteins exist, or whether two distinct mechanisms or signaling cascades lead to similar phenotypes remains to be answered.

Furthermore, several association studies linked *ATOH7* to human optic disc size, which is directly related to the number of RGCs [52]– [54], but also open-angle glaucoma [55], [56]. In one of these studies, two missense mutations in *ATOH7* have been described (p.Arg65Gly, p.Ala47Thr) in patients with optic nerve hypoplasia [52]. Recently, in a combinatory approach of auto-zygosity mapping and next generation sequencing, two homozygous mutations (p.Glu49Val, p.Pro18ArgfsX69) in two consanguineous families diagnosed with multiple ocular developmental defects were identified [57].

In summary, we report a new in-frame deletion of eight amino acids in the basic domain of ATOH7 and show its biological consequences. The analyses of wild type and mutant expression constructs provide direct evidence that the lack of ATOH7 in the nucleus causes human ocular developmental diseases with an autosomal recessive mode of inheritance.

Materials and Methods

Ethics statement

Written informed consent was obtained from all patients involved in this study. The Massachusetts General Hospital Institutional Review Board approved consent procedure. The Institute of Medical Molecular Genetics of the University of Zurich is approved for clinical genetic testing by the Federal Office of Public Health.

Genetic analysis

Informed consent for genetic testing was obtained from all the patients included in this study. Genomic DNA was extracted by standard methods from peripheral blood, PCR-amplified, and bi-directionally Sanger–sequenced using an ABI Prism 3170 genetic analyzer (Applied Biosystems, Rotkreuz, Switzerland). We sequenced the entire protein-coding exon 1 and 50-70 bp of flanking untranslated (exonic) regions. We divided the *ATOH7* gene into two overlapping PCR fragments for sequence analysis. Two primer pairs were used to generate two PCR products with a 180 bp overlap. Genomic DNA (50ng) was used for PCR amplification. For the first fragment Ampli Taq Gold 360 with 360 GC Enhancer (Applied Biosystems, Rotkreuz, Switzerland) was used. After an initial incubation at 95 °C for 10 min, 35 cycles were performed: 95 °C (1 min), 60 °C (1 min), 72 °C (2 min), and a final extension at 72 °C for 10 min. For the second fragment, HotFire Taq polymerase (Solis BioDyne, Tartu, Estonia) was used. Initial incubation at 95 °C for 15 min, followed by 35 cycles of 95 °C (1 min), 60 °C (1 min), 72 °C (2 min), and a final extension at 72 °C for 10 min. Primers were as follows:
ATOH7_Ex1_for1, 5'-TAG AAC AGA AGG CCG AGT CC-3'; ATOH7_Ex1_rev1, 5'- AGT GGA GAC CCA CCC AGT C-3'; ATOH7_Ex1_for2, 5'ATG CAG GGG CTC AAC ACT-3';ATOH7_Ex1_rev2, 5'- TGA TGC GAA TAA AGG TAA TCT GA-3'. PCR products were sequenced using the Big Dye terminator cycle sequencing Kit v.3.1 (Applied Biosystems, Rotkreuz, Switzerland) on the ABI 3170 genetic analyzer (Applied Biosystems, Rotkreuz, Switzerland). The obtained sequences were analyzed using SeqScape version 2.5 software (Applied Biosystems, Rotkreuz, Switzerland).

PCR products spanning the deletion

Genomic DNA (50ng) was used for PCR amplification. The amplification protocol consisted of the following polymerase and steps: Ampli Taq Gold 360 with 360 GC Enhancer (Applied Biosystems, Rotkreuz, Switzerland) was used: incubation at 95 °C for 10 min, 35 cycles of 95 °C (1 min), 60 °C (1 min), 72 °C (2 min), and a final extension at 72 °C for 10 min. As forward primer ATOH7_Ex1 del for (5'-GGGATGAAGTCCTGCAAGC-3') and as reverse primer ATOH7_Ex1 del rev (5'-GTCGAAGGCAGTGTTGAGC-3') were used. PCR products were run in a 2% agarose gel and stained with ethidium bromide.

Bioinformatic analysis

For multiple sequence alignment (MSA), the protein sequences of ATOH7 of different species were downloaded from NCBI (http://www.ncbi.nlm.nih.gov/protein) and the alignments of the bHLH domain were calculated using ClustalW2 (http://www.ebi.ac.uk/clustalw2). Sequence alignment was carried out with the following reference sequences: NP_660161.1 (human),

NP_058560.1 (mouse), NP_989999.1 (chicken), NP_001079290.1 (*Xenopus*), NP_731223.1 (*Drosophila*).

Protein modeling

The model of the protein structure of the wild type human ATOH7 (NP_660161) was generated by comparative protein structure modeling using the M4T server version 3.0 (http://manaslu.aecom.yu.edu/M4T) [58], [59]. The crystal structure of the basic helix-loop-helix domain of the mouse heterodimer E47/NeuroD1 bound to DNA (PDB code 2ql2) was used as a template [44]. Figures were generated using the molecular visualization program PYMOL version 1.4.1. (http://www.pymol.org).

Expression vectors

Human genomic DNA was used as template for cloning of expression vectors. Two primers were used to amplify the full-length coding sequence of human *ATOH7* directly from genomic DNA of the patient. The amplified fragment was cloned in the expression vector pcDNA3.1/nV5 using the Gateway cloning system (Invitrogen, Basel, Switzerland). This vector has a CMV promoter to express N-terminal V5 fusion proteins. We generated four different constructs, including wild type ATOH7 (ATOH7 wt), mutant (p.Arg41_Arg48del) ATOH7 (ATOH7 del), wild type ATOH7 with an artificial NLS (ATOH7 NLS_wt), and mutant (p.Arg41_Arg48del) ATOH7 with an artificial NLS (ATOH7 NLS_del). Verification of all constructs was done by direct sequencing. The same expression vectors were used for immunocytochemistry and Western blot analyses.

Cell culture and transfection

COS-7 cells were grown in Modified Eagle's medium containing 10% (v/v) fetal bovine serum at 37 °C in humidity-controlled incubator with 5% CO_2.

HEK293T cells were grown in Dulbecco's modified Eagle's medium containing 10% (v/v) fetal bovine serum at 37 °C in humidity-controlled incubator with 5% CO_2.

Cells were transfected with PEI (Sigma-Aldrich, Buchs, Switzerland) according to manufacturer's instructions.

Immunocytochemistry

COS-7 or HEK293T cells were seeded on glass cover slip coated with 0.01% poly-L-lysine (Sigma-Aldrich, Buchs, Switzerland) in 12 well plates at a density of $5*10^4$ cells / well. Cells were transiently transfected with 1 µg DNA per well of the respective expression vectors using PEI (Sigma-Aldrich, Buchs, Switzerland) according to manufacturer's instructions. 24 hours after transfection, cells were fixed with 4% paraformaldehyde for 10 min, washed with PBS and permeabilized with 0.1% Triton X-100 for 15 min to detect intracellular V5-tagged proteins. Non-specific binding was blocked with 1% BSA in PBS for 30 min. Immunocytochemistry was carried out with primary antibody anti-V5 (Sigma-Aldrich, 1:100) for 1 hour. Cells were washed three times with PBS. As a secondary antibody anti-Alexa Fluor 488 (green) (Invitrogen, 1:200) was used for 40 min. Cells were washed in PBS and mounted in DAPI containing mounting medium (Vectashield®, Vector Laboratories, Burlingame, CA, USA). Immunocytochemistry was performed at room temperature. Immunostaining was visualized by fluorescence microscopy using an

Axioplan microscope (Zeiss, Hombrechtikon, Switzerland). Quantitative studies were carried out in three independent transfections. At least 50 cells were counted for each transfected construct. The data is expressed as mean ± s.e.m.

Nuclear fractionation

HEK293T cells were seeded in 75cm^2 culture flasks at a density of 6*10^6 cells / flask. 24 hours later, 30 µg DNA/flask was used to transfect HEK293T cells, for each construct ten 75cm^2 culture flasks were used. 24 hours after transfection, flasks were rinsed with 2 ml of ice cold PBS. 300 µl/flask of ice-cold lysis buffer (0.01M Tris-Cl pH 7.4, 0.01M NaCl, 0.003M $MgCl_2$, 0.5% Triton X-100) was added. Cells were scraped off and collected in 5 ml lysis buffer and homogenized in a tissue glass Teflon dounce homogenizer, on ice. 2.5 ml were put aside as whole cell fraction. The remaining 2.5 ml of the homogenate was centrifuged for 10 min at 3'000 rpm in a Sorvall HB4 rotor at 4°C. The supernatant (cytoplasmic fraction) was collected and the pellet was vortexed for 30 seconds and then resuspended in 5 ml of ice-cold lysis buffer. The homogenate was layered over a 5 ml cushion of 30% sucrose prepared in lysis buffer and centrifuged for 10 min at 3'000 rpm in a Sorvall HB4 rotor at 4°C. The pellet (nuclear fraction) was resuspended in 2.5 ml of nuclear fraction buffer (40% glycerol, 0.05M Tris-Cl pH 7.4, 0.005M $MgCl_2$, 0.1mM EDTA). All fractions were sonicated prior to SDS-PAGE and Western blot analysis.

Proteasome-dependent protein stability assays

HEK293T cells were seeded in 75cm^2 culture flasks at a density of 6*10^6 cells / flask. 24 hours later 30 µg DNA/flask was used to transfect HEK293T cells. 24 hours after transfection, HEK293T cells were treated with 20 µM MG-132 (Merck, Darmstadt, Germany), 1 µM epoxomicin (Merck, Darmstadt, Germany), 20 mM ammonium chloride (Sigma-Aldrich, Buchs, Switzerland) or DMSO vehicle control followed by Western blot analysis.

Cycloheximide chase assay

To study protein decay of ATOH7 we transfected HEK293T cells and treated the cells 24 hours after transfection with MG-132 (20 µM) for 4 hours to stabilize protein levels. The reversible proteasome inhibitor MG-132 was removed and cells were then treated with cycloheximide CHX (100µg/ml, Sigma-Aldrich, Buchs, Switzerland) for the indicated times to block synthesis of new protein [60]. Protein extracts were examined by Western blot analysis. The protein bands were quantified using ImageJ software and normalized on β-tubulin loading control, all time points were compared with time 0 and expressed as a percentage thereof. The degradation rate is expressed as half-life ($t_{½}$), the time for degradation of 50% of ATOH7. The graph indicates the mean and ± s.e.m.

Western blot

Protein extracts were separated on 12% SDS-polyacrylamide gels and transferred onto polyvinylidene difluoride (PVDF) membranes (Roche Diagnostics, Rotkreuz, Switzerland), and probed with an anti-V5 antibody (1:1000, Sigma-Aldrich, Buchs, Switzerland). To normalize on nuclear and cytoplasmic protein amounts, blots were stripped and incubated with a polyclonal rabbit antibody against Histone H3 (1:1000, Abcam, Cambridge, MA, USA), β-tubulin (1:500,

Abcam, Cambridge, MA, USA) respectively. As a transfection efficiency control, GFP was cotransfected and blots were incubated with GFP antibody (1:2000, Santa Cruz Biotechnology Inc., Heidelberg, Germany). As a secondary antibody anti-rabbit HRP (1:2000, GE Healthcare, Glattbrugg, Switzerland) or anti-mouse HRP (Dianova GmbH, Hamburg, Germany) were used. All blots were visualized by enhanced chemiluminescence (ECL, Perkin Elmer, Waltham, MA, USA). The protein bands were quantified using ImageJ software and normalized on β-tubulin or Histone H3 loading control. The data is expressed as mean ± s.e.m.

Statistical Analyses

All data (immunocytochemistry and Western blot) were analyzed using parametric one-way ANOVA. Following the initial ANOVAs, Fisher's least significant difference post hoc comparisons were conducted whenever appropriate. Statistical significance was set at $p < 0.05$. All statistical analyses were performed using the statistical software StatView (version 5.0) implemented on a PC running the Windows XP operating system.

Websites

1000 Genome project database: http://www.1000genomes.org/
Human Gene Mutation Database (HGMD®) Professional: http://www.hgmd.org/
Ensemble Genome Browser: http://www.ensembl.org/index.html
National Center for Biotechnology Information: http://www.ncbi.nlm.nih.gov/
ClustalW2: http://www.ebi.ac.uk/clustalw2/
M4T server version 3.0: http://manaslu.aecom.yu.edu/M4T/
PYMOL version 1.4.1: http://www.pymol.org/

Acknowledgements

The authors express their special thanks to the family involved in this study and are grateful to Jean-Marc Matter and Tania Rodrigues (Department of Biochemistry, University of Geneva, Switzerland) for providing the nuclear fractionation protocol and helpful discussions.

References

1. Turner DL, Cepko CL (1987) A common progenitor for neurons and glia persists in rat retina late in development. Nature 328: 131-136.

2. Holt CE, Bertsch TW, Ellis HM, Harris WA (1988) Cellular determination in the Xenopus retina is independent of lineage and birth date. Neuron 1: 15-26.

3. Wetts R, Fraser SE (1988) Multipotent precursors can give rise to all major cell types of the frog retina. Science 239: 1142-1145.

4. Carter-Dawson LD, LaVail MM (1979) Rods and cones in the mouse retina. II. Autoradiographic analysis of cell generation using tritiated thymidine. J Comp Neurol 188: 263-272.

5. Young RW (1985) Cell differentiation in the retina of the mouse. Anat Rec 212: 199-205.

6. Livesey FJ, Cepko CL (2001) Vertebrate neural cell-fate determination: lessons from the retina. Nat Rev Neurosci 2: 109-118.

7. Cepko CL, Austin CP, Yang X, Alexiades M, Ezzeddine D (1996) Cell fate determination in the vertebrate retina. Proc Natl Acad Sci U S A 93: 589-595.

8. Tomita K, Nakanishi S, Guillemot F, Kageyama R (1996) Mash1 promotes neuronal differentiation in the retina. Genes Cells 1: 765-774.

9. Brown NL, Kanekar S, Vetter ML, Tucker PK, Gemza DL, Glaser T (1998) Math5 encodes a murine basic helix-loop-helix transcription factor expressed during early stages of retinal neurogenesis. Development 125: 4821-4833.

10. Morrow EM, Furukawa T, Lee JE, Cepko CL (1999) NeuroD regulates multiple functions in the developing neural retina in rodent. Development 126: 23-36.

11. Perron M, Opdecamp K, Butler K, Harris WA, Bellefroid EJ (1999) X-ngnr-1 and Xath3 promote ectopic expression of sensory neuron markers in the neurula ectoderm and have distinct inducing properties in the retina. Proc Natl Acad Sci U S A 96: 14996-15001.

12. Wang JC, Harris WA (2005) The role of combinational coding by homeodomain and bHLH transcription factors in retinal cell fate specification. Dev Biol 285: 101-115.

13. Hernandez J, Matter-Sadzinski L, Skowronska-Krawczyk D, Chiodini F, Alliod C, Ballivet M, Matter JM (2007) Highly conserved sequences mediate the dynamic interplay of basic helix-loop-helix proteins regulating retinogenesis. J Biol Chem 282: 37894-37905.

14. Jarman AP, Grell EH, Ackerman L, Jan LY, Jan YN (1994) Atonal is the proneural gene for Drosophila photoreceptors. Nature 369: 398-400.

15. Jarman AP, Sun Y, Jan LY, Jan YN (1995) Role of the proneural gene, atonal, in formation of Drosophila chordotonal organs and photoreceptors. Development 121: 2019-2030.

16. Kanekar S, Perron M, Dorsky R, Harris WA, Jan LY, Jan YN, Vetter ML (1997) Xath5 participates in a network of bHLH genes in the developing Xenopus retina. Neuron 19: 981-994.

17. Masai I, Stemple DL, Okamoto H, Wilson SW (2000) Midline signals regulate retinal neurogenesis in zebrafish. Neuron 27: 251-263.

18. Wang SW, Kim BS, Ding K, Wang H, Sun D, Johnson RL, Klein WH, Gan L (2001) Requirement for math5 in the development of retinal ganglion cells. Genes Dev 15: 24-29.

19. Liu W, Mo Z, Xiang M (2001) The Ath5 proneural genes function upstream of Brn3 POU domain transcription factor genes to promote retinal ganglion cell development. Proc Natl Acad Sci U S A 98: 1649-1654.

20. Brown NL, Dagenais SL, Chen CM, Glaser T (2002) Molecular characterization and mapping of ATOH7, a human atonal homolog with a predicted role in retinal ganglion cell development. Mamm Genome 13: 95-101.

21. Brennan TJ, Chakraborty T, Olson EN (1991) Mutagenesis of the myogenin basic region identifies an ancient protein motif critical for activation of myogenesis. Proc Natl Acad Sci U S A 88: 5675-5679.

22. Shimizu T, Toumoto A, Ihara K, Shimizu M, Kyogoku Y, Ogawa N, Oshima Y, Hakoshima T (1997) Crystal structure of PHO4 bHLH domain-DNA complex: flanking base recognition. EMBO J 16: 4689-4697.

23. Matter-Sadzinski L, Matter JM, Ong MT, Hernandez J, Ballivet M (2001) Specification of neurotransmitter receptor identity in developing retina: the chick ATH5 promoter integrates the positive and negative effects of several bHLH proteins. Development 128: 217-231.

24. Yang Z, Ding K, Pan L, Deng M, Gan L (2003) Math5 determines the competence state of retinal ganglion cell progenitors. Dev Biol 264: 240-254.

25. Matter-Sadzinski L, Puzianowska-Kuznicka M, Hernandez J, Ballivet M, Matter JM (2005) A bHLH transcriptional network regulating the specification of retinal ganglion cells. Development 132: 3907-3921.

26. Brown NL, Patel S, Brzezinski J, Glaser T (2001) Math5 is required for retinal ganglion cell and optic nerve formation. Development 128: 2497-2508.

27. Kay JN, Finger-Baier KC, Roeser T, Staub W, Baier H (2001) Retinal ganglion cell genesis requires lakritz, a Zebrafish atonal Homolog. Neuron 30: 725-736.

28. Brzezinski JA, Brown NL, Tanikawa A, Bush RA, Sieving PA, Vitaterna MH, Takahashi JS, Glaser T (2005) Loss of circadian photoentrainment and abnormal retinal electrophysiology in Math5 mutant mice. Invest Ophthalmol Vis Sci 46: 2540-2551.

29. Edwards MM, McLeod DS, Li R, Grebe R, Bhutto I, Mu X, Lutty GA (2011) The deletion of Math5 disrupts retinal blood vessel and glial development in mice. Exp Eye Res 96: 147-156.

30. Berger W, vandePol D, Bachner D, Oerlemans F, Winkens H, Hameister H, Wieringa B, Hendriks W, Ropers HH (1996) An animal model for Norrie disease (ND): Gene targeting of the mouse ND gene. Hum Mol Genet 5: 51-59.

31. Luhmann UFO, Lin JH, Acar N, Lammel S, Feil S, Grimm C, Seeliger MW, Hammes HP, Berger W (2005) Role of the Norrie disease pseudoglioma gene in sprouting angiogenesis during development of the retinal vasculature. Invest Ophthalmol Vis Sci 46: 3372-3382.

32. Ma W, Yan RT, Xie W, Wang SZ (2004) bHLH genes cath5 and cNSCL1 promote bFGF-stimulated RPE cells to transdifferentiate toward retinal ganglion cells. Dev Biol 265: 320-328.

33. Xie W, Yan RT, Ma W, Wang SZ (2004) Enhanced retinal ganglion cell differentiation by ath5 and NSCL1 coexpression. Invest Ophthalmol Vis Sci 45: 2922-2928.

34. Dokucu ME, Zipursky SL, Cagan RL (1996) Atonal, rough and the resolution of proneural clusters in the developing Drosophila retina. Development 122: 4139-4147.

35. Sun Y, Jan LY, Jan YN (2000) Ectopic scute induces Drosophila ommatidia development without R8 founder photoreceptors. Proc Natl Acad Sci U S A 97: 6815-6819.

36. Ghiasvand NM, Rudolph DD, Mashayekhi M, Brzezinski JA, Goldman D, Glaser T (2011) Deletion of a remote enhancer near ATOH7 disrupts retinal neurogenesis, causing NCRNA disease. Nat Neurosci 14: 578-586.

37. Warburg M (1966) Norrie's disease. A congenital progressive oculo-acoustico-cerebral degeneration. Acta Ophthalmol (Copenh) 85: Suppl 5-147.

38. Berger W (1998) Molecular dissection of Norrie disease. Acta Anat (Basel) 162: 95-100.

39. Berger W, Kloeckener-Gruissem B, Neidhardt J (2010) The molecular basis of human retinal and vitreoretinal diseases. Prog Retin Eye Res 29: 335-375.

40. Smith SE, Mullen TE, Graham D, Sims KB, Rehm HL (2012) Norrie disease: Extraocular clinical manifestations in 56 patients. Am J Med Genet 158A: 1909-1917.

41. Berger W, Vandepol D, Warburg M, Gal A, Bleekerwagemakers L, Desilva H, Meindl A, Meitinger T, Cremers F, Ropers HH (1992) Mutations in the Candidate Gene for Norrie Disease. Hum Mol Genet 1: 461-465.

42. Berger W, Meindl A, Vandepol TJR, Cremers FPM, Ropers HH, Doerner C, Monaco A, Bergen AAB, Lebo R, Warburg M, Zergollern L, Lorenz B, Gal A, Bleekerwagemakers EM, Meitinger T (1992) Isolation of A Candidate Gene for Norrie Disease by Positional Cloning. Nature Genet 1: 199-203.

43. The 1000 Genomes Project Consortium (2010) A map of human genome variation from population-scale sequencing. Nature 467: 1061-1073.

44. Longo A, Guanga GP, Rose RB (2008) Crystal structure of E47-NeuroD1/beta2 bHLH domain-DNA complex: heterodimer selectivity and DNA recognition. Biochemistry 47: 218-229.

45. Desterro JMP, Rodriguez MS, Hay RT (2000) Regulation of transcription factors by protein degradation. Cell Mol Life Sci 57: 1207-1219.

46. Voronova A, Baltimore D (1990) Mutations That Disrupt Dna-Binding and Dimer Formation in the E47 Helix-Loop-Helix Protein Map to Distinct Domains. Proc Natl Acad Sci U S A 87: 4722-4726.

47. Ellenberger T, Fass D, Arnaud M, Harrison SC (1994) Crystal-Structure of Transcription Factor E47 - E-Box Recognition by A Basic Region Helix-Loop-Helix Dimer. Genes & Development 8: 970-980.

48. Prasov L, Masud T, Khaliq S, Mehdi SQ, Abid A et al (2012) ATOH7 mutations cause autosomal recessive persistent hyperplasia of the primary vitreous. Hum Mol Genet 21: 3681-3694.

49. Richter M, Gottanka J, May CA, Welge-Lussen U, Berger W, Lutjen-Drecoll E (1998) Retinal vasculature changes in Norrie disease mice. Invest Ophthalmol Vis Sci 39: 2450-2457.

50. Zuercher J, Fritzsche M, Feil S, Mohn L, Berger W (2012) Norrin stimulates cell proliferation in the superficial retinal vascular plexus and is pivotal for the recruitment of mural cells. Hum Mol Genet 21: 2619-2630.

51. Schafer NF, Luhmann UFO, Feil S, Berger W (2009) Differential Gene Expression in Ndph-Knockout Mice in Retinal Development. Invest Ophthalmol Vis Sci 50: 906-916.

52. Macgregor S, Hewitt AW, Hysi PG, Ruddle JB, Medland SE, Henders AK, Gordon SD, Andrew T, McEvoy B, Sanfilippo PG, Carbonaro F, Tah V, Li YJ, Bennett SL, Craig JE, Montgomery GW, Tran-Viet KN, Brown NL, Spector TD, Martin NG, Young TL, Hammond CJ, Mackey DA (2010) Genome-wide association identifies ATOH7 as a major gene determining human optic disc size. Hum Mol Genet 19: 2716-2724.

53. Ramdas WD, van Koolwijk LM, Ikram MK, Jansonius NM, de Jong PT, Bergen AA, Isaacs A, Amin N, Aulchenko YS, Wolfs RC, Hofman A, Rivadeneira F, Oostra BA, Uitterlinden AG, Hysi P, Hammond CJ, Lemij HG, Vingerling JR, Klaver CC, van Duijn CM (2010) A genome-wide association study of optic disc parameters. PLoS Genet 6: e1000978.

54. Khor CC, Ramdas WD, Vithana EN, Cornes BK, Sim X, Tay WT, Saw SM, Zheng Y, Lavanya R, Wu R, Wang JJ, Mitchell P, Uitterlinden AG, Rivadeneira F, Teo YY, Chia KS, Seielstad M, Hibberd M, Vingerling JR, Klaver CC, Jansonius NM, Tai ES, Wong TY, van Duijn CM, Aung T (2011) Genome-wide association studies in Asians confirm the involvement of ATOH7 and

TGFBR3, and further identify CARD10 as a novel locus influencing optic disc area. Hum Mol Genet 20: 1864-1872.

55. Fan BJ, Wang DY, Pasquale LR, Haines JL, Wiggs JL (2011) Genetic variants associated with optic nerve vertical cup-to-disc ratio are risk factors for primary open angle glaucoma in a US Caucasian population. Invest Ophthalmol Vis Sci 52: 1788-1792.

56. Ramdas WD, van Koolwijk LM, Lemij HG, Pasutto F, Cree AJ, Thorleifsson G, Janssen SF, Jacoline TB, Amin N, Rivadeneira F, Wolfs RC, Walters GB, Jonasson F, Weisschuh N, Mardin CY, Gibson J, Zegers RH, Hofman A, de Jong PT, Uitterlinden AG, Oostra BA, Thorsteinsdottir U, Gramer E, Welgen-Lussen UC, Kirwan JF, Bergen AA, Reis A, Stefansson K, Lotery AJ, Vingerling JR, Jansonius NM, Klaver CC, van Duijn CM (2011) Common genetic variants associated with open-angle glaucoma. Hum Mol Genet 20: 2464-2471.

57. Khan K, Logan CV, McKibbin M, Sheridan E, Elcioglu NH, Yenice O, Parry DA, Fernandez-Fuentes N, Abdelhamed ZI, Al Maskari A, Poulter JA, Mohamed MD, Carr IM, Morgan JE, Jafri H, Raashid Y, Taylor GR, Johnson CA, Inglehearn CF, Toomes C, Ali M (2011) Next generation sequencing identifies mutations in Atonal homolog 7 (ATOH7) in families with global eye developmental defects. Hum Mol Genet 21: 776-783.

58. Fernandez-Fuentes N, Rai BK, Madrid-Aliste CJ, Fajardo JE, Fiser A (2007) Comparative protein structure modeling by combining multiple templates and optimizing sequence-to-structure alignments. Bioinformatics 23: 2558-2565.

59. Fernandez-Fuentes N, Madrid-Aliste CJ, Rai BK, Fajardo JE, Fiser A (2007) M4T: a comparative protein structure modeling server. Nucleic Acids Res 35: 363-368.

60. Schneider-Poetsch T, Ju JH, Eyler DE, Dang YJ, Bhat S, Merrick WC, Green R, Shen B, Liu JO (2010) Inhibition of eukaryotic translation elongation by cycloheximide and lactimidomycin. Nature Chem Biol 6: 209-217.

Figures

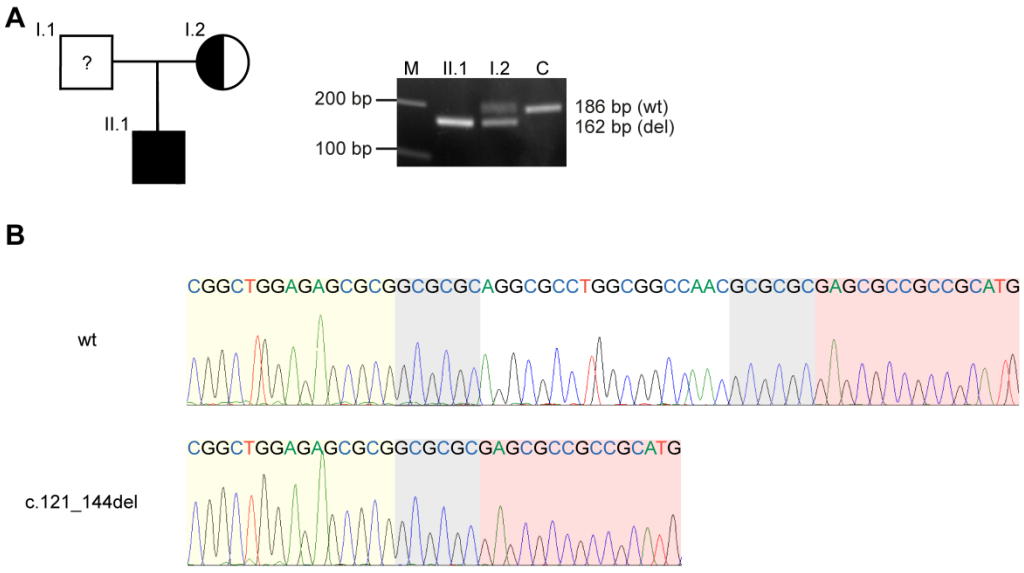

Figure I. Microhomology-mediated *ATOH7* deletion in a male patient with retinal dysplasia.
(A) Pedigree and genetic analysis of the patient and his mother. Deletion-flanking primers amplify a 186 bp fragment in the control (C). The mother (I.2) is heterozygous for the normal and the deleted allele while her son (II.1) only shows the deleted allele. DNA from the father was not available for genetic testing. (M= size marker)
(B) Sequence profiles from PCR products representing the wild type (wt) and mutant (c.121_144del) alleles of *ATOH7*. The deletion of 24 nucleotides is flanked on either side by a stretch of 6 completely identical nucleotides. This region of microhomology is indicated in grey. DNA sequences upstream and downstream of the deletion are indicated in yellow and red, respectively.

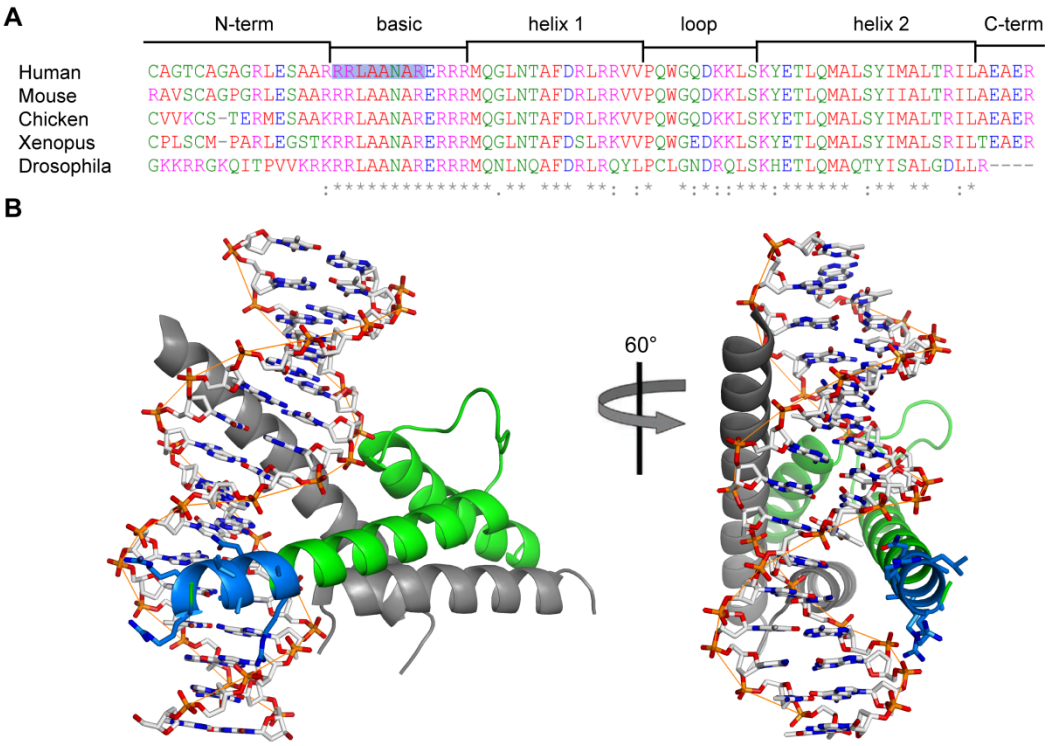

Figure II. Multiple sequence alignment and structural modeling of ATOH7 bHLH domain.
(A) Multiple sequence alignment of the bHLH domain of ATOH7 protein sequences from different species. The deletion of eight amino acids is highlighted in blue. All eight amino acids which are deleted in the patient are highly conserved between all the investigated species. Structural motifs of the bHLH domain of human ATOH7 are indicated above the amino acid sequence. The deletion affects the basic, DNA-binding domain of ATOH7.
(B) 3D model of the bHLH domain of human wild type ATOH7 (in green) dimerized with the transcription factor E47 (in grey) and bound to double-stranded DNA. Amino acid residues of the basic domain which are deleted in the patient (Arg41-Arg48, highlighted in blue) are in close connection to the major groove of the double-stranded DNA.

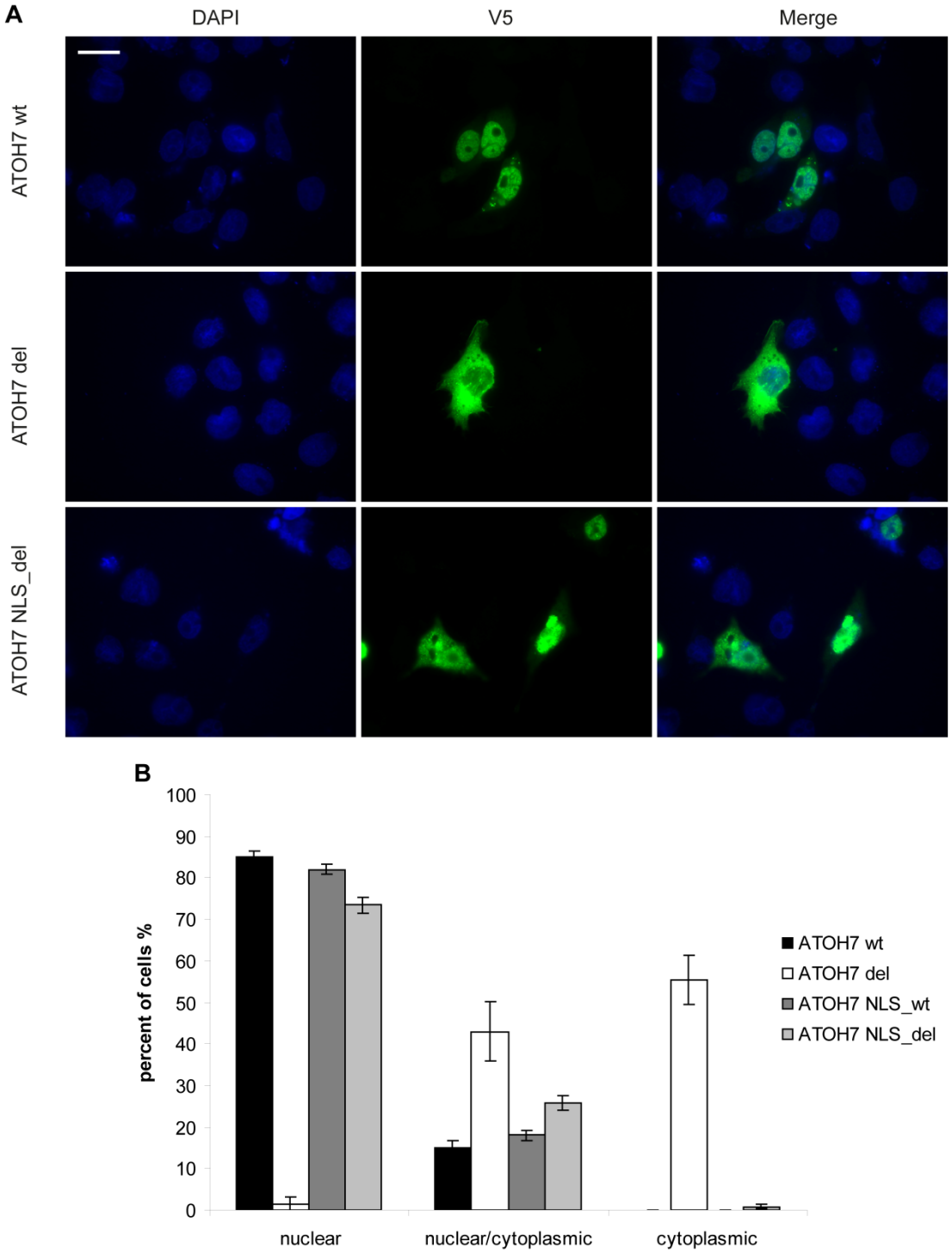

Figure III. Mislocalization of mutant human ATOH7.

(A) The sub-cellular localization of N-terminal V5- tagged human ATOH7 in COS-7 cells upon immunofluorescence staining with an antibody against V5. V5 antibody in green, DAPI in blue, scale bar 20µm.

(B) Quantification of the sub-cellular localization of the ATOH7 protein. Wild type N-terminal V5-tagged ATOH7 was predominantly localized in the nucleus, whereas nuclear localization of the mutant V5-tagged ATOH7 is significantly reduced compared to wt (P<0.0001). By adding an

artificial NLS, nuclear localization of the mutant V5-tagged ATOH7 (ATOH7 NLS_del) compared to ATOH7 del was significantly increased (*P*<0.001). Cells in which only cytoplasmic ATOH7 was observed, were almost exclusively found when transfected with ATOH7 del construct. For quantification, at least 50 cells were counted per construct in three independent transfections. All graphs show mean ± s.e.m of three independent transfections.

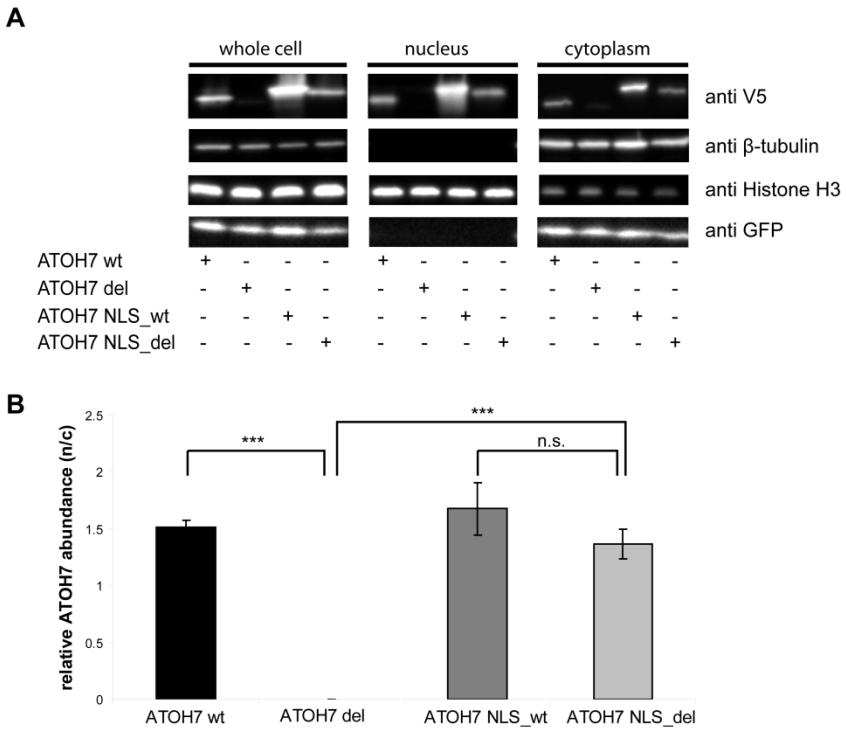

Figure IV. Sub-cellular localization of ATOH7 correlates with protein amount.

(A) Western blot analysis of whole cell, nuclear and cytoplasmic fractions from HEK293T cells transfected either with the wild type or mutant expression constructs of *ATOH7* with or without artificial NLS. Protein level in the whole cell extracts was higher for ATOH7 wt compared to ATOH7 del. By adding an artificial NLS, protein levels increased. Further, the wild type V5-tagged ATOH7 localizes to nucleus and cytoplasm while the mutant protein can only be detected in very small amounts in the nuclear fractions, but is present in the cytoplasmic extracts. By adding an artificial NLS to the mutant ATOH7, nuclear localization of the protein is rescued. anti-Histone H3, and anti-β-tubulin were used as loading controls. Anti-GFP was used to determine transfection efficientcy. (GFP: green fluorescence protein).

(B) Relative abundance of wild type and mutant ATOH7 protein with or without artificial NLS in the nuclear fractions. All graphs show mean ± s.e.m. of three independent transfections. Initial one-way ANOVA of relative nuclear abundance yielded a highly significant main effect of the genotype [$F(3,8)= 32.167$, $P< 0.0001$]. Subsequent post-hoc analyses verified the significant difference between ATOH7 wt and ATOH7 del (***, P<0.0001) and ATOH7 del and ATOH7 NLS_del (***, P<0.0001). Differences between ATOH7 wt and ATOH7 NLS_del were not significant.

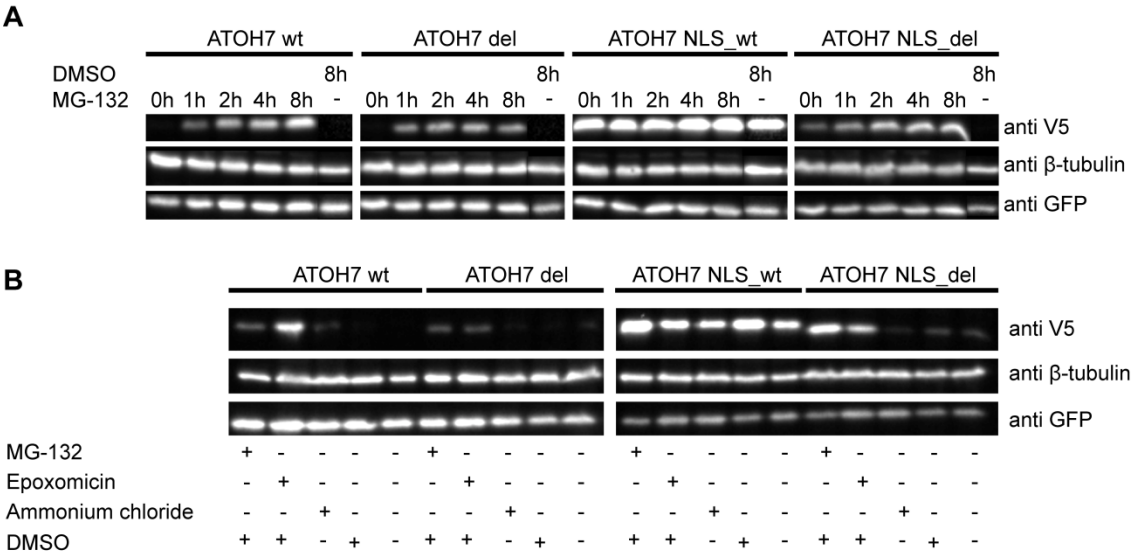

Figure V. Proteasomal inhibition stabilizes ATOH7 protein level.

(A) HEK293T cells were cotransfected with indicated ATOH7 constructs and GFP. 24 hours after transfection MG-132 was added for indicated times. Cells were harvested and subjected to Western blot analyses, which revealed stabilization of ATOH7 protein upon proteasomal inhibition for the ATOH7 wt, del, and NLS_del but not for NLS_wt.

(B) HEK293T cells were cotransfected with indicated ATOH7 constructs and GFP. 24 hours after transfection inhibitors were added for 4 hours. Cells were harvested and subjected to Western blot analyses, which revealed stabilization of ATOH7 protein upon proteasomal inhibition for the ATOH7 wt, del and NLS_del but not for NLS_wt. Inhibition of the lysosomal degradation with ammonium chloride had no effect on either of the ATOH7 variants.

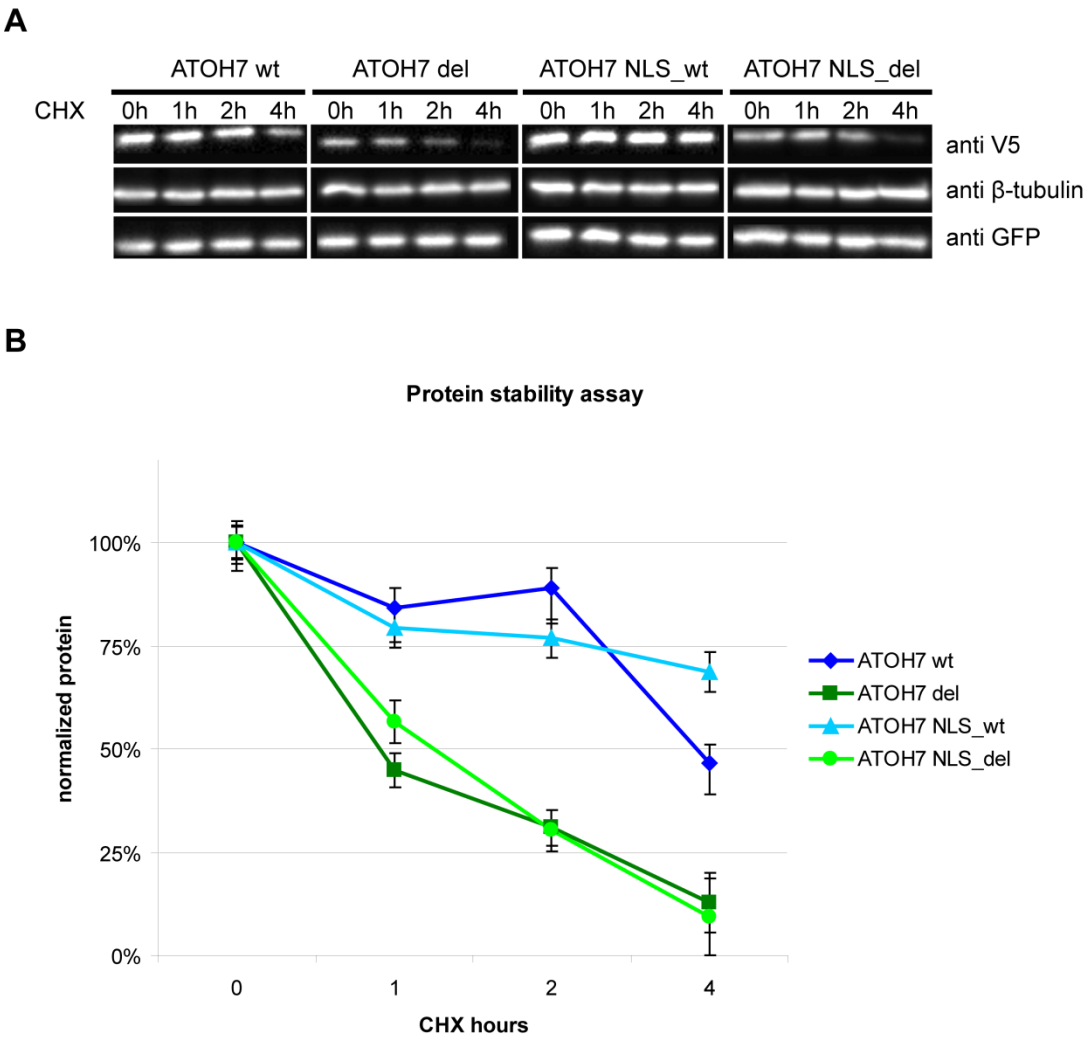

Figure VI. Increased turnover of the mutant ATOH7 protein.

(A) HEK293T cells were cotransfected with the indicated ATOH7 construct and GFP. 24 hours after transfection cells were treated with MG-132 for 4 hours to stabilize ATOH7 followed by CHX (Cycloheximide) treatment for the indicated times. Cells were harvested and analyzed by Western blot using antibodies as indicated. (GFP: green fluorescence protein).

(B) Protein stability was assessed by comparing the ATOH7 signal intensity, relative to endogenous β-tubulin. For each construct ATOH7 was set to 100% at time point 0h.

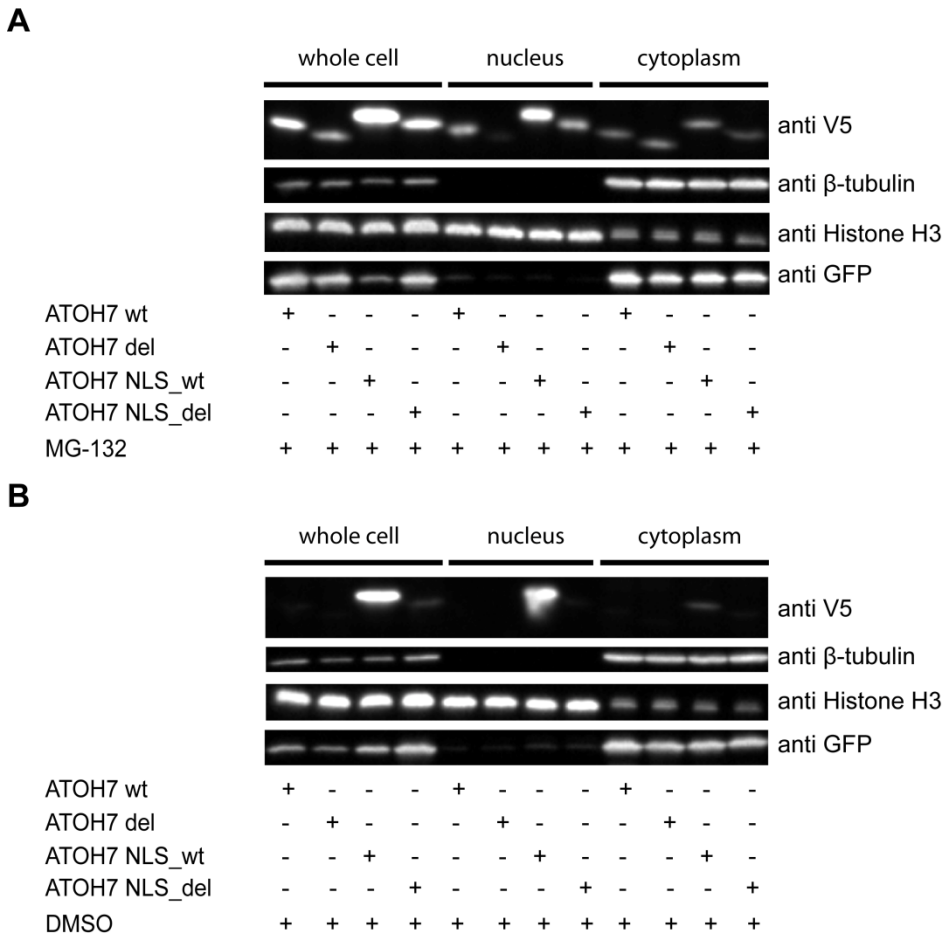

Figure VII. The basic domain of ATOH7 is important for its nuclear localization.
(A) HEK293T cells were cotransfected with the indicated ATOH7 construct and GFP. 24 hours after transfection cells were treated with MG-132 to stabilize ATOH7 or (B) with DMSO for 4 hours. Cells were harvested and fractionated, whole cell, nuclear, and cytoplasmic fractions were analyzed by Western blot using antibodies as indicated. (GFP: green fluorescence protein).

Tasks	Authors
Gene selection	LM
Study concept	LM, WB
Primer design	LM, SF
Genetic screening	SF
Sequence data analysis	SF, LM
Construct cloning	LM
3D model	LM
Immunocytochemical assay	LM
Cell fractionation	LM
Proteasomal degradation	LM, BS, SF
CHX experiment	LM, BS, SF
Figure preparation	LM
Contributed DNA material	KS, WB
Wrote the manuscript	LM, WB

Name	Abbrivation
Lucas Mohn	LM
Britta Seebauer	BS
Silke Feil	SF
Katherine Sims	KS
Wolfgang Berger	WB

Table I: Individual contributions in the ATOH7 project.

***NEUROD1* - Sequence variants and the predicted effect on the function**

One in-frame deletion (c.463_465del, p.Glu155del) was found in a female cousin of a Norrie male patient. It is an in-frame deletion of three nucleotides, which encode for a highly conserved amino acid. The deleted amino acid is located in a basic helix-loop-helix dimerization region of NEUROD1. The mutation might affect binding to its dimerization partners (NEUROD1, ATOH7, or TCF3) and might inhibit proper transcriptional regulation of downstream target genes.

NINJ1* – Sequence variants and the predicted effect on the function of *NINJ1

One missens mutation and two sequence alterations in the 5'UTR were found. The missense mutation leads to an exchange from alanine to threonine at position 42. The physiological difference of these two amino acids is small, but the alanine is very well conserved throughout evolution (Appendix B). All *in silico* prediction programs predicts this exchange to be deleterious. Both alterations in the 5'UTR were found in the same patient, and might affect promoter activity.

***NINJ1* mutation has no effect on Wnt signaling but causes a mislocalization of NINJ1**

To further investigate the function of this mutation, Lea Sollfrank compared the mutant and the wild type NINJ1 isoform in a Wnt reporter luciferase assay. She did not see any differences between wt and mutant NINJ1 (Master thesis Lea Sollfrank 2011). NINJ1 is known to be located in the cell membrane and function as a cell adhesions molecule and is involved in macrophage induced programmed cell death during early ocular development (Araki et al. 1997, Lee et al. 2009). Therefore, we transfected COS-7 and HEK293T cells with the mutant and the wild type isoform of *NINJ1* and performed an immunocytochemical staining to assess subcellular localization of the two protein isoforms. As exepted, the wild type NINJ1 was located in the cell membrane, but the mutant isoform was mislocalized in the cytoplasm (Figure 13). Lea Sollfrank quantified the ICC staining which reveald an 87.5% fraction of wild type NINJ1 to be localized in the cell membrane, whereas only 12.5% of the mutant *NINJ1* transfected cells show a membrane staining (Figure 14). The mutant isoform aggregated next to the nucleus and we speculated it might be trapped in the endoplasmic reticulum. Unfortunately an ER co-staining did not reveal a co-localization of mutant *NINJ1* and ER marker. *NINJ1* is involved in cell-cell interaction and adhesion of macrophages and the mutation (p.Ala42Thr) lies in the extracellular domain, behind the homophilic adhesion domain which consists of the proline and the asparagine at position 26 and 37 respectively. I tried to transfect BV-2 cells (a gift from Prof. Dr. Burkhard Becher) to perform an adhesions assay. Unfortunately, BV-2 cells could not be transfected so far.

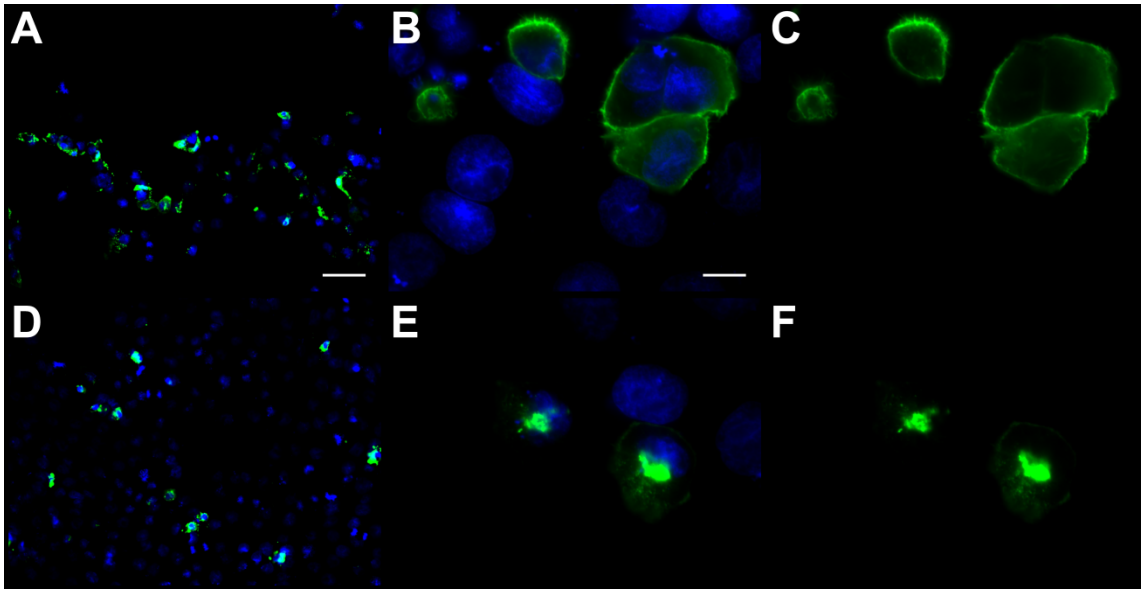

Figure 13: Subcellular localization of *NINJ1*. Wild type *NINJ1* is localized in the cell membrane of HEK293T cell (A-C), wherease mutant *NINJ1* isoform (p.Ala42Thr) is mislocalized in the cytoplasm (D-F). Blue: DAPI, green V5-tagged *NINJ1*. Scale bar A&D 50µm, B, C, E, F 10 µm. Figure is adapted from Lea Sollfrank Master thesis 2011.

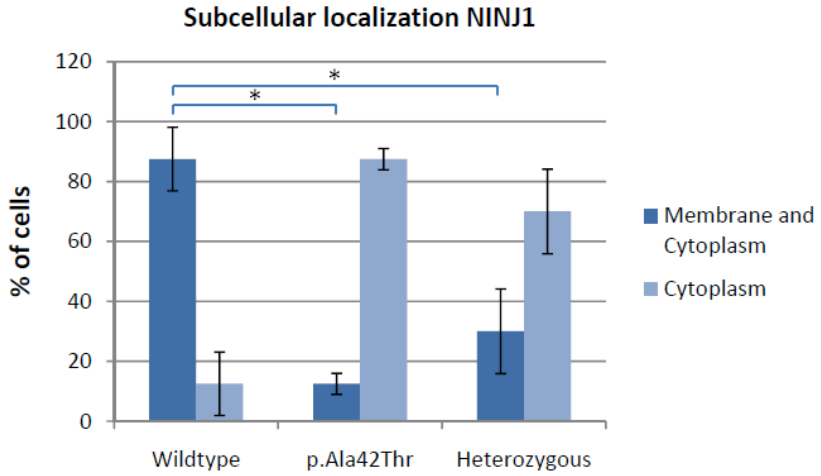

Figure 14: Quantification of subcellular localization of *NINJ1*. (Figure from Lea Sollfrank Master thesis 2011)

***ZNF408* – a new transcription factor involved in EVR pathogenesis**

We screened *ZNF408* in our patient cohort, in the framework of a collaboration with Frans Cremers at the University of Nijmegen (Holland) to investigate the role of ZNF408 in autosomal dominant FEVR. We could show that *ZNF408* is a novel gene underlying autosomal dominant FEVR. The manuscript regarding this project has recently been submitted to Proceedings of the National Academy of Sciences of the United States of America. We found two missense mutations, four synonymous mutations, and two sequence alterations in the 3'UTR. The amino acids at position 12 and 525 are only weakly conserved and the substituted residues found in our patients have only small physicochemical differences to the naturally occurring amino acids. Therefore, these missense mutations are predicted to be not deleterious by all three *in silico*

programs. Further, the mutations (p.Lys12Arg, p.Arg525His) showed no mislocalization of ZNF408 in a sub-cellular localization experiment; wild type and mutant ZNF408 both localized in the nucleus (personal communication Rob Collin).

Sequence variants in *ILK, ITGB3, PARVA* – and focal adhesion

We screend *ILK*, *ITGB3* and *PARVA* in our patients, in a collaborative effort regarding a project together with Prof. Ralf Adams at the Max-Planck Institute for Molecular Biomedicine (Münster, Germany). In this project we are interested in the focal adhesion (FA) complex, and the transition of extracellular signals to the cytoskeleton within the cell. We found several mutations in humans with retinal dysplasia in several genes involved in FA.

***ILK* - Sequence variants and the predicted effect on the function**

In *ILK* we found three different missense mutations one of which was found twice in two unrelated patients. Further, we found one synonymous mutation, and four intronic sequence alterations. All three missense mutations affect a highly conserved amino acid. In one mutation (p.Arg211Cys) the physicochemical difference between the mutated and the normally occurring amino acid is large. In one case (70159), where we found the p.Arg211Cys mutation, we were able to collect paternal DNA. The father of this female patient is homozygous for the C allel and the mother is heterozygous C/T as the affected daughter (Figure 15). For the other two mutations (p.Leu53Met, p.Arg317Gln) the physicochemical difference is small. p.Arg211Cys is predicted to be deleterious by all three prediction programs, p.Leu53Met is predicted to be deleterious by two prediction programs and p.Arg317Gln is predicted to be not deleterious by all prediction programs. The mutation at position 53 affects the ankyrin domain, which is responsible for protein-protein interaction and localizes ILK to focal adhesions, and induces an alternative start codon at this position. The mutation at position 211 lies within the PH-like domain of the ILK protein, which has been shown to bind phosphatidylinositol-3,4,5-trisphosphate (PIP3). The mutation at position 317 affects the catalytic kinase domain of ILK. ILK is highly conserved throughout evolution. The amino acids mutated in our patients are 100% conserved in vertebrates as it can be seen in a multiple sequence alignment of ILK (Appendix B). All intronic mutations are predicted to have an effect on splicing.

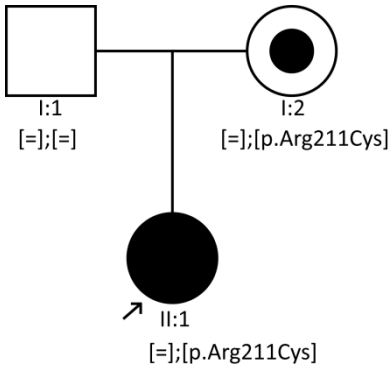

Figure 15: Pedigree of the family with an *ILK* mutation. The daughter (patient # 70159) and the mother are heterozygous for the c.631C>T exchange which is leading to a p.Arg211Cys. The father is homozygous for the wt allele.

To further investigate the effect of these mutations on protein function of ILK we conducted functional experiments/assays.

We hypothesized that the mutations might have an effect on the sub-cellular localization of ILK (especially the p.Leu53Met). Further, we suggested that they might influence cytoskeleton structure, especially for the p.Arg317Gln variant. Therefore, we did an immunocytochemical co-staining for V5-tagged ILK and phalloidin (F-actin marker) in HEK293T and COS-7 cells (Figure 16). Wild type, p.Arg211Cys, and p.Arg317Gln were localized in the cytoplasm and no clear localization at focal adhesions could be shown. p.Leu53Met was not detectable in all in four independent transfections. No differences in F-actin staining could be observed for all mutant constructs compared to wild type.

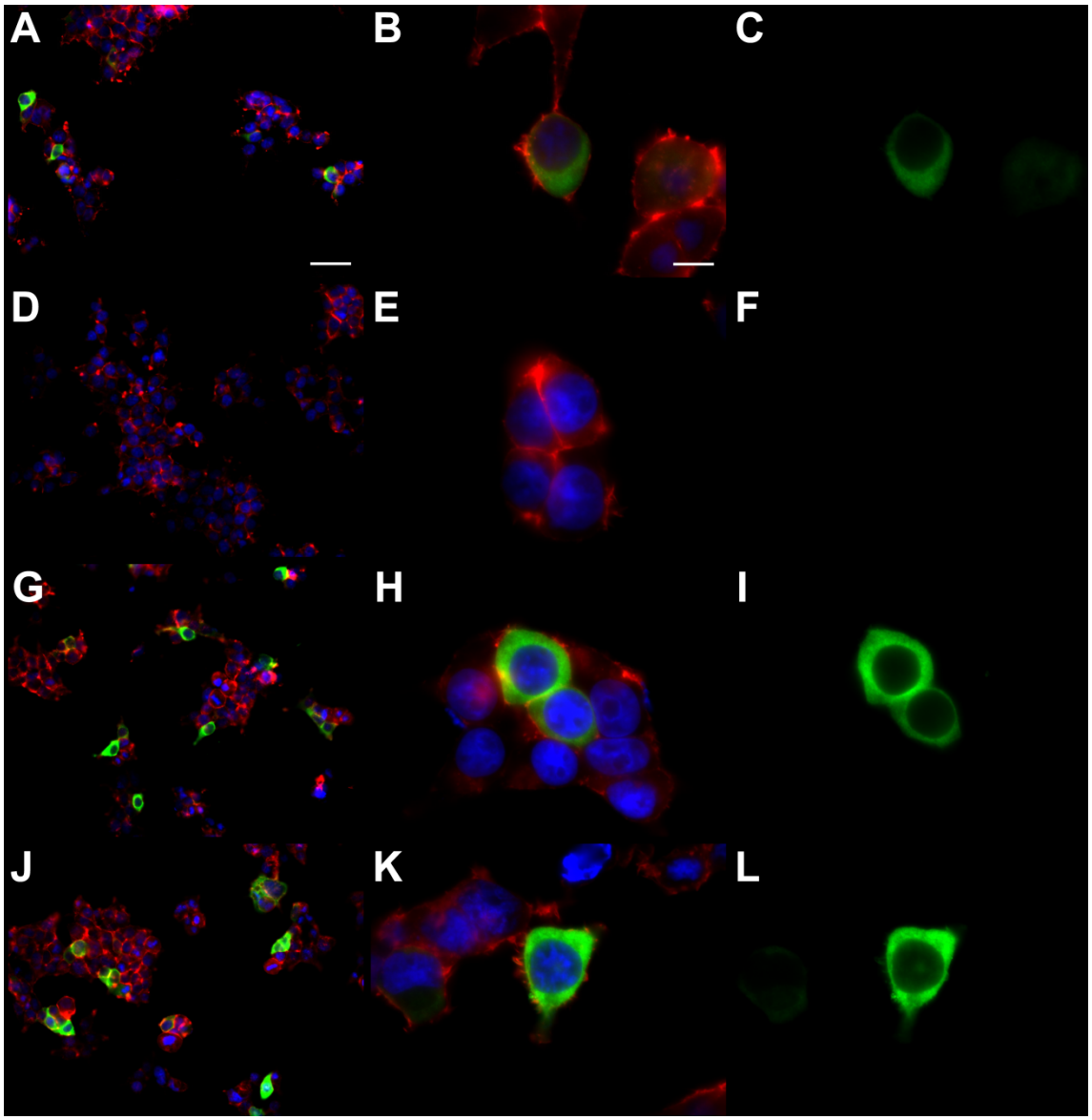

Figure 16: Sub-cellular localization of ILK. ILK wild type is localized in the cytoplasm (A-C), p.Leu53Met could not be detected (D-F), p.Arg211Cys (G-I), as well as p.Arg317Gln are localized in the cytoplasm (J-L). No differences in F-actin staining could be observed. Green: V5-tagged ILK, red: F-actin, blue: DAPI. Scale bar A, D, G, J 50µm, B, C, E, F, H, I, K, L 10 µm. Figure is adapted from Lea Sollfrank Master thesis 2011.

***ILK* has no effect on Wnt reporter assay**

ILK inhibits GSK3β, and therefore ILK might have an affect on Wnt signailing. To test if ILK affects Wnt signaling and whether ILK mutant isoforms abolish this effect we used the Wnt luciferase reporter assay to answer this question. However, we could not see an effect of neither wild type nor mutant ILK isoforms on Wnt reporter in transiently transfected HEK293T cells (Figure 17).

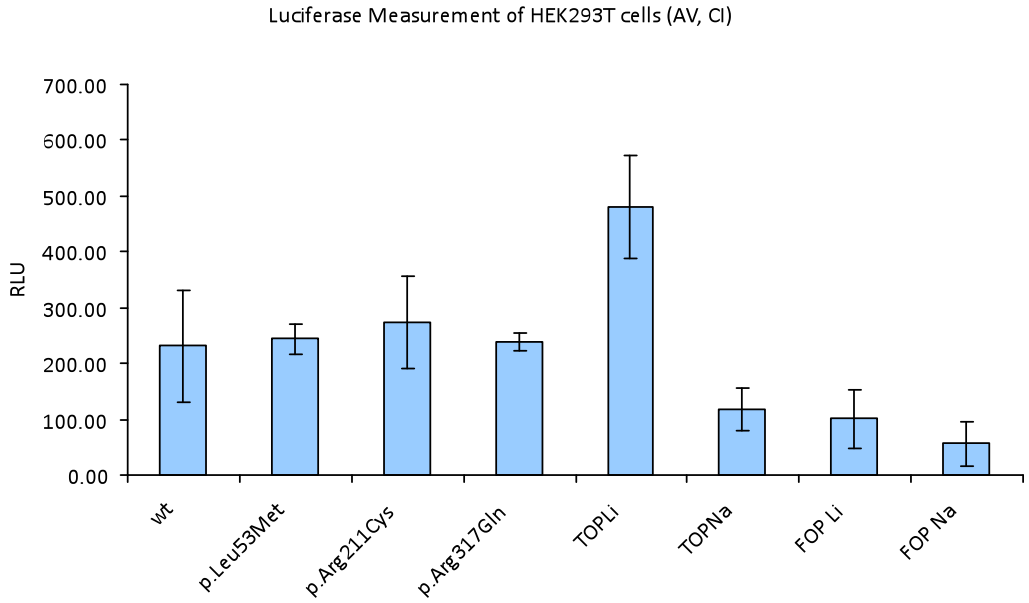

Figure17: Luciferase activity in response to ILK constructs in HEK293T cells. No significant effect of wild type or mutant ILK on Wnt reporter assay. Error bars represent the confidence interval (95%). RLU = Relative Luciferase Unit, AV = average, CI = confidence interval, n=3

We then examined whether endogenous ILK might already occupy all focal adhesion complexes and therefore the transfected ILK is not able to interact properly. Therefore, we tried to down regulate endogenous ILK in HEK293T using siRNA (Life Technologies, Zug, Switzerland), and overexpressed mouse ILK at the same time. Transfection effiecency was monitored using an EGFP (enhanced green fluorescence protein) plasmid (Figure 18).

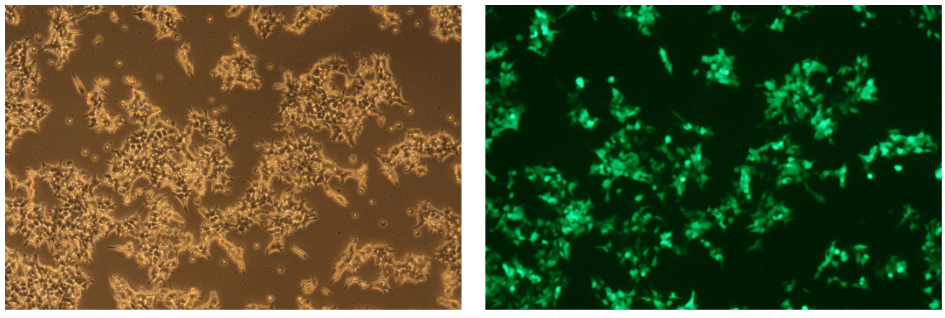

Figure 18: Transfection efficiency of eGFP in siRNA treated cells. HEK293T cells were transfected with GFP and siRNA against hILK using X-tremeGENE (Roche).

Also in this experiment we could not see any effect of wild type or mutant mouse ILK isoforms on Wnt reporter activity (data not shown). We then tested whether the siRNA knockdown is efficient and performed a RT-PCR for human ILK on HEK293T cells (Figure 19). No differences were observed between ILK specific siRNA (siRNA24 and siRNA43) and siRNA negative control

treated HEK293T cells. Thus the Prof. Ralf Adams group started to generate better siRNAs to knockdown endogenous ILK specifically.

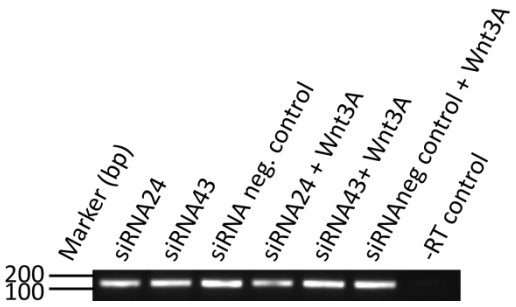

Figure 19: RT-PCR for hILK after siRNA transfection in HEK293T cells. Neither siRNA24 nor siRNA43 were efficient to knockdown endougenous hILK *in vitro*.

***ITGB3* - Sequence variants and the predicted effect on its function**

One missense mutation (p.Ala283Thr), two synonymous mutations and six intronic sequence alterations were found. The amino acid at position 283 is very well conserved throughout evolution and the exchange to a threonine is predicted to be deleterious by all prediction programs even though the physicochemical difference of the two amino acids is small. All intronic mutations are predicted to cause aberrant splicing. One mutation, which was detected twice, might lead to an extra branchpoint.

***PARVA* - Sequence variants and the predicted functional consequences**

Four synonymous mutations, three intronic mutations and two variants in the 3'UTR were found. All intronic mutations were predicted to cause aberrant splicing. One was predicted to generate a new splice donor site. The variants in the 3'UTR might have an effect on transcript stability.

Sequence variants in *SRF*, *MKL1*, and *MKL2* – and MAPK signaling molecules

***SRF* - Sequence variants and the predicted effects on the function**

One missense mutation (p.Thr239Ser) and three synonymous mutations were detected. The threonine at position 239 is highly conserved throughout evolution but the physicochemical difference between threonine and serine is small. The prediction programs revealed for this mutation contradictory results. PolyPhen predicted the mutation as possibly damaging, whereas SIFT and A-GVGD predicted the mutation as not deleterious.

***MKL1* - Sequence variants and the predicted effect on the function**

Seven missense mutations were detected. Three mutations (p.Ala567Thr, p.Ala569Thr, p.Pro574Ser) were predicted to be not deleterious by all three prediction programs. The prediction of the remaining mutations revealed contradictory results between the three programs. Three missense mutations p.Ser470Pro, p.Ala637Thr and p.Val668Ala are predicted to be deleterious by two prediction programs, whereas one program predicted these mutations as not deleterious. One mutation (p.Val575Met) is predicted to be deleterious by one prediction program, whereas the other two predict this mutation not to be deleterious. Only the amino acid at position 470 is highly conserved, all others are not 100% conserved. Three nucleotide variations were found in the 5'UTR and might influence the regulation of transcription or

translation. Further three synonymous mutations, four intronic variations and one variation in the 3'UTR were found. Some of them might affect splicing or transcript stability.

***MKL2* - Sequence variants and the predicted effect on the function**

Five missense mutations and two synonymous mutations were detected. The mutations at positions 122 and 328 (p.Glu122Asp, p.Arg328His) are predicted to be deleterious by all three prediction programs. The three mutations p.Pro254Arg, p.Val817Ile, p.Pro850Thr are predicted to be not deleterious by all three prediction programs. One sequence variation in the 5'UTR and six intronic variations were found.

3.2 New sequence variations in known disease causing genes

Beside the candidate genes, already known disease causing genes were sequenced. *NDP* was sequenced in a male patient with suspicion on Norrie disease. *TSPAN12* was sequenced in all the 208 individuals. In these two genes, eight sequence variations were found: Four missense muations, one synonymous mutation, one intronic mutation and two sequence variations in the 3'UTR. An overview is listed in table 37.

	Exon	Intron	3'UTR
NDP	1	0	0
TSPAN12	4	1	2

Table 37: Numbers of novel DNA sequence variations in genes, which are associated with retinal disorders.

***NDP* - Case history, clinical findings and genetic testing**

The index patient, a male infant was born on schedule (16th July 1990) after an inconspicuous pregnancy with normal birth weight. Postnatally, a retinopathy was diagnosed and the index patient was referred to a retinal specialist at the age of eleven months. In the right eye, an intraocular pressure of 25mm Hg, a cloudy cornea, vascular papillary membrane covering the papillary area, intraocular hemorrhages, total retinal detachment and subretinal hemorrhages were present. In the left eye, the cornea was sunken but clear, the papillary membrane was seen, old hemorrhages and old retinal detachment was seen, and subretinal hemorrhages were suspected. Open-sky vitrektomie was performed in the left eye at the age of eleven months, but the retina did not attach after surgery. In a follow up examination the cornea in the left eye was cloudy and total retinal detachment was suspected. At the age of three years phthisis bulbi in both eyes was evident. Beside this severe eye phenotype the proband also show some degenerative neuropathies such as mental retardation and seizures starting at the age of ten. So far no hearing loss is evident.

A new mutation (c.365A>T, p.Tyr122Phe) was found in exon 3 of the *NDP* gene. This mutation has not been described so far. It is the first time that this particular amino acid is affected in a Norrie Disease patient. The amino acid at position 122 is highly conserved throughout evolution. We also analyzed three other family members, the mother, the father and an unaffected brother of the index patient. The father and the brother do not have the mutation, whereas the mother seems to be a mosaic of this sequence variation in the *NDP* gene. We analyzed saliva from all four family members as well as blood from the mother. Currently we are analyzing whether the mother is a mosaic for the two *NDP* alelles by quantitative sequencing. To my knowledge no mosaic for sequence variations in the *NDP* gene has been described so far. This specific mutation has not been found in 400 control alleles.

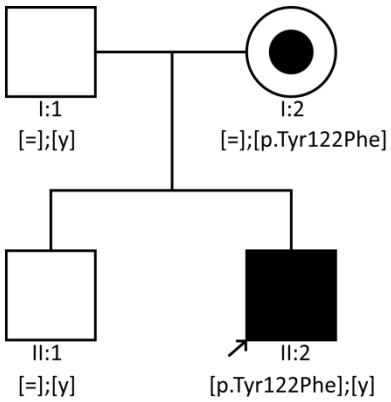

Figure 20: *NDP* family. A new mutation (p. Tyr122Phe) was identified in a male patient with a severe phenotype. The mother might be a mosaic for this mutation whereas the father and the son do not have the mutation.

TSPAN12

Four missense mutations, one intronic mutation and two variants in the 3'UTR were found. One missense mutation affects the translation initiation codon (p.Met1?) and is suspected to prevent translation initiation of TSPAN12. The second missense mutation (p.Leu10Gln) affects a highly conserved amino acid and this mutation is predicted to be deleterious by PolyPhen. The missense mutation (p.Met35Val) affects a moderately conserved amino acid and is predicted to be not deleterious by all prediction programs. The missense mutation (p.Ile103Val) affects a highly conserved amino acid and is predicted to be deleterious by tow prediction programs. The intronic mutation might influence splicing. The sequence variants in the 3'UTR, which were both found in the same patient, might affect transcript stability.

NDP								
Patient	**DNA variant**	**Protein variant**	**Location**	**PolyPhen**	**SIFT**	**A-GVGD**	**Effect**	**Zygosity**
70998	c.365A>T	p.Tyr122Phe	Exon 3	probably damaging (0.997)	not tolerated	Class C15	Misssense mutation	hemizygous
71075	c.365A>T	p.Tyr122Phe	Exon 3	probably damaging (0.997)	not tolerated	Class C15	Misssense mutation	ev. mosaic

TSPAN12								
Patient	**DNA variant**	**Protein variant**	**Location**	**PolyPhen**	**SIFT**	**A-GVGD**	**Effect**	**Zygosity**
70174	c.1A>G	p.Met1?	Exon 2	-	-	-	Startcodon affected	heterozygous
22439	c.29T>A	p.Leu10Gln	Exon 2	probably damaging (0.999)	tolerated	Class C0	Misssense mutation	heterozygous
70189	c.67-47A>G	p.?	Intron 2	-	-	-	Splicing	heterozygous
22439	c.103A>G	p.Met35Val	Exon 3	benign (0.000)	tolerated	Class C0	Misssense mutation	heterozygous
70231	c.307A>G	p.Ile103Val	Exon 5	possibly damaging (0.565)	not tolerated	Class C0	Misssense mutation	heterozygous
70138	c.*103 C>A	p.=	3'UTR	-	-	-	transcript regulation	heterozygous
70138	c.*104 C>A	p.=	3'UTR	-	-	-	transcript regulation	heterozygous

Table 38: New mutations identified in known disease causing genes.

3.3 Recombinant human Norrin – production, purification

Besides the screening of candidate genes involved in severe retinal dysplasia in humans and the identification of disease causing sequence variants, I am particularly interested in the function of Norrin. It seems that the Norrin protein is a very important protein in the early development of the eye but also in brain development and maintenance of the inner ear. A prerequisite to investigate the function of Norrin is the successful production and purification of recombinant Norrin protein. So far only a recombinant Norrin produced in an E. coli system is commercially available from R&D Bioscience. To ensure proper posttranslational modification and function of the recombinant Norrin we choose a mammalian expression system and included mutations, which are know to cause Norrie disease in humans as a negative control.

Generation of stably rhNorrin expressing cell lines

Human embryonic kidney (HEK293T) cells were stably transfected with wild type and four different disease-associated mutant Norrin expression constructs. Several clones for each Norrin isoform were isolated and further selected. Thus several mammalian cell line clones were established which express wild type rhNorrin or mutant rhNorrin proteins respectively. For each isoform twelve to eighteen clones were tested for rhNorrin expression and three of them, with the highest rhNorrin expression, were chosen for further selection and analysis.

Genotype verification of stably rhNorrin expressing cell lines

A cell pellet of each clone was harvested and DNA was extracted. Two pBudCE4.1 internal primers (CMV_pBud_for and MYC_pBud_rev) were used to amplify the insert of these vectors. PCR products were analysed on an agarose gel. For each cell line a specific band with the expected size was detected on an agarose gel. PCR products without insert was 192bp, and with insert 591bp long.

The same primers were used for sequencing of each insert. All mutations and the wild type sequence could be confirmed by direct sequencing (Figure 21).

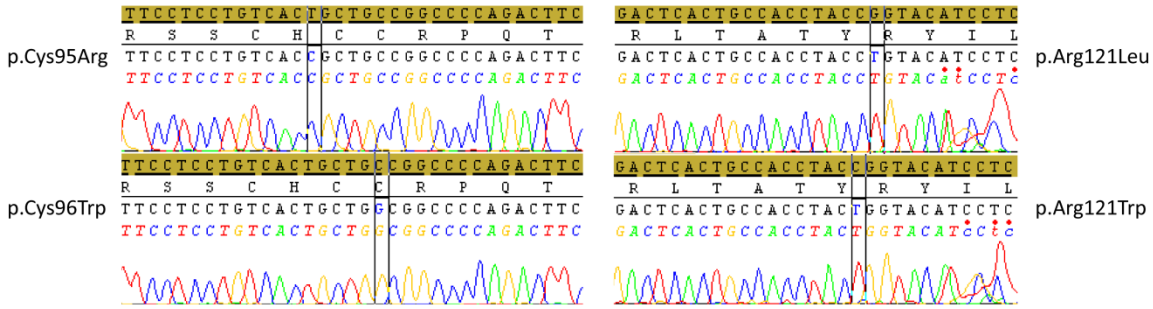

Figure 21: Sequences of mutant human Norrin in stably transfected HEK392T cells used in this work.

Examination of rhNorrin expression

rhNorrin has a predicted signal peptide and is supposed to be an extracellular protein. Therefore, cell culture supernatant was analyzed to see whether rhNorrin is secreted or not. Proteins in the supernatants of all cell lines were separated by SDS-PAGE, blotted on a PVDF membrane and probed with anti-myc antibody to verify that rhNorrin is expressed and secreted (Figure 22). The wild type protein was expressed and secreted at the highest level compared to the other genotypes.

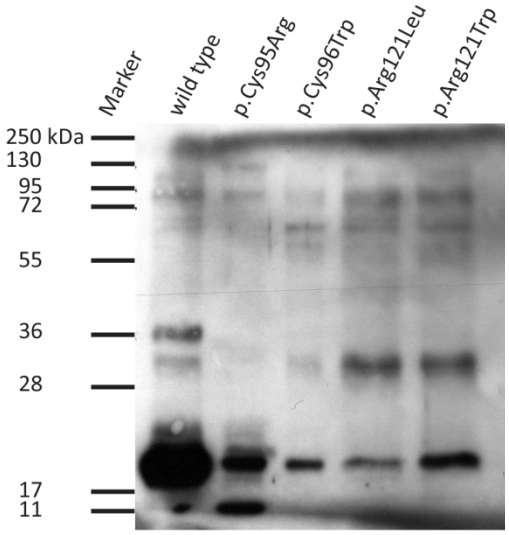

Figure 22: Western blot to examine expression and secretion of all rhNorrin isoforms by stable transfected HEK293T cells.

Recombinant protein production

Different approaches were used to produce rhNorrin in high amounts. Different cultivation devices as well as different media additives were used. The best result in respect to rhNorrin amount and purity was the production of rhNorrin using suspension-adapted cells. The reduced amount of FCS in the production medium simplifies purification of rhNorrin. Also higher cell densities could be reached compared to adherent cell cultivation. Cultivating suspension-adapted cells on an orbital shaker might further optimize this cultivation method, which helps to oxygenize the culture medium by agitation, and is routinely used in suspension cultivation nowadays. Suspension cell viability was monitored with trypan blue staining. In addition, the suspension adapted cell lines have to be resuspended from time to time to prevent cell clumping, the addition of heparin to the culture medium helps to minimize cell clumping as well. An example of a viable single cell suspension culture is given in figure 23.

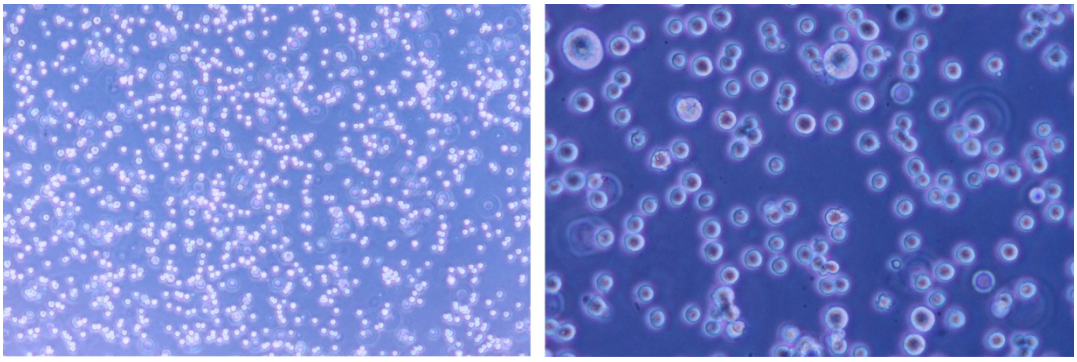

Figure 23: Trypan blue staining of suspension adapted HEK293T cells. Viable cells are white; trypan blue can not enter the cell as long as the cell membrane is intact. Magnification 5x, and 10x

Recombinant protein purification - IMAC

rhNorrin was purified from the supernatant of HEK293T cells stably expressing wild type or mutant rhNorrin. As a control, supernatant of a cell line stably transfected with empty pBudCE4.1 vector or mutant isoforms of rhNorrin were used. Initially, the Norrin constructs were designed to purifiy rhNorrin using the polyhistidine tag at the C-terminus with the immobilized metal affinity chromatography (IMAC)

technique. Cell culture supernatant was loaded on HisTrap FF crude columns (GE Healthcare) and eluted with increasing concentration of imidazole. With the IMAC purification approach and a simple single step purification protocol only low purity of rhNorrin was achieved. With increased amount of imidazole and NaCl in the binding buffer, only minor improvements in respect to purity were achieved. Therefore a two-step elution approach was established (Figure 24).

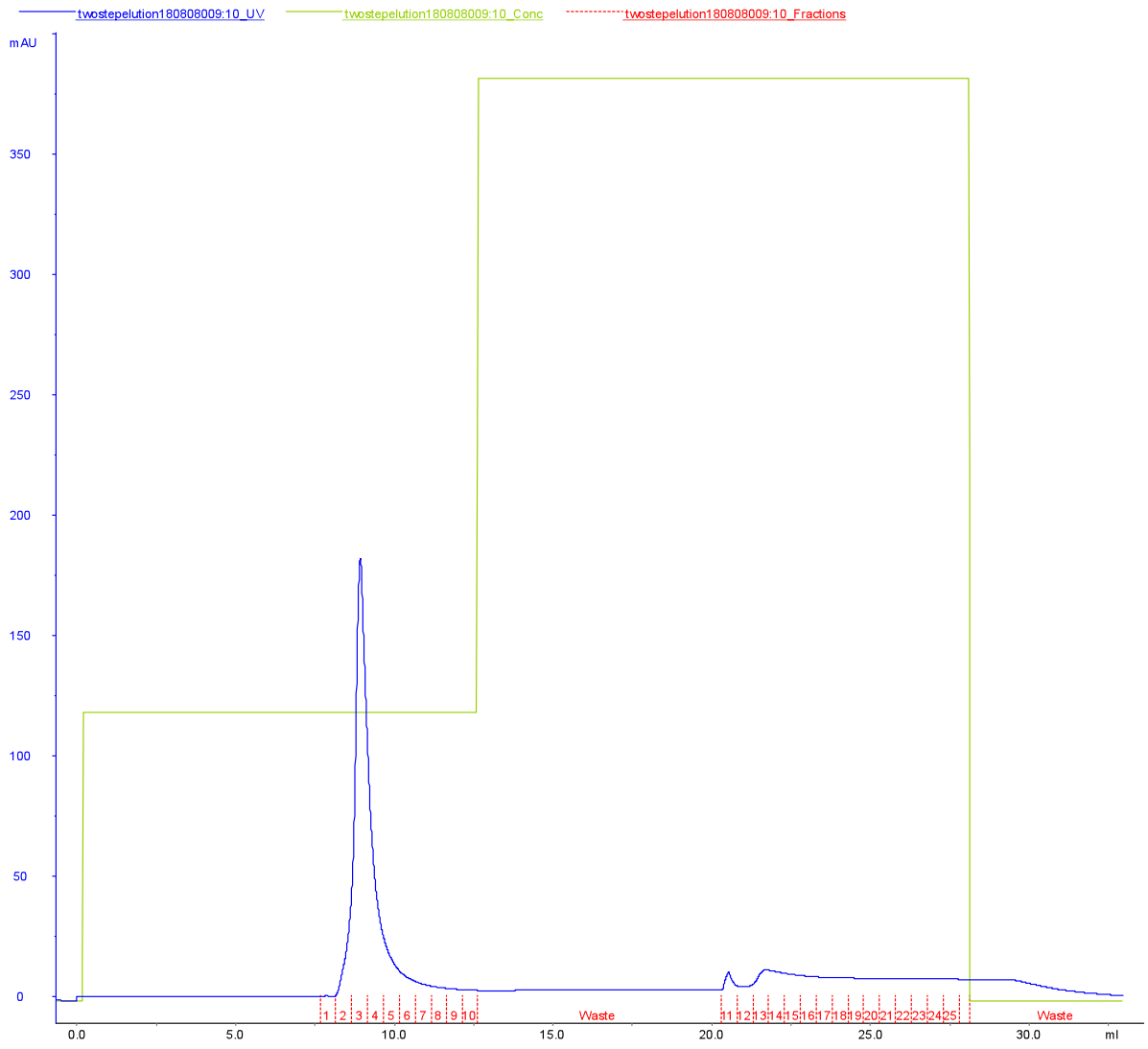

Figure 24: IMAC purification chromatogram. Two-step elution protocol. UV-A_{280} absorbtion (blue), concentration of elution buffer (green), fractions (red). x- axis: volume, y-axis: mAU

Western blot of purification fractions after separation on a 15% SDS-PAGE probed with anti-myc showed that column bound impurities were washed away by slightly increasing the imidazole concentration in the first step accepting a loss of rhNorrin at the same time (Figure 25). In a second purification step with substantial increased concentration of imidazole, higher purity of rhNorrin was achieved.

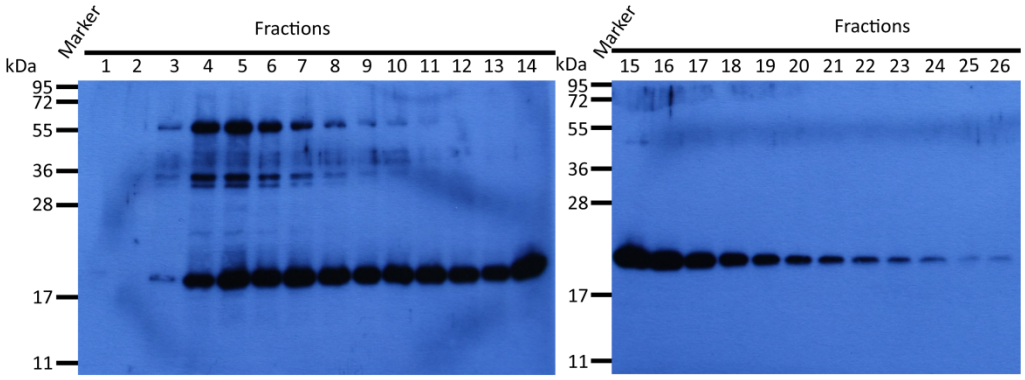

Figure 25: Western blot of IMAC purification. Using 1mL HisTrap FF crude columns and a two-step elution protocol.

The same purification protocol was applied for supernatant from p.Cys95Arg mutant rhNorrin expressing cells and mock transfected cells. The fractions of the second elution step were pooled and desalted by group filtration using two PD-10 columns in serie. Wild type and mutant rhNorrin were blotted and probed with anti-myc (Figure 26). Wild type rhNorrin was detected at the expected size of around 20kDa, whereas the majority of p.Cys95Arg mutant rhNorrin after purification was seen at around 14kDa and only minor amounts of three bands at 20kDa could be detected.

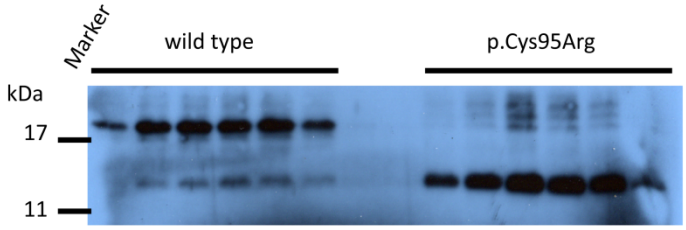

Figure 26: Western blot of IMAC purified and desalted rhNorrin. (wild type and p.Cys95Arg variant)

Recombinant protein purification - Heparin

Since it was possible to increase the amount of rhNorrin in the supernatant by adding heparin to the cell culture medium and due to the fact that similar growth factors like VEGF, FGF, and others are known to bind heparin sulfate proteoglycans (HSPG), which are structurally similar to heparin, I tried to purify rhNorrin using Heparin affinity chromatography. Cell culture supernatant was loaded on HiTrap Heparin HP columns (GE Healthcare) and eluted with a two-step elution protocol with increasing concentration of NaCl (Figure 27).

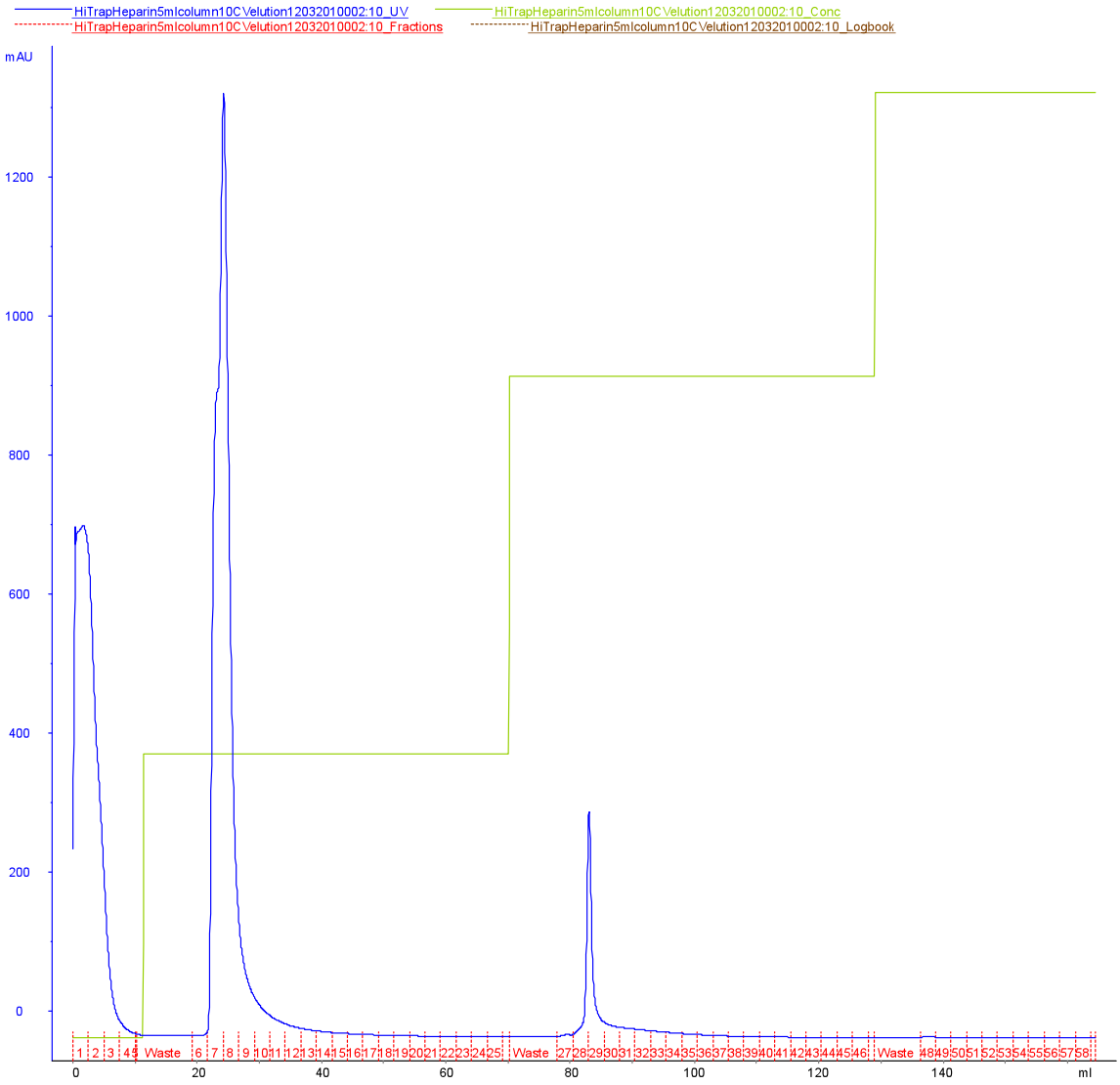

Figure 27: Heparin purification chromatogram. Two-step elution protocol. The third increase of elution buffer concentration is to wash out all impurities, which are still bound to the column. UV-A_{280} absorbtion (blue), concentration of elution buffer (green), fractions (red). x- axis: volume, y-axis: mAU

Western blot of Heparin purification fractions after separation on a 15% SDS-PAGE, probed with anti-myc antibody, revealed that most of the impurities were washed away from the column in the first purification step. Compared to the IMAC purification, less rhNorrin was lost in this step. The second purification step eluted high concentrations of rhNorrin in only six fractions (Figure 28).

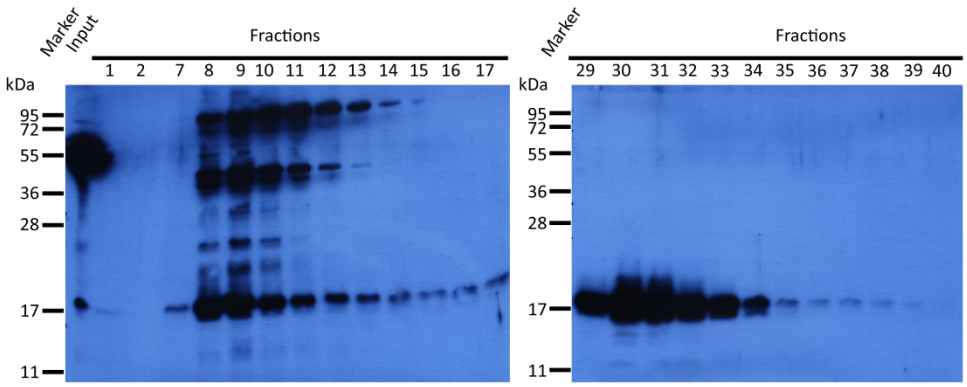

Figure 28: Western blot of Heparin purification. Using 1mL HiTrap Heparin HP columns and a two-step elution protocol.

The same purification protocol was applied for supernatant from mutant rhNorrin expressing cells and mock transfected cells. The fractions of the second elution step were pooled and desalted by group filtration using two PD-10 columns.

Mass spectrometric analysis of purified rhNorrin

To prove the identity of the detected protein on the Western blot, IMAC purified protein was separated with SDS-PAGE on a 15% gel and stained with silver nitrate. The band of the expected size of about 20 kDa was cut out of the silver-stained gel (Figure 29) and submitted for mass spectrometric analysis (Alphalyse, Denmark). The returned protein identification report confirmed the identity of rhNorrin (37% sequence coverage of the analyzed peptide to the Norrie disease protein). These analysis have been conducted during my Master thesis and have been repeated during the PhD thesis with the same result. rhNorrin was also send to FGCZ for MS analysis, data not shown.

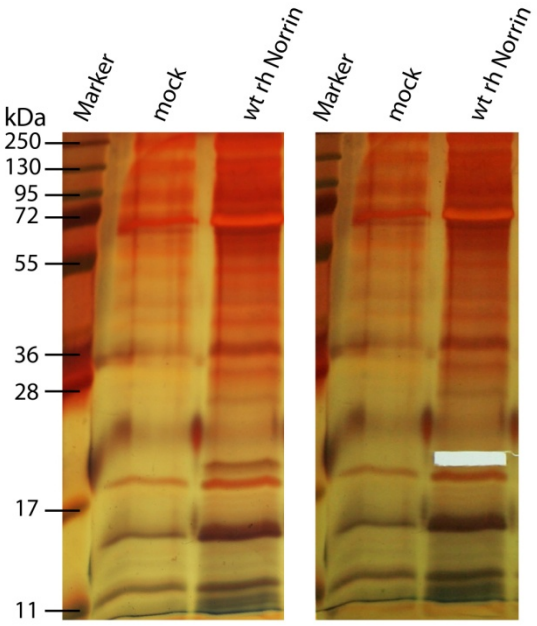

Figure 29: Silver-stained wild type rhNorrin, confirmed by mass spectrometry. Band with the expected size of wild type rhNorrin was cut out and submitted for mass spectrometric analysis (Alphalyse, Danmark).

Desalting of purified fractions and recovery rate of rhNorrin

After the elution of rhNorrin from the chromatography column, high salt or imidazole concentrations are present in the samples, which do have a toxic effect on endothelial cells in subsequent functional assays. To get rid of these substances, different methods were applied, including dialysis and group filtration (Figure 30). The best recovery rate of rhNorrin was achieved with PD-10 columns (GE Healthcare). Concentration of the sample is possible with ultrafiltration devices with a MWCO of 10kDa or less.

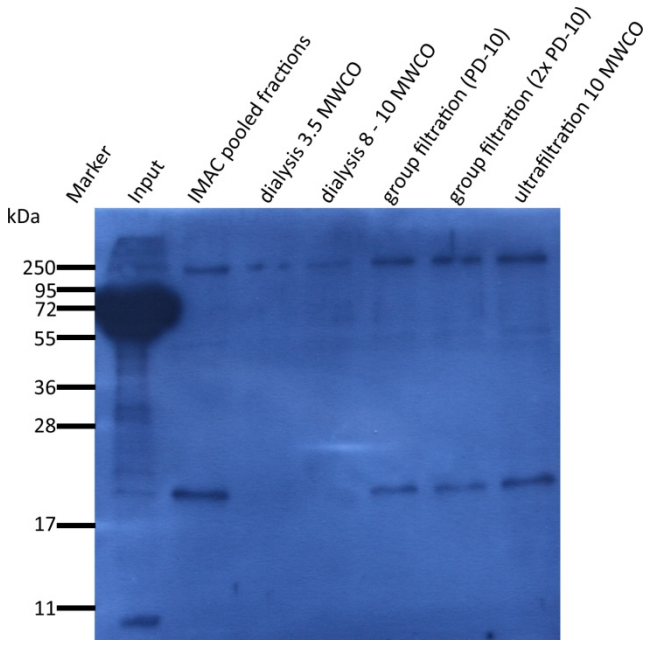

Figure 30: Western blot after desalting of purified fractions containing wt rhNorrin. Best recovery rate was achieved using PD-10 group separation columns.

Quantification of purified rhNorrin

To estimate the purity and the quantity of the purified and desalted rhNorrin, silver staining of SDS-PAGE was conducted with a dilution series of BSA for semi quantitative analysis of the purified rhNorrin. An example of silver-stained SDS-PAGE after single step IMAC purification is shown in figure 31.

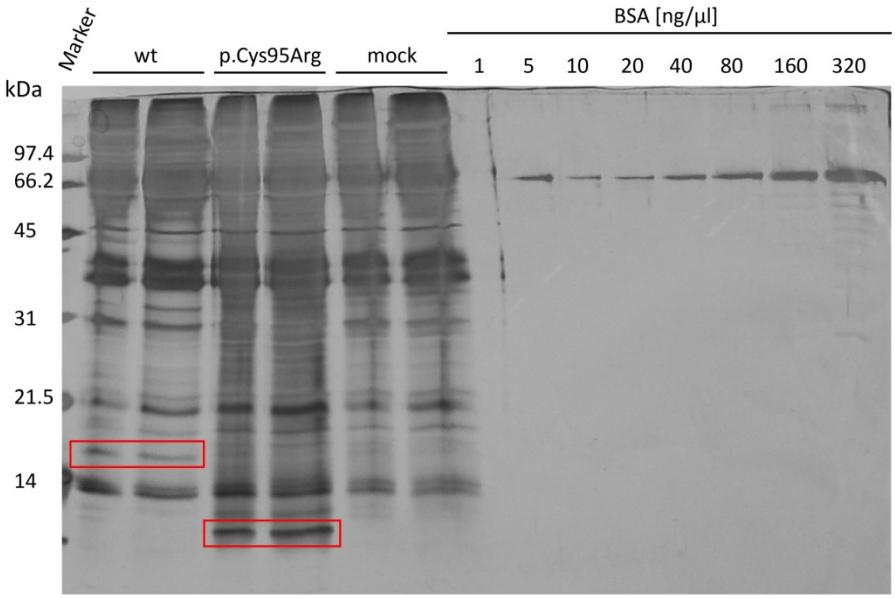

Figure 31: Silver staining of SDS-PAGE for semiquantitative analysis. Bands in red boxes were quantified.

Since the production of rhNorrin is dependent on the viability and the productivity of the cells and varies between different production batches, each batch of purified rhNorrin was analyzed by western blot and silver gel to estimate sample purity and quantities of rhNorrin.

3.4 Functional assays with rhNorrin

Purified rhNorrin has no effect on the proliferation of endothelial cells

Purified rhNorrin was applied on endothelial cells to test whether it has an effect on the proliferation and viability of endothelial cells *in vitro*. Equal amounts (20-100ng/µl) of wild type and mutant rhNorrin were added to HUVEC or HMEC-1 and incubated for 24-72h. Fresh rhNorrin was added every day. Proliferation of endothelial cells was measured with the WST-1 proliferation assay. No effect of rhNorrin on proliferation of endothelial cells could be detected (Figure 32). As a positive control endothelial cell culture medium was supplemented with FCS (ECM-2 complete medium was used). As a negative control, only ECM-2 basal medium without FCS and additional growth factors was used.

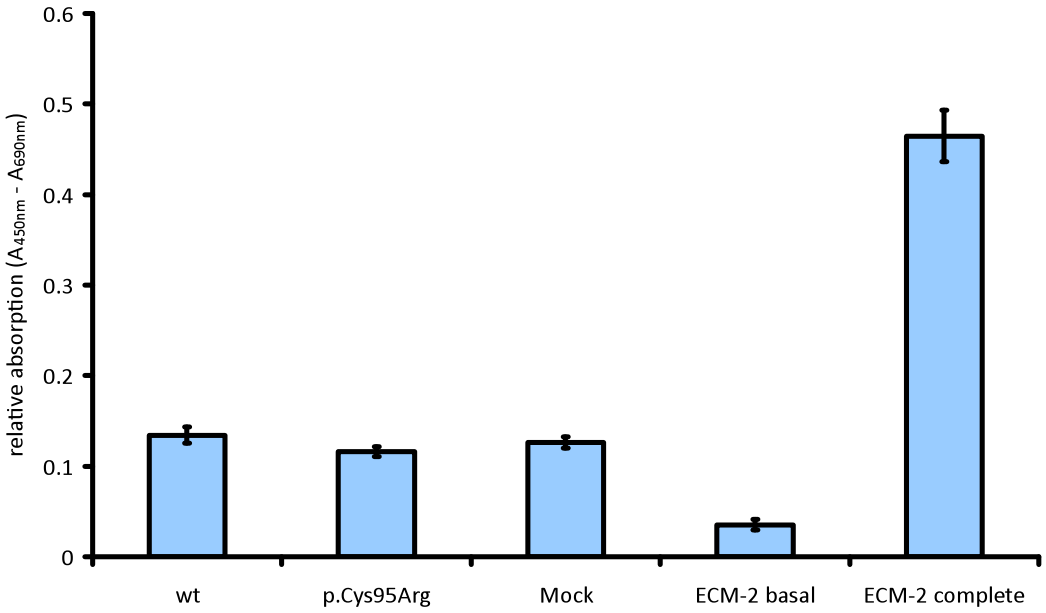

Figure 32: Purified rhNorrin has no effect on endothelial cells proliferation. HMEC-1 cells were treated with different isoforms of purified rhNorrin. Proliferation was measured using WST-1 assay. This graph shows the results of one representative experiment.

Purified rhNorrin has no effect on the migration of endothelial cells

In a second functional assay I tested the effect of purified rhNorrin on the migration of endothelial cells *in vitro*. Therefore I used the so called scratch or wound healing assay, which is a widely used and inexpensive assay to assess cell migration (Liang et al. 2007). A scratch is generated with a pipette tip in a monolayer of endothelial cells. The cells then start to migrate back into the scratch to close the gap. The area, which has become overgrown by the endothelial cells, was measured after 8 to 16 hours. In figure 33 a representative experiment is shown where the pictures were taken after creating the scratch (0h) and 24h later at the very same position of the scratch.

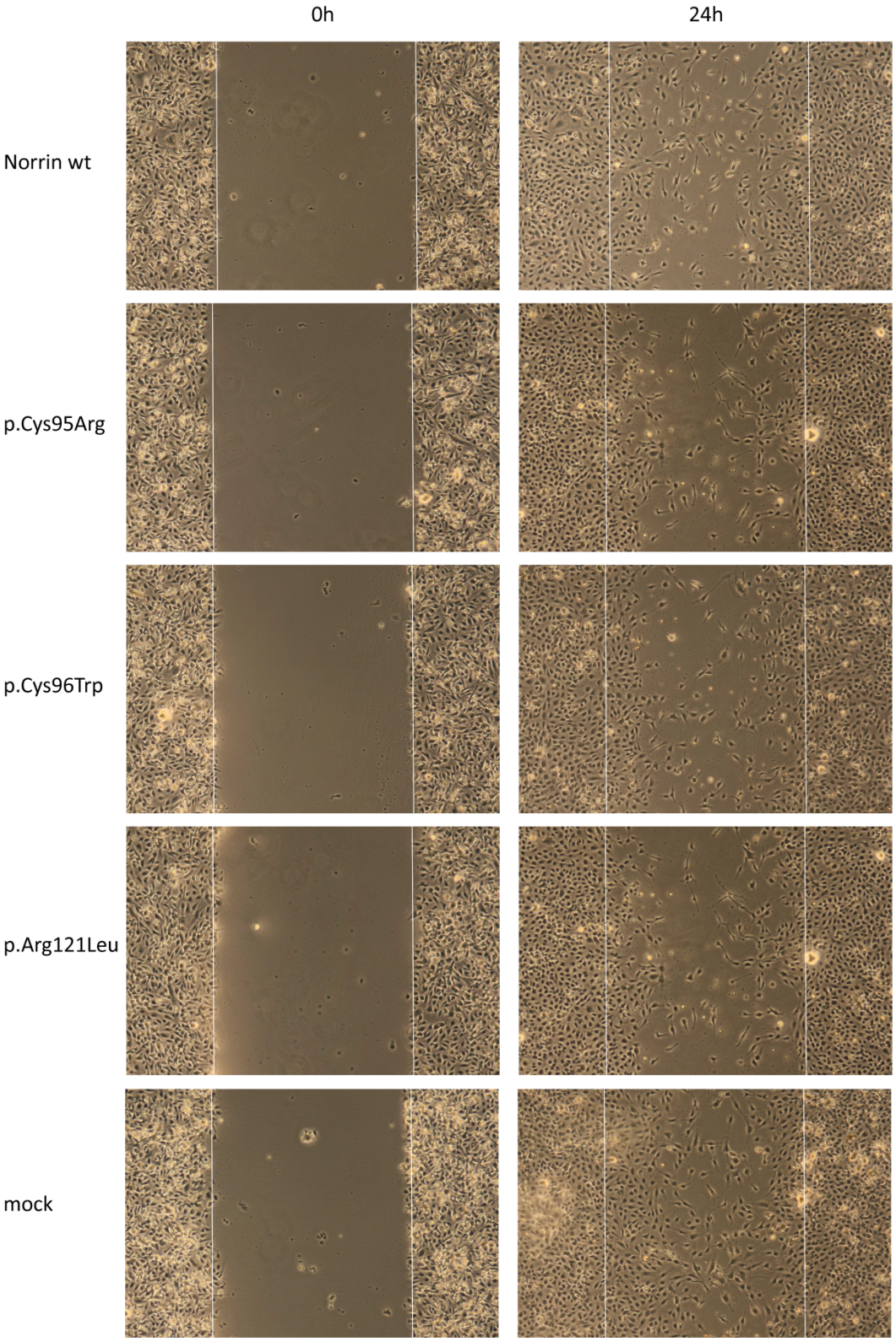

Figure 33: Purified rhNorrin has no effect on the migration of endothelial cells. Scratch assay using HMEC-1 cells and different purified rhNorrin isoforms.

The rate of migration was measured with two different methods. Either by counting the cells or measuring the area, which was reoccupied by endothelial cells after 24h. The area, which was

reoccupied by endothelial cells, was divided by the whole area of the initial scratch (marked by dotted lines). The scratch assay principally worked, but extensive tests of different rhNorrin batches could not show a difference of rhNorrin wild type and mutant isoforms on the migration of HUVEC or HMEC-1 cells. The quantitative analysis of a representative experiment is shown in figure 34.

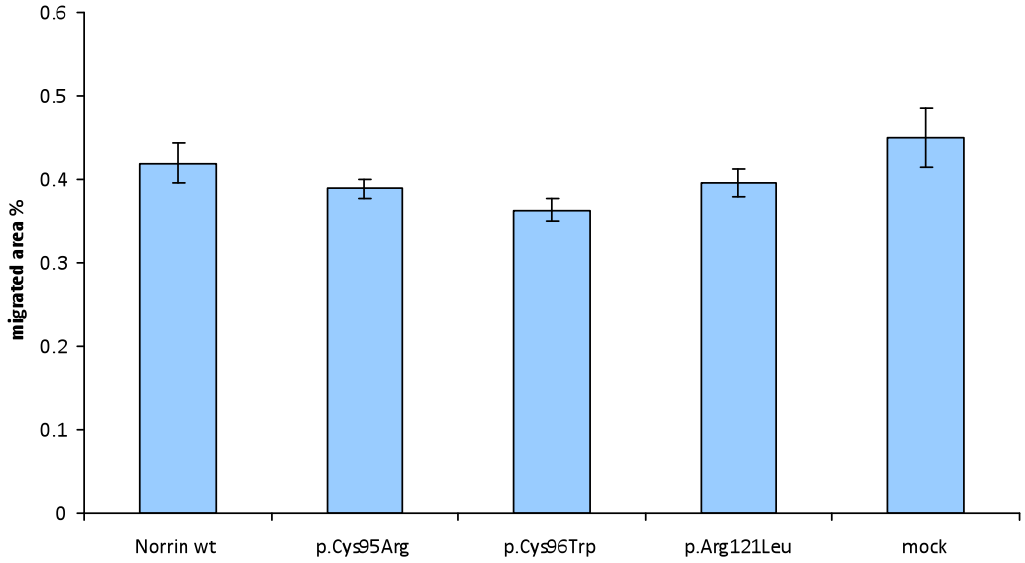

Figure 34: Quantitative analysis of endothelial cell migration. Measuring the area, which was reoccupied by endothelial cells after 24h upon protein addition**.**

Purified rhNorrin has no effect on the tube formation of endothelial cells

In a third functional assay I tested the effect of purified rhNorrin on tube formation of endothelial cells *in vitro*. Endothelial cells build a tubular-like network when they are grown on basement membrane matrix like matrigel (BD Bioscience). No differences on the tube formation of endothelail cells upon wild type rhNorrin and mutant rhNorrin isoforms was observed. As a positive control, EGF (100ng/µl) and FGF (100ng/µl) were used. No differences between wild type and mutant rhNorrin isoforms were seen in this assay. Pictures of a representative experiment are shown in figure 35.

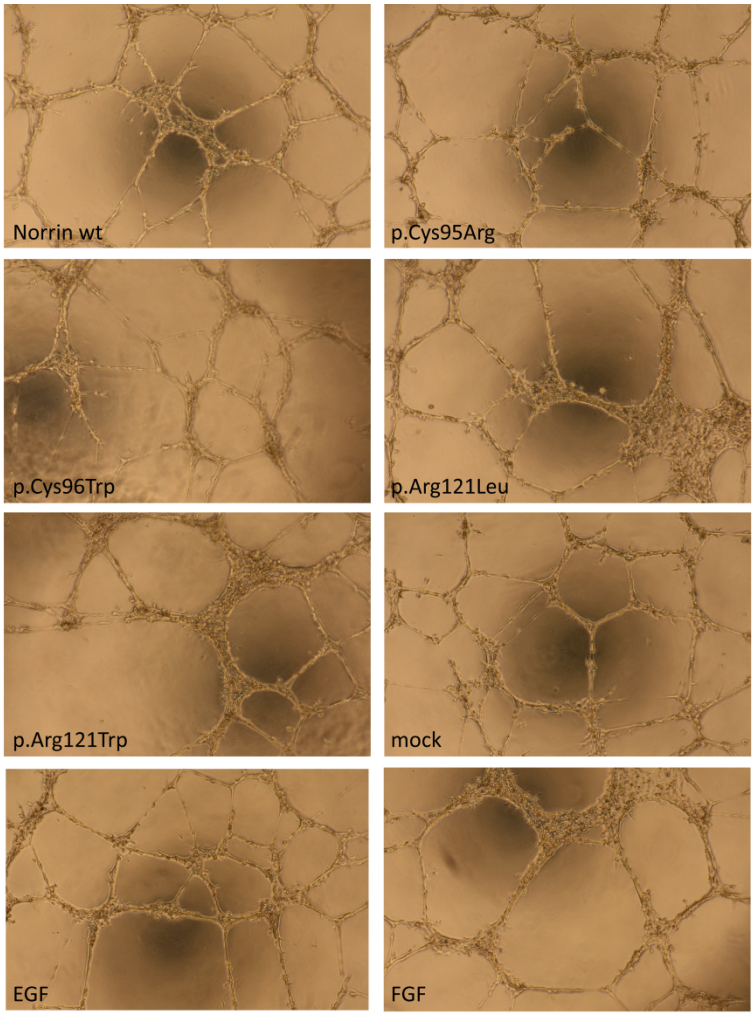

Figure 35: Tube formation assay. Purified rhNorrin has no effect on the tube formation of endothelial cells.

Establishment of 3D sprouting assay

In contrast to the other angiogenesis assays, this is a three-dimensional assay, which is supposed to mimic the *in vivo* situation better then the two-dimensional assays. In this assay the endothelial cells are grown on beads and endothelial sprouts can grow away from these beads. The length and number of sprouts can then be evaluated. To see the sprouts better, endothelial cells were stained with calcein AM. I established this angiogenesis assay using VEGF (1000ng/µl) as a positive controle but did not test rhNorrin in this assay.

Further biochemical characterization of rhNorrin

Norrin has been shown to be a secreted protein but conflicting results can be found in the literature regarding the association of Norrin with the extracellular matrix. Therefore one objective of this PhD thesis was to further elucidate the association of rhNorrin and the extracellular matrix.

Norrin might be bound to sulfated glycosaminoglycan chains of HSPGs

In our mammalian expression system rhNorrin is secreted into the cell culture supernatant, but the majority of rhNorrin is bound to the extracellular matrix. I suggested that Norrin might be bound to HSPG because similar secreted proteins like TGF-β, VEGF, and FGF can bind to HSPG as well (Whitelock and Iozzo 2005). To test this, three different experiments were performed. First, Heparin was added to the cell culture medium to compete with the heparan sulfate proteoglycans, produced by the cells. Heparin

is structurally similar to HSPG and can bind several growth factors as well. We could show that more soluble rhNorrin is present in the supernatant when heparin is added to the medium compared to medium without heparin (Figure 36A). Further we could show by western blot, when heparin is added to the medium in an increasing concentration, that the soluble amount of rhNorrin is increasing and the ECM bound amount is decreasing at the same time (Figure 36B).

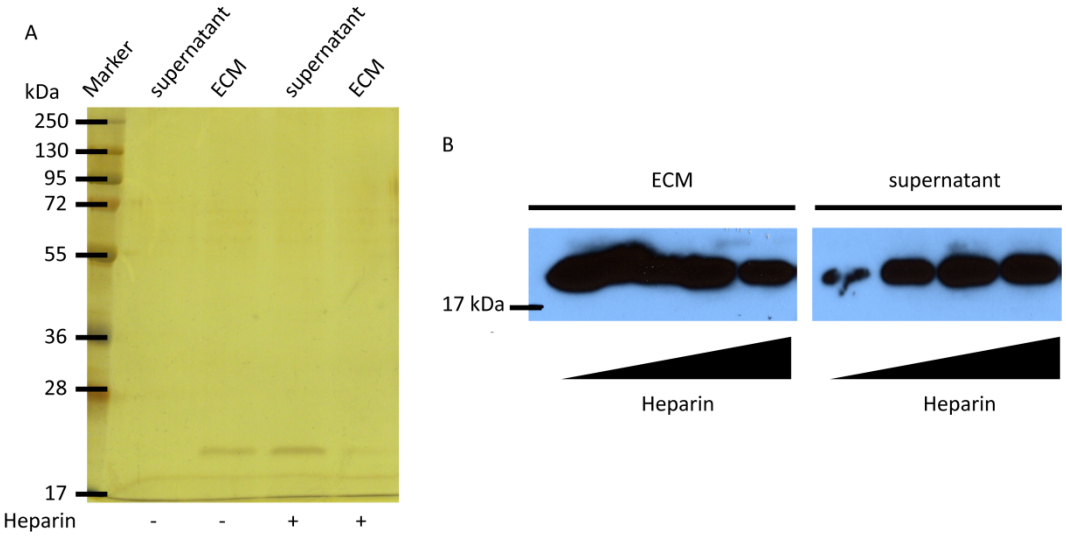

Figure 36: Norrins association with extracellular molecules. (A) Silver gel of rhNorrin. (B) Western blot of rhNorrin.

Second, enzymatic digestion of different extracellular molecules was performed to release rhNorrin into the supernatant. Only the digestion of heparan sulfate (HS), but not the digestion of chondroitin sulfate, (CS) released rhNorrin into the supernatant (Figure 37). In a third experimental approach, stably rhNorrin expressing cells were grown in sodium chlorate containing medium to inhibit sulfation of the glyosaminoglyan sidechains of proteoglycans (Safaiyan et al. 1999). With 20mM sodium chlorate in the cell culture medium it was possible to increase the soluble fraction of rhNorrin in the supernatant (Figure 37).

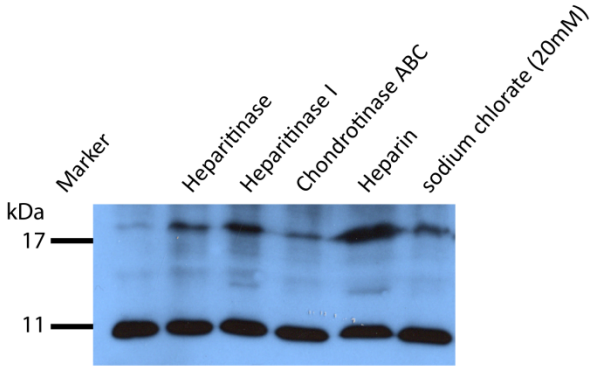

Figure 37: Norrins association with extracellular molecules. Western blot of supernatants derived from wild type rhNorrin expressing cells treated with indicated additives. Heparitinase, Heparintinase I, Heparin, and sodium chlorate release rhNorrin (~20kDa) from the ECM into the supernatant, which indicates that rhNorrin is bound to sulfated HSPG in HEKT293T cells. The band at 11kDa is unspecific.

All these experiments indicate the rhNorrin is bound to sulfated glycosaminoglycan sidechains of HSPGs. Whether the C-terminal polyhistidine tag in the rhNorrin construct has an influence on the association of

rhNorrin with the ECM could not be evaluated. To do so, these experiments should be repeated using a construct without polyhistidine tag.

Posttranslational modification of rhNorrin

We compared a commercially available rhNorrin (R&D Systems, Minneapolis, USA), which is produced in E. coli, and our rhNorrin derived from a mammalian system. A difference in size of about 4kDa was detected by silverstaing (Figure 38).

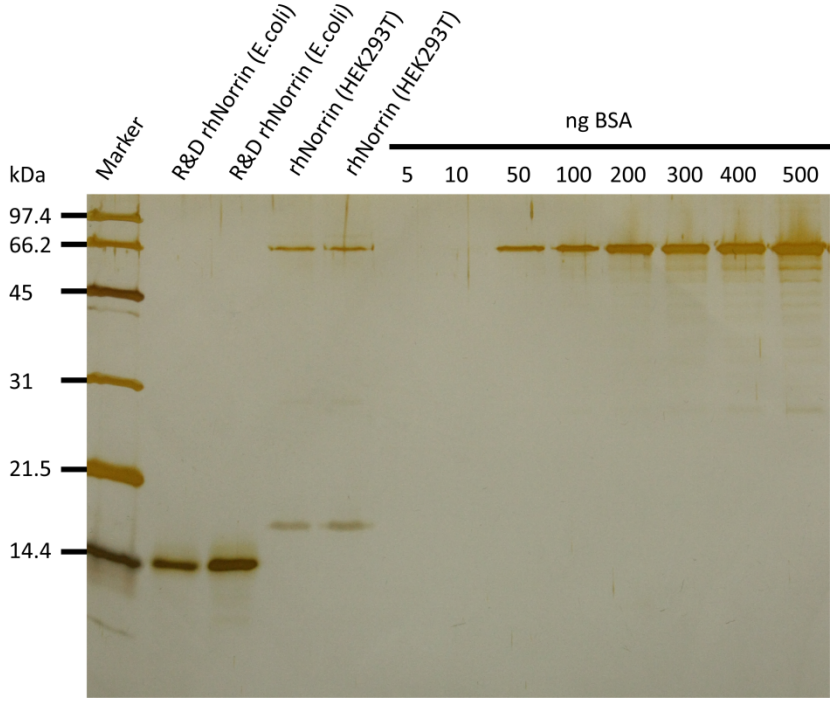

Figure 38: Silverstaining of rhNorrin. rhNorrin produced in a E. coli and in a mammalian system was compared on a silvergel.

Whether this difference derives from posttranslational modification (PM) of rhNorrin in the mammalian system remains to be elucidated. There are two potential PM for rhNorrin, O-glycosylation and lipide modification. No N-glycosylation sites were predicted in Norrin. Both O-glycosylation and palmytylation of rhNorrin have been tested but since no positive control was available in both experiments, no concluding result could be obtained. O-glycosylation of rhNorrin was investigated using O-glycosidase (Roche) and palmytylation was investigated using a Triton X-100 phase separation assay (Willert et al. 2003).

3.5 Ligand Receptor Capturing on living cells

To investigate whether Norrin can bind additional receptors beside FZD4, LRP5, and TSPAN12 we used the ligand-based receptor-capture (LRC) technology, which was developed by Andreas Frei and colleagues at the ETH Zurich. I worked with him on this project during the time the technology was developed at the ETH, recently they published the successful establishment of the method (Frei et al. 2012). Briefly, they developed a novel trifunctional reagent called “Triceps”. One function of this molecule is that it can be non-specifically coupled to primary amines of lysine side chains in any protein of interest. Then the ligand-Triceps complex is allowed to bind cell surface receptors. The second

function is the ability to capture aldehydes on the surface of living cells, which can be introduced into the carbohydrates of cell surface glycoproteins through exposure of cells to an oxidizing reagent. This is done after the ligand-Triceps complex has bound to the receptor. Therefore, it is possible to link the receptor to the ligand over the Triceps molecule. After the receptor-capture reaction, the cells are lysed and enzymatically digested with trypsin, and Triceps-labeled peptides are isolated using streptavidin beads. The ability to be purified is the third essential feature of Triceps. Subsequent analysis with mass spectrometry allows the identification of ligand receptor complexes. Unfortunately, a first attempt of a positive control experiment using rhNorrin and FZD4, LRP5 cotransfected HEK293T cells was not sucessfull in capturing the transfected known receptors. Since the known receptors could not be identified, we did not repeate the experiment with endothelial cells or other target cell.

4. Discussion

4.1 Variability of the human genome and potential consequences

Two independent groups released a first draft of the human genome sequence in 2001 (Lander et al. 2001, Venter et al. 2001). Three years later, a high-quality human genome assembly representing 99% of the human nucleotide sequence was published (Collins et al. 2004). The human genome sequence available in 2004 was a consensus sequence from multiple individuals. This first human genome sequence had a major impact on the field of human genetics. The rapid development of new, faster, and cheaper sequencing technologies allowed the sequencing of more and more individual genomes, thus increasing data of human genome variation could be achieved. Therefore these new technologies contribute to a better understanding of the variations between single individual genomes and will ultimately lead us to the new era of personalized medicine. The 1000 Genome Project (The 1000 Genomes Project Consortium 2010), combines the sequence data of 2500 individuals to detect sequence variants with frequencies as low as 1%. This ambitious project is the next milestone in human genome research and thus we will better understand the individual uniqueness of our genome in the future.

The DNA sequence of any individual contains many sequence variations, including single nucleotide polymorphisms, which represent about 90% of all human DNA polymorphisms, but also small indels (insertions and deletions), and structural alterations like copy number variations (CNV). The combination of these variations makes each individual unique - this genetic variability is the basis of the phenotypic differences between individuals. Single nucleotide polymorphisms (SNP, pronounced “snip”) are DNA sequence variations, which occur when a single nucleotide (A, T, G, and C) is altered. SNPs can fall in the coding or non-coding region of a gene or are even located in intergenic regions. A sequence variant is called polymorphism as soon as the frequency in the population is 1% or more. Sequence variants in the coding region do not have necessarily an effect on the protein sequence. Due to the degeneracy, the redundancy of the genetic code, different codons encode for the same amino acid. These sequence variants are called synonymous single nucleotide polymorphisms (sSNP). Synonymous SNPs or silent mutations do not have an effect on the protein sequence, but they still might have an effect on the function of the gene. As it has been described for a synonymous variant in *IRGM* with susceptibility to Crohn's disease, which had allele-specific consequences on protein expression (Brest et al. 2011). A nucleotide exchange in the coding region of a gene can also lead to an exchange of an amino acid and is then called non-synonymous single nucleotide polymorphism (nsSNP). A nsSNP that lead to a replacement of the naturally occurring amino acid with another amino acid and when it is pathogenic, it is called missense mutation. An exchange is called nonsense mutation when it results in a misplaced termination codon and lead to a truncated protein. Such an amino acid alteration has an influence on the function of a protein and is causative for a certain disease. Sequence variations in non-coding region of a gene can also have an influence on the gene product. Splicing of the respective gene can be affected, or when located in the regulatory sequences changes in gene expression or RNA stability can be the consequences. To interpret these individual sequence variations and to elucidate whether they play a role in the pathogenesis is difficult. This actually might be one of the biggest challenges of modern molecular genetics, to distinguish between neutral and disease causing sequence variations.

A part of this work was to look at DNA sequence variants located within the coding region and 50-100 bp of flanking intronic region of certain candidate genes for severe retinal dysplasia in more then 200

patients. Several sequence alterations in different candidate genes have been found during this work and functional effects thereof have been evaluated with different approaches.

4.2 Pathogenicity prediction - a combinatory approach of multiple methods

The best way to characterize individual sequence variations involves a combinatory approach of population genetics, computational approaches and experimental assays. The first step to identify disease causing sequence variations is to look at family members and to see whether a mutation co-segregates with the phenotype in the family. But often no family members are available for genetic testing or only a single family member is affected by the disease and no correlation can be drawn between disease and genetics. Further, it is important to check whether the sequence variation can be found in the general population, which might indicate its functional neutrality. It is estimated that every person harbors 200'000 nsSNPs (Cargill et al. 1999). Some sequence variations are so to say private and can only be found in one single family. Other variations are very rare and might have a frequency of less then 1% in the general population. But also more common variations are known which can be found with higher frequencies. Rare variants have long been underestimated in respect to their role in diseases.

In this work a combination of different approaches was used to assess functional consequences of each sequence variation. First, detected sequence variations were analyzed if they are synonymous or non-synonymous when they were located in the coding region. Missense mutations were further analyzed with three different *in silico* bioinformatic prediction algorithms including PolyPhen-2 (Adzhubei et al. 2010), SIFT (Ng and Henikoff 2001), and Align-GVGD (Mathe et al. 2006, Tavtigian et al. 2006) to predict potential deleterious effects of these substitutions (Table 36). The prediction results of the three different prediction programs have to be seen with care. These computational tools use certain algorithms, like evolutionary conservation or biophysical differences between amino acid to assess the possibility whether an amino acid exchange is pathogenic or not. The function of an amino acid in a protein can be rather difficult to be predicted by these computational approaches. Functional assays – where the effect of a mutation can be assessed experimentally – are often not available and have to be developed for most of the genes, which is laborious and time-consuming. Therefore, the computational approaches offer a cheap and straightforward method to predict the effect of a missense mutation. Nevertheless, they do not provide enough certainty to judge whether a single missense mutation is disease causing or not. For some genes, in which we have identified missense mutations functional studies were performed. I would like to discuss these genes in the following section grouped according to their functional properties.

4.3 Basic helix-loop-helix transcription factors and retinogenesis

The development of the retina is regulated by extrinsic and intrinsic factors. One group of these intrinsic factors are the proneural genes, which are expressed prior to neuronal differentiation in the retina. In one functional related group of transcription factors we found several mutations. The most prominent mutation was an in-frame deletion of almost the entire basic DNA binding domain in the *atonal homologe 7 (ATOH7)* gene. For the discussion regarding this mutation I refer to the manuscript. Beside the deletion we found an nsSNP three times in our cohort, which might be a risk allele for retinal dysplasia. In addition, we found a mutation in the 3'UTR that might affect ATOH7 RNA level. Since we do not have access to a patient cell-line, we could not further investigate the effect of this mutation

experimentally. In a second proneural gene (*NEUROD1)* an in-frame deletion of a single amino acid was found. Mutations in *NEUROD1* are associated with diabetes and neurological abnormalities similar to Norrie disease (Malecki et al. 1999, Rubio-Cabezas et al. 2010). It turned out that the individual in which we found the deletion in *NEUROD1* is a cousin of a Norrie male patient and is not affected. Whether the Norrie male cousin also has this deletion in *NEUROD1* could not be evaluated because we had no access to his DNA. NEUROD1 is implicated in early eye, ear and brain development and therefore might be a modifier gene for Norrie disease (Jahan et al. 2010, Liu et al. 2000). ATOH7 and NEUROD1 bind TCF3, another transcription factor which is also involved in Wnt signaling in the retina (Wu et al. 2012). Therefore, we established PCR to analyze the coding region of bHLH domain of TCF3 – so far the screening for this gene is outstanding. Other genes, which might be of interest to be screened for mutations, are *PAX6*, which is upstream of NEUROD1 and ATOH7 and also important for eye development. Other bHLH transcription factors of the atonal family, which are involved in the differentiation of retinal neurons might be interesting to be screened for mutations.

4.4 Adhesion of macrophages and endothelial cells

In the nerve injury induced protein 1 (NINJ1, Ninjurin1) we found one missense mutation near to the homophilic adhesion domain of this protein and two alterations in the 5'UTR that might affect transcriptional regulation. We tested the mutation in a localization assay using COS-7 cells and found a significant mis-localization of the mutant protein. To verify this observation, the localization experiment could be repeated in a human cell line like HEK293T. In addition, since the mutation was found heterozygous, a dominant-negative effect of the mutant NINJ1 could be considered due to its homophilic interaction, similar as it has been described for FZD4 (Kaykas et al. 2004). To further investigate the effect of the mutation we have identified, I suggest to use BV-2 cells in an adhesions assay. I organized BV-2 cells from Prof. Burkhard Becher's Group at the University of Zurich. So far these cells could not be transfect with PEI (Sigma-Aldrich), Ca^{2+}phosphate and X-treme reagent (Roche). I suggest trying lipofectamin (Life Technologies) which has been used successfully by other groups (Ahn et al. 2009). To further investigate the effect of the mutations in the 5'UTR which were both found in the same patient, the best would be to have a look at RNA level in a patient derived cell line (eg. skin fibroblast). But since these cells are not available, a luciferase reporter assay could be developed to see whether the mutations have an effect on the expression level of the reporter construct.

NINJ1 is a promising candidate gene for retinal vascular diseases since this protein has been linked to macrophage induced programmed cell death during early ocular development (Lee 2009). Further investigation might help to elucidate the functional relevance of the identified mutation. And it might be worthwhile to include other FEVR cohorts in the screening for NINJ1 mutations.

4.5 Extracellular signal transduction and cellular response to the ILK pathway

In *ILK* we found four missense mutations and four intronic mutations, which might affect splicing. The functional assays we performed to investigate *ILK* mutations are discussed in the following section.

We performed immunocytochemical stainings to see whether exogenous ILK can be localized at focal adhesions. But no clear, specific, and distinct stainings for the wt ILK protein was observed at focal adhesions. No differences between wt, p.Arg211Cys, and p.Arg317Gln variants were observed in the immunocytochemical stainings (Figure 16). This might be due to the fact that endogenous ILK is occupying all focal adhesion sites and the transiently expressed ILK is equally distributed in the

cytoplasm. Therefore this assay might not be suitable to test whether the mutations have an effect on protein localization or not. However, one ILK variant (p.Leu53Met) could not be detected by immunocytochemistry in four independent transfections. Since this variant has an alternative start codon, the N-terminal V5 tag is not fused to the protein when the alternative start codon is used to initiate translation. Therefore, we have cloned this variant in a vector with a C-terminal V5 tag and indeed we do see a signal of the C-terminal tagged p.Leu53Met ILK isoform in HEK293T cells. This is part of an ongoing internship by Sandra Dold. The mutation p.Arg317Gln affects the catalytic kinase domain of ILK. This domain interacts with α- and β-parvin as well as paxilin, all three proteins are connected to the actin cytoskeleton. Therefore the mutation might affect cytoskeleton organization in addition to catalytic kinase activity. We co-stained in the immunocytochemical assay with phalloidin, a marker for the cytoskeletal actin, and could not see any differences between this mutation and the wt ILK in the phalloidin staining. As mentioned before, the settings used in the immunocytochemical stainings might not be suitable for functional characterization of mutant ILK variants due to endogenous ILK that is occupying the focal adheision sites. Further, we could not observe any differences between p.Arg211Cys and the wt ILK, although it has been shown that a mutation at the same position (p.Arg211Ala) leads to a reduction in kinase activity (Persad et al. 2001). The p.Arg211Cys mutation was predicted to be deleterious by all prediction programs. It affects the PH-like domain, which binds to phosphatidylinositol-3,4,5-trisphosphate (PIP3) and is involved in the PI3K-Akt signaling pathway. Since ILK directly inhibits GSK3-beta by phosphorylation and thus stimulates nuclear localization of β-catenin and activation of the β-catenin-Lef-1 transcription factor (D'Amico et al. 2000, Delcommenne et al. 1998, Tan et al. 2001), we also looked whether the ILK mutations have an effect on Wnt signaling using the TCF/LEF luciferase reporter assay. But no differences between wt and mutant ILK has been observed in Wnt reporter assay (Figure 17).
In all these assays endogenous ILK might occupy the focal adhesion sites and therefore transfected ILK cannot access the places where it fulfills its function. We tried to knock down endogenous ILK with siRNA, to circumvent this problem, without any success so far.
Overall further investigations are necessary to investigate the functional relevance of the identified mutations. Several experiments are currently ongoing in the laboratory of Prof. Ralf Adams regarding functional analysis of *ILK* mutations. Especially Hiroyuki Yamamoto is working on this project; he is also doing some *in vivo* experiments using mouse and zebrafish.

Two other genes were screened, which are involved in the same molecular pathway: integrin beta 3 (*ITGB3*) and α-parvin (*PARVA*).
In *ITGB3* we found one missense mutation (p.Ala283Thr), which was predicted by all three programs as deleterious, that gives a high probability that this mutation has a functional effect. Regarding this mutation, no functional experiments have been performed so far. I suggest performing migration and/or adhesions assays. In addition we found six intronic mutations which all might affect splicing. Further functional experiments are required to elucidate the consequences of these identified variations.
In *PARVA* we did only find intronic and synonymous or silent mutations and two variations in the 3'UTR. Whether these sequence alterations have an effect on the function of PARVA was not assessed.

4.6 Vascular integrity might be altered by mutations in SRF, MKL1, and MKL2

We found 15 missense mutations in the coding region of these three genes, but also in the 5' and 3'UTRs we found some alterations, which might effect transcriptional or translational regulation, RNA stability or splicing. Further we found several synonymous substitutions and intronic sequence variations, some of them might affect splicing. In the *MKL1* gene we found 9 missense mutations, interestingly all of them located in exon 12. Thus we suggest that a functional domain is located in exon 12 of *MKL1*. There are several possibilities to test the functional relevance of these missense mutations. We do have a serum response element (SRE) lucifrease reporter construct which can be used to investigate the transcriptional activity of different SRF variants. Further, nuclear localization assays using immunocytochemical stainings or cell fractionation assays can be conducted. Overall this is an ongoing project, in which especially Britta Seebauer (PhD student in Prof. Wolfgang Bergers Lab) is involved in collabration with the Prof. Alfred Nordheims group (Department of Molecular Biology, University of Tuebingen). Functional consequences on splicing could be tested with a minigene approach and effects on transcript level could be assessed with reporter assays.

4.7 Differential diagnosis of ND

Beside FEVR, PFVS, ROP, and Coats' disease, the differential diagnosis of ND includes also bilateral retinoblastoma, endophthalmitis, and juvenile retinoschisis. If ND is considered, clinicians should be aware to look at X-linked inheritance pattern if family is available, lack of prematurity, bilaterality of the eye phenotype, and on extraocular findings, which can develop during childhood, adolescence or later in life. All these diseases have similar eye phenotypes and are difficult to distinguish. Overall I would like to stress that the clinical picture might be similar or quite divergent - also the genetic basis of these diseases might share some features but can also be very diverse. The development of the vertebrate eye is very complex and only little aberration can lead to distinctive developmental defects. To ensure a proper diagnosis genetical testing is essential.

4.8 Non-endothelial retinal cells and retinal vascular disesaes

The vertebrate retina is a highly organized and fragile structure. A proper interplay among different cell types is crucial for its faultless function. I would like to stress the function of different cell types in the retina, which might be implicated in retinal dysplasias.

Müller glia cells span from the ILM to the ELM, build a scaffold for blood vessels to grow into the deeper layers of the retina and are supposed to express Norrin (Stone et al. 1995, Ye et al. 2011). Further the play an important role to sustain neuronal homeostasis and ensure proper synaptic function by reabsorbing neurotransmitters (Bringmann et al. 2009). In mouse (Smith et al. 1994) and rat (Downie et al. 2007) Müller cells upregulate expression of GFAP in the avascular retina which is an indicator for gliosis and has been shown to be associated with neuronal degeneration and hypoxia (Eisenfeld et al. 1984, Smith et al. 1994). A defect in Müller cells, or mutant Norrin expressed by these cells, might lead to an avascular retina and cause gliosis.

Beside Müller cells, microglial cells, the macrophages of the CNS, play an important role during normal development of the retinal blood vessel system (Checchin et al. 2006, Ritter et al. 2006). Mis-regulation of microglia could influence proper retinal development on different levels. The invading microglia of myeloid origin could be disrupted which then leads to an under representation of microglia cells at the

paravascular space and might lead to inappropriate pruning and remodeling of the retinal vasculature. Further, mutations in FZD4 prevent paracrine WNT7b signaling suggesting a mechanism of Wnt ligands expressed by macrophages, which have an effect on FZD4 present on endothelial cells (Lobov et al. 2005). Endothelial cells and myeloid cells do not express Norrin but when Norrin is present in the extracellular space it might have the same effect as Wnt7b. It was shown that resident retinal myeloid cells express Wnt ligands and regulate blood vessel branching into deeper layers of the retina by non-canonical Wnt-Flt1 pathway (Stefater et al. 2011). Whether Norrin plays a role in this mechanism has to be investigated. Further, NINJ1 might be implicated in this process. NINJ1 might be crucial for the adherence of myeloid cells to the endothelial cells and could be essential for proper cell-cell interaction.
Further, exessive mural cell recruitment is evident in veins and capillaries of *Ndp*$^{y/-}$ mice, which might be due to the upregulation PDGFβ and PDGFRβ (Luhmann et al. 2005, Zuercher et al. 2012). This indicates that the retinal vessels in the superficial plexus rather appear as arterial vessels and venous identity is lost in *Ndp*$^{y/-}$ mice. Since sprouting occurs from veins, it might explain the inability of the SVP to sprout into depper plexi (Fruttiger 2007).
It is important to better understand the interplay among angiogenesis, neuronal development and glial response during the process of retinal development to understand the underlying pathophysiological mechanisms of retinal dysplasias including EVR, ROP, DR, and other retinal diseases.

4.9 Recombinant human Norrin (rhNorrin)

To obtain an unlimited amount of rhNorrin for structural and functional studies, I have been able to successfully produce the rhNorrin in a mammalian expression system. Stable gene expression technology has been chosen since up to 20-25 times higher productivity compared to transient gene expression approach has been suggested (Pham et al. 2006, Wurm 2004). To produce functional rhNorrin protein we chose a mammalian system to ensure proper posttranslational modification. Beside the wild type rhNorrin four diseases associated mutant rhNorrin isoforms were produced to ensure a proper negative control in functional assays and to further investigate mutation specific effects. These mutations could also be very helpful to further understand the structural properties of Norrin and how this small protein interacts with different binding partners.

Previous reports of rhNorrin

There are several reports in the literature about recombinant human Norrin. An N-terminal His-tagged rhNorrin protein produced in the baculovirus expression system was not secreted in the growth medium and the majority of the protein did not bind the purification column, which probably was due to insufficient cell lysis or inaccessible His tag (Shastry and Trese 2003). Perez Vilar and Hill used an eukaryotic system (COS-7) and could detect secreted C-terminal His-tagged rhNorrin only in the ECM but not in the cell culture supernatant (Perez-Vilar and Hill 1997). In contrast to the results from Perez Vilar and Hill, I was able to detect rhNorrin in both the ECM and the supernatant using HEK293T cells and a C-terminal tagged construct. Another group used HEK293T to produce a 3myc-Norrin and could also detect the recombinant protein in the supernatant and used heparin sepharose for the purification (Smallwood et al. 2007). The last report of rhNorrin used EBNA-HEK293T cell but exchanged the natural occurring signal peptide by an artificial one and could also detect secreted rhNorrin in the supernatant (Ohlmann et al. 2010). All different approaches revealed different sizes of recombinant human Norrin, which might be due to different posttranslational modifications in different expression systems. Whether our

rhNorrin is posttranslational modified by O-glycosylation or palmytylation or not, was investigated, but no clear result could be obtained, due to the lacking of a positive control. Thus, we cannot say whether these experiments worked properly and whether rhNorrin is modified or not.

Norrin is bound to ECM molecules

Norrin has a very high isoelectric point (pI 9.5) and a high density of cationic amino acid side chains (17 arginine or lysine residues in the mature polypeptide of 109 residues). This suggests a potential role of ionic interaction between Norrin and its binding partners. At physiological pH Norrin has a net positive charge and can bind negatively charged proteoglycans of the extracellular matrix. Heparin and heparan sulfate have strong anionic properties due to their sulfate groups and bind different proteins, which are similar to Norrin (Whitelock and Iozzo 2005). Heparan sulfate proteoglycans (HSPG) are described as extacellular binding molecules for growth factor like Wnt proteins, VEGF, FGF, TGF-beta (Houck et al. 1992, Mohammadi et al. 2005, Reichsman et al. 1996, Yayon et al. 1991). Perez-Vilar and Hill excluded the binding of Norrin to HSPG since they could not extract Norrin from the ECM by adding heparin or heparan sulfate to the cell culture medium. Further, they could not release Norrin from the ECM with heparinase I. The extraction of Norrin from the ECM was only successful with relatively harsh extraction buffer including 6M Guanidine hydrochloride (Perez-Vilar and Hill 1997). With our system, on the other hand, we could increase the amount of recombinant Norrin in the supernatant by adding heparin and we could show by enzymatic digestion of the ECM that Norrin is bound to HSPG. Similar to the results of two other groups (Ohlmann et al. 2010, Smallwood et al. 2007), both used Heparin sepharose to purify recombinant Norrin. In addition, Smallwood et al. showed a 10-fold increase of Norrin binding to a cystein-rich domain (CRD) upon heparin addition. Since our rhNorrin has a His-tag which might interfere with the binding to the ECM molecules we did not further investigate the ECM association of Norrin. To do so an untagged rhNorrin would be preferable.

Attempts to produce high amounts of rhNorrin

Unfortunately, we were not able to produce neither of the rhNorrin isoforms in a sufficient amount to conduct structural experiments. To enable a high concentration of rhNorrin several approaches were conducted including the expression of Norrin in different systems. Namely, in Pichia pastoris together with the Paul Scherrer Institute (PSI) and in a transient transfection approach together with the EPFL in Lausanne. But none of these attempts revealed significantly higher rhNorrin levels in the supernatant compared to our mammalian system.

Production and purification of rhNorrin

The production process has to be monitored precisely to ensure high cell viability and proper rhNorrin production. To eliminate unwanted impurities it is important to reduce as many impurities as possible from the beginning. HEK293T cells can be adapted to grow in medium with less or for a certain time even without any serum. These cells have to be adapted to grow in medium without serum over time otherwise the viability drops significantly. During low serum adaptation HEK cells round up and start to go in suspension, which allows a higher density of cells to be grown in one flask. The serum free adapted cells were grown in T-Flask without agitation. To improve oxygenation of this medium and cell viability, it would be important to agitate the flasks during the cultivation. A good starting material simplifies the

subsequent purification, more rhNorrin is available in less volume and fewer impurities have to be removed.
The purification of rhNorrin can be accomplished with different methods. In our approach we have a His-tag, which can be used to purify rhNorrin with IMAC. Alternatively, the heparin binding properties of Norrin can be used to purify untagged rhNorrin. Heparin purification should be preferred since less harsh elution conditions can be chosen. Heparin buffers might be better tolerated in the functional assays *in vitro* since no imidazole is present in these buffers. Nevertheless, a desalting step of elution fractions should be executed.

Norrins effect on endothelial cells

It has been shown that Norrin is a high affinity ligand for FZD4 and LRP5 and also binds TSPAN12. Upon binding to its receptors, Norrin triggers canonical Wnt signaling (Xu et al. 2004). The cell line we used for functional assays was tested by RT-PCR whether they express these receptors, which they do. However, we could not obtain any clear results regarding an effect of wild type rhNorrin compared to mutant rhNorrin isoforms in these functional assays. On the other hand, others could show an effect of rhNorrin on microvascular endothelial cells regarding proliferation, migration and tube formation (Ohlmann et al. 2010). This might be due to the different target cell or due to differences in the functionality of the different rhNorrins.

Norrin and neuronal differentiation

The expression of Norrin in astrocytes of the CNS and the subventricular zone (SVZ), which is a neurogenic region, indicates its involvment in embryonic neural stem cell differentiation (Doetsch 1999). Also other growth factors can act in a dual form in neuro- and angiogenesis, like recently shown VEGF3 (Calvo 2011). The inhibition of TGF-β family signaling directs commitment of embryonic stem cells to neuroectoderm lineages, resulting in the formation of embryonic neural stem cells. Embryonic neural stem cells differentiate into neurons and glia (astrocytes and oligodendrocytes) of the central nervous system. Norrin seems to play an important role in early neurectoderm induction (Xu et al. 2012). Norrin might have similar functions like chordin during neural induction and gastrulation. These two proteins might even have redundant activities. During neuronal tissue formation Wnt signaling pathways play different roles. At early blastula stages, canonical Wnt signaling is important for the formation of the dorsal-ventral axis formation via activation of Tcf3 (Schneider et al. 1996, Harland 2000, Heasman 2006). Later during neurula stage, it regulates neuronal differentiation via inhibition of NeuroD (Marcus et al. 1998). Further, the inhibition of Wnt signaling promotes neural differentiation in Xenopus, chicken and mouse ES cell (Glinka et al. 1998, Wilson and Edlund 2001, Aubert et al. 2002). Thus Norrin might be helpful to differentiate human embryonic stem cells to anterior neural ectoderm by inhibition of bone morphogenic protein (BMP) and Nodal/Activin signaling.

Acknowledgements

First of all, I am indebted to Prof. Wolfgang Berger, who gave me the opportunity to work in his lab. I thank him for his constant support and guidance throughout the whole duration of my thesis.

I would like to thank all the members of the Berger lab – colleagues who have become friends over the years. I truly enjoyed working with all of you and will always treasure this valuable experience.

Many thanks also to the Norrie-team: Dr. Ulrich Luhmann, who introduced me to the topic and helped me to come to terms in the lab. Dr. Nikolaus Schäfer, Dr. Jurian Zürcher, Britta Seebauer, Silke Feil for your constant support, technical assistance and helpful discussions.

Lea Sollfrank, who performed her Master thesis in the lab. It was a great year and personal enrichment working with you.

Dr. Sandra Brunner, Dr. Fabian Schmid, Dr. Istvan Magyar, Romain DaCosta, and Dr. Amit Tiwari for all the fertile discussions as well as your friendly support.

Dr. Barbara Kloeckener and PD Dr. John Neidhardt for many helpful discussions not only in lab meetings but also during experiments, lunchs or BBQs.

Esther Glaus, Mariana Wittmer, Jaya Balakrishnan for your readiness to help in every situation.

Furthermore, I would like to thank my collaborators for scientific exchange and discussions: In particular, Prof. Kathrine B. Sims for sharing of patient DNA which helped us advance our knowledge of the pathophysiology of Norrie disease.

Prof. Ralf Adams, Prof. Alfred Nordheim, Prof. Frans Cremers for the inspiring collaboration aiming at the elucidation of the molecular mechanisms of retinal diseases. Three very interesting projects were initiated by these excellent scientists.

Prof. Kurt Ballmer, Dr. Rolf Jaussi, and Dr. David Hacker for the collaboration which helped me to succesfully produce rhNorrin. I learned a lot from these experienced scientists.

Last but not least, I would like to thank my family and friends! My beloved wife, Vanessa, for your persistent encouragement, sympathy, love, and for always believing in me. My little son, Lias, for existing. You are truly the most wonderful creature all over the world. My parents, Wilma and Hans Peter, my brother, Jean Pierre, and my parents-in-law, Marc and Silvia, for your constant support and friendship. My friends for the constancy of your friendship.

Thank you very much indeed!

References

Adzhubei, I. A., Schmidt, S., Peshkin, L., Ramensky, V. E., Gerasimova, A., Bork, P., Kondrashov, A. S., and Sunyaev, S. R. (2010) A method and server for predicting damaging missense mutations. *Nature Methods*, **7**, 248-249.

Ahn, B. J., Lee, H. J., Shin, M. W., Choi, J. H., Jeong, J. W., and Kim, K. W. (2009) Ninjurin1 is expressed in myeloid cells and mediates endothelium adhesion in the brains of EAE rats. *Biochemical and Biophysical Research Communications*, **387**, 321-325.

Allen, R.C., Russell, S.R., Streb, L.M., Alsheikheh, A., and Stone, E.M. (2006) Phenotypic heterogeneity associated with a novel mutation (Gly112Glu) in the Norrie disease protein. *Eye*, **20**, 234-241.

Amasheh, S., Schmidt, T., Mahn, M., Florian, P., Mankertz, J., Tavalali, S., Gitter, A., Schulzke, J.D., and Fromm, M. (2005) Contribution of claudin-5 to barrier properties in tight junctions of epithelial cells. *Cell and Tissue Research*, **321**, 89-96.

Andersen, S.R., and Warburg, M. (1961) Norries Disease - Congenital Bilateral Pseudotumor of Retina with Recessive X-Chromosomal Inheritance - Preliminary Report. *Archives of Ophthalmology*, **66**, 614.

Angers, S. and Moon, R.T. (2009) Proximal events in Wnt signal transduction. Nature Reviews *Molecular Cell Biology*, **10**, 468-477.

Antonetti, D.A., Klein, R., and Gardner, T.W. (2012) Mechanisms of Disease Diabetic Retinopathy. *New England Journal of Medicine*, **366**, 1227-1239.

Araki, T. and Milbrandt, J. (1996) Ninjurin, a novel adhesion molecule, is induced by nerve injury and promotes axonal growth. *Neuron*, **17**, 353-361.

Araki, T., Zimonjic, D.B., Popescu, N.C., and Milbrandt, J. (1997) Mechanism of homophilic binding mediated by ninjurin, a novel widely expressed adhesion molecule. *Journal of Biological Chemistry*, **272**, 21373-21380.

Aubert, J., Dunstan, H., Chambers, I., and Smith, A. (2002) Functional gene screening in embryonic stem cells implicates Wnt antagonism in neural differentiation. *Nature Biotechnology*, **20**, 1240-1245.

Bakrania, P., Efthymiou, M., Klein, J.C., Salt, A., Bunyan, D.J., Wyatt, A., Ponting, C.P., Martin, A., Williams, S., Lindley, V., Gilmore, J., Restori, M., et al. (2008) Mutations in BMP4 cause eye, brain, and digit developmental anomalies: overlap between the BMP4 and hedgehog signaling pathways. *American Journal of Human Genetics*. **82**, 304-319.

Bergen, A.A.B., Wapenaar, M.C., Schuurman, E.J.M., Diergaarde, P.J., Lerach, H., Monaco, A.P., Bakker, E., Bleekerwagemakers, E.M., and Vanommen, G.J.B. (1993) Detection of A New Submicroscopic Norrie Disease Deletion Interval with A Novel Dna Probe Isolated by Differential Alu-Pcr Fingerprint Cloning. *Cytogenetics and Cell Genetics*, **62**, 231-235.

Berger, W., Kloeckener-Gruissem, B., and Neidhardt, J. (2010) The molecular basis of human retinal and vitreoretinal diseases. *Progress in Retinal and Eye Research*, **29**, 335-375.

Berger, W., Meindl, A., Vandepol, T.J.R., Cremers, F.P.M., Ropers, H.H., Doerner, C., Monaco, A., Bergen, A.A.B., Lebo, R., Warburg, M., Zergollern, L., Lorenz, et al. (1992a) Isolation of A Candidate Gene for Norrie Disease by Positional Cloning. *Nature Genetics*, **1**, 199-203.

Berger, W., Vandepol, D., Bachner, D., Oerlemans, F., Winkens, H., Hameister, H., Wieringa, B., Hendriks, W., and Ropers, H.H. (1996) An animal model for Norrie disease (ND): Gene targeting of the mouse ND gene. *Human Molecular Genetics*, **5**, 51-59.

Berger, W., Vandepol, D., Warburg, M., Gal, A., Bleekerwagemakers, L., Desilva, H., Meindl, A., Meitinger, T., Cremers, F., and Ropers, H.H. (1992b) Mutations in the Candidate Gene for Norrie Disease. *Human Molecular Genetics*, **1**, 461-465.

Bhanot, P., Brink, M., Samos, C.H., Hsieh, J.C., Wang, Y., Macke, J.P., Andrew, D., Nathans, J., and Nusse, R. (1996) A new member of the frizzled family from Drosophila functions as a Wingless receptor. *Nature*, **382**, 225-230.

Black, G.C.M., Perveen, R., Bonshek, R., Cahill, M., Clayton-Smith, J., Lloyd, I.C., and McLeod, D. (1999) Coats' disease of the retina (unilateral retinal telangiectasis) caused by somatic mutation in the NDP gene: a role for norrin in retinal angiogenesis. *Human Molecular Genetics*, **8**, 2031-2035.

Blanco, C.L., Baillargeon, J.G., Morrison, R.L., and Gong, A.K. (2006) Hyperglycemia in extremely low birth weight infants in a predominantly Hispanic population and related morbidities. *Journal of Perinatology*, **26**, 737-741.

Bleekerwagemakers, L.M., Friedrich, U., Gal, A., Wienker, T.F., Warburg, M., and Ropers, H.H. (1985) Close Linkage Between Norrie Disease, A Cloned Dna-Sequence from the Proximal Short Arm, and the Centromere of the X-Chromosome. *Human Genetics*, **71**, 211-214.

Brest, P., Lapaquette, P., Souidi, M., Lebrigand, K., Cesaro, A., Vouret-Craviari, V., Mari, B., Barbry, P., Mosnier, J. F., Hebuterne, X., Harel-Bellan, A., Mograbi, B., et al. (2011) A synonymous variant in IRGM alters a binding site for miR-196 and causes deregulation of IRGM-dependent xenophagy in Crohn's disease. *Nature Genetics*, **43**, 242-U24.

Bringmann, A., Pannicke, T., Biedermann, B., Francke, M., Iandiev, I., Grosche, J., Wiedemann, P., Albrecht, J., and Reichenbach, A. (2009) Role of retinal glial cells in neurotransmitter uptake and metabolism. *Neurochemistry International*, **54**, 143-160.

Cargill, M., Altshuler, D., Ireland, J., Sklar, P., Ardlie, K., Patil, N., Shaw, N., Lane, C.R., Lim, E.P., Kalyanaraman, N., Nemesh, J., Ziaugra, L., et al. (1999) Characterization of single-nucleotide polymorphisms in coding regions of human genes. *Nature Genetics*, **22**, 231-238.

Carson-Walter, E.B., Hampton, J., Shue, E., Geynisman, D.M., Pillai, P.K., Sathanoori, R., Madden, S.L., Hamilton, R.L., and Walter, K.A. (2005) Plasmalemmal vesicle associated protein-1 is a novel marker implicated in brain tumor angiogenesis. *Clinical Cancer Research*, **11**, 7643-7650.

Carterdawson, L.D., and Lavail, M.M. (1979) Rods and Cones in the Mouse Retina .2. Autoradiographic Analysis of Cell Generation Using Tritiated-Thymidine. *Journal of Comparative Neurology*, **188**, 263-272.

Caprara, C., and Grimm, C. (2012) From oxygen to erythropoietin: Relevance of hypoxia for retinal development, health and disease. *Progress in Retinal and Eye Research*, **31**, 89-119.

Cen, B., Selvaraj, A., Burgess, R. C., Hitzler, J. K., Ma, Z. G., Morris, S. W., and Prywes, R. (2003) Megakaryoblastic leukemia 1, a potent transcriptional coactivator for serum response factor (SRF), is required for serum induction of SRF target genes. *Molecular and Cellular Biology*, **23**, 6597-6608.

Cepko, C.L., Austin, C.P., Yang, X.J., and Alexiades, M. (1996) Cell fate determination in the vertebrate retina. *Proceedings of the National Academy of Sciences of the United States of America*, **93**, 589-595.

Chang, B., Smith, R S., Peters, M., Savinova, O.V., Hawes, N.L., Zabaleta, A., Nusinowitz, S., Martin, J. E., Davisson, M.L., Cepko, C.L., Hogan, B.L., and John, S.W. (2001) Haploinsufficient Bmp4 ocular phenotypes include anterior segment dysgenesis with elevated intraocular pressure. *BMC Genetics*, **2**, 18.

Chai, J.Y., Jones, M.K., and Tarnawski, A.S. (2004) Serum response factor is a critical requirment for VEGF signaling in endothelial cells and VEGF-induced angiogenesis. *Faseb Journal*, **18**, 1264.

Checchin, D., Sennlaub, F., Levavasseur, E., Leduc, M., and Chemtob, S. (2006) Potential role of microglia in retinal blood vessel formation. *Investigative Ophthalmology & Visual Science*, **47**, 3595-3602.

Chen, J., Stahl, A., Krah, N.M., Seaward, M.R., Joyal, J.S., Juan, A.M., Hatton, C.J., Aderman, C.M., Dennison, R.J., Willett, K.L., Sapieha, P., and Smith, L.E.H. (2012) Retinal Expression of Wnt-Pathway Mediated Genes in Low-Density Lipoprotein Receptor-Related Protein 5 (Lrp5) Knockout Mice. *Plos One*, **7**.

Chen, Z.Y., Hendriks, R.W., Jobling, M.A., Powell, J.F., Breakefield, X.O., Sims, K.B., and Craig, I.W. (1992) Isolation and Characterization of A Candidate Gene for Norrie Disease. *Nature Genetics*, **1**, 204-208.

Chynn, E.W., Walton, D.S., Hahn, L.B., and Dryja, T.P. (1996) Norrie disease - Diagnosis of a simplex case by DNA analysis. *Archives of Ophthalmology*, **114**, 1136-1138.

Clevers, H. (2006) Wnt/beta-catenin signaling in development and disease. *Cell*, **127**, 469-480.

Clevers H., and Nusse R. (2012) Wnt/β-catenin signaling and disease. *Cell,* **149**,1192-1205

Coats, G. (1908) Forms of retinal disease with massive exudation. *Roy London Ophthalmol Hosp Rep* **17**, 440-525.

Collins, F. S., Lander, E. S., Rogers, J., and Waterston, R. H. (2004) Finishing the euchromatic sequence of the human genome. *Nature*, **431**, 931-945.

D'Amico, M., Hulit, J., Amanatullah, D.F., Zafonte, B.T., Albanese, C., Bouzahzah, B., Fu, M.F., Augenlicht, L.H., Donehower, L.A., Takemaru, K.I., Moon, R.T., Davis, R., et al. (2000) The integrin-linked kinase regulates the cyclin D1 gene through glycogen synthase kinase 3 beta and cAMP-responsive element-binding protein-dependent pathways. *Journal of Biological Chemistry*, **275**, 32649-32657.

de La Chapelle, A., Sankila, E.M., Lindlof, M., Aula, P., and Norio, R. (1985) Norrie Disease Caused by A Gene Deletion Allowing Carrier Detection and Prenatal-Diagnosis. *Clinical Genetics*, **28**, 317-320.

Del Bene, F., Ettwiller, L., Skowronska-Krawczyk, D., Baier, H., Matter, J.M., Birney, E., and Wittbrodt, J. (2007) In vivo validation of a computationally predicted conserved Ath5 target gene set. *PLoS Genetics*, **3**, 1661-1671.

Delcommenne, M., Tan, C., Gray, V., Rue, L., Woodgett, J., and Dedhar, S. (1998) Phosphoinositide-3-OH kinase-dependent regulation of glycogen synthase kinase 3 and protein kinase B/AKT by the integrin-linked kinase. *Proceedings of the National Academy of Sciences of the United States of America*, **95**, 11211-11216.

Diazaraya, C.M., Provis, J.M., Penfold, P.L., and Billson, F.A. (1995) Development of Microglial Topography in Human Retina. *Journal of Comparative Neurology*, **363**, 53-68.

Dickinson, J.L., Sale, M.M., Passmore, A., FitzGerald, L.M., Wheatley, C.M., Burdon, K.P., Craig, J.E., Tengtrisorn, S., Carden, S.M., Maclean, H., and Mackey, D.A. (2006) Mutations in the NDP gene: contribution to Norrie disease, familial exudative vitreoretinopathy and retinopathy of prematurity. *Clinical and Experimental Ophthalmology*, **34**, 682-688.

Donnai, D., Mountford, R.C., and Read, A.P. (1988) Norrie Disease Resulting from A Gene Deletion - Clinical-Features and Dna Studies. *Journal of Medical Genetics*, **25**, 73-78.

Doetsch, F., Caillé, I., Lim, D.A., García-Verdugo, J.M., and Alvarez-Buylla, A. (1999) Subventricular zone astrocytes are neural stem cells in the adult mammalian brain. *Cell*, **97**, 703-716.

Downie, L. E., Pianta, M. J., Vingrys, A. J., Wilkinson-Berka, J. L., and Fletcher, E. L. (2007) Neuronal and glial cell changes are determined by retinal vascularization in retinopathy of prematurity. *Journal of Comparative Neurology*, **504**, 404-417..

Eisenfeld, A. J., Buntmilam, A. H., and Sarthy, P. V. (1984) Muller Cell Expression of Glial Fibrillary Acidic Protein After Genetic and Experimental Photoreceptor Degeneration in the Rat Retina. *Investigative Ophthalmology & Visual Science*, **25**, 1321-1328.

Ells, A., Guernsey, D.L., Wallace, K., Zheng, B.Y., Vincer, M., Allen, A., Ingram, A., DaSilva, O., Siebert, L., Sheidow, T., Beis, J., and Robitaille, J.M. (2010) Severe retinopathy of prematurity associated with FZD4 mutations. *Ophthalmic Genetics*, **31**, 37-43.

Ertl, T., Gyarmati, J., Gaal, V., and Szabo, I. (2006) Relationship between hyperglycemia and retinopathy of prematurity in very low birth weight infants. *Biology of the Neonate*, **89**, 56-59.

Farooqui, A.A. (1980) Purification of enzymes by heparin-sepharose affinity chromatography. *Journal of Chromatography*, **184**, 335–345.

Feng, Y.X., Wang, Y.M., Li, L., Wu, L.A., Hoffmann, S., Gretz, N., and Hammes, H.P. (2011) Gene Expression Profiling of Vasoregression in the Retina-Involvement of Microglial Cells. *Plos One*, **6**.

Fielding, A. B., Dobreva, I., and Dedhar, S. (2008) Beyond focal adhesions - Integrin-linked kinase associates with tubulin and regulates mitotic spindle organization. *Cell Cycle*, **7**, 1899-1906.

Franco, C. A., Mericskay, M., Parlakian, A., Gary-Bobo, G., Gao-Li, J., Paulin, D., Gustafsson, E., and Li, Z. L. (2008) Serum response factor is required for sprouting angiogenesis and vascular integrity. *Developmental Cell*, **15**, 448-461.

Friedrich, E. B., Liu, E., Sinha, S., Cook, S., Milstone, D. S., Macrae, C. A., Mariotti, M., Kuhlencordt, P. J., Force, T., Rosenzweig, A., St Arnaud, R., Dedhar, S., and Gerszten, R. E. (2004) Integrin-linked kinase

regulates endothelial cell survival and vascular development. *Molecular and Cellular Biology*, **24**, 8134-8144.

Friedrich, E. B., Sinha, S., Li, L., Dedhar, S., Force, T., Rosenzweig, A., and Gerszten, R. E. (2002) Role of integrin-linked kinase in leukocyte recruitment. *Journal of Biological Chemistry*, **277**, 16371-16375.

Frei, A.P., Jeon, O.Y., Kilcher, S., Moest, H., Henning, L.M., Jost, C., Plückthun, A., Mercer, J., Aebersold, R., Carreira, E.M., and Wollscheid, B. (2012) Direct identification of ligand-receptor interactions on living cells and tissues. *Nature Biotechnology*, **30**, 997-1001.

Fruttiger, M. (2007) Development of the retinal vasculature. *Angiogenesis*, **10,** 77-88.

Gal, A., Wieringa, B., Smeets, D.F.C.M., Bleekerwagemakers, L., and Ropers, H.H. (1986) Submicroscopic Interstitial Deletion of the X-Chromosome Explains A Complex Genetic Syndrome Dominated by Norrie Disease. *Cytogenetics and Cell Genetics*, **42**, 219-224.

Gilbert, C. (2008) Retinopathy of prematurity: A global perspective of the epidemics, population of babies at risk and implications for control. *Early Human Development*, **84**, 77-82.

Gineitis, D., and Treisman, R. (2001) Differential usage of signal transduction pathways defines two types of serum response factor target gene. *Journal of Biological Chemistry*, **276**, 24531-24539.

Glinka, A., Wu, W., Delius, H., Monaghan, A.P., Blumenstock, C., and Niehrs, C. (1998) Dickkopf-1 is a member of a new family of secreted proteins and functions in head induction. *Nature*, **391**, 357-362.

Goldberg, M.F. (1997) Persistent fetal vasculature (PFV): An integrated interpretation of signs and symptoms associated with persistent hyperplastic primary vitreous (PHPV) LIV Edward Jackson Memorial Lecture. *American Journal of Ophthalmology*, **124**, 587-626.

Gregory-Evans, K., Talks, S.J., Hykin, P., Adams, G., Yang, Y.F., Schulenberg, E., and Gregory-Evans, C.Y. (2001) De novo mutations in the 5 regulatory region of the Norrie's disease gene in retinopathy of prematurity in the UK. *Investigative Ophthalmology & Visual Science*, **42**, 682.

Ha, A., Perez-Iratxeta, C., Liu, H., Mears, A.J., and Wallace, V.A. (2012) Identification of Wnt/β-catenin modulated genes in the developing retina. *Molecular Vision*, **18**, 645-656.

Haddad, R., Font, R.L., and Reeser, F. (1978) Persistent hyperplastic primary vitreous: a clinicopathologic study of 62 cases and review of the literature. *Survey* of *Ophthalmology,* **23**, 123-124.

Hallmann, R., Mayer, D.N., Berg, E.L., Broermann, R., and Butcher, E.C. (1995) Novel Mouse Endothelial-Cell Surface Marker Is Suppressed During Differentiation of the Blood-Brain-Barrier. *Developmental Dynamics*, **202**, 325-332.

Halpin, C., Owen, G., Gutierez-Espeleta, G.A., Sims, K., and Rehm, H.L. (2005) Audiologic features of Norrie disease. *Annals of Otology Rhinology and Laryngology*, **114**, 533-538.

Halpin, C., and Sims, K. (2008) Twenty years of audiology in a patient with Norrie disease. *International Journal of Pediatric Otorhinolaryngology*, **72**, 1705-1710.

Harland, R. (2000) Neural induction. *Current Opinion in Genetics & Development*, **10**, 357-362.

Hartzer, M.K., Cheng, M., Liu, X., and Shastry, B.S. (1999) Localization of the Norrie disease gene mRNA by in situ hybridization. *Brain Research Bulletin*, **49**, 355-358.

Hayashi, H., Sano, H., Seo, S., and Kume, T. (2008) The Foxc2 transcription factor regulates angiogenesis via induction of integrin beta 3 expression. *Journal of Biological Chemistry*, **283**, 23791-23800.

Heasman, J. (2006) Patterning the early Xenopus embryo. *Development*, **133**, 1205-1217.

Hiraoka, M., Berinstein, D.M., Trese, M.T., and Shastry, B.S. (2001) Insertion and deletion mutations in the dinucleotide repeat region of the Norrie disease gene in patients with advanced retinopathy of prematurity. *Journal of Human Genetics*, **46**, 178-181.

Ho, B., and Bendeck, M.P. (2009) Integrin linked kinase (ILK) expression and function in vascular smooth muscle cells. *Cell Adhesion & Migration*, **3**, 174-176.

Hochuli, E., Dobeli, H., Schacher, A. (1987) New metal chelate adsorbent selective for proteins and peptides containing neighbouring histidine residues. *Journal of Chromatography*, **411**, 177–184.

Holt, C.E., Bertsch, T.W., Ellis, H.M., and Harris, W.A. (1988) Cellular Determination in the Xenopus Retina Is Independent of Lineage and Birth Date. *Neuron*, **1**, 15-26.

Holtz, M.L., and Misra, R.P. (2008) Endothelial-specific ablation of Serum Response Factor causes hemorrhaging, yolk sac vascular failure, and embryonic lethality. *Bmc Developmental Biology*, **8**, 65.

Houck, K.A., Leung, D.W., Rowland, A.M., Winer, J., and Ferrara, N. (1992) Dual Regulation of Vascular Endothelial Growth-Factor Bioavailability by Genetic and Proteolytic Mechanisms. *Journal of Biological Chemistry*, **267**, 26031-26037.

Hsieh, M., Boerboom, D., Shimada, M., Lo, Y., Parlow, A.F., Luhmann, U.F.O., Berger, W., and Richards, J.S. (2005) Mice null for Frizzled4 (Fzd4(-/-)) are infertile and exhibit impaired corpora lutea formation and function. *Biology of Reproduction*, **73**, 1135-1146.

Isaacs, N.W. (1995) Cystine Knots. *Current Opinion in Structural Biology*, **5**, 391-395.

Jahan, I., Kersigo, J., Pan, N., and Fritzsch, B. (2010) Neurod1 regulates survival and formation of connections in mouse ear and brain. *Cell and Tissue Research*, **341**, 95-110.

Jian, R., Longping, W., Xinjiao, G., Changjiang, J., Yu X., and Xuebiao, Y. (2008) CSS-Palm 2.0: an update software for palmitoylation sites prediction. *Protein Engineering, Design and Selection*, **21**, 639-644.

Jiao, X., Ventruto, V., Trese, M.T., Shastry, B.S., and Hejtmancik, J.F. (2004) Autosomal recessive familial exudative vitreoretinopathy is associated with mutations in LRP5. *American Journal of Human Genetics*, **75**, 878-884.

Junge, H.J., Yang, S., Burton, J.B., Paes, K., Shu, X., French, D.M., Costa, M., Rice, D.S., and Ye, W.L. (2009) TSPAN12 Regulates Retinal Vascular Development by Promoting Norrin- but Not Wnt-Induced FZD4/beta-Catenin Signaling. *Cell*, **139**, 299-311.

Kaloglu, C., Cesur, I., and Bulut, H.E. (2011) Norrin immunolocalization and its possible functions in rat endometrium during the estrus cycle and early pregnancy. *Development Growth & Differentiation*, **53**, 887-896.

Kaykas, A., Yang-Snyder, J., Heroux, M., Shah, K.V., Bouvier, M., and Moon, R.T. (2004) Mutant Frizzled 4 associated with vitreoretinopathy traps wild-type Frizzled in the endoplasmic reticulum by oligomerization. *Nature Cell Biology*, **6**, 2-13.

Kenyon, J.R., and Craig, I.W. (1999) Analysis of the 5 ' regulatory region of the human Norrie's disease gene: evidence that a non-translated CT dinucleotide repeat in exon one has a role in controlling expression. *Gene*, **227**, 181-188.

Knöll, B. and Nordheim, A. (2009) Functional versatility of transcription factors in the nervous system: the SRF paradigm. *Trends in Neurosciences*, **32**, 432-442.

Kogata, N., Tribe, R.M., Fassler, R., Way, M., and Adams, R.H. (2009) Integrin-linked kinase controls vascular wall formation by negatively regulating Rho/ROCK-mediated vascular smooth muscle cell contraction. *Genes & Development*, **23**, 2278-2283.

Kondo, H., Qin, M., Kusaka, S., Tahira, T., Hasebe, H., Hayashi, H., Uchio, E., and Hayashi, K. (2007) Novel mutations in Norrie disease gene in Japanese patients with Norrie disease and familial exudative vitreoretinopathy. *Investigative Ophthalmology & Visual Science*, **48**, 1276-1282.

Lander, E.S., Linton, L.M., Birren, B., Nusbaum, C., Zody, M.C., Baldwin, J., Devon, K., Dewar, K., Doyle, M., FitzHugh, W., Funke, R., et al. (2001) Initial sequencing and analysis of the human genome. *Nature*, **409**, 860-921.

Lee, H.J., Ahn, B.J., Shin, M.W., Choi, J.H., and Kim, K.W. (2010) Ninjurin1: a potential adhesion molecule and its role in inflammation and tissue remodeling. *Molecules and Cells*, **29**, 223-227.

Lee, H.J., Ahn, B.J., Shin, M.W., Jeong, J.W., Kim, J.H., and Kim, K.W. (2009) Ninjurin1 mediates macrophage-induced programmed cell death during early ocular development. *Cell Death and Differentiation*, **16**, 1395-1407.

Lev, D., Weigl, Y., Hasan, M., Gak, E., Davidovich, M., Vinkler, C., Leshinsky-Silver, E., Lerman-Sagie, T., and Watemberg,N. (2007) A novel missense mutation in the NDP gene in a child with Norrie disease and severe neurological involvement including infantile spasms. *American Journal of Medical Genetics Part A*, **143A**, 921-924.

Liang, C.C., Park, A.Y., and Guan, J.L. (2007) In vitro scratch assay: a convenient and inexpensive method for analysis of cell migration in vitro. *Nature Protocols*, **2**, 329-333.

Liebner, S., Corada, M., Bangsow, T., Babbage, J., Taddei, A., Czupalla, C.J., Reis, M., Felici, A., Wolburg, H., Fruttiger, M., Taketo, M.M., von Melchner, H., et al. (2008) Wnt/beta-catenin signaling controls development of the blood-brain barrier. *Journal of Cell Biology*, **183**, 409-417.

Lin, S., Cheng, M., Dailey, W., Drenser, K., and Chintala, S. (2009) Norrin attenuates protease-mediated death of transformed retinal ganglion cells. *Molecular Vision*, **15**, 26-37.

Ling, E.A., and Wong, W.C. (1993) The Origin and Nature of Ramified and Ameboid Microglia - A Historical Review and Current Concepts. *Glia*, **7**, 9-18.

Liu, M., Pereira, F.A., Price, S.D., Chu, M.J., Shope, C., Himes, D., Eatock, R.A., Brownell, W.E., Lysakowski, A., and Tsai, M.J. (2000) Essential role of BETA2/NeuroD1 in development of the vestibular and auditory systems. *Genes & Development*, **14**, 2839-2854.

Livesey, F.J., and Cepko, C.L. (2001) Vertebrate neural cell-fate determination: Lessons from the retina. *Nature Reviews Neuroscience*, **2**, 109-118.

Lobov, I.B., Rao, S., Carroll, T.J., Vallance, J.E., Ito, M., Ondr, J.K., Kurup, S., Glass, D.A., Patel, M.S., Shu, W.G., Morrisey, E.E., McMahon, A.P., et al. (2005) WNT7b mediates macrophage-induced programmed cell death in patterning of the vasculature. *Nature*, **437**, 417-421.

Logan, C.Y. and Nusse, R. (2004) The Wnt signaling pathway in development and disease. *Annual Review of Cell and Developmental Biology*, **20**, 781-810.

Luhmann, U.F.O., Lin, J.H., Acar, N., Lammel, S., Feil, S., Grimm, C., Seeliger, M.W., Hammes, H.P., and Berger, W. (2005a) Role of the Norrie disease pseudoglioma gene in sprouting angiogenesis during development of the retinal vasculature. *Investigative Ophthalmology & Visual Science*, **46**, 3372-3382.

Luhmann, U.F.O., Meunier, D., Shi, W., Luttges, A., Pfarrer, C., Fundele,R., and Berger, W. (2005b) Fetal loss in homozygous mutant norrie disease mice: A new role of norrin in reproduction. *Genesis*, **42**, 253-262.

Luhmann, U.F.O., Neidhardt, J., Kloeckener-Gruissem, B., Schafer, N.F., Glaus, E., Feil, S., and Berger, W. (2008) Vascular changes in the cerebellum of Norrin/Ndph knockout mice correlate with high expression of Norrin and Frizzled-4. *European Journal of Neuroscience*, **27**, 2619-2628.

Mack, C.P., and Hinson, J.S. (2005) Regulation of smooth muscle differentiation by the myocardin family of serum response factor co-factors. *Journal of Thrombosis and Haemostasis*, **3**, 1976-1984.

Malecki, M.T., Jhala, U.S., Antonellis, A., Fields, L., Doria, A., Orban, T., Saad, M., Warram, J.H., Montminy, M., and Krolewski, A.S. (1999) Mutations in NEUROD1 are associated with the development of type 2 diabetes mellitus. *Nature Genetics*, **23**, 323-328.

Marcus, E.A., Kintner, C., and Harris, W. (1998) The role of GSK3beta in regulating neuronal differentiation in Xenopus laevis. *Molecular and Cellular Neuroscience*, **12**, 269-280.

Massari, M.E. and Murre, C. (2000) Helix-loop-helix proteins: regulators of transcription in eucaryotic organisms. *Molecular and Cellular Biology*, **20**, 429-440.

Mathe, E., Olivier, M., Kato, S., Ishioka, C., Hainaut, P., and Tavtigian, S.V. (2006) Computational approaches for predicting the biological effect of p53 missense mutations: a comparison of three sequence analysis based methods. *Nucleic Acids Research*, **34**, 1317-1325.

MacDonald, B.T., Tamai, K., and He, X. (2009) Wnt/beta-catenin signaling: components, mechanisms, and diseases. *Developmental Cell*, **17**, 9-26.

McDonald, P.C., Fielding, A.B., and Dedhar, S. (2008) Integrin-linked kinase - essential roles in physiology and cancer biology. *Journal of Cell Science*, **121**, 3121-3132.

MacDonald, M.L.E., Goldberg, Y.P., MacFarlane, J., Samuels, M.E., Trese, M.T., and Shastry, B.S. (2005) Genetic variants of frizzled-4 gene in familial exudative vitreoretinopathy and advanced retinopathy of prematurity. *Clinical Genetics*, **67**, 363-366.

Mcdonald, N.Q., and Hendrickson, W.A. (1993) A Structural Superfamily of Growth-Factors Containing A Cystine Knot Motif. *Cell*, **73**, 421-424.

McMahon, A.P. and Moon, R.T. (1989) Ectopic expression of the proto-oncogene int-1 in Xenopus embryos leads to duplication of the embryonic axis. *Cell*, **58**, 1075-1084.

Meindl, A., Berger, W., Meitinger, T., Vandepol, D., Achatz, H., Dorner, C., Haasemann, M., Hellebrand, H., Gal, A., Cremers, F., and Ropers, H.H. (1992) Norrie Disease Is Caused by Mutations in An Extracellular Protein Resembling C-Terminal Globular Domain of Mucins. *Nature Genetics*, **2**, 139-143.

Meitinger, T., Meindl, A., Bork, P., Rost, B., Sander, C., Haasemann, M., and Murken, J. (1993) Molecular Modeling of the Norrie Disease Protein Predicts A Cystine Knot Growth-Factor Tertiary Structure. *Nature Genetics*, **5**, 376-380.

Miano, J.M., Long, X., and Fujiwara, K. (2007) Serum response factor: master regulator of the actin cytoskeleton and contractile apparatus. *American Journal of Physiology* , **292**, 70-81.

Michaelides,M., Luthert,P.J., Moore,A.T., Michaelides,M., Cooling,R., Moore,A.T., and Firth,H. (2004) Norrie disease and peripheral venous insufficiency. *British Journal of Ophthalmology*, **88**, 1475.

Mintz-Hittner,H.A., Ferrell,R.E., Sims,K.B., Fernandez,K.M., Gemmell,B.S., Satriano,D.R., Caster,J., and Kretzer,F.L. (1996) Peripheral retinopathy in offspring of carriers of Norrie disease gene mutations - Possible transplacental effect of abnormal Norrin. *Ophthalmology*, **103**, 2128-2134.

Mohammadi, M., Olsen, S. K., and Goetz, R. (2005) A protein canyon in the FGF-FGF receptor dimer selects from an a la carte menu of heparan sulfate motifs. *Current Opinion in Structural Biology*, **15**, 506-516.

Moon, R.T., Kohn, A.D., De Ferrari, G.V., and Kaykas, A. (2004) WNT and beta-catenin signalling: diseases and therapies. *Nature Reviews Genetics*, **5**, 691-701.

Mu, X., Fu, X., Sun, H., Beremand, P. D., Thomas, T. L., and Klein, W. H. (2005) A gene network downstream of transcription factor Math5 regulates retinal progenitor cell competence and ganglion cell fate. *Developmental Biology*, **280**, 467-481.

Muletarow,J., Paditz,E., Petersen,H., and Kreuz,F. (2004) Coats' disease in conjunction with other disorders. *Monatsschrift Kinderheilkunde*, **152**, 403-412.

Mullis, K., Faloona, F., Scharf, S., Saiki, R., Horn, G., and Erlich, H. (1986) Specific Enzymatic Amplification of DNA In Vitro: The Polymerase Chain Reaction. *Cold Spring Harbor Symposia on Quantitative Biology,* **51**, 263-273.

Ng, P.C. and Henikoff, S. (2001) Predicting deleterious amino acid substitutions. *Genome Research*, **11**, 863-874.

Nikopoulos, K., Gilissen, C., Hoischen, A., van Nouhuys, C.E., Boonstra, F.N., Blokland, E.A.W., Arts, P., Wieskamp, N., Strom, T.M., Ayuso, C., Tilanus, M.A.D., Bouwhuis, S., et al. (2010) Next-Generation Sequencing of a 40 Mb Linkage Interval Reveals TSPAN12 Mutations in Patients with Familial Exudative Vitreoretinopathy. *American Journal of Human Genetics*, **86**, 240-247.

Norrie, G. (1927) Causes of blindness in children. *Acta Opthalmologie,* **5**, 357-364.

Ohlmann, A., Scholz, M., Goldwich, A., Chauhan, B.K., Hudl, K., Ohlmann, A.V., Zrenner, E., Berger, W., Cvekl, A., Seeliger, M.W., and Tamm, E.R. (2005) Ectopic norrin induces growth of ocular capillaries and restores normal retinal angiogenesis in Norrie disease mutant mice. *Journal of Neuroscience*, **25**, 1701-1710.

Ohlmann, A., Seitz, R., Braunger, B., Seitz, D., Bosl, M.R., and Tamm, E.R. (2010) Norrin Promotes Vascular Regrowth after Oxygen-Induced Retinal Vessel Loss and Suppresses Retinopathy in Mice. *Journal of Neuroscience*, **30**, 183-193.

Ooto, S., Akagi, T., Kageyama, R., Akita, J., Mandai, M., Honda, Y., and Takahashi, M. (2004) Potential for neural regeneration after neurotoxic injury in the adult mammalian retina. *Proceedings of the National Academy of Sciences of the United States of America*, **101**, 13654-13659.

Osakada, F., Ooto, S., Akagi, T., Mandai, M., Akaike, A., and Takahashi, M. (2007) Wnt signaling promotes regeneration in the retina of adult mammals. *Journal of Neuroscience*, **27**, 4210-4219.

Perez-Vilar, J., and Hill, R.L. (1997) Norrie disease protein (norrin) forms disulfide-linked oligomers associated with the extracellular matrix. *Journal of Biological Chemistry*, **272**, 33410-33415.

Persad, S., Attwell, S., Gray, V., Mawji, N., Deng, J.T., Leung, D., Yan, J., Sanghera, J., Walsh, M.P., and Dedhar, S. (2001) Regulation of protein kinase B/Akt-serine 473 phosphorylation by integrin-linked kinase - Critical roles for kinase activity and amino acids arginine 211 and serine 343. *Journal of Biological Chemistry*, **276**, 27462-27469.

Pham, P.L., Kamen, A., and Durocher, Y. (2006) Large-scale Transfection of mammalian cells for the fast production of recombinant protein. *Molecular Biotechnology*, **34**, 225-237.

Piccolo, S., Agius, E., Leyns, L., Bhattacharyya, S., Grunz, H., Bouwmeester, T., and De Robertis, E.M. (1999) The head inducer Cerberus is a multifunctional antagonist of Nodal, BMP and Wnt signals. *Nature*, **397**, 707-710.

Pipes, G.C.T., Creemers, E.E., and Olson, E.N. (2006) The myocardin family of transcriptional coactivators: versatile regulators of cell growth, migration, and myogenesis. *Genes & Development*, **20**, 1545-1556.

Porath, J., Carlsson, J., Olsson, I., Belfrage, G. (1975) Metal chelate affinity chromatography, a new approach to protein fractionation. *Nature* **258**, 598–599.

Poulter, J.A., Ali, M., Gilmour, D.F., Rice, A., Kondo, H., Hayashi, K., Mackey, D.A., Kearns, L.S., Ruddle, J.B., Craig, J.E., Pierce, E.A., Downey, L.M., et al. (2010) Mutations in TSPAN12 Cause Autosomal-Dominant Familial Exudative Vitreoretinopathy. *American Journal of Human Genetics*, **86**, 248-253.

Prasov, L., Masud, T., Khaliq, S., Mehdi, S.Q., Abid, A., Oliver, E.R., Silva, E.D., Lewanda, A., Brodsky, M.C., Borchert, M., Kelberman, D., Sowden, J.C., et al. (2012) ATOH7 mutations cause autosomal recessive persistent hyperplasia of the primary vitreous. *Human Molecular Genetics*, **21**, 3681-3694.

Pula, G., Garonna, E., Dunn, W.B., Hirano, M., Pizzorno, G., Campanella, M., Schwartz, E.L., el Kouni, M.H., and Wheeler-Jones, C.P.D. (2010) Paracrine Stimulation of Endothelial Cell Motility and Angiogenesis by Platelet-Derived Deoxyribose-1-Phosphate. *Arteriosclerosis Thrombosis and Vascular Biology*, **30**, 2631-2638.

Rattner, A., and Nathans, J. (2006) Macular degeneration: recent advances and therapeutic opportunities. *Nature Reviews Neuroscience*, **7**, 860-872.

Reese, A.B. (1955) Persistent Hyperplastic Primary Vitreous - the Jackson Memorial Lecture. *American Journal of Ophthalmology*, **40**, 317.

Rehm, H.L., GutierrezEspeleta, G.A., Garcia, R., Jimenez, G., Khetarpal, U., Priest, J.M., Sims, K.B., Keats, B.J.B., and Morton, C.C. (1997) Norrie disease gene mutation in a large Costa Rican kindred with a novel phenotype including venous insufficiency. *Human Mutation*, **9**, 402-408.

Rehm, H.L., Zhang, D.S., Brown, M.C., Burgess, B., Halpin, C., Berger, W., Morton, C.C., Corey, D.P., and Chen, Z.Y. (2002) Vascular defects and sensorineural deafness in a mouse model of Norrie disease. *Journal of Neuroscience*, **22**, 4286-4292.

Reichsman, F., Smith, L., and Cumberledge, S. (1996) Glycosaminoglycans can modulate extracellular localization of the wingless protein and promote signal transduction. *Journal of Cell Biology*, **135**, 819-827.

Reis, L.M., Tyler, R.C., Schilter, K.F., Abdul-Rahman, O., Innis, J.W., Kozel, B.A., Schneider, A.S., Bardakjian, T.M., Lose, E.J., Martin, D.M., Broeckel, U., and Semina, E.V. (2011) BMP4 loss-of-function mutations in developmental eye disorders including SHORT syndrome. *Human Genetics*, **130**, 495-504.

Richter, M., Gottanka, J., May, C.A., Welge-Lussen, U., Berger, W., and Lutjen-Drecoll, E. (1998) Retinal vasculature changes in Norrie disease mice. *Investigative Ophthalmology & Visual Science*, **39**, 2450-2457.

Robitaille, J., MacDonald, M.L.E., Kaykas, A., Sheldahl, L.C., Zeisler, J., Dube, M.P., Zhang, L.H., Singaraja, R.R., Guernsey, D.L., Zheng, B.Y., Siebert, L.F., Hoskin-Mott, A., et al. (2002) Mutant frizzled-4 disrupts retinal angiogenesis in familial exudative vitreoretinopathy. *Nature Genetics*, **32**, 326-330.

Rohen, J.W. (1971) Funktionelle Anatomie des Nervensystems. *F.K. Schattauer*

Rider, C.C. (2006) Heparin/heparan sulphate binding in the TGF-beta cytokine superfamily", *Biochemical Society Transactions*, **34**, 458-460.

Ritter, M.R., Banin, E., Moreno, S.K., Aguilar, E., Dorrell, M.I., and Friedlander, M. (2006) Myeloid progenitors differentiate into microglia and promote vascular repair in a model of ischemic retinopathy", *Journal of Clinical Investigation*, **116**, 3266-3276.

Rubio-Cabezas, O., Minton, J.A.L., Kantor, I., Williams, D., Ellard, S., and Hattersley, A.T. (2010) Homozygous Mutations in NEUROD1 Are Responsible for a Novel Syndrome of Permanent Neonatal Diabetes and Neurological Abnormalities. *Diabetes*, **59**, 2326-2331.

Safaiyan, F., Kolset, S.O., Prydz, K., Gottfridsson, E., Lindahl, U., and Salmivirta, M. (1999) Selective effects of sodium chlorate treatment on the sulfation of heparan sulfate. *Journal of Biological Chemistry*, **274**, 36267-36273.

Saiki, R., Gelfand, D., Stoffel, S., Scharf, S., Higuchi, R., Horn, G., Mullis, K.B., and Erlich, H.A. (1988) Primer-directed enzymatic amplification of DANN with a thermostable DNA polymerase. *Science, **239***, 487-491.

Sambrook, J., Maniatis, T., and Fritsch, E. (1989) *Molecular Cloning: A Laboratory Manual* (Bd. 1). Cold Spring Harbor Laboratory Press.

Sanger, F., Nicklen, S., and Coulson, A. (1977) DNA sequencing with chain-terminating inhibitors. *Proceedings of the National Academy of Sciences of the United States of America,* **74**, 5463-7.

Schaefer, N.F., Luhmann, U.F.O., Feil, S., and Berger, W. (2009) Differential Gene Expression in Ndph-Knockout Mice in Retinal Development. *Investigative Ophthalmology & Visual Science*, **50**, 906-916.

Schneider, S., Steinbeisser, H., Warga, R.M., and Hausen, P. (1996) Beta-catenin translocation into nuclei demarcates the dorsalizing centers in frog and fish embryos. *Mechanisms of Development*, **57**, 191-198.

Seitz, R., Hackl, S., Seibuchner, T., Tamm, E.R., and Ohlmann, A. (2010) Norrin Mediates Neuroprotective Effects on Retinal Ganglion Cells via Activation of the Wnt/beta-Catenin Signaling Pathway and the Induction of Neuroprotective Growth Factors in Muller Cells. *Journal of Neuroscience*, **30**, 5998-6010.

Shastry, B.S., Pendergast, S.D., Hartzer, M.K., Liu, X.Y., and Trese, M.T. (1997) Identification of missense mutations in the Norrie disease gene associated with advanced retinopathy of prematurity. *Archives of Ophthalmology*, **115**, 651-655.

Shastry, B.S., and Trese, M.T. (2003) Overproduction and partial purification of the Norrie disease gene product, norrin, from a recombinant baculovirus. *Biochemical and Biophysical Research Communications*, **312**, 229-234.

Sims, K.B., Lebo, R.V., Benson, G., Shalish, C., Schuback, D., Chen, Z.Y., Bruns, G., Craig, I.W., Golbus, M.S., and Breakefield, X.O. (1992) The Norrie disease gene maps to a 150 kb region on chromosome Xp11.3. *Human Molecular Genetics*, **2**, 89-93.

Smallwood, P.M., Williams, J., Xu, Q., Leahy, D.J., and Nathans, J. (2007) Mutational analysis of Norrin-Frizzled4 recognition. *Journal of Biological Chemistry*, **282**, 4057-4068.

Smith, L.E.H., Wesolowski, E., Mclellan, A., Kostyk, S.K., Damato, R., Sullivan, R., and Damore, P.A. (1994) Oxygen-Induced Retinopathy in the Mouse", *Investigative Ophthalmology & Visual Science*, **35**, 101-111.

Smith, S.E., Mullen, T.E., Graham, D., Sims, K.B., and Rehm, H.L. (2012) Norrie disease: Extraocular clinical manifestations in 56 patients. *American Journal of Medical Genetics Part A*, **158A**, 1909-1917.

Sparks, D.L., Kuo, Y.M., Roher, A., Martin, T., and Lukas, R.J. (2000) Alterations of Alzheimer's disease in the cholesterol-fed rabbit, including vascular inflammation - Preliminary observations. *Vascular Factors in Alzheimer'S Disease*, **903**, 335-344.

Stan, R.V., Tkachenko, E., and Niesman, I.R. (2004) PV1 is a key structural component for the formation of the stomatal and fenestral diaphragms. *Molecular Biology of the Cell*, **15**, 3615-3630.

Stenman, J.M., Rajagopal, J., Carroll, T.J., Ishibashi, M., McMahon, J., and McMahon, A.P. (2008) Canonical Wnt Signaling Regulates Organ-Specific Assembly and Differentiation of CNS Vasculature. *Science*, **322**, 1247-1250.

Stefater, J.A., Lewkowich, I., Rao, S., Mariggi, G., Carpenter, A.C., Burr, A.R., Fan, J.Q., Ajima, R., Molkentin, J.D., Williams, B.O., Wills-Karp, M., Pollard, J.W., et al. (2011) Regulation of angiogenesis by a non-canonical Wnt-Flt1 pathway in myeloid cells. *Nature*, **474**, 511-515.

Stone, J., Dreher, Z. (1987) Relationship Between Astrocytes, Ganglion-Cells and Vasculature of the Retina. *Journal of Comparative Neurology*, **255**, 35-49.

Stone, J., Itin, A., Alon, T., Peer, J., Gnessin, H., Chanling, T., and Keshet, E. (1995) Development of Retinal Vasculature Is Mediated by Hypoxia-Induced Vascular Endothelial Growth-Factor (Vegf) Expression by Neuroglia. *Journal of Neuroscience*, **15**, 4738-4747.

Streit, W.J. (2001) Microglia and macrophages in the developing CNS. *Neurotoxicology*, **22**, 619-624.

Sun, P.D., and Davies, D.R. (1995) The Cystine-Knot Growth-Factor Superfamily. *Annual Review of Biophysics and Biomolecular Structure*, **24**, 269-291.

Sullivan, A.L., Benner, C., Heinz, S., Huang, W., Xie, L., Miano, J.M., and Glass, C.K. (2011) Serum Response Factor Utilizes Distinct Promoter- and Enhancer-Based Mechanisms To Regulate Cytoskeletal Gene Expression in Macrophages. *Molecular and Cellular Biology*, **31**, 861-875.

Tamai, K., Semenov, M., Kato, Y., Spokony, R., Liu, C., Katsuyama, Y., Hess, F., Saint-Jeannet, J.P., and He, X. (2000) LDL-receptor-related proteins in Wnt signal transduction. *Nature*, **407**, 530-535.

Tan, C., Costello, P., Sanghera, J., Dominguez, D., Baulida, J., de Herreros, A.G., and Dedhar, S. (2001) Inhibition of integrin linked kinase (ILK) suppresses beta-catenin-Lef/Tcf-dependent transcription and expression of the E-cadherin repressor, snail, in APC-/- human colon carcinoma cells. *Oncogene*, **20**, 133-140.

Tavtigian, S.V., Deffenbaugh, A.M., Yin, L., Judkins, T., Scholl, T., Samollow, P.B., de Silva, D., Zharkikh, A., and Thomas, A. (2006) Comprehensive statistical study of 452 BRCA1 missense substitutions with classification of eight recurrent substitutions as neutral. *Journal of Medical Genetics*, **43**, 295-305.

Terry, T.L. (1946) Retrolental Fibroplasia. *Journal of Pediatrics*, **29**, 770-773.

The 1000 Genomes Project Consortium (2010) A map of human genome variation from population-scale sequencing. *Nature*, **467**, 1061-1073.

Toomes, C., Bottomley, H.M., Jackson, R.M., Towns, K.V., Scott, S., Mackey, D.A., Craig, J.E., Jiang, L., Yang, Z.L., Trembath, R., Woodruff, G., Gregory-Evans, C.Y., et al. (2004) Mutations in LRP5 or FZD4

underlie the common familial exudative vitreoretinopathy locus on chromosome 11q. *American Journal of Human Genetics*, **74**, 721-730.

Turner, D.L., and Cepko,C.L. (1987) A Common Progenitor for Neurons and Glia Persists in Rat Retina Late in Development. *Nature*, **328**, 131-136.

Unoki, N., Murakami, T., Nishijima, K., Ogino, K., van Rooijen, N., and Yoshimura, N. (2010) SDF-1/CXCR4 Contributes to the Activation of Tip Cells and Microglia in Retinal Angiogenesis. *Investigative Ophthalmology & Visual Science*, **51**, 3362-3371.

Van Bergen, N.J., Wood, J.P.M., Chidlow, G., Trounce, I.A., Casson, R.J., Ju, W.K., Weinreb, R.N., and Crowston, J.G. (2009) Recharacterization of the RGC-5 Retinal Ganglion Cell Line. *Investigative Ophthalmology & Visual Science*, **50**, 4267-4272.

Vartiainen, M.K., Guettler, S., Larijani, B., and Treisman, R. (2007) Nuclear actin regulates dynamic subcellular localization and activity of the SRF cofactor MAL. *Science*, **316**, 1749-1752.

Veeman, M.T., Axelrod, J.D., and Moon, R.T. (2003) A second canon. Functions and mechanisms of beta-catenin-independent Wnt signaling. *Developmental Cell*, **5**, 367-377.

Venter, J.C., Adams, M.D., Myers, E.W., Li, P.W., Mural, R.J., Sutton, G.G., Smith, H.O., Yandell, M., Evans, C.A., Holt, R.A., Gocayne, J.D., Amanatides, P., et al. (2001) The sequence of the human genome", *Science*, **291**, 1304.

Vouret-Craviari, V., Boulter, E., Grall, D., Matthews, C., and Obberghen-Schilling, E. (2004) ILK is required for the assembly of matrix-forming adhesions and capillary morphogenesis in endothelial cells. *Journal of Cell Science*, **117**, 4559-4569.

Wang, Y.S., Huso, D., Cahill, H., Ryugo, D., and Nathans, J. (2001) Progressive cerebellar, auditory, and esophageal dysfunction caused by targeted disruption of the frizzled-4 gene. *Journal of Neuroscience*, **21**, 4761-4771.

Warburg, M. (1963) Norries Disease - (Atrofia Bulborum Hereditaria) - A Report of 11 Cases of Heridatary Bilateral Pseudotumour of Retina, Complicated by Deafness and Mental Deficiency. *Acta Ophthalmologica*, **41**, 134-146.

Warburg, M. (1966) Norries Disease - Congenital Progressive Oculo-Acoustico-Cerebral Degeneration. *Acta Ophthalmologica*, Suppl. 89, 1-47

Warburg, O. (1928) Über die klassifizierung tierischer gewebe nach ihrem stoffwechsel. *Biochememische Zeitschrift,* **184**, 484-488.

Watanabe, T., and Raff, M.C. (1988) Retinal Astrocytes Are Immigrants from the Optic-Nerve. *Nature*, **332**, 834-837.

Wetts, R., and Fraser, S.E. (1988) Multipotent Precursors Can Give Rise to All Major Cell-Types of the Frog Retina. *Science*, **239**, 1142-1145.

Whitelock, J.M. and Iozzo, R.V. (2005). Heparan sulfate: a complex polymer charged with biological activity. *Chemical Reviews*, **105**, 2745-2764.

Willert, K., Brown, J.D., Danenberg, E., Duncan, A.W., Weissman, I.L., Reya, T., Yates, J.R., and Nusse, R. (2003) Wnt proteins are lipid-modified and can act as stem cell growth factors. *Nature*, **423**, 448-452.

Wilson, S.I. and Edlund, T. (2001) Neural induction: toward a unifying mechanism. *Nature Neuroscience*, **4**, 1161-1168.

Wordinger, R.J., Fleenor, D.L., Hellberg, P.E., Pang, I.H., Tovar, T.O., Zode, G.S., Fuller, J.A., and Clark, A.F. (2007) Effects of TGF-beta2, BMP-4, and gremlin in the trabecular meshwork: implications for glaucoma. *Investigative Ophthalmology & Visual Science*, **48**, 1191-1200.

Wu, C.I., Hoffman, J.A., Shy, B.R., Ford, E.M., Fuchs, E., Nguyen, H., and Merrill, B.J. (2012) Function of Wnt/beta-catenin in counteracting Tcf3 repression through the Tcf3-beta-catenin interaction. *Development*, **139**, 2118-2129.

Wurm, F.M. (2004) Production of recombinant protein therapeutics in cultivated mammalian cells. *Nature Biotechnology*, **22**, 1393-1398.

Xia, C.H., Liu, H.Q., Cheung, D., Wang, M., Cheng, C., Du, X., Chang, B., Beutler, B., and Gong, X.H. (2008) A model for familial exudative vitreoretinopathy caused by LPR5 mutations. *Human Molecular Genetics*, **17**, 1605-1612.

Xu, Q., Wang, Y.S., Dabdoub, A., Smallwood, P.M., Williams, J., Woods, C., Kelley, M.W., Jiang, L., Tasman, W., Zhang, K., and Nathans, J. (2004) Vascular development in the retina and inner ear: Control by Norrin and Frizzled-4, a high-affinity ligand-receptor pair. *Cell*, **116**, 883-895.

Xu, S.H., Cheng, F., Liang, J., Wu, W., and Zhang, J. (2012) Maternal xNorrin, a Canonical Wnt Signaling Agonist and TGF-beta Antagonist, Controls Early Neuroectoderm Specification in Xenopus. *Plos Biology*, **10**.

Yang-Snyder, J., Miller, J.R., Brown, J.D., Lai, C.J., and Moon, R.T. (1996) A frizzled homolog functions in a vertebrate Wnt signaling pathway. *Current Biology*, **6**, 1302-1306.

Yayon, A., Klagsbrun, M., Esko, J.D., Leder, P., and Ornitz, D.M. (1991) Cell-Surface, Heparin-Like Molecules Are Required for Binding of Basic Fibroblast Growth-Factor to Its High-Affinity Receptor. *Cell*, **64**, 841-848.

Ye, X., Smallwood, P., and Nathans, J. (2011) Expression of the Norrie disease gene (Ndp) in developing and adult mouse eye, ear, and brain. *Gene Expression Patterns*, **11**, 151-155.

Ye, X., Wang, Y.S., Cahill, H., Yu, M.Z., Badea, T.C., Smallwood, P.M., Peachey, N.S., and Nathans, J. (2009) Norrin, Frizzled-4, and Lrp5 Signaling in Endothelial Cells Controls a Genetic Program for Retinal Vascularization. *Cell*, **139**, 285-298.

Young, R.W. (1985) Cell-Differentiation in the Retina of the Mouse. *Anatomical Record*, **212**, 199-205.

Zaremba, J., Feil, S., Juszko, J., Myga, W., van Duijnhoven, G., Berger, W. (1998) Intrafamilial variability of the ocular phenotype in a Polish family with a missense mutation (A63D) in the Norrie disease gene. Ophthalmic Genet., **3**, 157-164.

Zuercher, J., Fritzsche, M., Feil, S., Mohn, L., and Berger, W. (2012) Norrin stimulates cell proliferation in the superficial retinal vascular plexus and is pivotal for the recruitment of mural cells. *Human Molecular Genetics*, **21**, 2619-2630.

Appendix A – Electropherograms

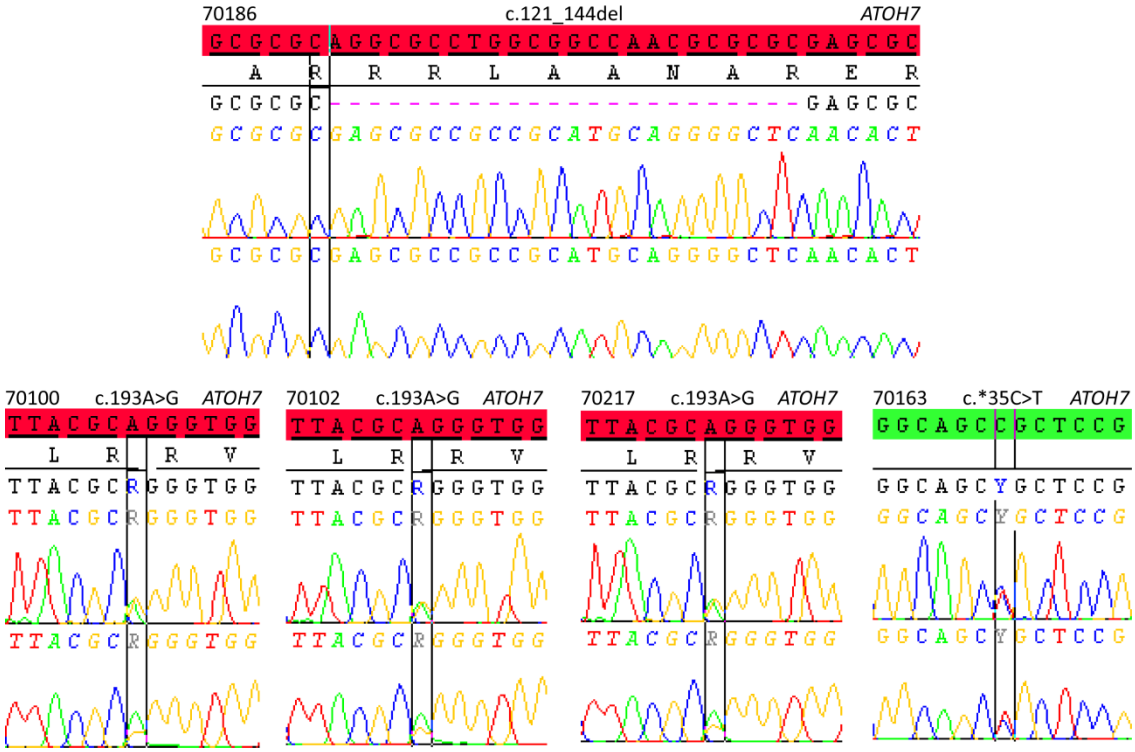

Figure 1A: Electropherograms from the *ATOH7* sequence analysis.

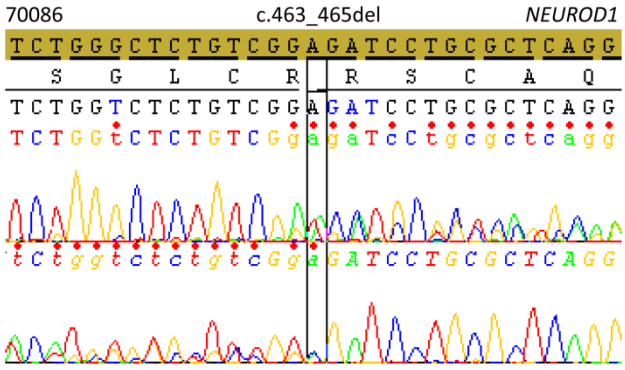

Figure 2A: Electropherogram from the *NEUROD1* sequence analysis.

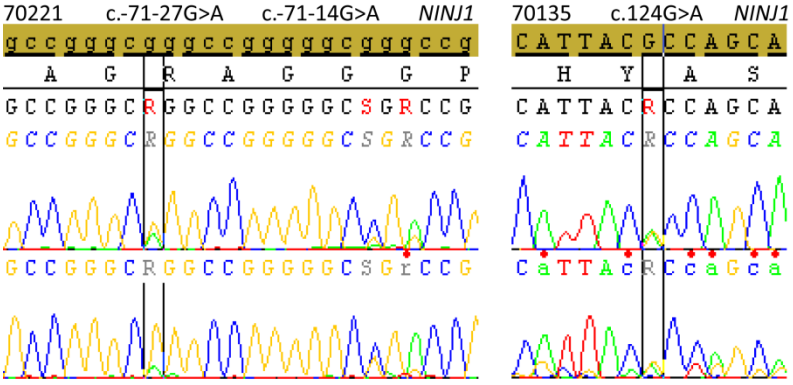

Figure 3A: Electropherogram from the *NINJ1* sequence analysis.

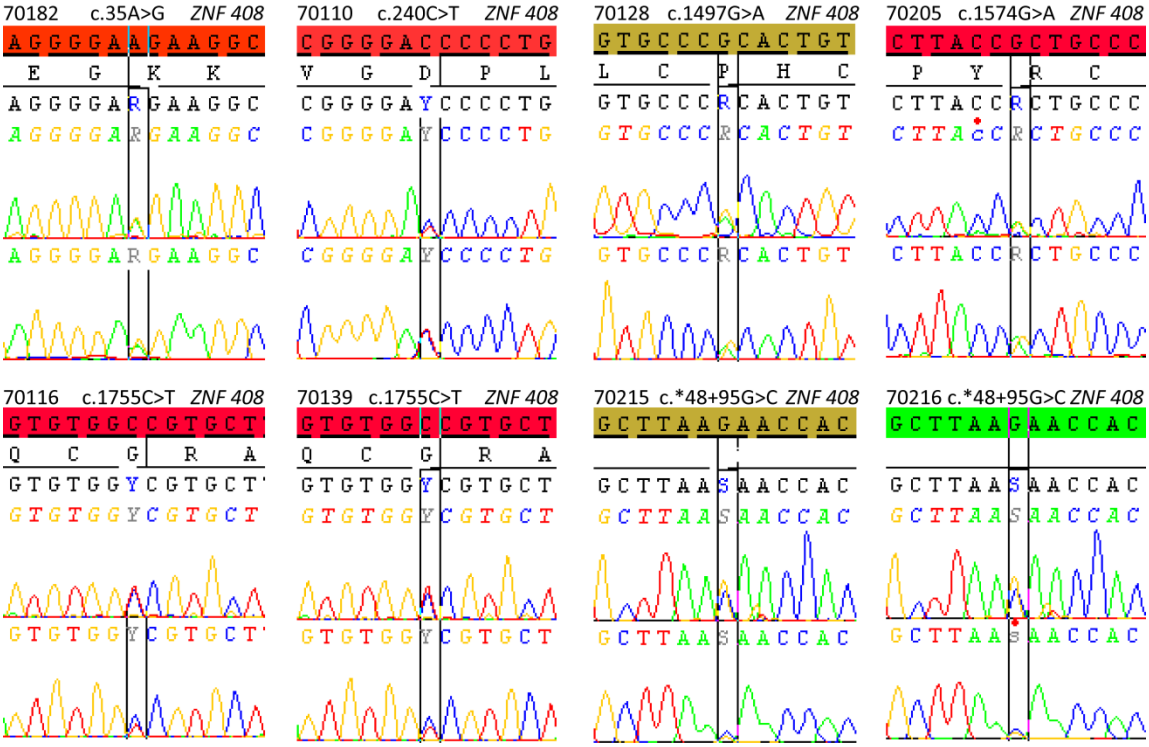

Figure 4A: Electropherograms from the *ZNF 408* sequence analysis.

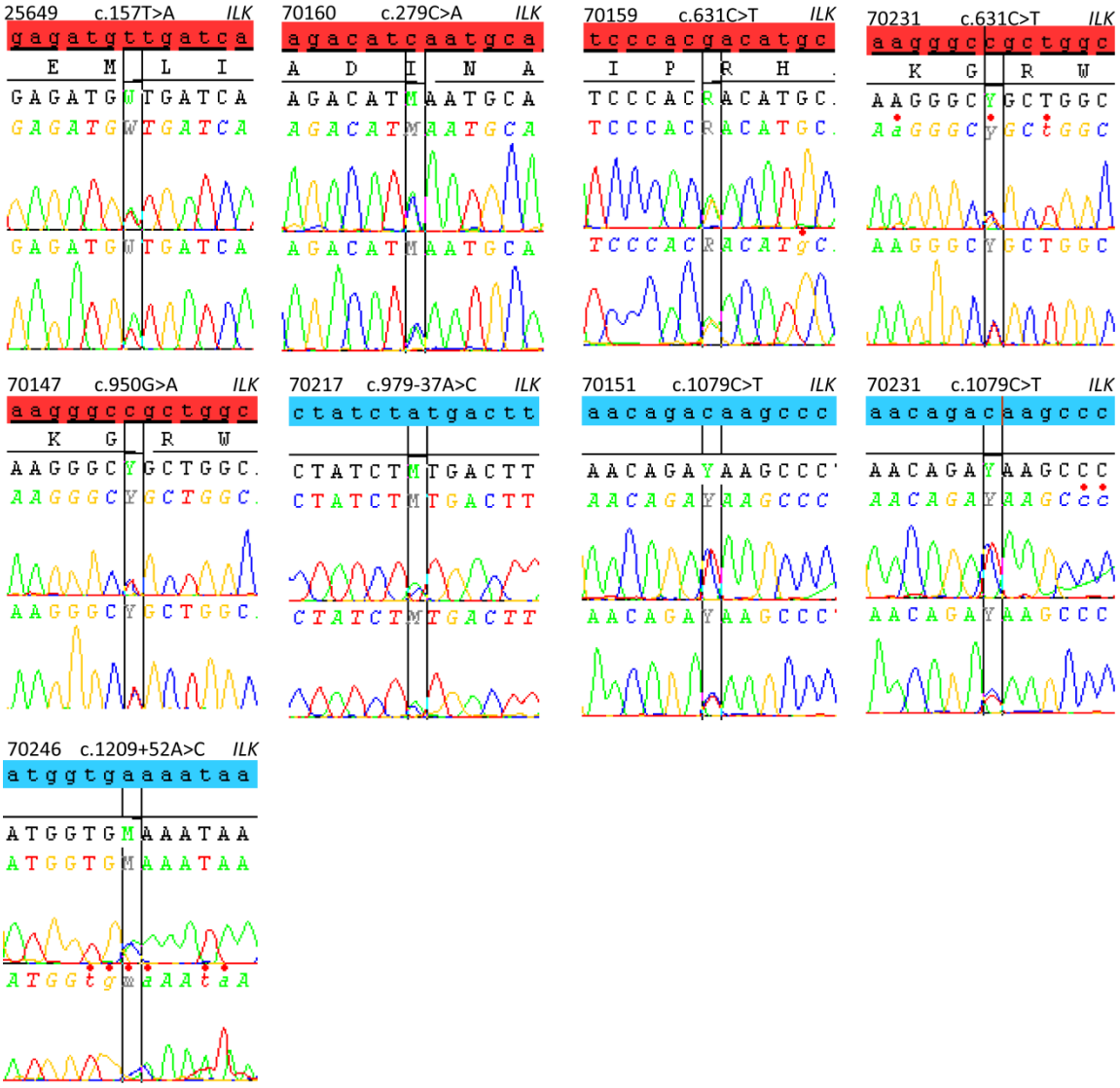

Figure 5A: Electropherograms from the *ILK* sequence analysis.

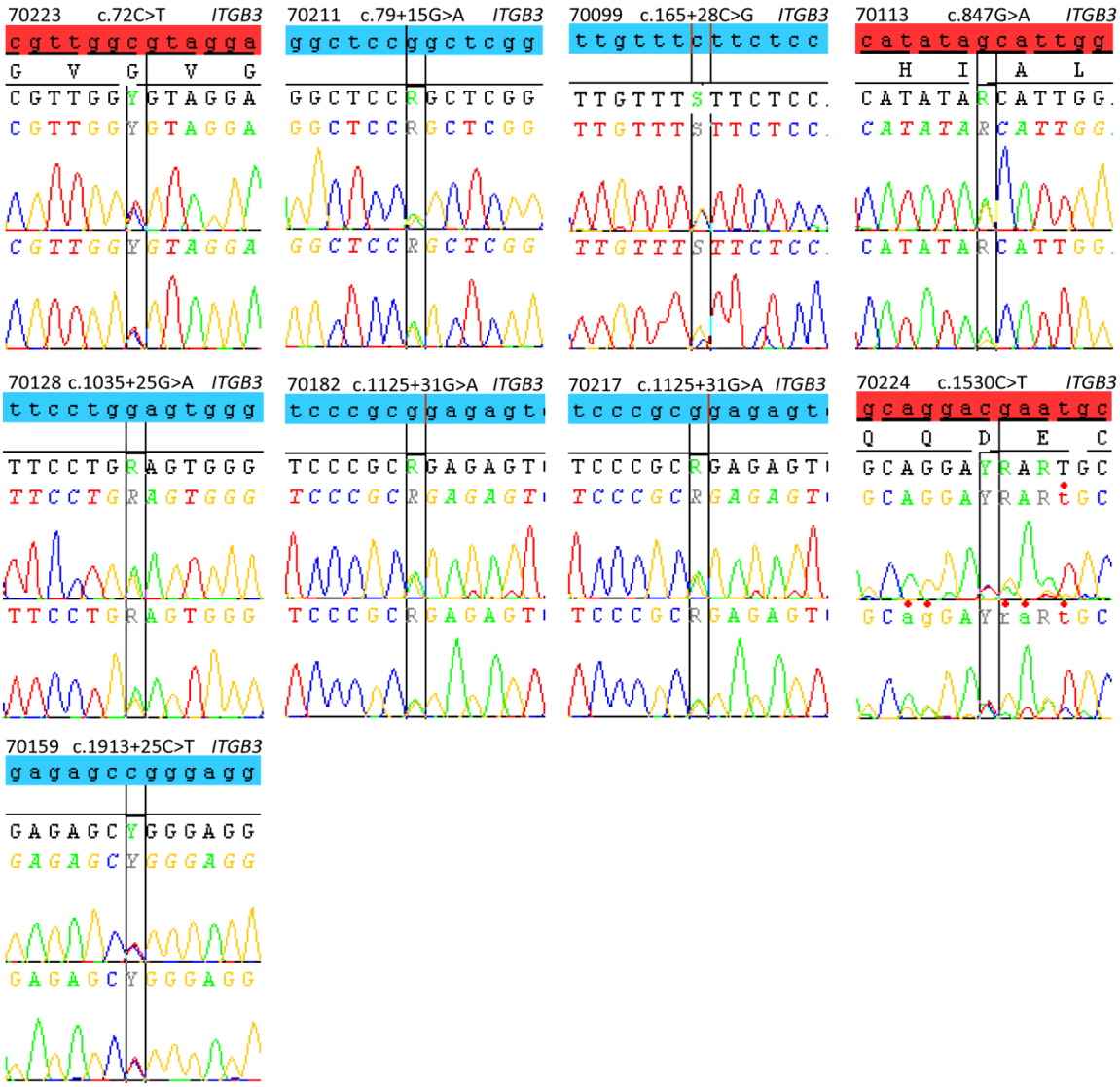

Figure 6A: Electropherograms from the *ITGB3* sequence analysis.

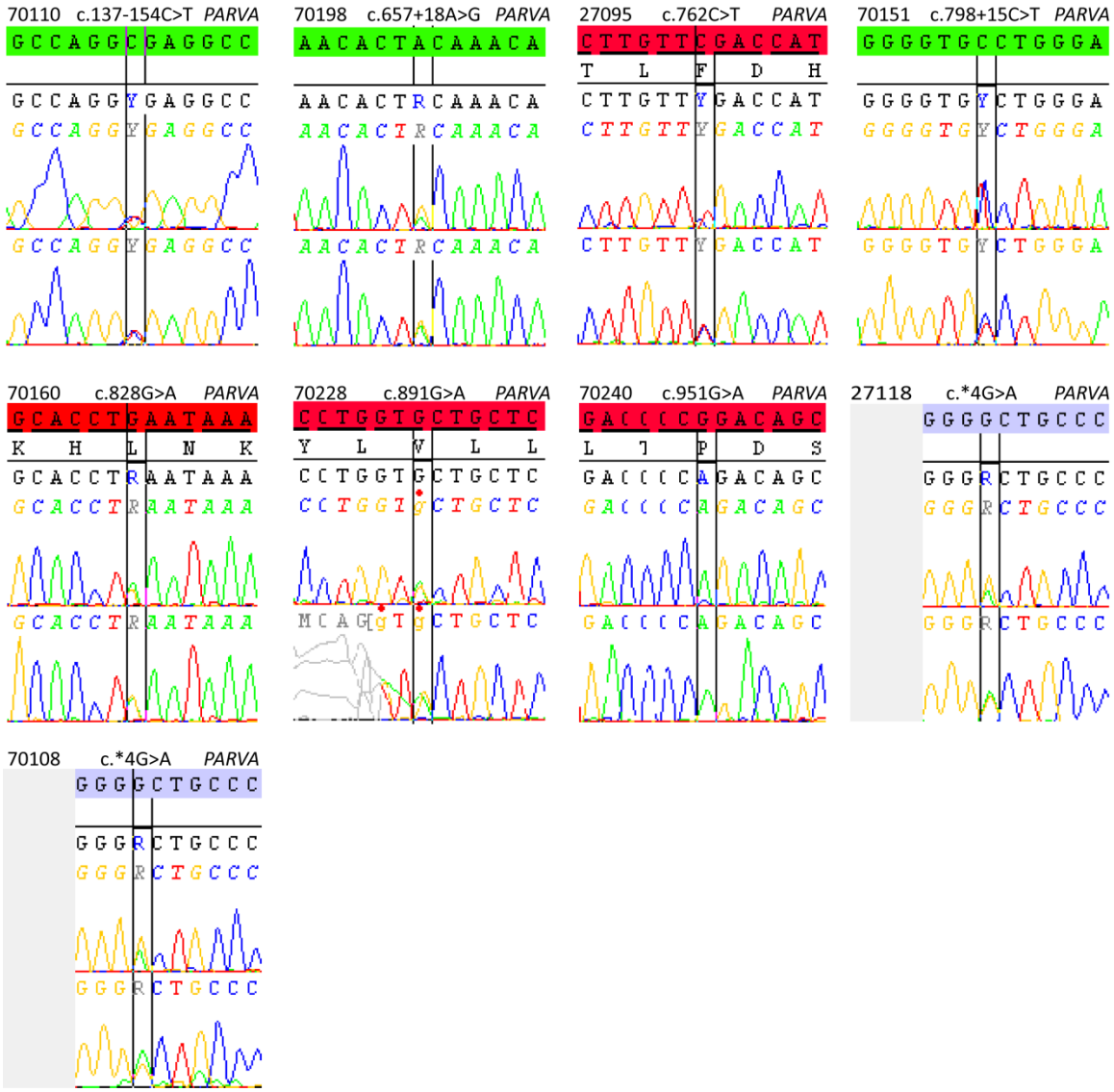

Figure 7A: Electropherograms from the *PARVA* sequence analysis.

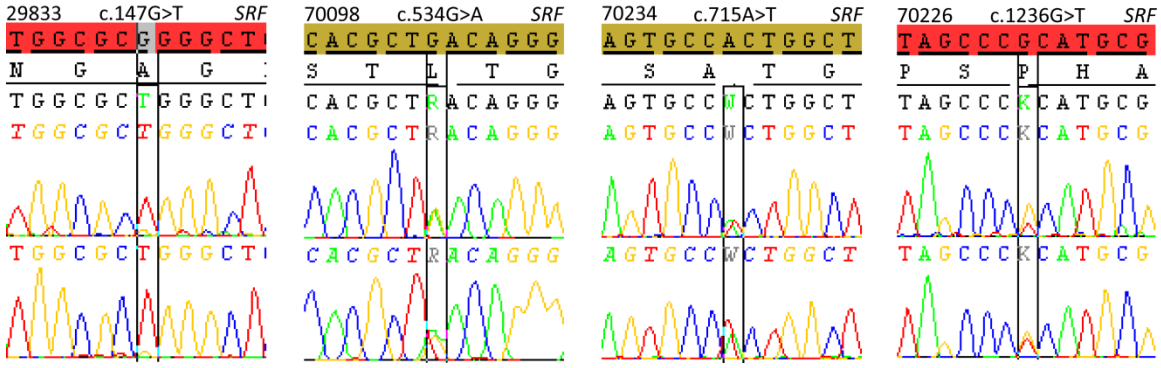

Figure 8A: Electropherograms from the *SRF* sequence analysis.

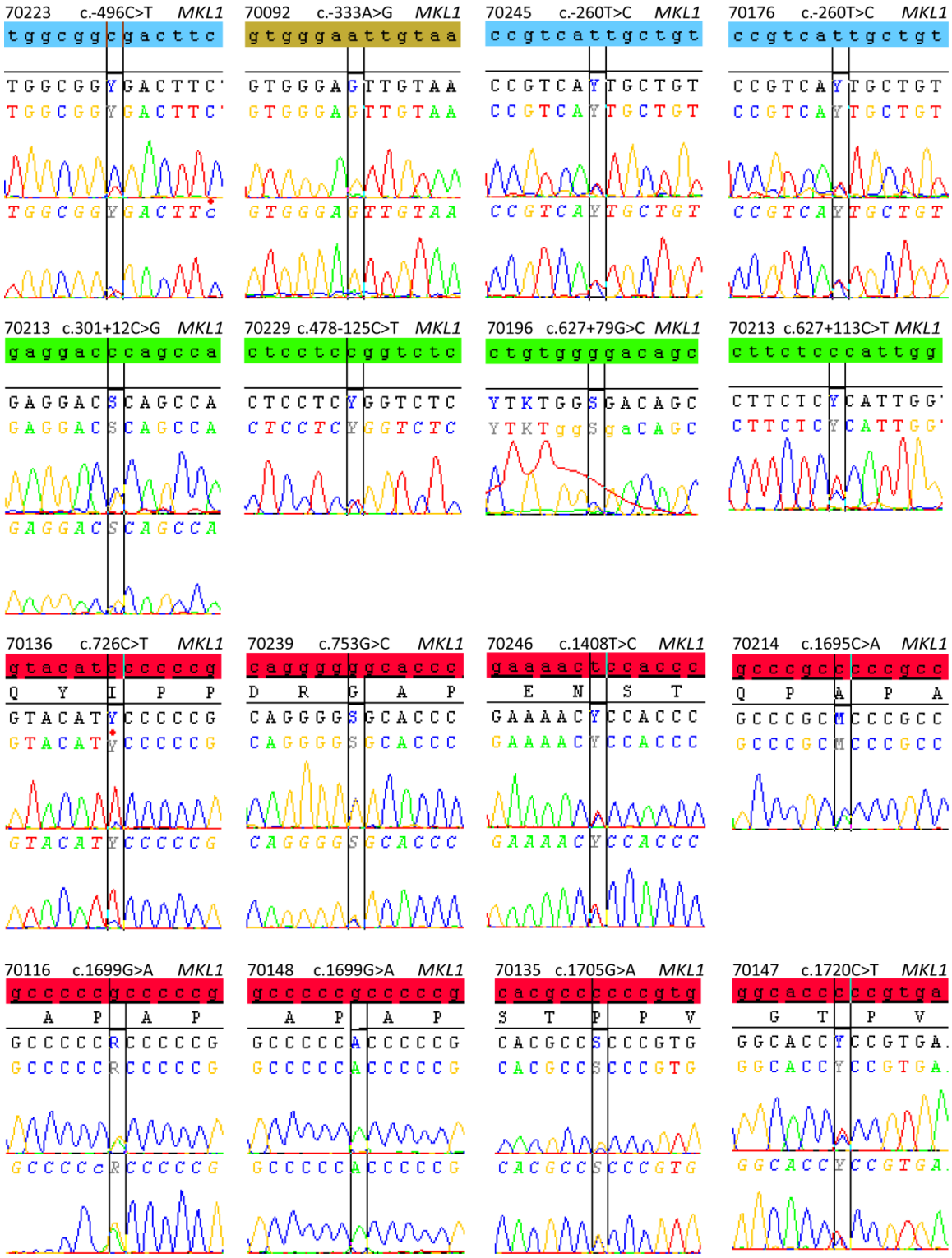
70223 c.-496C>T MKL1
70092 c.-333A>G MKL1
70245 c.-260T>C MKL1
70176 c.-260T>C MKL1
70213 c.301+12C>G MKL1
70229 c.478-125C>T MKL1
70196 c.627+79G>C MKL1
70213 c.627+113C>T MKL1
70136 c.726C>T MKL1
70239 c.753G>C MKL1
70246 c.1408T>C MKL1
70214 c.1695C>A MKL1
70116 c.1699G>A MKL1
70148 c.1699G>A MKL1
70135 c.1705G>A MKL1
70147 c.1720C>T MKL1

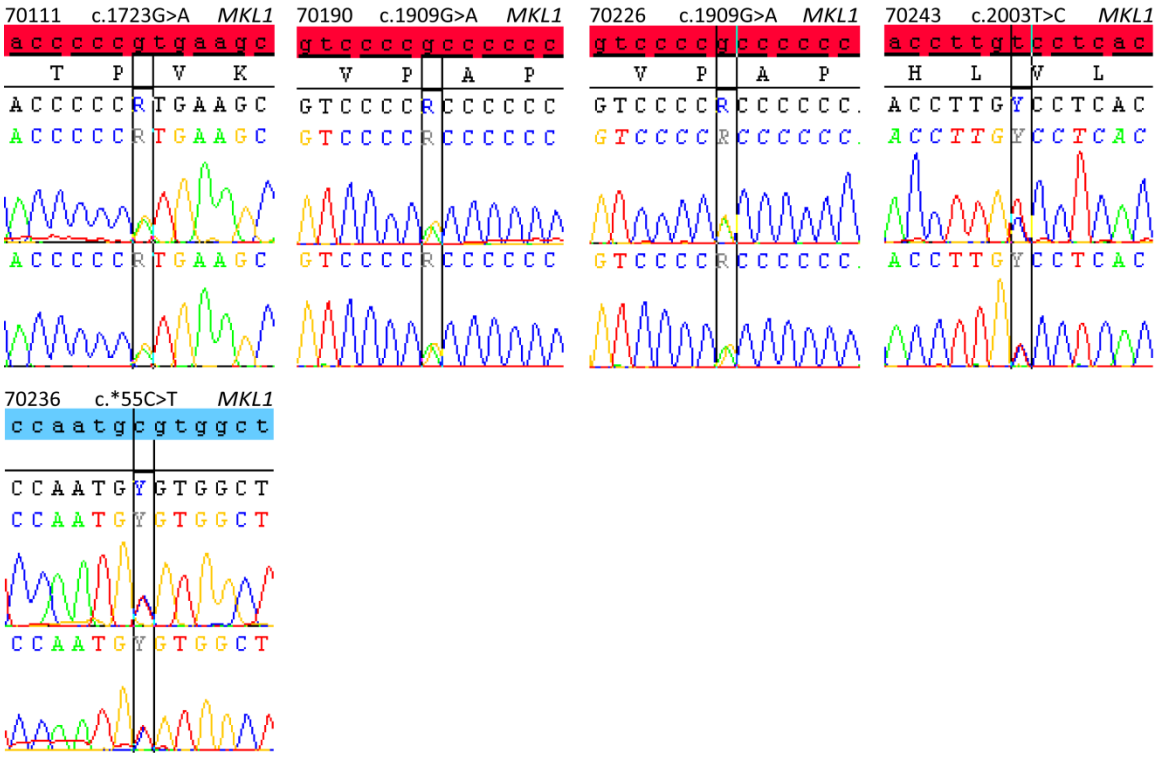

Figure 9A: Electropherograms from the *MKL1* sequence analysis.

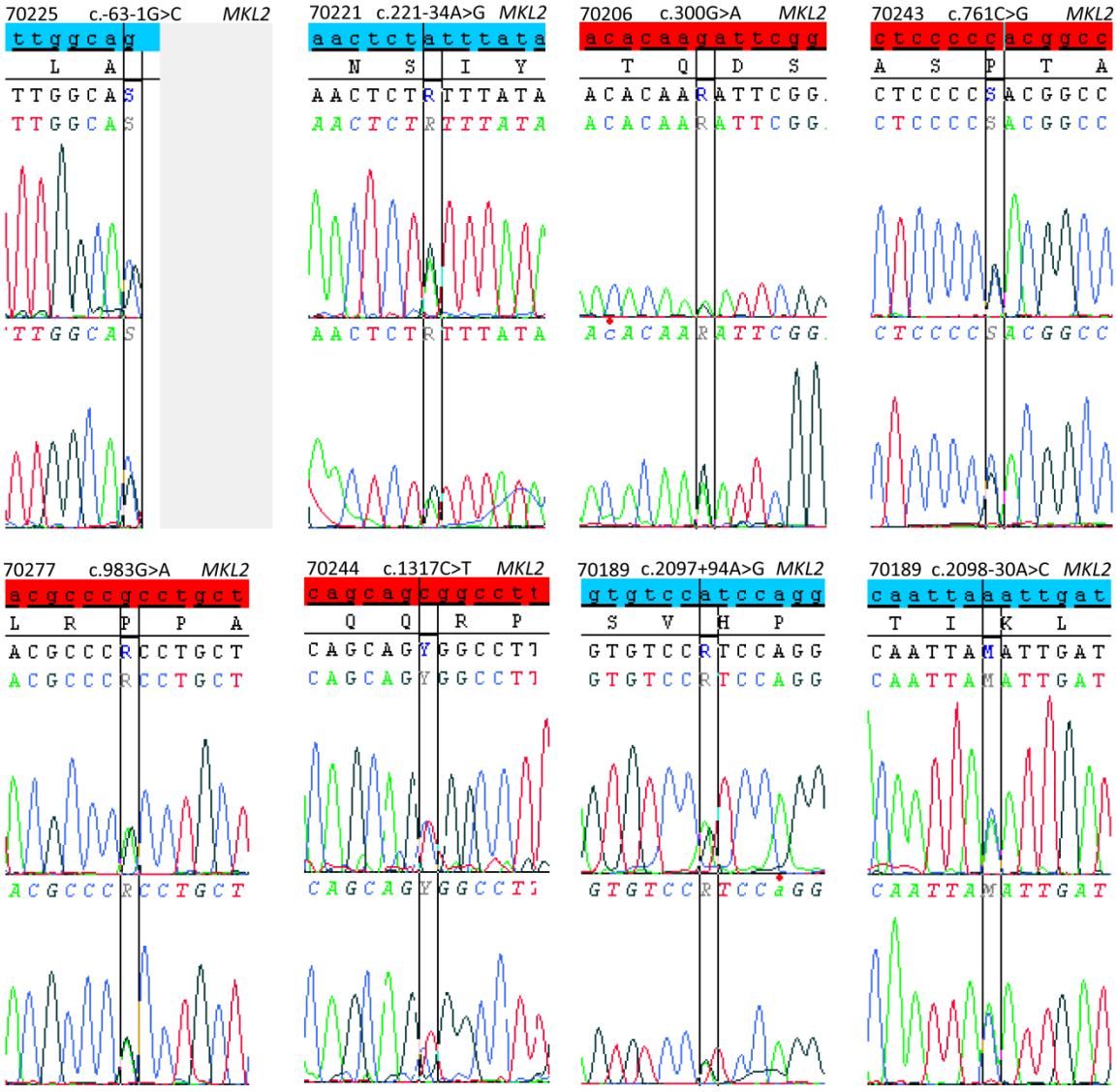
70225 c.-63-1G>C MKL2
70221 c.221-34A>G MKL2
70206 c.300G>A MKL2
70243 c.761C>G MKL2
70277 c.983G>A MKL2
70244 c.1317C>T MKL2
70189 c.2097+94A>G MKL2
70189 c.2098-30A>C MKL2

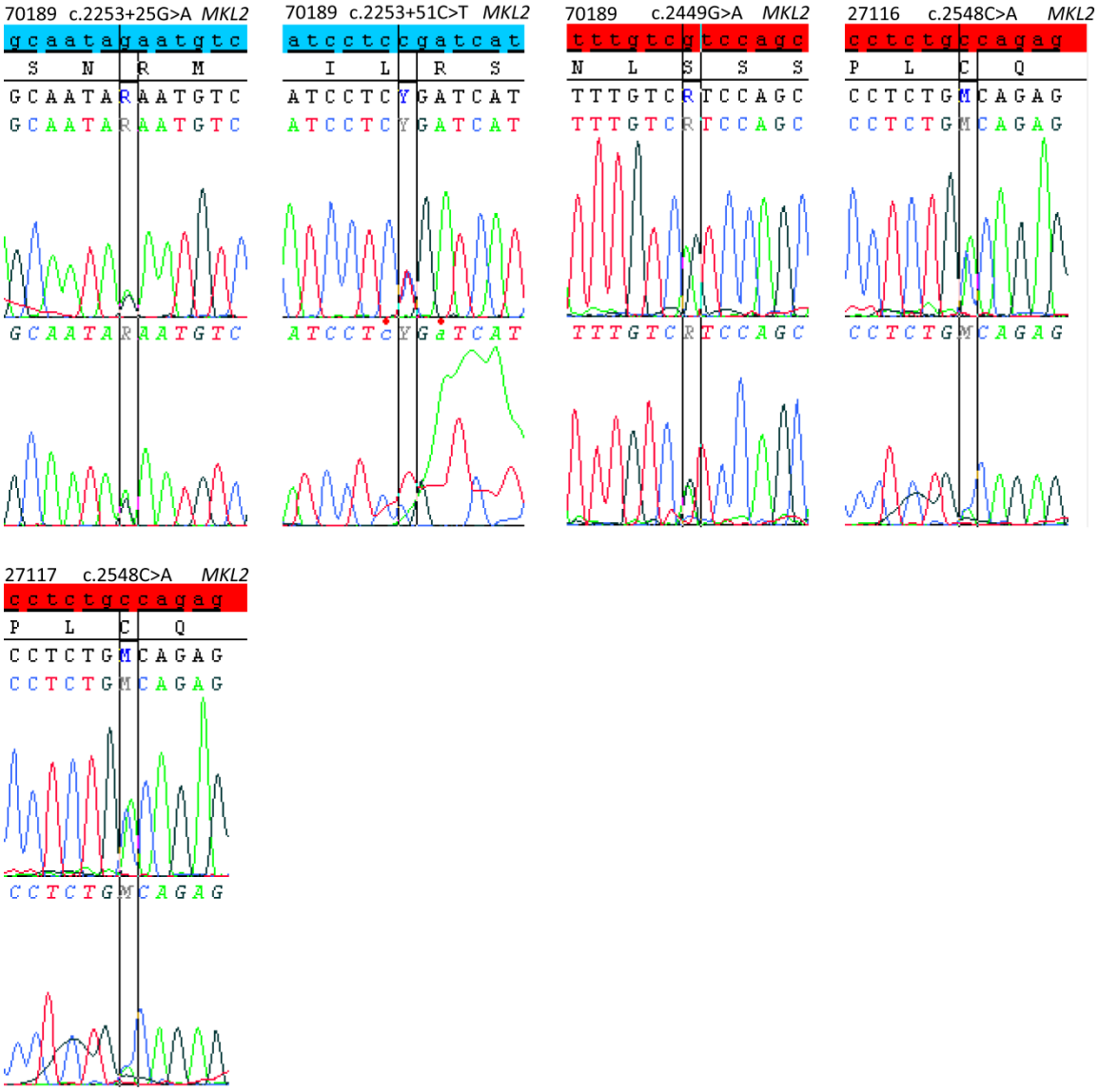

Figure 10A: Electropherograms from the *MKL2* sequence analysis.

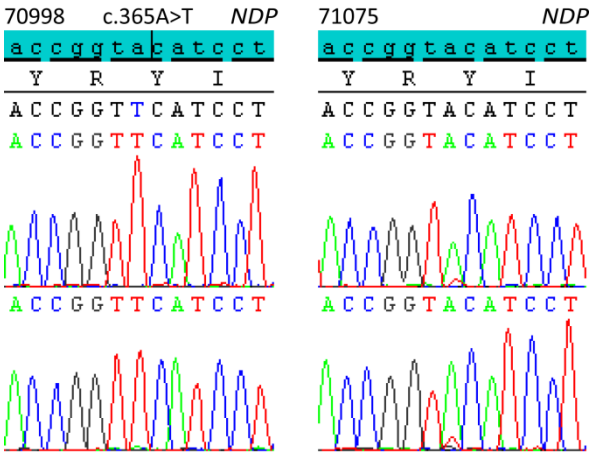

Figure 11A: Electropherograms from the *NDP* sequence analysis.

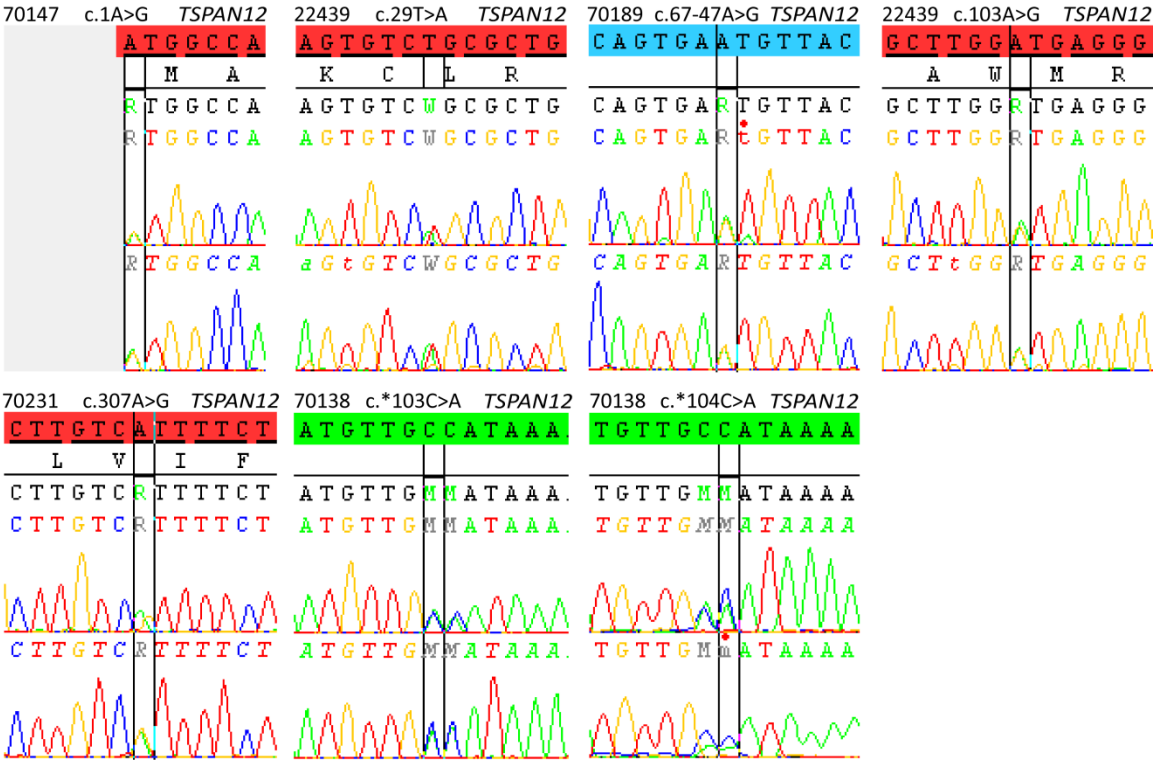

Figure 12A: Electropherograms from the *TSPAN12* sequence analysis.

Appendix B – Multiple sequence alignments

Colored multiple sequence alignments (MSA) of all proteins in which new missense mutations have been found. New missense mutations are indicated with a grey box.

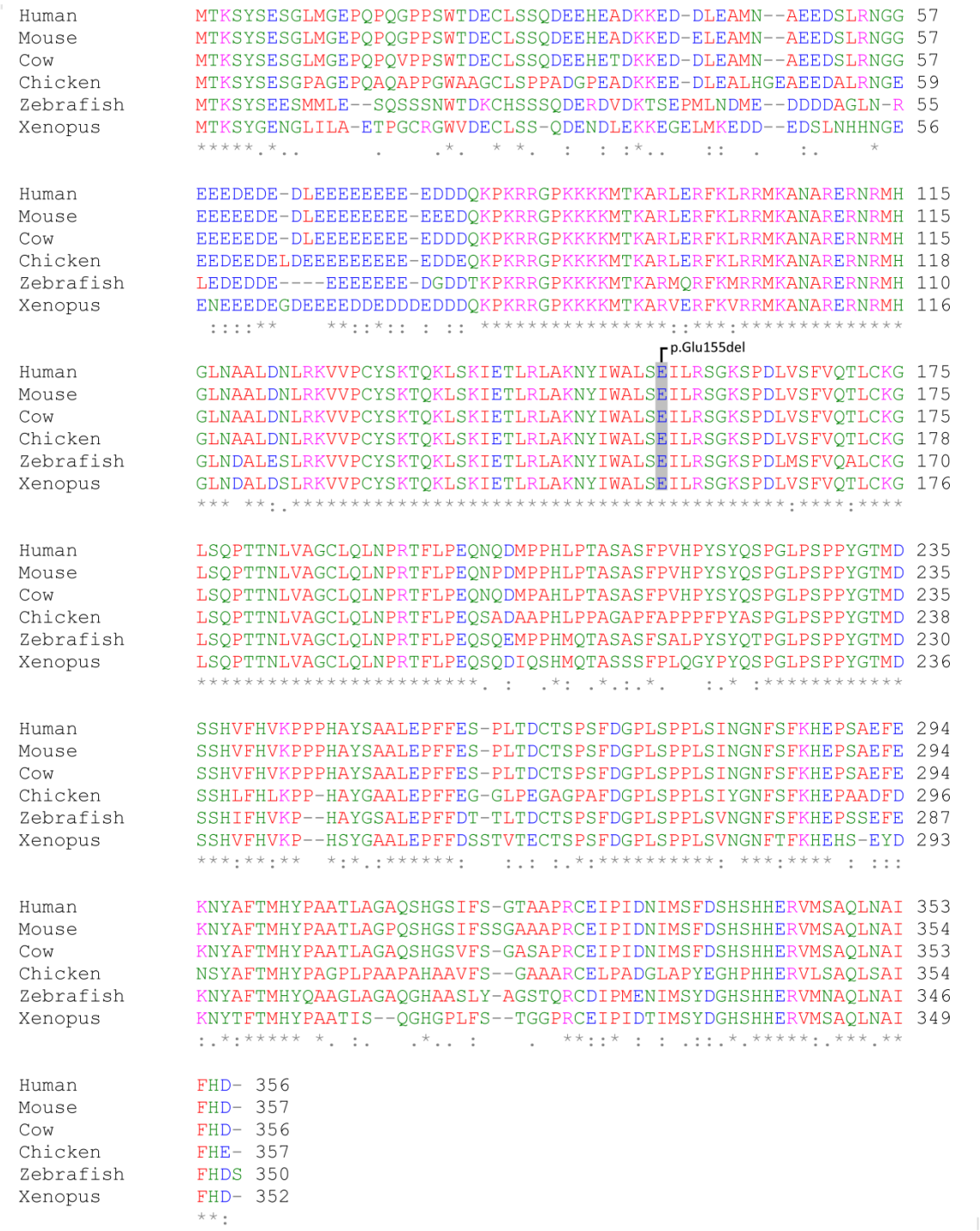

Figure 1B: MSA of *NEUROD1* sequences using CLUSTALW-2.1. Mutation site is indicated in grey.

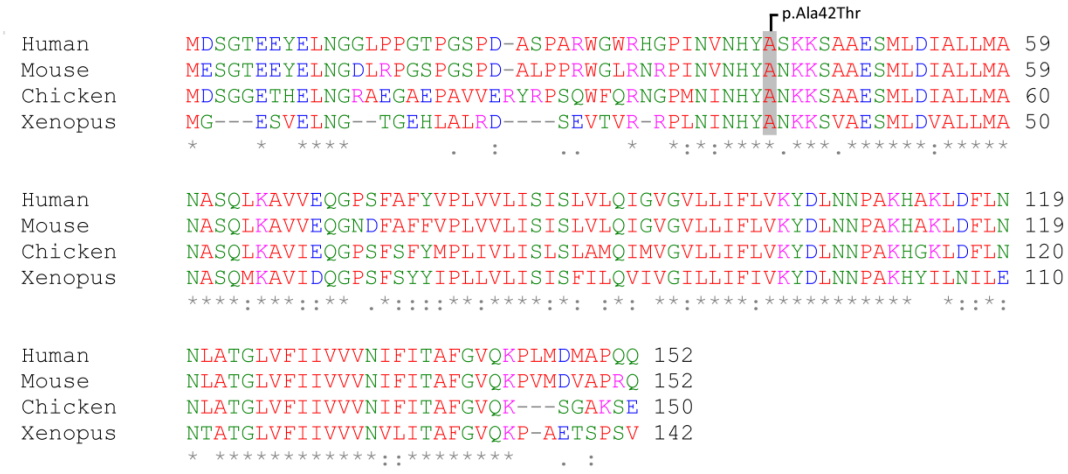

Figure 2B: MSA of *NINJ1* sequences using CLUSTALW-2.1. Mutation site is indicated in grey.

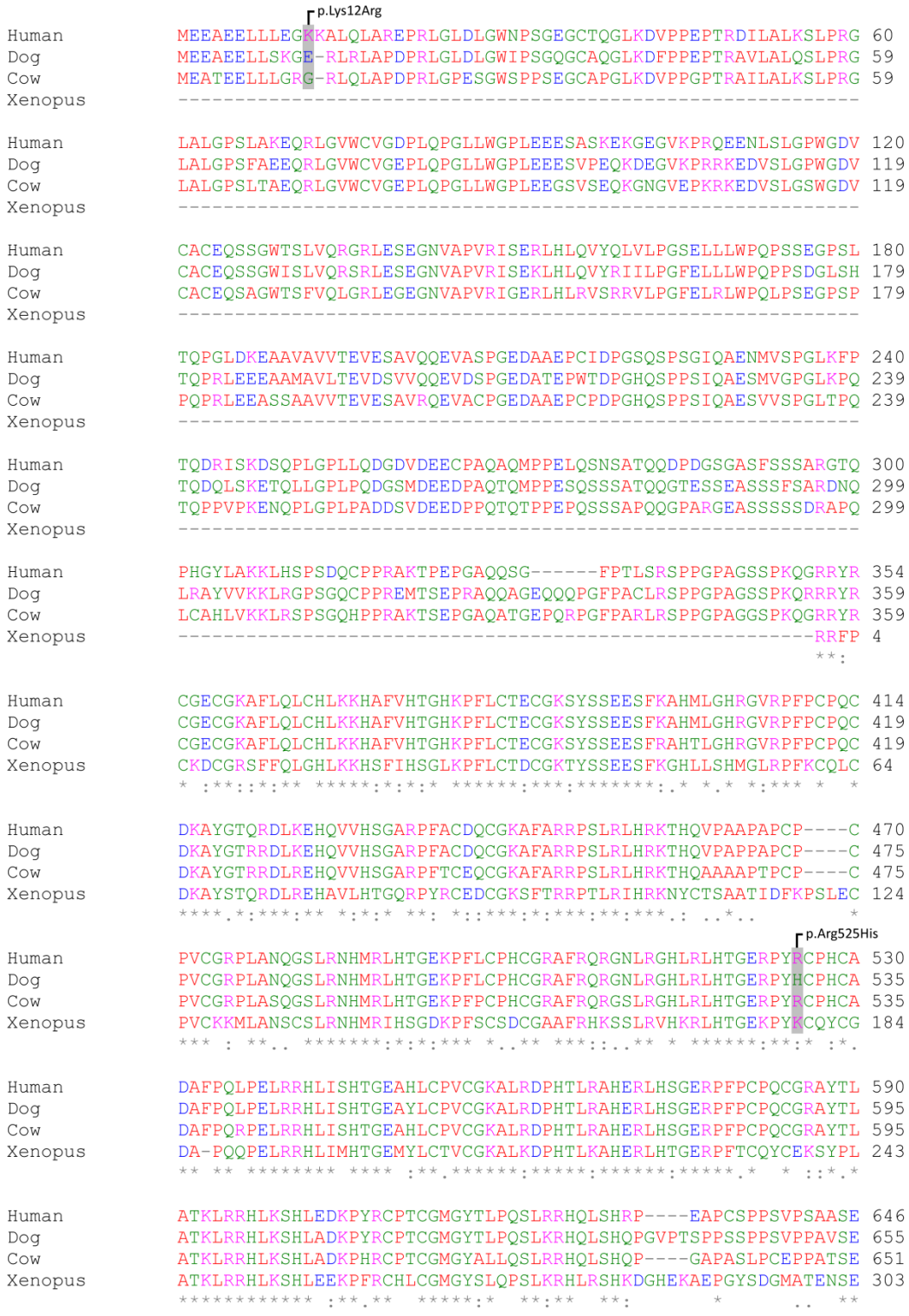
p.Lys12Arg
p.Arg525His
Human MEEAEELLLEGKKALQLAREPRLGLDLGWNPSGEGCTQGLKDVPPEPTRDILALKSLPRG 60
Dog MEEAEELLSKGE-RLRLAPDPRLGLDLGWIPSGQGCAQGLKDFPPEPTRAVLALQSLPRG 59
Cow MEATEELLLGRG-RLQLAPDPRLGPESGWSPPSEGCAPGLKDVPPGPTRAILALKSLPRG 59
Xenopus ----------
Human LALGPSLAKEQRLGVWCVGDPLQPGLLWGPLEEESASKEKGEGVKPRQEENLSLGPWGDV 120
Dog LALGPSFAEEQRLGVWCVGEPLQPGLLWGPLEEESVPEQKDEGVKPRRKEDVSLGPWGDV 119
Cow LALGPSLTAEQRLGVWCVGEPLQPGLLWGPLEEGSVSEQKGNGVEPKRKEDVSLGSWGDV 119
Xenopus ----------
Human CACEQSSGWTSLVQRGRLESEGNVAPVRISERLHLQVYQLVLPGSELLLWPQPSSEGPSL 180
Dog CACEQSSGWISLVQRSRLESEGNVAPVRISEKLHLQVYRIILPGFELLLWPQPPSDGLSH 179
Cow CACEQSAGWTSFVQLGRLEGEGNVAPVRIGERLHLRVSRRVLPGFELRLWPQLPSEGPSP 179
Xenopus ----------
Human TQPGLDKEAAVAVVTEVESAVQQEVASPGEDAAEPCIDPGSQSPSGIQAENMVSPGLKFP 240
Dog TQPRLEEEAAMAVLTEVDSVVQQEVDSPGEDATEPWTDPGHQSPPSIQAESMVGPGLKPQ 239
Cow PQPRLEEASSAAVVTEVESAVRQEVACPGEDAAEPCPDPGHQSPPSIQAESVVSPGLTPQ 239
Xenopus ----------
Human TQDRISKDSQPLGPLLQDGDVDEECPAQAQMPPELQSNSATQQDPDGSGASFSSSARGTQ 300
Dog TQDQLSKETQLLGPLPQDGSMDEEDPAQTQMPPESQSSSATQQGTESSEASSSFSARDNQ 299
Cow TQPPVPKENQPLGPLPADDSVDEEDPPQTQTPPEPQSSSAPQQGPARGEASSSSSDRAPQ 299
Xenopus ----------
Human PHGYLAKKLHSPSDQCPPRAKTPEPGAQQSG------FPTLSRSPPGPAGSSPKQGRRYR 354
Dog LRAYVVKKLRGPSGQCPPREMTSEPRAQQAGEQQQPGFPACLRSPPGPAGSSPKQRRRYR 359
Cow LCAHLVKKLRSPSGQHPPRAKTSEPGAQATGEPQRPGFPARLRSPPGPAGGSPKQGRRYR 359
Xenopus ----------RRFP 4
**:
Human CGECGKAFLQLCHLKKHAFVHTGHKPFLCTECGKSYSSEESFKAHMLGHRGVRPFPCPQC 414
Dog CGECGKAFLQLCHLKKHAFVHTGHKPFLCTECGKSYSSEESFKAHMLGHRGVRPFPCPQC 419
Cow CGECGKAFLQLCHLKKHAFVHTGHKPFLCTECGKSYSSEESFRAHTLGHRGVRPFPCPQC 419
Xenopus CKDCGRSFFQLGHLKKHSFIHSGLKPFLCTDCGKTYSSEESFKGHLLSHMGLRPFKCQLC 64
Human DKAYGTQRDLKEHQVVHSGARPFACDQCGKAFARRPSLRLHRKTHQVPAAPAPCP----C 470
Dog DKAYGTRRDLKEHQVVHSGARPFACDQCGKAFARRPSLRLHRKTHQVPAPPAPCP----C 475
Cow DKAYGTRRDLREHQVVHSGARPFTCEQCGKAFARRPSLRLHRKTHQAAAAPTPCP----C 475
Xenopus DKAYSTQRDLREHAVLHTGQRPYRCEDCGKSFTRRPTLRIHRKNYCTSAATIDFKPSLEC 124
Human PVCGRPLANQGSLRNHMRLHTGEKPFLCPHCGRAFRQRGNLRGHLRLHTGERPYRCPHCA 530
Dog PVCGRPLANQGSLRNHMRLHTGEKPFLCPHCGRAFRQRGNLRGHLRLHTGERPYHCPHCA 535
Cow PVCGRPLASQGSLRNHMRLHTGEKPFPCPHCGRAFRQRGSLRGHLRLHTGERPYRCPHCA 535
Xenopus PVCKKMLANSCSLRNHMRIHSGDKPFSCSDCGAAFRHKSSLRVHKRLHTGEKPYKCQYCG 184
Human DAFPQLPELRRHLISHTGEAHLCPVCGKALRDPHTLRAHERLHSGERPFPCPQCGRAYTL 590
Dog DAFPQLPELRRHLISHTGEAYLCPVCGKALRDPHTLRAHERLHSGERPFPCPQCGRAYTL 595
Cow DAFPQRPELRRHLISHTGEAHLCPVCGKALRDPHTLRAHERLHSGERPFPCPQCGRAYTL 595
Xenopus DA-PQQPELRRHLIMHTGEMYLCTVCGKALKDPHTLKAHERLHTGERPFTCQYCEKSYPL 243
Human ATKLRRHLKSHLEDKPYRCPTCGMGYTLPQSLRRHQLSHRP----EAPCSPPSVPSAASE 646
Dog ATKLRRHLKSHLADKPYRCPTCGMGYTLPQSLKRHQLSHQPGVPTSPPSSPPSVPPAVSE 655
Cow ATKLRRHLKSHLADKPHRCPTCGMGYALLQSLRRHQLSHQP----GAPASLPCEPPATSE 651
Xenopus ATKLRRHLKSHLEEKPFRCHLCGMGYSLQPSLKRHLRSHKDGHEKAEPGYSDGMATENSE 303

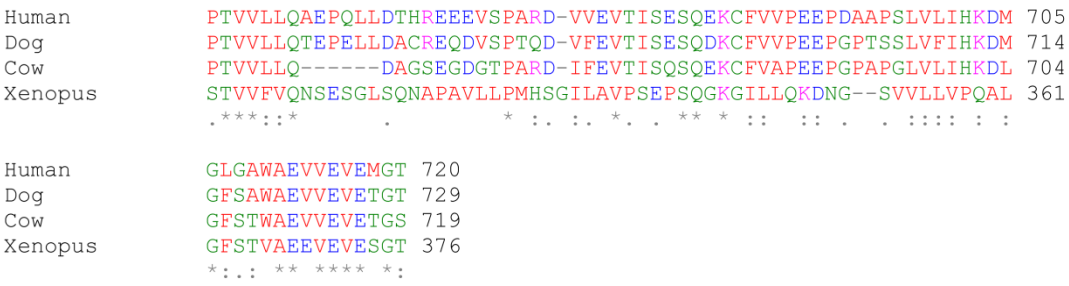

Figure 3B: MSA of *ZNF408* sequences using CLUSTALW-2.1. Mutation sites are indicated in grey.

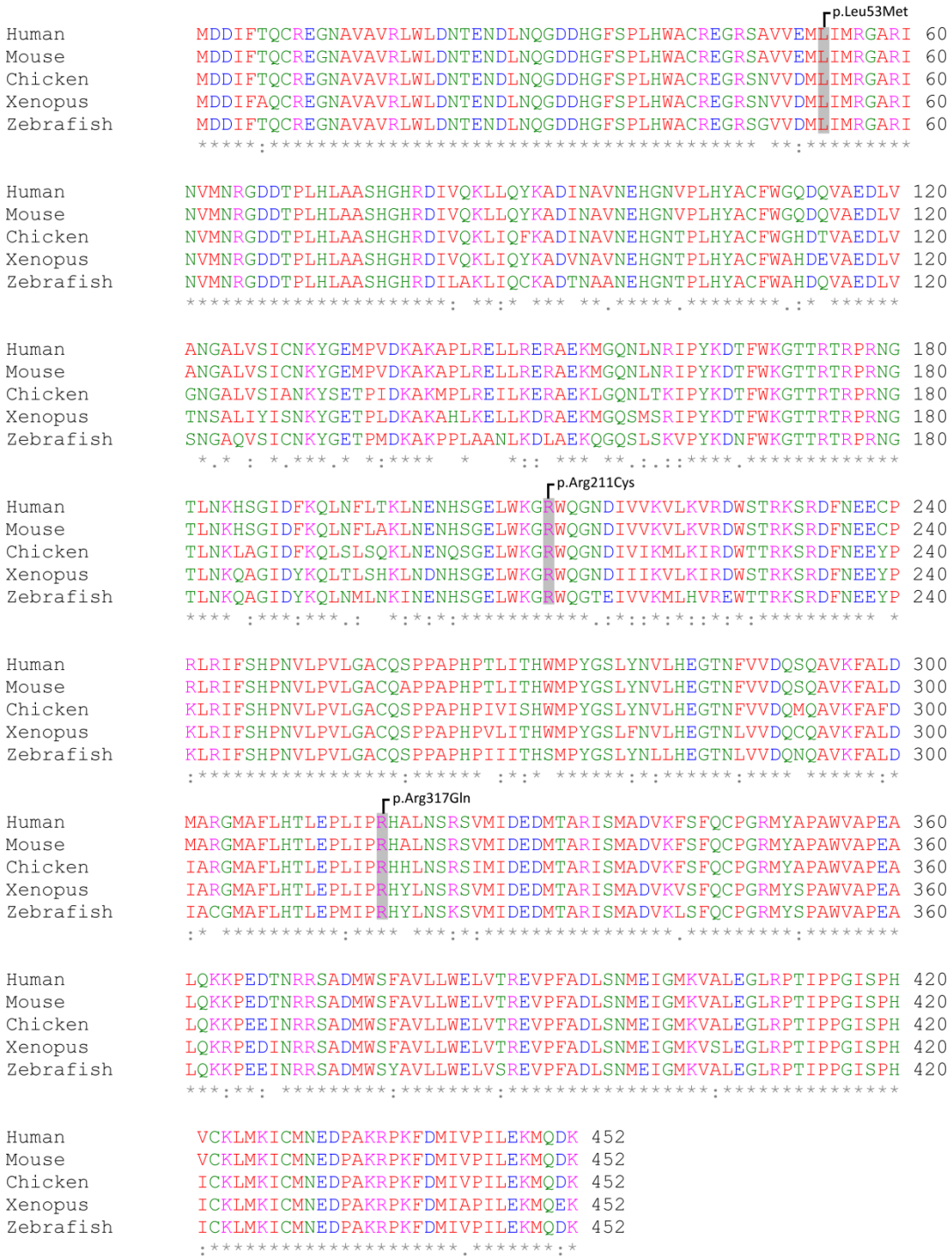

Figure 4B: MSA of *ILK* sequences using CLUSTALW-2.1. Mutation sites are indicated in grey.

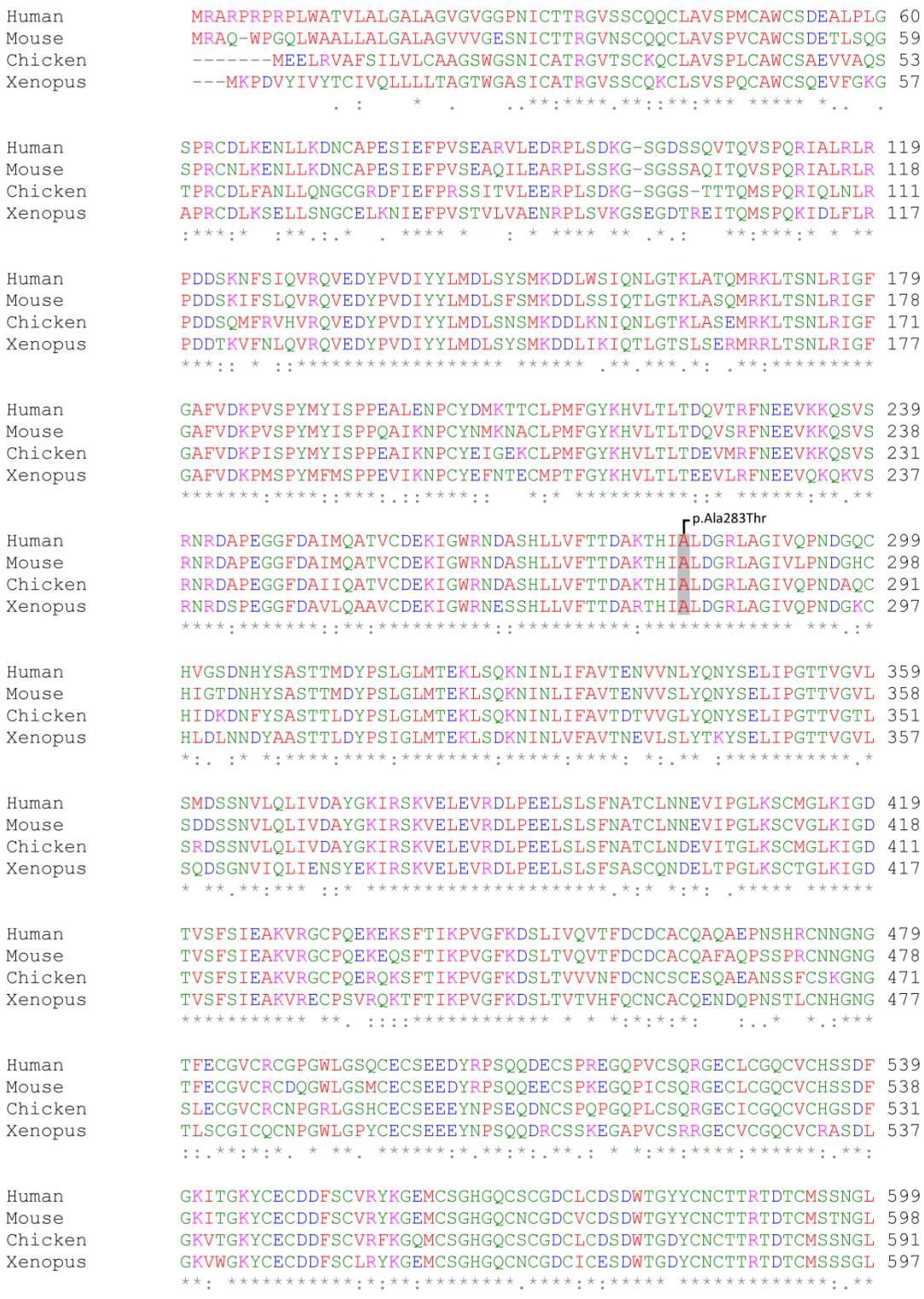
Human MRARPRPRPLWATVLALGALAGVGVGGPNICTTRGVSSCQQCLAVSPMCAWCSDEALPLG 60
Mouse MRAQ-WPGQLWAALLALGALAGVVVGESNICTTRGVNSCQQCLAVSPVCAWCSDETLSQG 59
Chicken -------MEELRVAFSILVLCAAGSWGSNICATRGVTSCKQCLAVSPLCAWCSAEVVAQS 53
Xenopus ---MKPDVYIVYTCIVQLLLLTAGTWGASICATRGVSSCQKCLSVSPQCAWCSQEVFGKG 57
Human SPRCDLKENLLKDNCAPESIEFPVSEARVLEDRPLSDKG-SGDSSQVTQVSPQRIALRLR 119
Mouse SPRCNLKENLLKDNCAPESIEFPVSEAQILEARPLSSKG-SGSSAQITQVSPQRIALRLR 118
Chicken TPRCDLFANLLQNGCGRDFIEFPRSSITVLEERPLSDKG-SGGS-TTTQMSPQRIQLNLR 111
Xenopus APRCDLKSELLSNGCELKNIEFPVSTVLVAENRPLSVKGSEGDTREITQMSPQKIDLFLR 117
Human PDDSKNFSIQVRQVEDYPVDIYYLMDLSYSMKDDLWSIQNLGTKLATQMRKLTSNLRIGF 179
Mouse PDDSKIFSLQVRQVEDYPVDIYYLMDLSFSMKDDLSSIQTLGTKLASQMRKLTSNLRIGF 178
Chicken PDDSQMFRVHVRQVEDYPVDIYYLMDLSNSMKDDLKNIQNLGTKLASEMRKLTSNLRIGF 171
Xenopus PDDTKVFNLQVRQVEDYPVDIYYLMDLSYSMKDDLIKIQTLGTSLSERMRRLTSNLRIGF 177
Human GAFVDKPVSPYMYISPPEALENPCYDMKTTCLPMFGYKHVLTLTDQVTRFNEEVKKQSVS 239
Mouse GAFVDKPVSPYMYISPPQAIKNPCYNMKNACLPMFGYKHVLTLTDQVSRFNEEVKKQSVS 238
Chicken GAFVDKPISPYMYISPPEAIKNPCYEIGEKCLPMFGYKHVLTLTDEVMRFNEEVKKQSVS 231
Xenopus GAFVDKPMSPYMFMSPPEVIKNPCYEFNTECMPTFGYKHVLTLTEEVLRFNEEVQKQKVS 237
p.Ala283Thr
Human RNRDAPEGGFDAIMQATVCDEKIGWRNDASHLLVFTTDAKTHIALDGRLAGIVQPNDGQC 299
Mouse RNRDAPEGGFDAIMQATVCDEKIGWRNDASHLLVFTTDAKTHIALDGRLAGIVLPNDGHC 298
Chicken RNRDAPEGGFDAIIQATVCDEKIGWRNDASHLLVFTTDAKTHIALDGRLAGIVQPNDAQC 291
Xenopus RNRDSPEGGFDAVLQAAVCDEKIGWRNESSHLLVFTTDARTHIALDGRLAGIVQPNDGKC 297
Human HVGSDNHYSASTTMDYPSLGLMTEKLSQKNINLIFAVTENVVNLYQNYSELIPGTTVGVL 359
Mouse HIGTDNHYSASTTMDYPSLGLMTEKLSQKNINLIFAVTENVVSLYQNYSELIPGTTVGVL 358
Chicken HIDKDNFYSASTTLDYPSLGLMTEKLSQKNINLIFAVTDTVVGLYQNYSELIPGTTVGTL 351
Xenopus HLDLNNDYAASTTLDYPSIGLMTEKLSDKNINLVFAVTNEVLSLYTKYSELIPGTTVGVL 357
Human SMDSSNVLQLIVDAYGKIRSKVELEVRDLPEELSLSFNATCLNNEVIPGLKSCMGLKIGD 419
Mouse SDDSSNVLQLIVDAYGKIRSKVELEVRDLPEELSLSFNATCLNNEVIPGLKSCVGLKIGD 418
Chicken SRDSSNVLQLIVDAYGKIRSKVELEVRDLPEELSLSFNATCLNDEVITGLKSCMGLKIGD 411
Xenopus SQDSGNVIQLIENSYEKIRSKVELEVRDLPEELSLSFSASCQNDELTPGLKSCTGLKIGD 417
Human TVSFSIEAKVRGCPQEKEKSFTIKPVGFKDSLIVQVTFDCDCACQAQAEPNSHRCNNGNG 479
Mouse TVSFSIEAKVRGCPQEKEQSFTIKPVGFKDSLTVQVTFDCDCACQAFAQPSSPRCNNGNG 478
Chicken TVSFSIEAKVRGCPQERQKSFTIKPVGFKDSLTVVVNFDCNCSCESQAEANSSFCSKGNG 471
Xenopus TVSFSIEAKVRECPSVRQKTFTIKPVGFKDSLTVTVHFQCNCACQENDQPNSTLCNHGNG 477
Human TFECGVCRCGPGWLGSQCECSEEDYRPSQQDECSPREGQPVCSQRGECLCGQCVCHSSDF 539
Mouse TFECGVCRCDQGWLGSMCECSEEDYRPSQQEECSPKEGQPICSQRGECLCGQCVCHSSDF 538
Chicken SLECGVCRCNPGRLGSHCECSEEEYNPSEQDNCSPQPGQPLCSQRGECICGQCVCHGSDF 531
Xenopus TLSCGICQCNPGWLGPYCECSEEEYNPSQQDRCSSKEGAPVCSRRGECVCGQCVCRASDL 537
Human GKITGKYCECDDFSCVRYKGEMCSGHGQCSCGDCLCDSDWTGYYCNCTTRTDTCMSSNGL 599
Mouse GKITGKYCECDDFSCVRYKGEMCSGHGQCNCGDCVCDSDWTGYYCNCTTRTDTCMSTNGL 598
Chicken GKVTGKYCECDDFSCVRFKGQMCSGHGQCSCGDCLCDSDWTGDYCNCTTRTDTCMSSNGL 591
Xenopus GKVWGKYCECDDFSCLRYKGEMCSGHGQCNCGDCICESDWTGDYCNCTTRTDTCMSSSGL 597

```
Human          LCSGRGKCECGSCVCIQPGSYGDTCEKCPTCPDACTFKKECVECKKFDRGALHDENTCNR 659
Mouse          LCSGRGNCECGSCVCVQPGSYGDTCEKCPTCPDACSFKKECVECKKFNRGTLHEENTCSR 658
Chicken        VCSGHGICVCGKCDCIQPGSYGNTCEKCPTCSDACTIKKECVECKKYERGTLVEQQSCGR 651
Xenopus        LCSGRGQCVCGKCECTQPGSYGDTCEKCPTCPDACTFKKGCVECKKFERGPWFEDSSCKQ 657
               :***:* * **.* * ******:********.***::** ******::**.  ::.:* :

Human          YCRDEIESVKELKDTGKDAVNCTYKNEDDCVVRFQYYEDSSGKSILYVVEEPECPKGPDI 719
Mouse          YCRDDIEQVKELTDTGKNAVNCTYKNEDDCVVRFQYYEDTSGRAVLYVVEEPECPKGPDI 718
Chicken        VCRDEIETVQELGDRGKDAVNCTYKDENDCVVRFQYYEDSSGKSILYVIEEPECPKGPDI 711
Xenopus        ICRDEIESVTELVDNGKNAVNCTYKDENDCVVRFQYHEDASGKSVLYVINEAECPQGPDI 717
                ***:** * ** * **:********:*:*********:**:**:::***::*.***:****

Human          LVVLLSVMGAILLIGLAALLIWKLLITIHDRKEFAKFEEERARAKWDTANNPLYKEATST 779
Mouse          LVVLLSVMGAILLIGLATLLIWKLLITIHDRKEFAKFEEERARAKWDTANNPLYKEATST 778
Chicken        LVVLLSVMGAILLIGLAALLIWKLLITIHDRREFARFEEEKARAKWDTGNNPLYKEATST 771
Xenopus        LVVLMSVMGAILLIGLVALLIWKLLITIHDRREFAKFEEERAKAKWDTAHNPLYKGATST 777
               ****:***********.:**************:***:****:*:*****.:***** ****

Human          FTNITYRGT-- 788
Mouse          FTNITYRGT-- 787
Chicken        FTNITYRGNM- 781
Xenopus        FTNITYRGNTE 788
                ********.
```

Figure 5B: MSA of *ITGB3* sequences using CLUSTALW-2.1. Mutation site is indicated in grey.

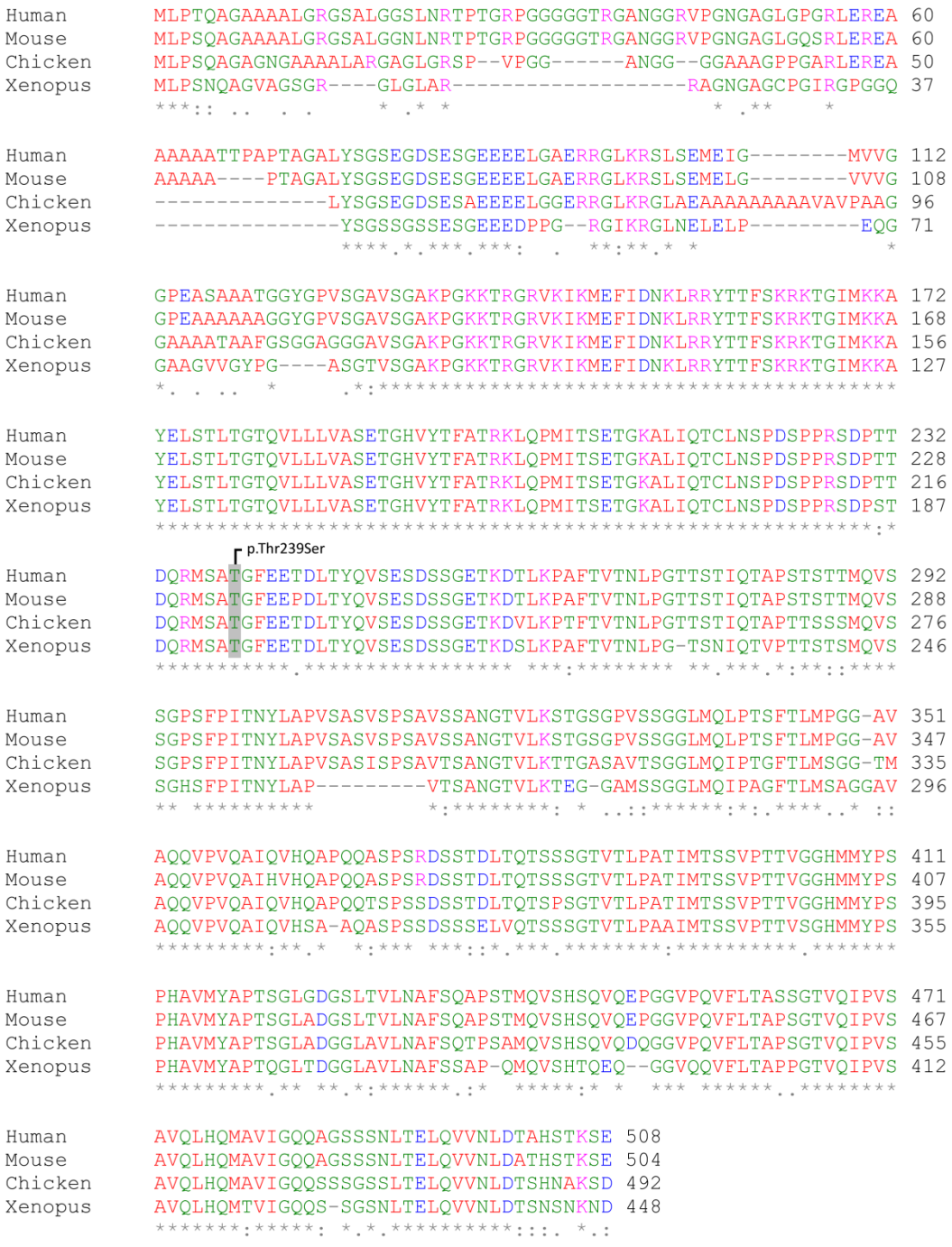

Figure 6B: MSA of *SRF* sequences using CLUSTALW-2.1. Mutation site is indicated in grey.

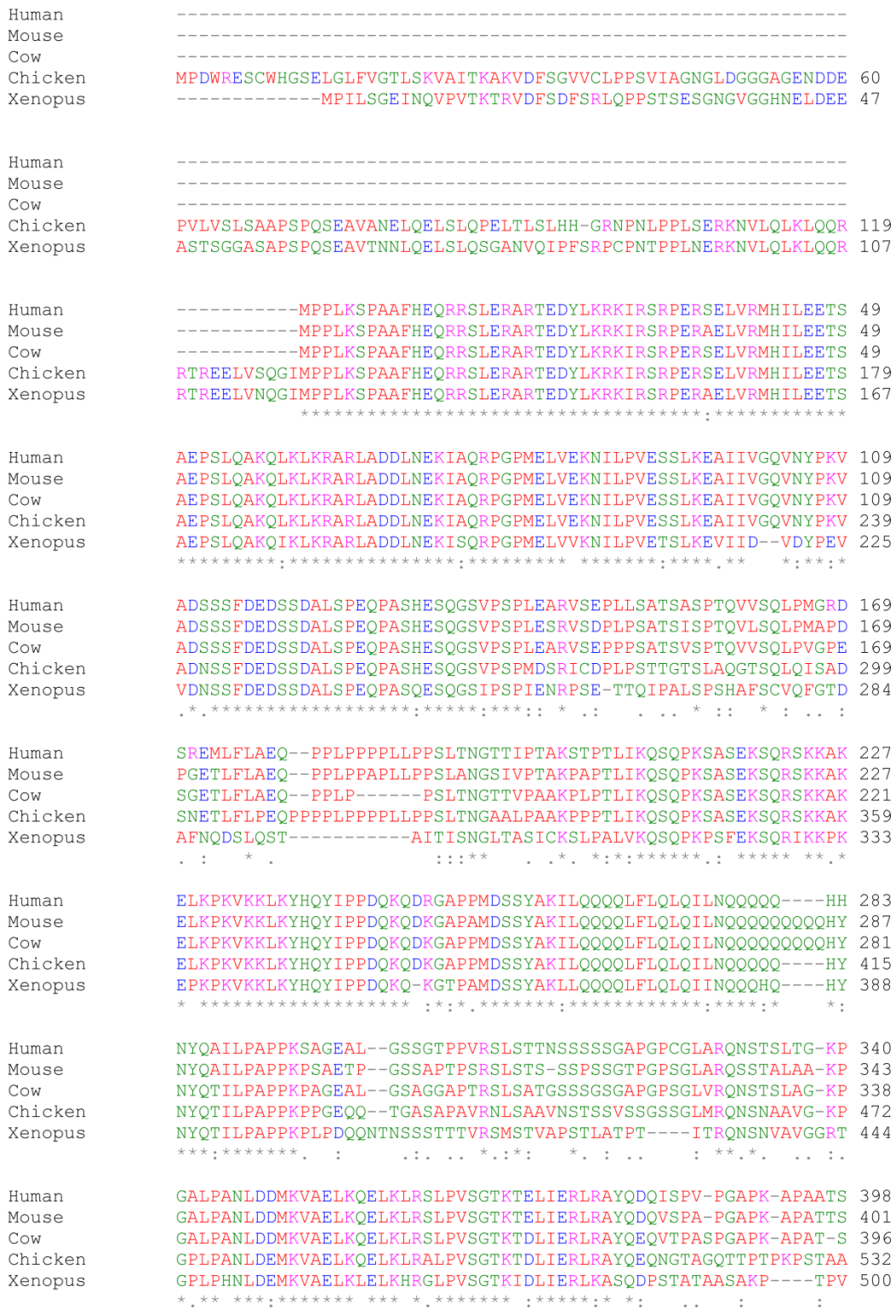
Human ----------
Mouse ----------
Cow ----------
Chicken MPDWRESCWHGSELGLFVGTLSKVAITKAKVDFSGVVCLPPSVIAGNGLDGGGAGENDDE 60
Xenopus ----------MPILSGEINQVPVTKTRVDFSDFSRLQPPSTSESGNGVGGHNELDEE 47
Human ----------
Mouse ----------
Cow ----------
Chicken PVLVSLSAAPSPQSEAVANELQELSLQPELTLSLHH-GRNPNLPPLSERKNVLQLKLQQR 119
Xenopus ASTSGGASAPSPQSEAVTNNLQELSLQSGANVQIPFSRPCPNTPPLNERKNVLQLKLQQR 107
Human ----------MPPLKSPAAFHEQRRSLERARTEDYLKRKIRSRPERSELVRMHILEETS 49
Mouse ----------MPPLKSPAAFHEQRRSLERARTEDYLKRKIRSRPERAELVRMHILEETS 49
Cow ----------MPPLKSPAAFHEQRRSLERARTEDYLKRKIRSRPERSELVRMHILEETS 49
Chicken RTREELVSQGIMPPLKSPAAFHEQRRSLERARTEDYLKRKIRSRPERSELVRMHILEETS 179
Xenopus RTREELVNQGIMPPLKSPAAFHEQRRSLERARTEDYLKRKIRSRPERAELVRMHILEETS 167
Human AEPSLQAKQLKLKRARLADDLNEKIAQRPGPMELVEKNILPVESSLKEAIIVGQVNYPKV 109
Mouse AEPSLQAKQLKLKRARLADDLNEKIAQRPGPMELVEKNILPVESSLKEAIIVGQVNYPKV 109
Cow AEPSLQAKQLKLKRARLADDLNEKIAQRPGPMELVEKNILPVESSLKEAIIVGQVNYPKV 109
Chicken AEPSLQAKQLKLKRARLADDLNEKIAQRPGPMELVEKNILPVESSLKEAIIVGQVNYPKV 239
Xenopus AEPSLQAKQIKLKRARLADDLNEKISQRPGPMELVVKNILPVETSLKEVIID--VDYPEV 225
Human ADSSSFDEDSSDALSPEQPASHESQGSVPSPLEARVSEPLLSATSASPTQVVSQLPMGRD 169
Mouse ADSSSFDEDSSDALSPEQPASHESQGSVPSPLESRVSDPLPSATSISPTQVLSQLPMAPD 169
Cow ADSSSFDEDSSDALSPEQPASHESQGSVPSPLEARVSEPPPSATSVSPTQVVSQLPVGPE 169
Chicken ADNSSFDEDSSDALSPEQPASHESQGSVPSPMDSRICDPLPSTTGTSLAQGTSQLQISAD 299
Xenopus VDNSSFDEDSSDALSPEQPASQESQGSIPSPIENRPSE-TTQIPALSPSHAFSCVQFGTD 284
Human SREMLFLAEQ--PPLPPPPLLPPSLTNGTTIPTAKSTPTLIKQSQPKSASEKSQRSKKAK 227
Mouse PGETLFLAEQ--PPLPPAPLLPPSLANGSIVPTAKPAPTLIKQSQPKSASEKSQRSKKAK 227
Cow SGETLFLAEQ--PPLP------PSLTNGTTVPAAKPLPTLIKQSQPKSASEKSQRSKKAK 221
Chicken SNETLFLPEQPPPPLPPPPLLPPSLTNGAALPAAKPPPTLIKQSQPKSASEKSQRSKKAK 359
Xenopus AFNQDSLQST----------AITISNGLTASICKSLPALVKQSQPKPSFEKSQRIKKPK 333
Human ELKPKVKKLKYHQYIPPDQKQDRGAPPMDSSYAKILQQQQLFLQLQILNQQQQQ----HH 283
Mouse ELKPKVKKLKYHQYIPPDQKQDKGAPAMDSSYAKILQQQQLFLQLQILNQQQQQQQQQHY 287
Cow ELKPKVKKLKYHQYIPPDQKQDKGAPPMDSSYAKILQQQQLFLQLQILNQQQQQQQQQHY 281
Chicken ELKPKVKKLKYHQYIPPDQKQDKGAPPMDSSYAKILQQQQLFLQLQILNQQQQQ----HY 415
Xenopus EPKPKVKKLKYHQYIPPDQKQ-KGTPAMDSSYAKLLQQQQLFLQLQIINQQQHQ----HY 388
Human NYQAILPAPPKSAGEAL--GSSGTPPVRSLSTTNSSSSSGAPGPCGLARQNSTSLTG-KP 340
Mouse NYQAILPAPPKPSAETP--GSSAPTPSRSLSTS-SSPSSGTPGPSGLARQSSTALAA-KP 343
Cow NYQTILPAPPKPAGEAL--GSAGGAPTRSLSATGSSSGSGAPGPSGLVRQNSTSLAG-KP 338
Chicken NYQTILPAPPKPPGEQQ--TGASAPAVRNLSAAVNSTSSVSSGSSGLMRQNSNAAVG-KP 472
Xenopus NYQTILPAPPKPLPDQQNTNSSSTTTVRSMSTVAPSTLATPT----ITRQNSNVAVGGRT 444
Human GALPANLDDMKVAELKQELKLRSLPVSGTKTELIERLRAYQDQISPV-PGAPK-APAATS 398
Mouse GALPANLDDMKVAELKQELKLRSLPVSGTKTELIERLRAYQDQVSPA-PGAPK-APATTS 401
Cow GALPANLDDMKVAELKQELKLRSLPVSGTKTDLIERLRAYQEQVTPASPGAPK-APAT-S 396
Chicken GPLPANLDEMKVAELKQELKLRALPVSGTKTDLIERLRAYQEQNGTAGQTTPTPKPSTAA 532
Xenopus GPLPHNLDEMKVAELKLELKHRGLPVSGTKIDLIERLKASQDPSTATAASAKP----TPV 500

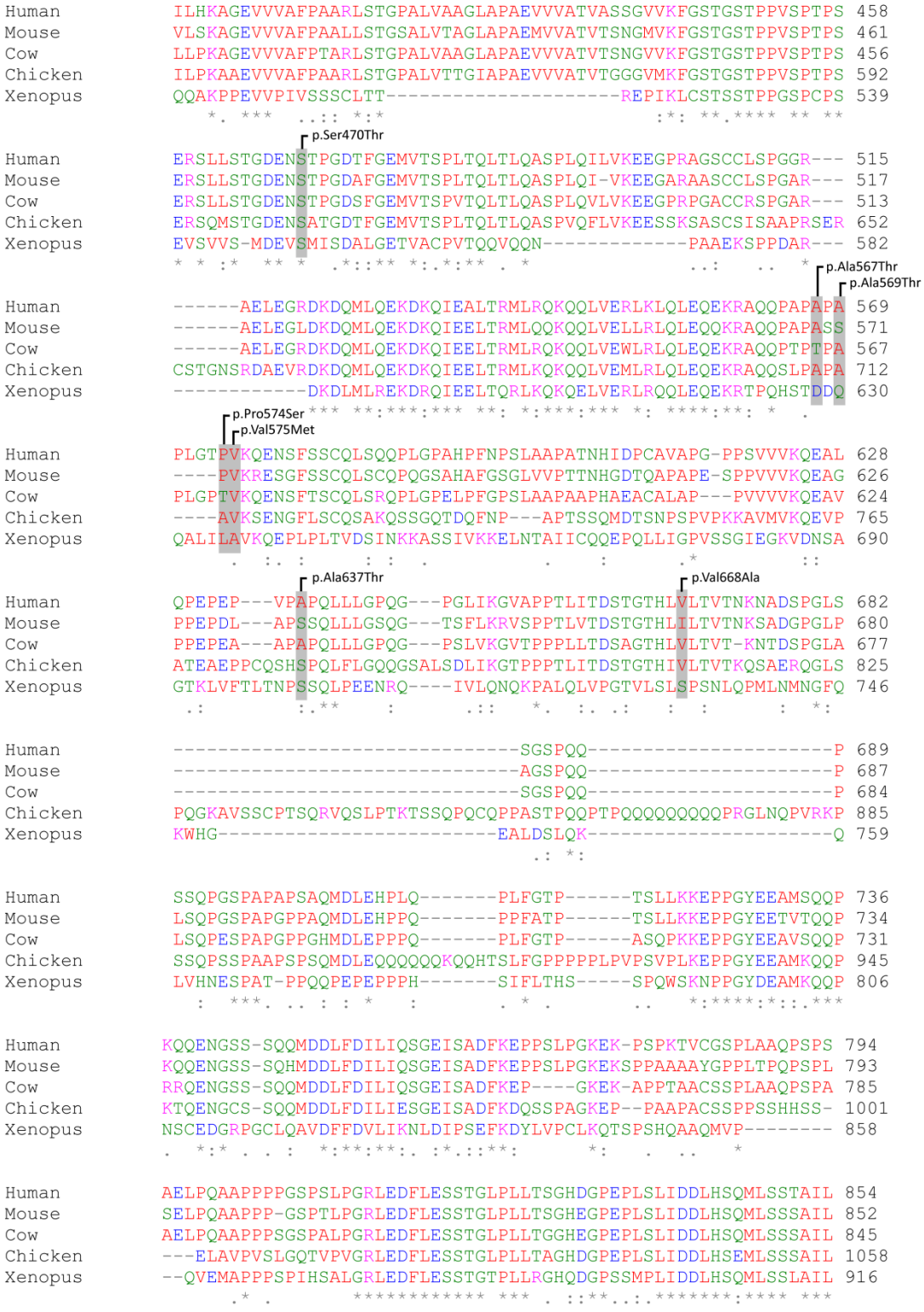
p.Ser470Thr
p.Ala567Thr
p.Ala569Thr
p.Pro574Ser
p.Val575Met
p.Ala637Thr
p.Val668Ala

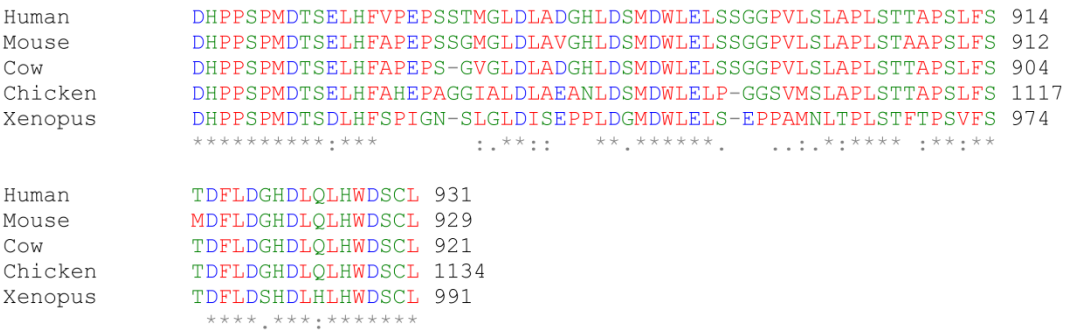

Figure 7B: MSA of *MKL1* sequences using CLUSTALW-2.1. Mutation sites are indicated in grey.

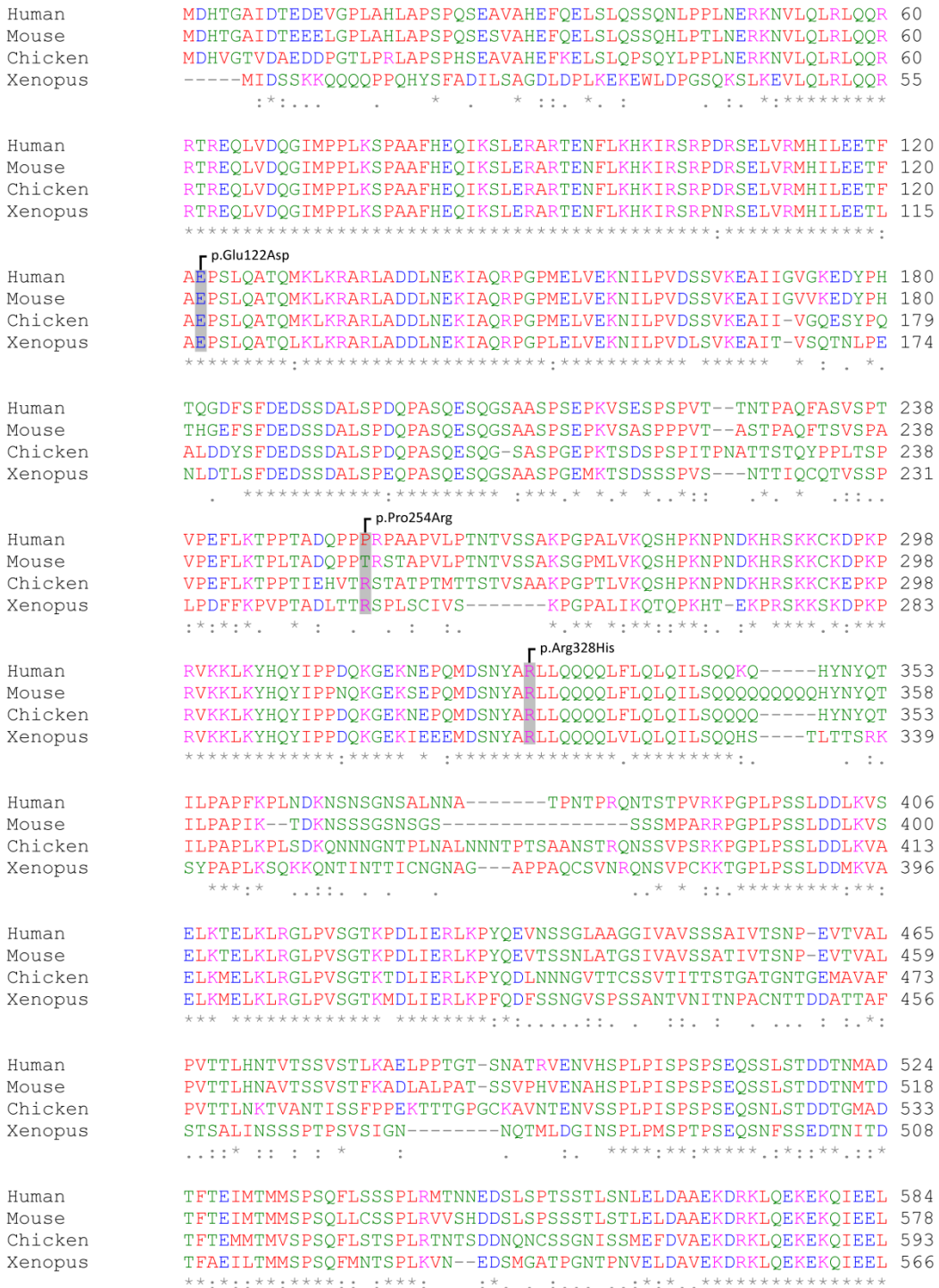
Human MDHTGAIDTEDEVGPLAHLAPSPQSEAVAHEFQELSLQSSQNLPPLNERKNVLQLRLQQR 60
Mouse MDHTGAIDTEEELGPLAHLAPSPQSESVAHEFQELSLQSSQHLPTLNERKNVLQLRLQQR 60
Chicken MDHVGTVDAEDDPGTLPRLAPSPHSEAVAHEFKELSLQPSQYLPPLNERKNVLQLRLQQR 60
Xenopus -----MIDSSKKQQQQPPQHYSFADILSAGDLDPLKEKEWLDPGSQKSLKEVLQLRLQQR 55
Human RTREQLVDQGIMPPLKSPAAFHEQIKSLERARTENFLKHKIRSRPDRSELVRMHILEETF 120
Mouse RTREQLVDQGIMPPLKSPAAFHEQIKSLERARTENFLKHKIRSRPDRSELVRMHILEETF 120
Chicken RTREQLVDQGIMPPLKSPAAFHEQIKSLERARTENFLKHKIRSRPDRSELVRMHILEETF 120
Xenopus RTREQLVDQGIMPPLKSPAAFHEQIKSLERARTENFLKHKIRSRPNRSELVRMHILEETL 115
p.Glu122Asp
Human AEPSLQATQMKLKRARLADDLNEKIAQRPGPMELVEKNILPVDSSVKEAIIGVGKEDYPH 180
Mouse AEPSLQATQMKLKRARLADDLNEKIAQRPGPMELVEKNILPVDSSVKEAIIGVVKEDYPH 180
Chicken AEPSLQATQMKLKRARLADDLNEKIAQRPGPMELVEKNILPVDSSVKEAII-VGQESYPQ 179
Xenopus AEPSLQATQLKLKRARLADDLNEKIAQRPGPLELVEKNILPVDLSVKEAIT-VSQTNLPE 174
Human TQGDFSFDEDSSDALSPDQPASQESQGSAASPSEPKVSESPSPVT--TNTPAQFASVSPT 238
Mouse THGEFSFDEDSSDALSPDQPASQESQGSAASPSEPKVSASPPPVT--ASTPAQFTSVSPA 238
Chicken ALDDYSFDEDSSDALSPDQPASQESQG-SASPGEPKTSDSPSPITPNATTSTQYPPLTSP 238
Xenopus NLDTLSFDEDSSDALSPEQPASQESQGSAASPGEMKTSDSSSPVS---NTTIQCQTVSSP 231
p.Pro254Arg
Human VPEFLKTPPTADQPPPRPAAPVLPTNTVSSAKPGPALVKQSHPKNPNDKHRSKKCKDPKP 298
Mouse VPEFLKTPLTADQPPTRSTAPVLPTNTVSSAKSGPMLVKQSHPKNPNDKHRSKKCKDPKP 298
Chicken VPEFLKTPPTIEHVTRSTATPTMTTSTVSAAKPGPTLVKQSHPKNPNDKHRSKKCKEPKP 298
Xenopus LPDFFKPVPTADLTTRSPLSCIVS-------KPGPALIKQTQPKHT-EKPRSKKSKDPKP 283
p.Arg328His
Human RVKKLKYHQYIPPDQKGEKNEPQMDSNYARLLQQQQLFLQLQILSQQKQ-----HYNYQT 353
Mouse RVKKLKYHQYIPPNQKGEKSEPQMDSNYARLLQQQQLFLQLQILSQQQQQQQQQHYNYQT 358
Chicken RVKKLKYHQYIPPDQKGEKNEPQMDSNYARLLQQQQLFLQLQILSQQQQ-----HYNYQT 353
Xenopus RVKKLKYHQYIPPDQKGEKIEEEMDSNYARLLQQQQLVLQLQILSQQHS----TLTTSRK 339
Human ILPAPFKPLNDKNSNSGNSALNNA-------TPNTPRQNTSTPVRKPGPLPSSLDDLKVS 406
Mouse ILPAPIK--TDKNSSSGSNSGS----------------SSSMPARRPGPLPSSLDDLKVS 400
Chicken ILPAPLKPLSDKQNNNGNTPLNALNNNTPTSAANSTRQNSSVPSRKPGPLPSSLDDLKVA 413
Xenopus SYPAPLKSQKKQNTINTTICNGNAG---APPAQCSVNRQNSVPCKKTGPLPSSLDDMKVA 396
Human ELKTELKLRGLPVSGTKPDLIERLKPYQEVNSSGLAAGGIVAVSSSAIVTSNP-EVTVAL 465
Mouse ELKTELKLRGLPVSGTKPDLIERLKPYQEVTSSNLATGSIVAVSSATIVTSNP-EVTVAL 459
Chicken ELKMELKLRGLPVSGTKTDLIERLKPYQDLNNNGVTTCSSVTITTSTGATGNTGEMAVAF 473
Xenopus ELKMELKLRGLPVSGTKMDLIERLKPFQDFSSNGVSPSSANTVNITNPACNTTDDATTAF 456
Human PVTTLHNTVTSSVSTLKAELPPTGT-SNATRVENVHSPLPISPSPSEQSSLSTDDTNMAD 524
Mouse PVTTLHNAVTSSVSTFKADLALPAT-SSVPHVENAHSPLPISPSPSEQSSLSTDDTNMTD 518
Chicken PVTTLNKTVANTISSFPPEKTTTGPGCKAVNTENVSSPLPISPSPSEQSNLSTDDTGMAD 533
Xenopus STSALINSSSPTPSVSIGN--------NQTMLDGINSPLPMSPTPSEQSNFSSEDTNITD 508
Human TFTEIMTMMSPSQFLSSSPLRMTNNEDSLSPTSSTLSNLELDAAEKDRKLQEKEKQIEEL 584
Mouse TFTEIMTMMSPSQLLCSSPLRVVSHDDSLSPSSSTLSTLELDAAEKDRKLQEKEKQIEEL 578
Chicken TFTEMMTMVSPSQFLSTSPLRTNTSDDNQNCSSGNISSMEFDVAEKDRKLQEKEKQIEEL 593
Xenopus TFAEILTMMSPSQFMNTSPLKVN--EDSMGATPGNTPNVELDAVEKDRKLQEKEKQIEEL 566

Figure 8B: MSA of *MKL2* sequences using CLUSTALW-2.1. Mutation sites are indicated in grey.

Figure 9B: MSA of *NDP* sequences using CLUSTALW-2.1. Mutation site is indicated in grey.

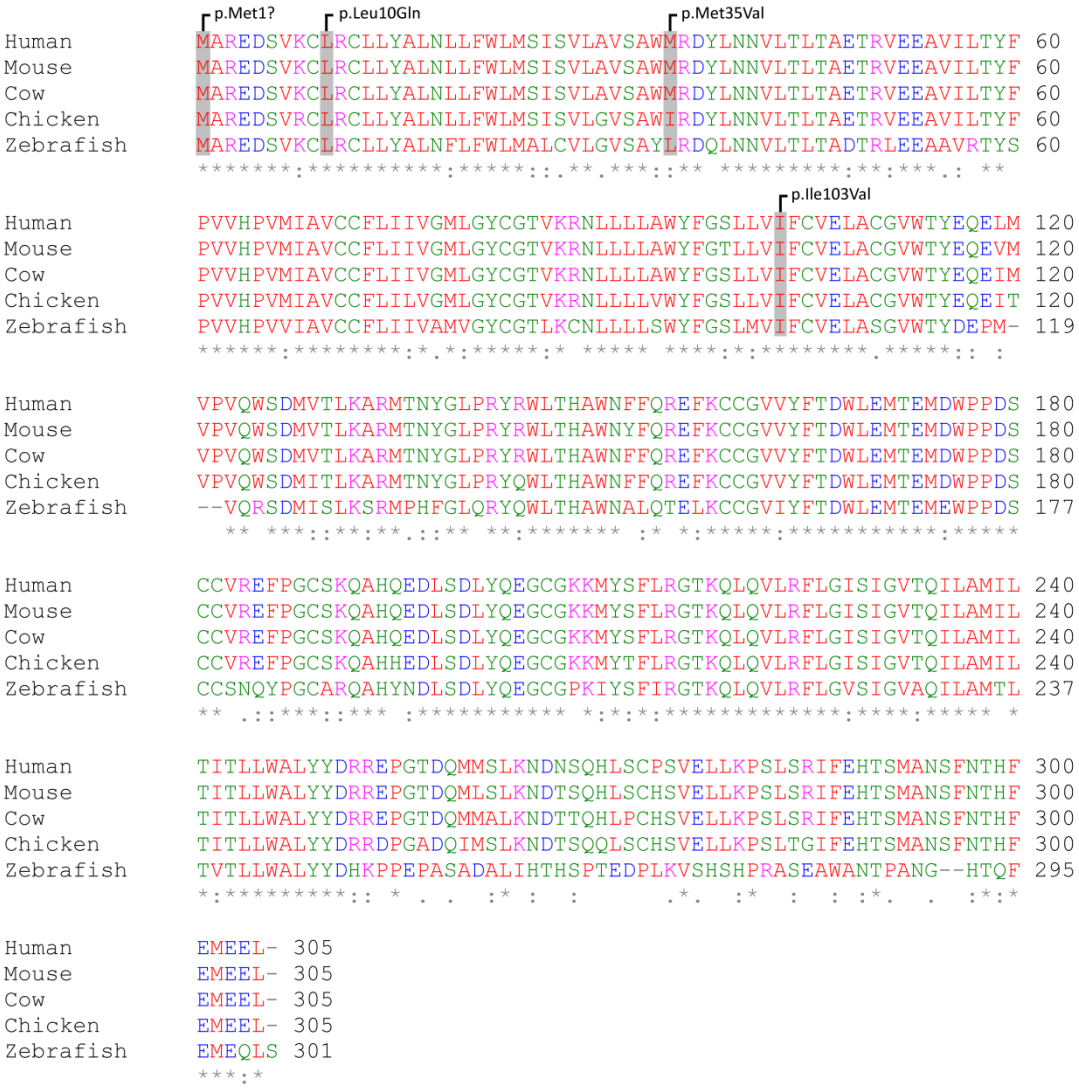

Figure 10B: MSA of *TSPAN12* sequences using CLUSTALW-2.1. Mutation sites are indicated in grey.

Residue	Colour	Property
AVFPMILW	RED	Small (small+ hydrophobic (incl.aromatic -Y))
DE	BLUE	Acidic
RK	MAGENTA	Basic - H
STYHCNGQ	GREEN	Hydroxyl + sulfhydryl + amine + G
Others	Grey	Unusual amino/imino acids etc

Table 1B: Colors indicate the residues according to their physicochemical properties.

Appendix C – Primer- and Vectorcollection

Primercollection

Cloning Sequencing Primers	
Name	**Sequenze 5'-3'**
FWD ILK pENTRY	CACCATGGACGACATTTTCAC
REV ILK STOP	TCATTACTACTTGTCCTGCATC
REV ILK w/o STOP	CTTGTCCTGCATCTTCTCAAGG
M13_FWD (-20)	GTAAAACGACGGCCAG
M13_REV	CAGGAAACAGCTATGAC
T7	gtaatacgactcactatagggc
V5_rev	ACCGAGGAGAGGGTTAGGGAT
CMV_pBud_for	CGTGTACGGTGGGAGGTCTA
MYC_pBud_rev	TGAGTTTTTGTTCGGATCCTC
ATOH7_NLS_for1	CACCATGCCCAAGAAGAAGCGAAAGGTGAAGTCCTGCAAGCCCAGC
ATOH7_NLS_for2	AGCGAAAGGTGAAGTCCTGCAAGCCCA
Atoh_NLS_For3	CACCATGCCCAAGAAGAAGCGAAAGGTGAA
ATOH7_CACC_FWD	CACCATGAAGTCCTGCAAGC
ATOH7_STOP_REV	TCATTACTAGGTGGCCATCTGG
CACC NeuroD1 F3	CACCATGGATTACAAGGATGACGATGAC
cloning NeuroD1 F2	aggatgacgatgacaagGGATCCGGAAC
cloning NeuroD1 F1	aagGGATCCGGAACCAAATCGTACAGC
cloning NeuroD1 Rev	TCATTACTAATCATGAAATATGGCATTGAGCTGG
NINJ1_EntryVector_CACC_for	CACCATGGACTCGGGAACCGA
NINJ1_Frag1_rev	AGATGTTGACTACCACGATG
NINJ1_Frag1_rev_2	CACATAGAAGGCGAAGCTG
NINJ1_Frag2_for	ATCTCCATCTCCCTTGTGCTG
NINJ1_EntryVector_STOP_rev	TCATTACTACTGCTGGGGTGCCAT
VP1.5_for	GGACTTTCCAAAATGTCG
XL39_rev	ATTAGGACAAGGCTGGTGGG
M_ILK_cDNA_F1_R	TGAAGTCAATACCGGAGTG
M_ILK_cDNA_F2_F	TTCTCCGAGAACGGGCAG
M_ILK_cDNA_F2_R	ACTTAACATCAGCCATGCTG
M_ILK_cDNA_F3_F	AGGATTTTCTCACACCCTAAC
M_ILK_F1_SeqREV2	TGCTCATTCACTGCATTGATG
M_ILK_F3_SeqFWD2	ACGAGAGGTGCCCTTTGC
H_ILK_cDNA_F1_R	TCTCGGAGAAGCTCTCTC
H_ILK_cDNA_F2_F	TGGCAGAGGACCTGGTGG
H_ILK_cDNA_F2_R	CCCTTGCCATGTCCAAAGC
H_ILK_cDNA_F3_F	CTACTCTCATCACACACTG
H_ILK_F1_SeqREV2	ATGACTGGCTGCCAGATGC
H_ILK_F3_SeqFWD2	CGAAGCTCTGCAGAAGAAGC
ITGB3_CACC_EntryVector_for	CACCATGCGAGCGCGGCCGC
ITGB3_Frag1_rev	GGTTACTGGTGAGCTTTC
ITGB3_Frag2_for	GAGTACTAGAGGACAGGCC
ITGB3_Frag2_rev	ACCAGCAAGTGGGATG
ITGB3_Frag3_for	TCGAAAACCCCTGCTATG
ITGB3_Frag3_rev	ACTCTTCAGGGAGGTCACG

ITGB3_Frag4_for	TGGGGCTGATGACTGAGAAGCT
ITGB3_Frag4_rev	ACTCGCCCCGCTGGCTG
ITGB3_Frag5_for	ATCGTCCAGGTCACCTTTG
ITGB3_Frag5_rev	AGGTATTTTCGTCATGTAGGG
ITGB3_Frag6_for	GGCTACTACTGCAACTGTACC
ITGB3_STOP_EntryVector_rev	CTATCATTAAGTGCCCCGGTACGTGATATTGGTGA

Mutagenesis Primers	
Name	Sequenze 5'-3'
M_ILK FWD Mut 157	GGTGGTTGAAATGATGATCATGCGTGGAGCACGGATTAATG
M_ILK REV Mut 157	GCATGATCATCATTTCAACCACCGCAGAGCGGCCT
M_ILK FWD Mut 631	TTGGAAAGGCTGCTGGCAGGGCAATGATATTGTTGTGAAGGTG
M_ILK REV Mut 631	TTGCCCTGCCAGCAGCCTTTCCAAAGCTCTCCAGAATGATTCTC
M_ILK FWD Mut 950	TCTCATACCCCAGCATGCACTCAATAGCCGCAGTGTAATG
M_ILK REV Mut 950	TGAGTGCATGCTGGGGTATGAGAGGCTCTAGTGTGTGAAGAAAAG
H_ILK FWD Mut 157	TGTGGTTGAGATGATGATCATGCGGGGGGCACG
H_ILK REV Mut 157	CCCGCATGATCATCATCTCAACCACAGCAGAGCGGC
H_ILK FWD Mut 631	AGCTATGGAAGGGCTGCTGGCAGGGCAATGACATTGTCGTG
H_ILK REV Mut 631	ATTGCCCTGCCAGCAGCCCTTCCATAGCTCTCCAGAGTGATTCTC
H_ILK FWD Mut 950	CCTCATCCCACAACATGCACTCAATAGCCGTAGTG
H_ILK REV Mut 950	TGAGTGCATGTTGTGGGATGAGGGGCTCTAGTG
NINJ1_pAla42Thr_for	ATCAACGTGAACCATTACACCAGCAAGAAGAGCGCAGC
NINJ1_pAla42Thr_rev	CTTGCTGGTGTAATGGTTCACGTTGATGGGCCCG
NINJ1_rs2275848_corr_for	GACCTTAACAACCCGGCCAAGCACGCCAAGCTGGACTTC
NINJ1_rs2275848_corr_rev	CTTGGCGTGCTTGGCCGGGTTGTTAAGGTCGTACTTGACAAG
ITGB3_pAla283Thr_for	GATGCCAAGACTCATATAACATTGGACGGAAGGCTGG
ITGB3_pAla283Thr_rev	CGTCCAATGTTATATGAGTCTTGGCATCAGTGGTAAACACCAG

RT-PCR Primers		
Name	**Sequenze 5'-3'**	**Product bp**
hNDP fwd	cataatggactcggaccctc	313
hNDP rev	cctcaggaattgcattcctc	
hFZD4 fwd	ctacaacgtgaccaagatgc	275
hFZD4 rev	gggaatttgctgcagttcag	
hLRP5 fwd	ggacttccagttttccaagg	392
hLRP5 rev	ccattgggccagtaaatgtc	
hTSAPN12 fwd	GGTCACTTTGAAAGCCAGGA	282
hTSAPN12 rev	ACCTGCAGTTGTTTGGTTCC	
hVEGF165 fwd	TCTTCAAGCCATCCTGTGTG	218
$hVEGF_{165}$ rev	CCCACAGGGATTTTCTTGTCT	
hFLT fwd	CTTTTACCGAATGCCACCTC	201
hFLT rev	ACAGCTGGAATGGCAGAAAC	
hKDR fwd	TGCCTACCTCACCTGTTTCC	279
hKDR rev	GCACCATTCCACCAAAAGAT	
18S for	GTAACCCGTTGAACCCCATT	
18s rev	CCATCCAATCGGTAGTAGCG	
H-Atoh7_RT_F	AGAGACTCTTCGGCTTCCAG	123
H_Atoh7_RT_R	AGGCTTCTGGGCTACTTGG	

EMSA Primers	
hNDP E-Box rev	AGTCCCAAAGCAGGTGGGAGACAGGAC
hNDP E-Box for	GTCCTGTCTCCCACCTGCTTTGGGACT
Ndph E-Box for	ATTATACTTGCCACCTGCTTGCTGTGC
Ndph E-Box rev	GCACAGCAAGCAGGTGGCAAGTATAAT
Atoh7_Ebox_rev	AGGGAACAGGTGGTGGCAGGTGGGCG
Atoh7_Ebox_for	CGCCCACCTGCCACCACCTGTTCCCT
hCHRNB3_E-Box_rev	TGCACTTCATTGATTTGCAGTCAGCTGTCAGATCG
hCHRNB3 E-Box_for	CGATCTGACAGCTGACTGCAAATCAATGAAGTGCA

PCR and DNA Sequencing Primers		
Name	**Sequenze 5'-3'**	**Product bp**
ATOH7_Ex1_for	ATTGCACGTGAGTTGCTTTG	474
ATOH7_Ex1_rev2	AGTGTTGAGCCCCTGCAT	
ATOH7_Ex1_for2	ATGCAGGGGCTCAACACT	454
ATOH7_Ex1_rev	TGATGCGAATAAAGGTAATCTGA	
ATOH7_Ex1_for3	CCCTAAATTTGGGCAAGTGA	mit rev2 564
ATOH7_Ex1_for4	TAGAACAGAAGGCCGAGTCC	mit rev2 520
ATOH7_deletion_FWD	GGGATGAAGTCCTGCAAGC	186-24
ATOH7_deletion_REV	GTCGAAGGCAGTGTTGAGC	
NEUROD1_Ex1_for1	tgcctctttcacctctgtcc	416
NEUROD1_Ex1_rev1	CCTCCTCCCCACTTCTCC	
NEUROD1_Ex1_for2	GTAGGGGTGGAGGGTGAGG	485
NEUROD1_Ex1_rev2	GGGGGTACTTGAGTGACACG	
NEUROD1_Ex2_for1	gaagctgaaggcgtatctgg	506
NEUROD1_Ex2_rev1	TGGACAGCTTCTGCGTCTTA	
NEUROD1_Ex2_for2	AATTGAGACGCATGAAGGCTA	500
NEUROD1_Ex2_rev2	GCTGGTGCAATCAGTCAGAG	
NEUROD1_Ex2_for3	ACAGCTCCCATGTCTTCCAC	653
NEUROD1_Ex2_rev3	CGATCTGAATACAGCCACACC	
NEUROD1_Ex2_for4	CTGCCTTTGGAAGAAACAGG	584
NEUROD1_Ex2_rev4	TTTTAGGGAGACGGAAAGACT	
NEUROD1_Ex2_for5	CCAGCAGAAAAGTGCTTAGAAA	365
NEUROD1_Ex2_rev5	AAAATCATGGAATGCAAAGGA	
NEUROD1_Ex2_for6	TCAAAAGCTGCTTGACTATCACA	623
NEUROD1_Ex2_rev6	GGTGACTCCCTGTGCAAGAT	
NINJ1_Ex1_for	GACGGAGGTTCAGAGCAAGA	490
NINJ1_Ex1_rev	ACGTCCCCCAACACTCTG	
NINJ1_Ex2_for	CACTTCTGTCTGAGCACTTACCA	472
NINJ1_Ex2_rev	TTGAGAGCCAAGTGTGCAAG	
NINJ1_Ex3_for	CGCTGTTGTCCATGTTTCAG	466
NINJ1_Ex3_rev	GGCCTAGGAAGGTGTCCAA	
NINJ1_Ex4_for	CTGACACTCGGGGCTTGT	457
NINJ1_Ex4_rev	AGTCAGAGCAAGGGCTGGT	
ZNF408_Exon1_for	CAGAGTTCTGCCTCCC	402
ZNF408_Exon1_rev	CTAAGGAGGGCCCTGAAAG	
ZNF408_Exon2_for	ACCTGGACCTGCGGTTTC	497
ZNF408_Exon2_rev	CTGAAGAGAAGGGACAAGACTATC	

ZNF408_Exon3_for	CCAGAGGCTTCTAACCTTCCA	310
ZNF408_Exon3_rev	GTGCCTTTGGAACATTCACTG	
ZNF408_Exon4_for	CCTTTAGGACCCAGACTGCTT	832
ZNF408_Exon4_rev	CCTTCCCACCTTAGCTCATCT	
ZNF408_Exon4_Seq	ACCGCAATGAGCCATAAACT	
ZNF408_Exon5A_for	TCTCAGGAGTGCTTCTCCAAA	562
ZNF408_Exon5A_rev	GAGAGTGTAGGGAAGCCAGACT	
ZNF408_Exon_5Fa	AGACCTCAAAGAGCACCAGGT	
ZNF408_E5A(Seq)rev	CTGTGTAACTTCTTGGCCAGG	
ZNF408_Exon5B_for	CCTGGCCAAGAAGTTACACAG	569
ZNF408_Exon5B_rev	TTTCTCCTGTATGGAGCCTCA	
ZNF408_Ex5BSeqfor	AGTCTGGCTTCCCTACACTCTC	
ZNF408_Exon5C_for	AGCACCAGGTGGTACATTCAG	657
ZNF408_Exon5C_rev	AAGCAGCAGAAGGCACAGAG	
ZNF408_Ex5CSeqfor	TGAGGCTCCATACAGGAGAAA	
ZNF408_Exon5D_for	CACTTGGAGGACAAGCCCTA	597
ZNF408_Exon5D_rev	GCAGAACAACAAGCTCTACCG	
ZNF408 ex 5 seq5d	CTCTGTGCCTTCTGCTGCTT	
ILK_Ex2_for	CTTCACAGACCCCCACTAGC	327
ILK_Ex2_rev	GACATGAGCACTCCACTCCA	
ILK_Ex3_for	GTTGCTGGCATGAATGAGAA	426
ILK_Ex3_rev	CCCTCATGGCATGTATGTGA	
ILK_Ex4_for	CATACATGCCATGAGGGTCA	318
ILK_Ex4_rev	TTCCAAAATCTCCCACCAAG	
ILK_Ex5_for	CTTGGTGGGAGATTTTGGAA	374
ILK_Ex5_rev	GAAGGGACGAGAGGACACAA	
ILK_Ex6&7_for	CCCTAGCTTGTGTCCTCTCG	483
ILK_Ex6&7_rev	GGTAGGGGTTAGGAGGCTTG	
ILK_Ex8_for	TCCCTCACTAAACCCCCATA	325
ILK_Ex8_rev	AGGGAGGGAGTGGTTGAGAC	
ILK_Ex9_for	GGAAGCTGCTAGTTCCAAGG	295
ILK_Ex9_rev	TGAGAGGAGGCAAAAGTCAAA	
ILK_Ex10&11_for	GGGATGTTGAATTTCCTTGG	500
ILK_Ex10&11_rev	TGGAGAGATAGGGCTTGTCTG	
ILK_Ex12_for	AAGTCATCATGTCGGGAGGT	355
ILK_Ex12_rev	CCCTTGGGACAGGATTACTGTAT	
ILK_Ex13_for	GCCTTGGCTCCTCACATATT	389
ILK_Ex13_rev	CATGGCTGGGGTAGTACCAT	
ILK_Ex12&Ex13_for	AAGTCATCATGTCGGGAGGT	508
ILK_Ex12&Ex13_rev	CATGGCTGGGGTAGTACCAT	
PARVA_Ex1_for	CTGCCTCAAATGCTTGGAAT	629
PARVA_Ex1_rev	TACTGGATCGCACTGTCTGC	
PARVA_Ex2&3_for	ACAGCTGGCAGAGGTGAGAT	563
PARVA_Ex2&3_rev	GGGCTGCCATGACTTTTTAC	
PARVA_Ex4_for	TGTTTAGGATAAGAAAGCTGGTCTG	329
PARVA_Ex4_rev	TGTTATTCCATGCTCCACACA	
PARVA_Ex5_for	AGTGTCCCTCTGCTGGTAGG	483
PARVA_Ex5_rev	ATTTTTCCCCAAGGGTATGG	
PARVA_Ex6_for	TCCAAACTCTATCAGTGGGGTA	426
PARVA_Ex6_rev	AGCACACGCTCTTCCATCTT	

PARVA_Ex7_for	GGTTCAGTCCAGTCCCTGAA	348
PARVA_Ex7_rev	CCTCCTGCAATCCCAATAAA	
PARVA_Ex8_for	AGGCCGTGCAGAATAAAATG	371
PARVA_Ex8_rev	CTTCTTCCCGCCAGTAAGC	
PARVA_Ex9_for	ATGACTAATCCCGGGTCACA	457
PARVA_Ex9_rev	GGTTAGGTGATGCCACCAGT	
PARVA_Ex10_for	GCCTGATCCTCTGCTTTCAC	325
PARVA_Ex10_rev	CCACCCCTCAGAGTAGGACA	
PARVA_Ex11_for	GGTAGGCTTCAGGTGGTGGCATA	348
PARVA_Ex11_rev	TATAATGGGTCCCACCTCCA	
PARVA_Ex12_for	TCCCAACAGCAAGCTAGGAT	359
PARVA_Ex12_rev	CAGAAAATGCTTCCCTCTGC	
PARVA_Ex13_for	CTTCCCCTCCTTTTCACCAC	485
PARVA_Ex13_rev	GCACAGTGCAAGAGACAGGA	
ITGB3 Ex1 for	GGCGAGAGAGGAGCAATAGTT	505
ITGB3 Ex1 rev	GCACCAGGCACCTCTCAG	
ITGB3 Ex2 for	GTTTGTGTGCACCTGAGAGC	317
ITGB3 Ex2 rev	AGAAGGGATAAGGGGCATGT	
ITGB3 Ex3 for	GCTCCAATGTACGGGGTAAA	382
ITGB3 Ex3 rev	CTCCTCAGACCTCCACCTTG	
ITGB3 Ex4 for	GGAAGAGGAAAAGGGACCAG	582
ITGB3 Ex4 rev	GCCTTAGGCTCCATTGACAC	
ITGB3 Ex5 for	TGAACTGTCTGGGTAACTGTGG	484
ITGB3 Ex5 rev	AGGCCAGGGAGTGGATCTAA	
ITGB3 Ex6 for	GTTCCAAGGACTGGGACTGA	476
ITGB3 Ex6 rev	ACGGTGTCCAGTTGGTAAGG	
ITGB3 Ex7 for	CCCAGGCTCTTGTCTCACTT	394
ITGB3 Ex7 rev	GGCCCAGAGTGCAATCTTTA	
ITGB3 Ex8 for	AGGGGTGTGAGAGGTTTCCT	399
ITGB3 Ex8 rev	AAGGCAGTAAGACCGTGTGG	
ITGB3 Ex9 for	GCGCAGGAAACAGAGTCCTA	512
ITGB3 Ex9 rev	TACGCAACAGAAGCCTCAGA	
ITGB3 Ex10 for	GCTGAGGAACTCCAGATTGC	656
ITGB3 Ex10 rev	GGCCTTCACCTATGTTTCCA	
ITGB3 Ex11 for	CCTTGGGACCCCTAGAAAAC	587
ITGB3 Ex11 rev	TATTCCAACTTGCCCAAAGC	
ITGB3 Ex12 for	CCCCAGGATTGTCTTACAGG	404
ITGB3 Ex12 rev	ATTGTTCCTCAAGCCTGCAC	
ITGB3 Ex13 for	GACACAACAGCCACCTTGAA	403
ITGB3 Ex13 rev	GGCCCCTAACTTATCACTTGC	
ITGB3 Ex14 for	TGCTGTCCTAATGATTGTCTCC	411
ITGB3 Ex14 rev	AACATGACCACCCAAAGCAT	
ITGB3 Ex15 for	CCCATGCCAAGAACTAAAGTG	303
ITGB3 Ex15 rev	AAACATGATGGCAGGGACTC	
SRF_Ex1_for	GATAGCGGCACTAGCAGCAG	760
SRF_Ex1_rev	ATCCCCTCCCACACACCT	
SRF_Ex1_int_seq_for	TCTACAGCGGCAGCGAGGGC	
SRF_Ex1_int_seq_rev	CCACCATACCGATCTCCATC	
SRF_Ex2_for	GACGAAGGTCATTATGGGAATG	468
SRF_Ex2_rev	GCACCTATCCACCTGTCCTG	

SRF_Ex3_for	GGATTTGAACCCAAGCTCACT	480
SRF_Ex3_rev	CTTCTGAGCAGGGAAAGAGGT	
SRF_Ex4_for	GAGTGGATACTTGGGCCTGA	360
SRF_Ex4_rev	AGGGTTACTGTTGGGCACCT	
SRF_Ex5_for	ACCTGGGAAATGGCAAGAG	391
SRF_Ex5_rev	AGGCATCAGTGCATATGTGTGT	
SRF_Ex6_for	CCTTTCCCTTGGGCTCTTAC	318
SRF_Ex6_rev	AGAAAAGCAGATGGGCTTCC	
SRF_Ex7_for	GGAAGCCCATCTGCTTTTCT	299
SRF_Ex7_rev	CCCGTCAACGTGTGTGTAAA	
MKL1 Ex1 for	ccgtcagtcacaggaagtca	562
MKL1 Ex1 rev	agaaggccggcaagaagag	
MKL1 Ex2 for	tgtgcatggagaggattgaa	350
MKL1 Ex2 rev	ggcacgatgagtgagactga	
MKL1 Ex3 for	accacccctgtgattcagtt	599
MKL1 Ex3 rev	ggaactttcacggaacatcaa	
MKL1 Ex4 for	tcaggccacttctgcaatta	382
MKL1 Ex4 rev	ttgagctctaaacttggaaagtca	
MKL1 Ex5 for	gcctcagcctcccaaagt	341
MKL1 Ex5 rev	cagggctggccctagagt	
MKL1 Ex6 for	gaaccctgcagtcaccaagt	405
MKL1 Ex6 rev	cacagctgtcgtacggtgtt	
MKL1 Ex7 for	gacaggccactcttctctgc	476
MKL1 Ex7 rev	ctgtgcatgaggctctcaaa	
MKL1 Ex8 for	ggaccaagaaagcagattgg	516
MKL1 Ex8 rev	gcccacatctcccaccac	
MKL1 Ex9 for	cctagctcctccttgctcct	509
MKL1 Ex9 rev	gtggctatgattgcaacagc	
MKL1 Ex10 for	gaagagtggaaatgggcaaa	581
MKL1 Ex10 rev	gcaggattgggtacagatgg	
MKL1 Ex11 for	ggatgctacagagtggtctgc	470
MKL1 Ex11 rev	agagcctaaagccctgctct	
MKL1 Ex12_1 for	agaggatgctgttggctcag	527
MKL1 Ex12_1 rev	GTTTTCATCGCCCGTGCT	
MKL1 Ex12_2 for	GTGGTGAAGTTTGGCAGCAC	524
MKL1 Ex12_2 rev	GCCACAGCACAAGGGTCTAT	
MKL1 Ex12_3 for	CGTGAAGCAGGAGAACAGC	575
MKL1 Ex12_3 rev	tctcaacagccagagaggtg	
MKL1 Ex13 for	agctccctaaaagccagtgc	444
MKL1 Ex13 rev	gtcccctaacaacccactcc	
MKL1 Ex14 for	cagcttcagggtcagagagg	512
MKL1 Ex14 rev	ctccacaagggcaaatgtct	
MKL1 Ex15_1 for	aagtctttgatccgttttatttttg	435
MKL1 Ex15_1 rev	AGGTGTCCATGGGTGACG	
MKL1 Ex15_2 for	GCTGACCAGTGGGCATGA	489
MKL1 Ex15_2 rev	TGAACCAGGAGTAAGGGCTTC	
MKL1 Ex12_2r_seq	CTGGAGCAGGAGAAGCGA	
MKL2_Ex2_for	tgcttgtttttaggtgggaag	523
MKL2_Ex2_rev	CCTCCATGACAGACTGCTGA	
MKL2_Ex3_for	agctttggtcatcaaaatagga	461

MKL2_Ex3_rev	AGGTGCCTGATTTTTCCTTG	
MKL2_Ex4_for	tttgcaggtctcctaatggaa	382
MKL2_Ex4_rev	TCTGCAAACCTCCAGATCAA	
MKL2_Ex5_for	ttcgtctcaaacacatgacca	313
MKL2_Ex5_rev	TGGAGGAAGTAAGGCTGTGG	
MKL2_Ex6_for	gagtctgtgggcatccaaat	502
MKL2_Ex6_rev	AACCCAGAAAACAATACTCACGA	
MKL2_Ex7_for	ttgcactgggaggtacattg	550
MKL2_Ex7_rev	TCAACTCTCCAAGATTTCAGGA	
MKL2_Ex8_for	caccatctggcctcagacat	524
MKL2_Ex8_rev	CATCCAGCCCCTAGTGTTTT	
MKL2_Ex9_for	gcaaacgttttcatggcttt	589
MKL2_Ex9_rev	CCACTCTCACCATGTGGACTT	
MKL2_Ex10_for	aacct gcagggatttcattg	526
MKL2_Ex10_rev	TGCCTGCACAAGGTACACAC	
MKL2_Ex11_for1	gccgtaacgcagagttgtc t	518
MKL2_Ex11_rev1	CAAGAACTGTGAAGGCGACA	
MKL2_Ex11_for2	TGCCGGTTACAACACTACACA	535
MKL2_Ex11_rev2	GAGGCCTCATCTTTGATGGA	
MKL2_Ex11_for3	AGAGCAGAAGCTCGTGGAAG	543
MKL2_Ex11_rev3	TCCTTAGCAGGGTTTGCATT	
MKL2_Ex12_for	agcatgcagtgactggtctg	522
MKL2_Ex12_rev	GCCAAATGGCATCTGACCTA	
MKL2_Ex13_for	acagccacacccatttatcc	535
MKL2_Ex13_rev	AGCTGAGCTCCTCCTTCACA	
MKL2_Ex14_for	accagtgctgtcagcctca	401
MKL2_Ex14_rev	TCTATTGAGGCAAGTCAGTTTCA	
MKL2_Ex15_for	ccctgttcttgctgtgtcaa	431
MKL2_Ex15_rev	TGGCCATAAGTTCTTTTAATGG	
MKL2_Ex16_for1	tgtcaaggattgtacctgacca	422
MKL2_Ex16_rev1	GGGCTCTCTGTCTTCACTGC	
MKL2_Ex16_for2	TGGCACCACCTGTATCTTTAG	524
MKL2_Ex16_rev2	CATATTTTGATTGCAACAATGC	
NDP PCR_1 fwd	tggcattcccatttgctagt	369
NDP PCR_1 rev	aggatgaaatgctcggtttg	
NDP PCR_2 fwd	tgggttccattagtggttctg	525
NDP PCR_2 rev	ttctccatcccctgacaaag	
NDP PCR_3 fwd	gcaacgagtgtgagggtctt	442
NDP PCR_3 rev	AGAGTCCCGGGAGAATTGTT	
TSPAN12 E1 fwd	TCACCCCCCTTCTCAAAC	588
TSPAN12 E1 rev	AGCCAGCCCTTAAGTAGT	
TSPAN12 E2 fwd	CGATGTCTCGAATGCACT	354
TSPAN12 E2 rev	CTTAGCCATGCCCTTTGG	
TSPAN12 E3 fwd	GCAGCAAATGGTAATTGGG	353
TSPAN12 E3 rev	TCTGGAGGATGCAAGTGT	
TSPAN12 E4 fwd	AGCAACCGAGCAAATAAAC	410
TSPAN12 E4 rev	ACTGCTCCCTAATCTTGTG	
TSPAN12 E5 fwd	TGCCTCTGTTTTCTTGGT	383
TSPAN12 E5 rev	GGTGTCTTGCTTCCTCTT	
TSPAN12 E6 fwd	ATTCCGAGTATGCGTGTG	403

TSPAN12 E6 rev	ACATGGGAAGAAAAGCAGG	
TSPAN12 E7 fwd	ATCGTTAGCCATGGTGTT	472
TSPAN12 E7 rev	CTTCTGCTTCTCCCCATATT	
TSPAN12 E8.1 fwd	CTCCCTCTCTCCTTCTTCT	438
TSPAN12 E 8.1 rev	TTTGCCATGGATGTGTGT	
TSPAN12 E 8.2 fwd	TTCTCACCATTACTCTGCTCT	492
TSPAN12 E 8.2 rev	AAACCATGCTGCCTCAAA	
TSPAN12 E6 fwd2 Seq	GCTGTTGATATTTTGCTTT	
TSPAN12 E1 fwd2 Seq	AGAGGAAGAGAAAGAAGCGT	
TSPAN12 E1 rev2 Seq	CTCTGCTAAGCCACCTCC	
TCF3_Ex18_fwd	ACCCTCACCCCATCAGGAC	
TCF3_Ex18_rev	GTCACTGCAAGGAGGCAACT	

TaqMan probes		
Gene	**Probe**	**RNA**
Atoh7 mouse	Mm00844064_s1	60ng
Stmn1 Mouse	Mm01185262_m1	60ng
Ndp mouse	Mm00477754_m1	60ng
Gapdh mouse	Mm99999915_g1	10ng
NDP human	Hs00181129_m1	60ng
GAPDH Human	Hs02758991_g1	10ng

Vectorcollection

Insert	Backbone	Description	Tag	Origin
non	pENTR™/D-TOPO®	Gateway Entry	non	Life Technologies, Zug, Switzerland
non	pcDNA3.1/nV5-DEST	Mammalian Expression	V5 (N-term)	Life Technologies, Zug, Switzerland
non	pcDNA3.1/V5-His	Mammalian Expression	V5, 6xHis(C-term)	Life Technologies, Zug, Switzerland
non	pcDNA3.2/V5-DEST	Mammalian Expression	V5 (C-term)	Life Technologies, Zug, Switzerland
non	pBudCE4.1	Mammalian Expression	V5 (N-term), 6xHis (C-term)	Life Technologies, Zug, Switzerland
EGFP	pEGFP-C1	transfection control	non	Institute of Medical Molecular Genetics, Zürich, J. Neidhardt group
hAtoh7 wt	pENTR™/D-TOPO®	Gateway Entry	non	Institute of Medical Molecular Genetics, Zürich, L. Mohn
hAtoh7 del	pENTR™/D-TOPO®	Gateway Entry	non	Institute of Medical Molecular Genetics, Zürich, L. Mohn
NLS_hAtoh7 wt	pENTR™/D-TOPO®	Gateway Entry	non	Institute of Medical Molecular Genetics, Zürich, L. Mohn
NLS_hAtoh7 del	pENTR™/D-TOPO®	Gateway Entry	non	Institute of Medical Molecular Genetics, Zürich, L. Mohn
hATOH7 p.Arg65Gly	pENTR™/D-TOPO®	Gateway Entry	non	Institute of Medical Molecular Genetics, Zürich, L. Mohn
hAtoh7 wt	pcDNA3.1/nV5-DEST	Mammalian Expression	V5 (N-term)	Institute of Medical Molecular Genetics, Zürich, L. Mohn
hAtoh7 del	pcDNA3.1/nV5-DEST	Mammalian Expression	V5 (N-term)	Institute of Medical Molecular Genetics, Zürich, L. Mohn
NLS_hAtoh7 wt	pcDNA3.1/nV5-DEST	Mammalian Expression	V5 (N-term)	Institute of Medical Molecular Genetics, Zürich, L. Mohn
NLS_hAtoh7 del	pcDNA3.1/nV5-DEST	Mammalian Expression	V5 (N-term)	Institute of Medical Molecular Genetics, Zürich, L. Mohn
hATOH7 p.Arg65Gly	pcDNA3.1/nV5-DEST	Mammalian Expression	V5 (N-term)	Institute of Medical Molecular Genetics, Zürich, L. Mohn
hAtoh7 wt	pcDNA3.1/V5-His	Mammalian Expression	non	Institute of Medical Molecular Genetics, Zürich, L. Mohn
hAtoh7 del	pcDNA3.1/V5-His	Mammalian Expression	non	Institute of Medical Molecular Genetics, Zürich, L. Mohn
NLS_hAtoh7 wt	pcDNA3.1/V5-His	Mammalian Expression	non	Institute of Medical Molecular Genetics, Zürich, L. Mohn
NLS_hAtoh7 del	pcDNA3.1/V5-His	Mammalian Expression	non	Institute of Medical Molecular Genetics, Zürich, L. Mohn
hATOH7 p.Arg65Gly	pcDNA3.1/V5-His	Mammalian Expression	non	Institute of Medical Molecular Genetics, Zürich, L. Mohn
hILK wt	pDONR223	Template for cloning	non	Addgene, Cambridge, MA, USA
hILK wt	pENTR™/D-TOPO®	Gateway Entry	non	Institute of Medical Molecular Genetics, Zürich, L. Mohn & L. Sollfrank
hILK p.Leu53Met	pENTR™/D-TOPO®	Gateway Entry	non	Institute of Medical Molecular Genetics, Zürich, L. Mohn & L. Sollfrank
hILK p.Arg211Cys	pENTR™/D-TOPO®	Gateway Entry	non	Institute of Medical Molecular Genetics, Zürich, L. Mohn & L. Sollfrank
hILK p.Arg317Gln	pENTR™/D-TOPO®	Gateway Entry	non	Institute of Medical Molecular Genetics, Zürich, L. Mohn & L. Sollfrank
hILK wt	pcDNA3.1/nV5-DEST	Mammalian Expression	V5 (N-term)	Institute of Medical Molecular Genetics, Zürich, L. Mohn & L. Sollfrank
hILK wt	pcDNA3.2-DEST	Mammalian Expression	V5 (C-term)	Institute of Medical Molecular Genetics, Zürich, L. Mohn & S. Dold
hILK p.Leu53Met	pcDNA3.1/nV5-DEST	Mammalian Expression	V5 (N-term)	Institute of Medical Molecular Genetics, Zürich, L. Mohn & L. Sollfrank
hILK p.Leu53Met	pcDNA3.2-DEST	Mammalian Expression	V5 (C-term)	Institute of Medical Molecular Genetics, Zürich, L. Mohn & S. Dold
hILK p.Arg211Cys	pcDNA3.1/nV5-DEST	Mammalian Expression	V5 (N-term)	Institute of Medical Molecular Genetics, Zürich, L. Mohn & L. Sollfrank
hILK p.Arg317Gln	pcDNA3.1/nV5-DEST	Mammalian Expression	V5 (N-term)	Institute of Medical Molecular Genetics, Zürich, L. Mohn & L. Sollfrank

mILK wt	pENTR™/D-TOPO®	Gateway Entry	non	Institute of Medical Molecular Genetics, Zürich, L. Mohn
mILK p.Leu53Met	pENTR™/D-TOPO®	Gateway Entry	non	Institute of Medical Molecular Genetics, Zürich, L. Mohn
mILK p.Arg211Cys	pENTR™/D-TOPO®	Gateway Entry	non	Institute of Medical Molecular Genetics, Zürich, L. Mohn
mILK p.Arg317Gln	pENTR™/D-TOPO®	Gateway Entry	non	Institute of Medical Molecular Genetics, Zürich, L. Mohn
mILK wt	pcDNA3.1/nV5-DEST	Mammalian Expression	V5 (N-term)	Institute of Medical Molecular Genetics, Zürich, L. Mohn
mILK p.Leu53Met	pcDNA3.1/nV5-DEST	Mammalian Expression	V5 (N-term)	Institute of Medical Molecular Genetics, Zürich, L. Mohn
mILK p.Arg211Cys	pcDNA3.1/nV5-DEST	Mammalian Expression	V5 (N-term)	Institute of Medical Molecular Genetics, Zürich, L. Mohn
mILK p.Arg317Gln	pcDNA3.1/nV5-DEST	Mammalian Expression	V5 (N-term)	Institute of Medical Molecular Genetics, Zürich, L. Mohn
hITGB3 wt	pENTR™/D-TOPO®	Gateway Entry	non	Institute of Medical Molecular Genetics, Zürich, L. Mohn & L. Sollfrank
hITGB3 p.Ala283Thr	pcDNA3.1/nV5-DEST	Mammalian Expression	V5 (N-term)	Institute of Medical Molecular Genetics, Zürich, L. Mohn & L. Sollfrank
hNDP wt	pBudCE4.1	Mammalian Expression	myc, 6xHis (C-term)	Institute of Medical Molecular Genetics, Zürich, U. Luhmann
hNDP p.Cys95Arg	pBudCE4.1	Mammalian Expression	myc, 6xHis (C-term)	Institute of Medical Molecular Genetics, Zürich, U. Luhmann
hNDP p.Cys96Trp	pBudCE4.1	Mammalian Expression	myc, 6xHis (C-term)	Institute of Medical Molecular Genetics, Zürich, U. Luhmann
hNDP p.Arg121Leu	pBudCE4.1	Mammalian Expression	myc, 6xHis (C-term)	Institute of Medical Molecular Genetics, Zürich, U. Luhmann
hNDP p.Arg121Trp	pBudCE4.1	Mammalian Expression	myc, 6xHis (C-term)	Institute of Medical Molecular Genetics, Zürich, U. Luhmann
hNINJ1	pCMV6-XL5	Template for cloning	non	OriGene Technologies, Rockville, USA
hNINJ1 wt	pENTR™/D-TOPO®	Gateway Entry	non	Institute of Medical Molecular Genetics, Zürich, L. Sollfrank
hNINJ1 p.Ala42Thr	pcDNA3.1/nV5-DEST	Mammalian Expression	V5 (N-term)	Institute of Medical Molecular Genetics, Zürich, L. Sollfrank
pTopflash	pTA-Luc backbone	TCF/LEF luciferase reporter	non	Institute of Molecular Life Sciences, Zürich, K. Basler group
pFopflash	pTA-Luc backbone	no TCF/LEF reporter	non	Institute of Molecular Life Sciences, Zürich, K. Basler group
pRL	pRL-CMV	normalization	non	Promega, Madison, USA
pE7-βA	pPGV	(CANNAG) reporter	non	Institute of Virus Research, Kyoto University, Ryoichiro Kageyama
pβA	pPGV	no (CANNAG)	non	Institute of Virus Research, Kyoto University, Ryoichiro Kageyama

Appendix D – Co-author publication

Human Molecular Genetics, 2012, Vol. 21, No. 12 **2619–2630**
doi:10.1093/hmg/dds087
Advance Access published on March 6, 2012

Norrin stimulates cell proliferation in the superficial retinal vascular plexus and is pivotal for the recruitment of mural cells

Jurian Zuercher[1,2,†], Martin Fritzsche[1,†], Silke Feil[1], Lucas Mohn[1,2] and Wolfgang Berger[1,2,3,*]

[1]Institute of Medical Molecular Genetics, [2]Neuroscience Center Zurich (ZNZ) and [3]Center for Integrative Human Physiology (ZIHP), University of Zurich, Zurich, Switzerland

Received January 20, 2012; Revised and Accepted February 28, 2012

Mutations in Norrin, the ligand of a receptor complex consisting of FZD4, LRP5 and TSPAN12, cause severe developmental blood vessel defects in the retina and progressive loss of the vascular system in the inner ear, which lead to congenital blindness and progressive hearing loss, respectively. We now examined molecular pathways involved in developmental retinal angiogenesis in a mouse model for Norrie disease. Comparison of morphometric parameters of the superficial retinal vascular plexus (SRVP), including the number of filopodia, vascular density and number of branch points together with inhibition of Notch signaling by using DAPT, suggest no direct link between Norrin and Notch signaling during formation of the SRVP. We noticed extensive vessel crossing within the SRVP, which might be a loss of Wnt- and MAP kinase-characteristic feature. In addition, endomucin was identified as a marker for central filopodia, which were aligned in a thorn-like fashion at P9 in Norrin knockout (*Ndp*$^{y/-}$) mice. We also observed elevated mural cell coverage in the SRVP of *Ndp*$^{y/-}$ mice and explain it by an altered expression of *PDGFβ* and its receptor (*PDGFRβ*). *In vivo* cell proliferation assays revealed a reduced proliferation rate of isolectin B4-positive cells in the SRVP from *Ndp*$^{y/-}$ mice at postnatal day 6 and a decreased mitogenic activity of mutant compared with the wild-type Norrin. Our results suggest that the delayed outgrowth of the SRVP and decreased angiogenic sprouting in *Ndp*$^{y/-}$ mice are direct effects of the reduced proliferation of endothelial cells from the SRVP.

INTRODUCTION

Mutations in the human *NDP* (*Norrie disease pseudoglioma*) gene, encoding Norrin, cause congenital blindness, progressive deafness and mental retardation, a triad of symptoms characteristic for Norrie disease (ND) (1–5). Alternatively, mutations in *NDP* can exclusively lead to ocular symptoms in X-linked exudative vireoretinopathy (EVR) (6), Coats' disease and retinopathy of prematurity (7,8). EVR is also caused by mutations in Frizzled-4 (*FZD4*, FZD4), low-density lipoprotein receptor-related protein 5 (*LRP5*, LRP5) or tetraspanin-12 (*TSPAN12*, TSPAN12) (9–11). Recessive mutations in *LRP5* may also cause osteoporosis pseudoglioma syndrome (OPPG), which manifests with low bone mass in addition to the ocular phenotype in patients (OMIM: #259770). It has been shown *in vitro* that Norrin is a ligand for the canonical Wnt signaling receptor complex consisting of FZD4, LRP5 and TSPAN12 (12,13). Furthermore, the outgrowth of the superficial retinal vascular plexus (SRVP) from *Ndp*$^{y/-}$, *Fzd4*$^{-/-}$, *Lrp5*$^{-/-}$ and *Tspan12*$^{-/-}$ is delayed and incomplete and all of these knockout mice lack the deep and intermediate retinal vascular plexuses (12–16). We generated and examined a Norrin knockout mouse model (*Ndp*$^{y/-}$) that resembles the human Norrie disease phenotype with respect to blindness and hearing loss (4,14,17). Hyaloid vessels do not completely regress in *Ndp*$^{y/-}$, *Fzd4*$^{-/-}$, *Lrp5*$^{-/-}$ and *Tspan12*$^{-/-}$ knockout mice (12–14,16). Retinal vascular hemorrhage and exudation from retinal blood vessels in *Ndp* knockout mice (*Ndp*$^{y/-}$) are characteristic features. We previously demonstrated that expression of the plasmalemma vesicle-associated protein (PLVAP), which mediates vascular fenestration and promotes vascular leakiness, is highly

*To whom correspondence should be addressed at: Schorenstrasse 16, CH-8603 Schwerzenbach. Tel: +41 446557031; Fax: +41 446557213; Email: berger@medmolgen.uzh.ch
†These two authors contributed equally.

upregulated in $Ndp^{y/-}$ retinas (18). Upregulation of PLVAP/MECA32 in retinal endothelial cells (ECs) has also been shown for $Lrp5^{-/-}$ and $Tspan12^{-/-}$ mice (13). Furthermore, it was shown that upregulation of PLVAP indicates the loss of canonical Wnt signaling (19). The delayed outgrowth of the SRVP and the absence of deep sprouting could be caused either by defects in sprouting angiogenesis or by reduced proliferation of the SRVP. Sprouting angiogenesis is mediated by endothelial tip cells that guide the growing SRVP from the optic nerve head towards the retinal periphery along a vascular endothelial growth factor (VEGF) gradient (20). Stalk cells following tip cells divide ensuring proliferation and growth. Thus, an imbalance of tip and stalk cells could lead to both observed effects. The proper differentiation of tip and stalk cells is mediated by a balanced expression and interaction of Notch1 with its ligands Dll4 and Jagged1 (21–23). Dll4 is expressed in tip cells and induces Notch signaling in adjacent stalk cells. In contrast, Jagged1 is expressed in stalk cells impeding Notch signaling in adjacent tip cells. Disruption of Notch signaling has been shown to alter morphometric parameters, such as the number of peripheral tip cell filopodia, vascular density and the number of vascular branch points. The outgrowth of the SRVP along the VEGF gradient involves MAPK signaling. VEGF, provided by astrocytes or retinal ganglion cells, binds a receptor complex consisting of VEGF receptor 2 (VEGFR2) and neuropilin 1 (Nrp1) activating downstream MAPK signaling. Loss of the cytoplasmatic Nrp1 domain ($Nrp1^{cyto\Delta/\Delta}$) or nestin-specific knockout of VEGF ($VEGF_{NES\text{-}CRE}$) in mice causes artery/vein crossing (A/V crossing) in the SRVP of these mice. $VEGF_{NES\text{-}CRE}$ mice additionally show aberrant deep sprouting (24,25).

Here, we focused on defects during development of the SRVP in $Ndp^{y/-}$ mice. We quantified several vascular and angiogenic parameters and observed extensive vessel crossing within the SRVP which might be a MAPK-characteristic feature. We found reduced cell proliferation in the SRVP at the vascular front at P6 in $Ndp^{y/-}$ mice which may explain the delayed outgrowth of the SRVP. We also detected elevated mural cell (MC) coverage of the SRVP starting at P9, which is consistent with previously found upregulation of *Tie1*, *Pdgfβ* and *Pdgfrβ*. Finally, we report for the first time endomucin-positive supernumerary central filopodia of the SRVP in $Ndp^{y/-}$ retinas culminating at P9, the time point when the deep retinal vascular plexus (DRVP) normally would develop.

RESULTS

Vascular development in Norrin knockout mice

The wild-type mouse retina is avascular at birth and outgrowth of the SRVP progresses from the center towards the periphery from P1 until P8. Because the outgrowth of the SRVP is incomplete and delayed in $Ndp^{y/-}$ mice (14), we hypothesized that there might be an imbalance between tip cell filopodia and/or adjacent stalk cell proliferation. We quantified the number of filopodia as well as the vascular density and number of branch points in the central plexus at the vascular front at P5 and P7 (Fig. 1) (Supplementary Material, Table S1). The number of filopodia was significantly increased but the vascular density (Fig. 1A, C, E, G, I, K) and the number of branch points (Fig. 1A, C, E, G, J, L) were significantly decreased at P5 and P7 in $Ndp^{y/-}$ mice. Moreover, filopodial protrusions in $Ndp^{y/-}$ mice are straighter and expand with a narrower angle than filopodia of wild-type littermates (Fig. 1O) (Supplementary Material, Table S2). In contrast to the increased number of filopodia, the vascular front in general appears to be less ramified with a reduced amount of long tip cell protrusions (Fig. 1B and F).

Comparison of vascular development in different mouse models

Available morphometric data from three Norrin-Wnt signaling knockout mice ($Fzd4^{-/-}$, $Lrp5^{-/-}$ and $Tspan12^{-/-}$), three Notch signaling knockout mice ($Dll4^{+/-}$, $Jag1^{i\Delta EC}$, $Nrarp^{-/-}$), $Ang2^{LZ/LZ}$ and Pax6 dependent hypoxia inducible factor 1 α ($HIF1\alpha^{\Delta Pax6}$) knockout mice were compared (Table 1). The morphometric comparison of $Jag1^{i\Delta EC}$ with $Ndp^{y/-}$ mice was of special interest since Jag1 has been shown to be a canonical Wnt target gene in hair follicle cells comprising two LEF/TCF-binding sites within its promoter region (26,27). We compared our morphometric data from Norrin KO mice with published morphometric data from $Jag1^{i\Delta EC}$ mice and recognized delayed and incomplete outgrowth of the SRVP, together with a reduced vascular density and a decreased number of branch points in $Jag1^{i\Delta EC}$ and $Ndp^{y/-}$ mice. In contrast to $Ndp^{y/-}$ mice, the number of tip cell filopodia was reduced in $Jag1^{i\Delta EC}$ mice. $Dll4^{+/-}$ mice have an increased number of filopodia, increased number of branchpoints and a denser vascular SRVP. Hence, the $Ndp^{y/-}$ phenotype of the SRVP displays as an intermingled picture, with a peripheral *Jag1* gain of function but central *Jag1* loss of function features. We asked the question whether or not Norrin is a negative regulator of Notch signaling. To answer this question, we examined the effect of Notch inhibition in $Ndp^{y/-}$ mice in order to see if this may rescue the abnormal vascular development. We quantified and compared morphometric parameters in Norrin knockout and wild-type mice after inhibition of Notch signaling by injection of the γ-secretase inhibitor DAPT (Fig. 2). Administration of DAPT increased vascular density in wild-type and $Ndp^{y/-}$ mice (Fig. 2A–E), while the number of filopodia only increased in wild-type but not in $Ndp^{y/-}$ retinas (Fig. 2F–J) (Supplementary Material, Table S3).

Retinal EC proliferation in Norrin-deficient mice

To test the hypothesis if Norrin acts as a mitogen for cells in the SRVP, which would explain the reduced vascular density as well as the delayed and incomplete radial vascular outgrowth in $Ndp^{y/-}$ mice, we quantified central EC proliferation after systemic bromodeoxyuridine (BrdU) injection and found significantly reduced proliferation rates of isolectin B4 (IB4)-positive ECs from the SRVP in $Ndp^{y/-}$ mice at P6 (WT: ME ± SD 101.71 ± 16.54; KO: ME ± SD 52.17 ± 9.62; *P*-value: 1.8E−5) (Fig. 3A and C). The only exceptions from this observation are local hotspots of proliferation within bulky unorganized regions at the vascular front (Fig. 3D). Additionally, we monitored the effect of Norrin on cell cycle progression in cell culture experiments by using an

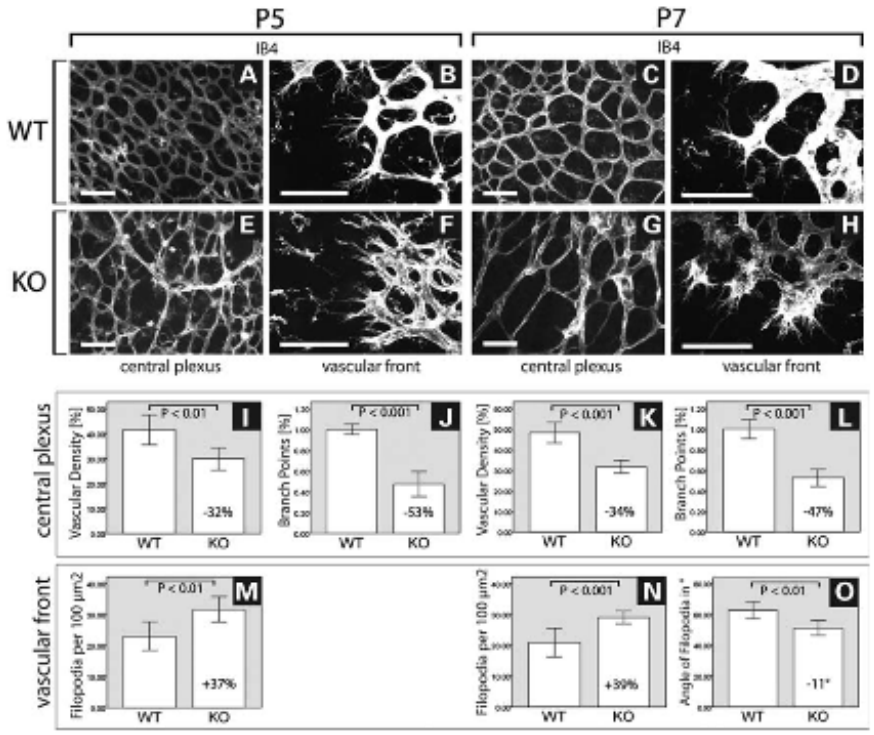

Figure 1. Morphometric parameters in Norrin knockout versus wild-type mice. $Ndp^{y/-}$ mice show decreased vascular density, a decreased number of branch points but supernumerary filopodia, which are aligned in a more narrow angle compared with wild-type mice at P5 and P7. (**A**, **E**, **C**, **G**) Representative central retinal whole-mounts from wild-type (WT) and $Ndp^{y/-}$ (KO) retinas stained with IB4. (**B**, **D**, **F**, **H**) Representative peripheral retinal whole-mounts from WT and $Ndp^{y/-}$ retinas stained with IB4. Emerging filopodia are visible. Quantification of vascular density (**I** and **K**), number of branch points (**J** and **L**), number of filopodia (**M** and **N**) and angle of filopodia (**O**). Average and confidence intervals are shown. *P*-values below $\alpha = 0.05$ were considered statistically significant. Scale bars = 100 µm.

E2F transcription factor-mediated reporter assay (cell proliferation controlling transcription factor-dependent luciferase reporter construct, reviewed in 28). For this, we transiently transfected pE2F luciferase reporter constructs into HEK293T cells which ectopically express the same amount of either human wild-type or a pathogenic variant of Norrin containing the p.C95R mutation (Supplementary Material, Fig. S1), which has been associated with the classic picture of Norrie disease (29). HEK293T cells do not endogenously express Norrin, but were positive in RT–PCR for transcripts from *FZD4*, *LRP5* and *TSPAN12* (Supplementary Material, Fig. S1). Similarly to our BrdU data in $Ndp^{y/-}$ mice, we found almost 6-fold increased cell cycle progression in cells that stably express human wild-type Norrin compared with cells that express the mutant Norrin isoform (Fig. 3F, Supplementary Material, Table S4).

Vascular remodeling in Norrin-deficient mice

Despite the reduced vascular outgrowth of the SRVP, we occasionally noticed bulky vascular areas at the front of $Ndp^{y/-}$ mice, comprising three-dimensional accumulations of ECs (Fig. 4D). To monitor vascular remodeling across the plexus, retinal whole-mounts were double stained for IB4 and collagen IV (ColIV). ColIV-positive tubes lacking IB4 staining represent empty basement membrane sleeves at positions where blood vessels have regressed (30,31). We noticed that vascular remodeling was elevated in $Ndp^{y/-}$ mice at peripheral bulky vascular areas of the SRVP, but not in central areas (Fig. 4C, white dots). Furthermore, we noticed vessel-crossing in $Ndp^{y/-}$ retinas. Vessels that morphologically resemble veins [venous character (VC)] cross and grow below vessels that resemble arteries [arterial character (AC)] between P7 and P21 (A/V crossing) (Fig. 5, Supplementary Material, Fig. S3). ACs in Norrin knockout mice also interconnect less to the central plexus compared with the wild-type and instead grow further into the periphery (Fig. 6D). At P21, disorganized twisted and tangled blood vessels form above the superficial plexus resembling fibrosis (Supplementary Material, Fig. S3t and w). We hypothesized that A/V crossing could be caused by altered astrocyte–EC interaction and therefore co-stained astrocytes against PDGFRα and blood

Table 1. Morphometric data among mutant mice with comparable retinal vascular phenotype

	Ndp$^{y/-}$	*Fzd4*$^{-/-}$	*Lrp5*$^{-/-}$	*Tspan12*$^{-/-}$	*Dll4*$^{+/-}$	*Jag1*$^{i\Delta EC}$	*Nrarp*$^{-/-}$	*Angpt2*$^{LZ/LZ}$	*HIF1α*$^{\Delta PAS}$
Pathway affected	Canonical Wnt-signaling	Canonical Wnt-signaling	Canonical Wnt-signaling	Canonical Wnt-signaling	Notch signaling	Notch signaling; tamoxifen-induced EC-specific deletion	Notch, β-catenin/Lef1-dependent Wnt signaling	Tie2 signaling; LZ = lacZ	Hypoxia
Vascular outgrowth of SRVP	Delayed and incomplete	Delayed and incomplete	Delayed and incomplete	Delayed and incomplete	Delayed	Delayed (−44%)	Delayed but complete	Periphery remains avascular	Not delayed nor reduced
Vascular density of SRVP	Reduced (−34%, P7)	Not available	Not available	Reduced	Increased (+58%[a])	Reduced (−32%, P6)	Reduced at P5 but not different in adult	Not available	Not available
Number of branch points of SRVP	Reduced (−47%, P7)	Not available	Not available	Not available	Increased (+96%[a])	Reduced (−65%, P6)	Reduced at P5 but not different in adult	Not available	Not available
Number of filopodia of SRVP	Increased (+39%, P7)	Not available	Not available	Not available	Increased (sprouts increased +63%[a])	Reduced (−27%, P6)	Not different at P5	Not available	Not available
A/V crossing in SRVP till P7	Present	Present	Present	Present	Absent	Absent	Present	Not deducible due to picture quality	Absent
DRVP	Absent	Absent	Absent	Absent	Present	Present	Present	Absent	Present
Intermediate retinal vascular plexi	Absent	Absent	Absent	Absent	Present	Present	Present	Absent	Absent
References	Luhmann *et al.* (14), this work	Xu *et al.* (12)	Xia *et al.* (16,41) and Chen *et al.* (42)	Junge *et al.* (13)	Lobov *et al.* (21)	Benedito *et al.* (22)	Phng *et al.* (43)	Gale *et al.* (44)	Caprara *et al.* (45)

[a]% estimated from graph.

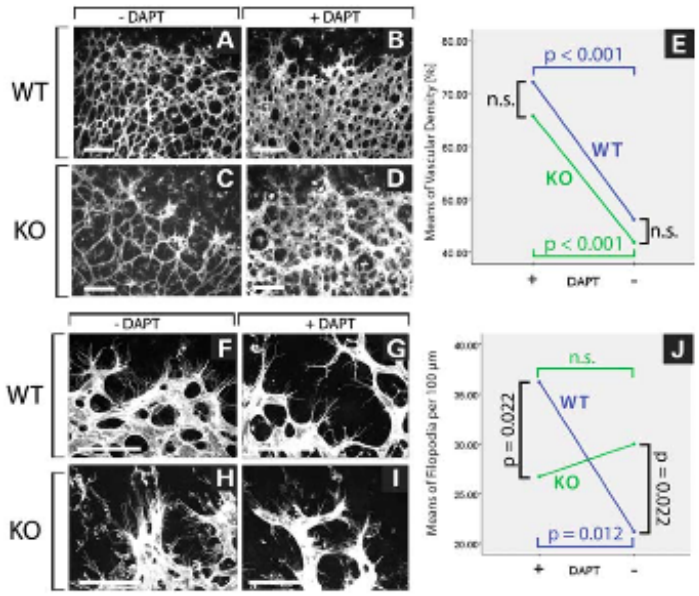

Figure 2. Effects of Notch signaling inhibition in wild-type and Norrin knockout mice. Pharmacological administration of DAPT increases vascular density at the vascular front in wild-type and $Ndp^{y/-}$ mice. The number of filopodia only increases in wild-type but not in $Ndp^{y/-}$ mice upon DAPT treatment. (**A**–**D**) Representative retinal whole-mounts stained with IB4 48 h after DAPT injection in P7 wild-type (WT) and $Ndp^{y/-}$ (KO) animals. (**E**) Statistical analysis shows that peripheral vascular density increases in both genotypes upon DAPT treatment. (**F**–**I**) Representative retinal whole-mounts of IB4 staining 48 h after DAPT treatment of P7 wild-type (WT) and $Ndp^{y/-}$ (KO) animals. Filopodia at the vascular front are visible. (**J**) Statistical analysis shows that number of filopodia increases only after DAPT treatment in the WT but not in $Ndp^{y/-}$ mice. *P*-values below $\alpha = 0.05$ were considered statistically significant. Scale bars = 100 µm.

vessels with IB4 (Supplementary Material, Fig. S2). We did not observe an altered astrocytic network in $Ndp^{y/-}$ retinas compared with wild-type and alignment between astrocytes and ECs was normal.

Mice lacking the Nrp1 cytoplasmatic domain or $VEGF_{NES\text{-}CRE}$ mice also show A/V crossing in the SRVP (24,25). This suggests that the loss of MAPK signaling might cause this phenotype. Therefore, we made use of our stably wild-type or p.C95R Norrin expressing HEK293T cell lines (Supplementary Material, Fig. S1) to monitor MAPK activity. We found a 1.9-fold increase in MAPK signaling in cells that express wild-type Norrin compared with those that expressed the mutant, disease-associated variant (Fig. 5I, Supplementary Material, Table S5).

Because of the above-described, strong SRVP phenotype in $Ndp^{y/-}$ mice, it was crucial to examine whether the VCs and ACs exhibit characteristic molecular features of the respective vessel types. Retinal flatmounts were stained either for endomucin or for smooth muscle actin (SMA) at P7, P9, P12 and P21. In both, wild-type and $Ndp^{y/-}$ mice, endomucin stained veins and venous portions while staining of arteries and arterioles was less intense (Fig. 6, Supplementary Material, Fig. S4) (32,33). Interestingly, the endomucin staining revealed supernumerary thorn-like assembled central filopodia around veins and capillaries of $Ndp^{y/-}$ retinas (Fig. 6D and E). In contrast, capillary sprouts were much less abundant and, if present, much shorter in wild-type mice. Staining for the arterial and MC marker α-SMA in wild-type mice specifically labeled arteries at P7, P9 and P12 as well as arteries and large veins at P21. In $Ndp^{y/-}$ retinas, arteries, veins and capillaries were covered with SMA-positive cells at P9, P12 and P21 (Fig. 7, Supplementary Material, Fig. S5). Thus, MC recruitment to the SRVP is abnormally increased in $Ndp^{y/-}$ retinas.

DISCUSSION

Deficiency of Norrin is known to cause Norrie disease, a severe X-linked recessive human disease characterized by congenital blindness, progressive hearing loss and, in some patients, mental retardation. We made use of a mouse model which mimics the human disease in eye and ear and applied morphometric analyses, Notch-inhibition by DAPT administration, as well as cell proliferation assays to characterize the angiogenic processes in the retina. We provide evidence that Norrin is a mitogenic stimulus for cells in the SRVP. Consistently, wild-type Norrin promotes E2F transcription factor-mediated cell cycle progression in a cell culture assay. Further, we identified endomucin as a marker for central filopodia, which were aligned in a thorn-like fashion at P9 in $Ndp^{y/-}$ mice. Finally, we found aberrant vascular SMA-positive MC coverage of veins and capillaries in the SRVP

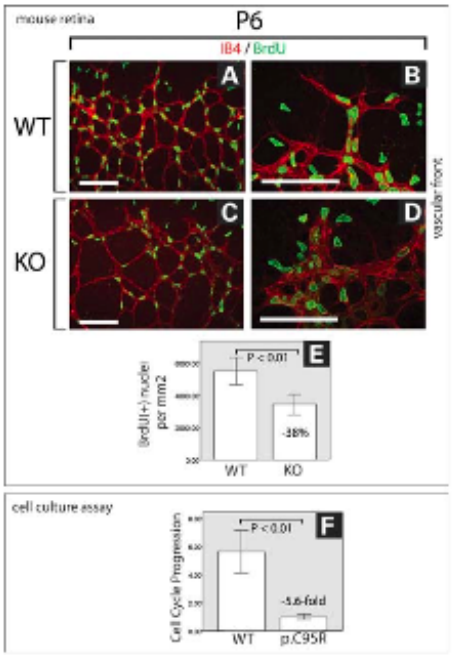

Figure 3. Decreased proliferation rate of ECs in Norrin knockout mice and reduced cell cycle progression due to a mutation (p.C95R) in human Norrin. Overall proliferation is reduced in $Ndp^{y/-}$ mice at P6. Representative retinal whole-mounts of wild-type (WT) (**A** and **B**) and $Ndp^{y/-}$ mice (KO) (**C** and **D**) were stained for blood vessels with IB4 (red) and for proliferating cells after BrdU incorporation (green). (D) Local hotspots of proliferation within thickened areas of the vascular front are occasionally seen in $Ndp^{y/-}$ mice and were excluded from quantification of proliferation. (**E**) Quantification of proliferating vascular ECs after BrdU-incorporation revealed a reduced proliferation rate (−38%) in $Ndp^{y/-}$ mice. (**F**) Expression of wild-type Norrin (WT) leads to 5.6-fold increase in the proliferation rate in HEK293T cells compared with cells expressing a mutant (p.C95R) human Norrin. Average and confidence intervals are shown. *P*-values below $\alpha = 0.05$ were considered statistically significant. Scale bars = 100 μm.

in $Ndp^{y/-}$ mice which indicates abnormally increased MC recruitment of the SRVP from Norrin KO mice.

Norrin and Notch signaling are not directly linked

We examined features of the SRVP in $Ndp^{y/-}$ mice by quantifying and comparing morphometric parameters (Figs 1 and 2, Supplementary Material, Tables S1–S3) with published data from different mouse models with retinal vascular phenotypes (Table 1). We did not quantify later stages than P7 since the outgrowth of the superficial plexus in wild-type mice ends soon after this stage of development.

We noticed that the outgrowth of the SRVP is delayed in all mouse models (Table 1), but incomplete vascular outgrowth was only observed in mutants with disrupted canonical Wnt signaling ($Ndp^{y/-}$, $Fzd4^{-/-}$ and $Lrp5^{-/-}$). Both the deep

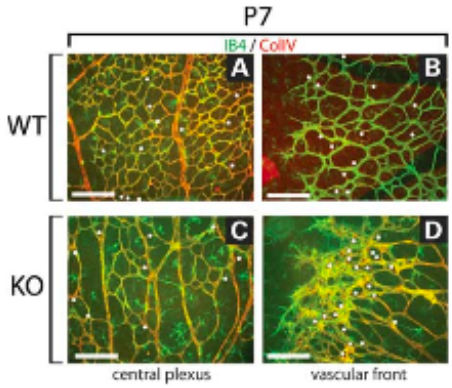

Figure 4. Massive vessel regression at the bulky vascular front in $Ndp^{y/-}$ mice at P7. IB4 (green) and ColIV (red) co-stained retinal whole-mounts from wild-type (WT) (**A** and **B**) and $Ndp^{y/-}$ mice (KO) (**C** and **D**). ColIV+, IB4-stainings represent empty membrane sleeves, where blood vessels have regressed (white dots). Regression was increased at the bulky vascular front in $Ndp^{y/-}$ retinas (D). Scale bars = 100 μm.

and intermediate retinal vascular plexuses (DRVP, IRVP) are absent in mice with deficient Wnt signaling components ($Ndp^{y/-}$, $Fzd4^{-/-}$, $Lrp5^{-/-}$ and $Tspan12^{-/-}$) and in $Ang2^{LacZ/LacZ}$ mice, but not in Notch signaling deficient mice ($Dll4^{+/-}$ or $Jag1^{i\Delta EC}$). The intermediate plexus is absent in $HIF1\alpha^{\Delta Pax6}$ mice, while the deep plexus is present (Table 1). We hypothesized that the canonical Wnt target gene *Jag1* might link Norrin-Wnt and Notch signaling during development of the SRVP, since knocking out *Ndp* or *Jag1* leads to aberrant SRVP development. However, we found significant differences in morphometric parameters between $Ndp^{y/-}$ and $Jag1^{i\Delta EC}$ retinas, which are in conflict with this hypothesis. The number of filopodia was increased in $Ndp^{y/-}$ and reduced $Jag1^{i\Delta EC}$ mice. $Jag1^{i\Delta EC}$ retinas also do not display defects in deep vascular development (22) which is a characteristic feature in $Ndp^{y/-}$ retinas. All these phenotypic differences suggest that there is no direct link between Norrin-Wnt and Notch signaling via Jag1.

Inhibiting Notch signaling through systemic DAPT administration led to an increased vascular density in $Ndp^{y/-}$ mice, but it did not reduce the supernumerary filopodia. Furthermore, vascular density increased similarly in wild-type and $Ndp^{y/-}$ retinas after DAPT treatment, excluding a synergistic effect (Fig. 2E). Accordingly, interaction effects were rejected by univariate analysis of variance (data not shown). Although the peripheral vascular network at the front is denser in DAPT-treated $Ndp^{y/-}$ mice (Fig. 2D), it still seems disorganized, three-dimensional and not planar. This implies that Notch inhibition can induce a peripheral hyper angiogenic response in $Ndp^{y/-}$ mice but not re-establish normal vascular development. The diameter of the peripheral blood vessels increased, which might be due to involvement of Dll4-Notch signaling in A/V differentiation, leading to a more pronounced venous phenotype after DAPT injection and to an increase in vessel diameter (Fig. 2A–D). The number of filopodia significantly

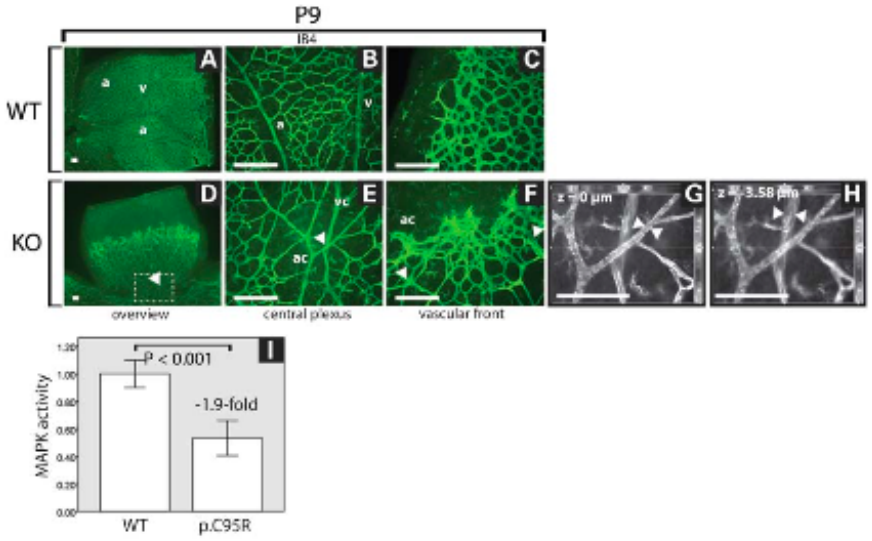

Figure 5. Blood vessel crossing in Norrin knockout mice. Arteries and veins often cross each other in $Ndp^{y/-}$ retinas. Retinal whole-mounts of wild-type (WT) (**A**–**C**) and $Ndp^{y/-}$ mice (KO) (**D**–**H**) were stained with IB4 to label blood vessels (green A–F, or grey G + H). We noticed abundant A/V crossings at the center (E, arrowheads) and periphery (F, arrowheads) of the SRVP from $Ndp^{y/-}$ retinas. Note, that (E) represents the box indicated in (D). (G) and (H) are confocal images from the blood vessels marked in (E), focused on the upper artery (G), and on the lower vein (H). The distance between both vessels is 3.58 µm. (I) Ectopic expression of wild-type Norrin (WT) leads to 1.9-fold increase in MAPK signaling in HEK293T cells compared with cells expressing a mutant (p.C95R), disease-associated human Norrin. a, artery; ac, arterial character; v, vein; vc, venous character. Scale bars = 100 µm.

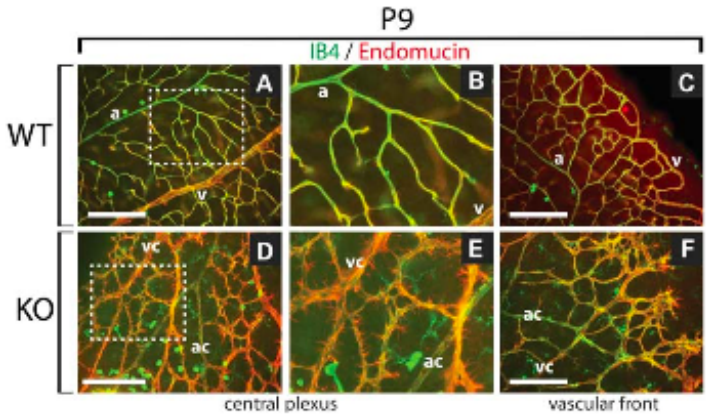

Figure 6. Large central filopodia in $Ndp^{y/-}$ mice at P9. Retinal whole-mounts from wild-type (WT) (**A**–**C**) and $Ndp^{y/-}$ mice (KO) (**D**–**F**) were co-stained with IB4 (green) to label blood vessels and with endomucin (red) which preferentially stains veins, venous vessels and central filopodia. (B) represents box in (A) and (E) represents box in (D). Endomucin staining revealed that vessels with a venous character (vc) but not with an arterial character (ac) are laced with supernumerary central filopodia. a, artery; v, vein. Scale bars = 100 µm.

increased in wild-type mice, but was unaltered in $Ndp^{y/-}$ retinas upon DAPT administration (Fig. 2G, I, J).

Vascular remodeling in Norrin-deficient mice

We found enhanced vascular proliferation (Fig. 3) and also enhanced vascular regression/remodeling (Fig. 4) at the vascular bulky front in $Ndp^{y/-}$ mice after BrdU injection and by co-staining of ColIV and IB4. We interpret the vessel regression of $Ndp^{y/-}$ retinas as secondary effect which ensures a planar vascular plexus at positions where bulky vascular fronts were present before moving towards the periphery. Disorganized vascular fronts are also present in $Fzd4^{-/-}$, $Lrp5^{-/-}$ and $Tspan12^{-/-}$ retinas (12,13,34).

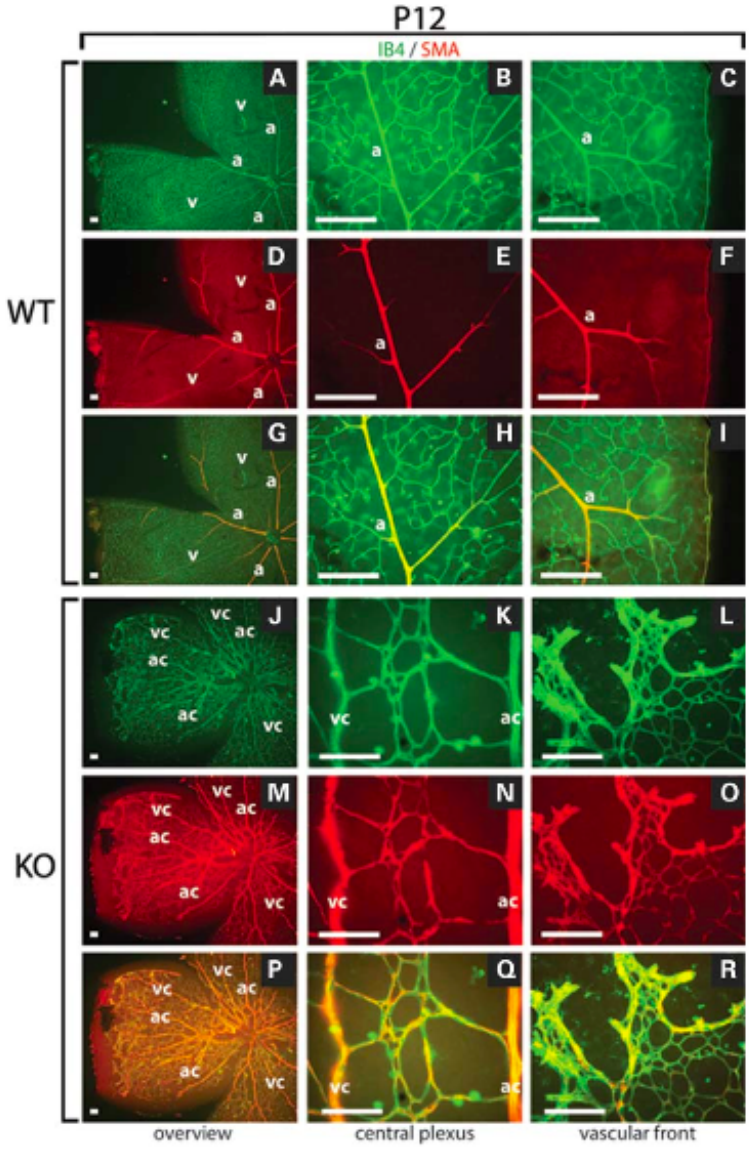

Figure 7. Retinal veins and capillaries are abundantly covered by mural cells (MCs) in $Ndp^{y/-}$ mice at P12. Retinal whole-mounts were co-stained with IB4 to label blood vessels (green) and against SMA to label arteries covered by MCs (red). Only arteries were covered by MCs in wild-type (WT) retinas. In contrast, arteries, veins and capillaries were covered by MCs in $Ndp^{y/-}$ retinas (KO). a, artery; ac, arterial character; v, vein; vc, venous character. Scale bars = 100 μm.

Further, we observed extensive crossing of arteries and veins (A/V) in $Ndp^{y/-}$ retinas and we excluded an altered astrocytic scaffold to be the reason for these observations (Supplementary Material, Fig. S2).

Loss of Norrin signaling might alter MAPK signaling

A/V crossing is a feature of all Norrin-Wnt signaling deficient mice and also (12,13,16,24,25) the lack of the cytoplasmatic

domain of Nrp1 ($Nrp1^{cyto\Delta/\Delta}$) or dosage-dependent reduction in neuronal VEGF-A paracrine signaling (VEGF-$A_{NES\text{-}CRE}$) lead to A/V crossing (24,25). The receptor pair consisting of VEGFR2 and Nrp1 triggers VEGF-mediated downstream MAPK signaling. Thus, the existence of A/V crossing in $Ndp^{y/-}$ retinas and in retinas from VEGF-$A_{NES\text{-}CRE}$ and $Nrp1^{cyto\Delta/\Delta}$ mice suggests that both pathways influence each other. Supporting this, Norrin-stimulated cells have elevated MAPK signaling activity compared with cells stimulated with mutant Norrin (Fig. 5I). Similarly, we previously reported MAPK signaling to be the major pathway influenced by Norrin signaling according to transcriptome analyses using microarray data from $Ndp^{y/-}$ retinas (18). Therefore, it will be intriguing to investigate the putative link between Norrin-Wnt and VEGF/Nrp1/MAPK signaling.

Norrin stimulates mitogenic activity in retinal ECs

Since the loss of Norrin leads to delayed and incomplete outgrowth of the SRVP, we analyzed the mitogenic activity of Norrin in mouse retinas and in cell culture using systemic BrdU injection and reporter assays, respectively. The reduced proliferation of IB4-positive ECs from the SRVP in $Ndp^{y/-}$ retinas, as revealed after BrdU injection, indicates that Norrin might act as a mitogenic stimulus (Fig. 3). Additionally, we monitored cell cycle progression by using the pE2F luciferase reporter construct. As expected, HEK293T cells, which endogenously express FZD4, LRP5 and TSPAN12 but not Norrin, and ectopically express human wild-type Norrin had an increased cell cycle progression compared with ectopically p.C95R mutant Norrin expressing cells (Fig. 3F). Consistently, Ohlmann *et al*. (35) observed, by using a BrdU ELISA, that Norrin efficiently stimulates proliferation of human retinal microvascular ECs *in vitro* in a Wnt-dependent manner. Our findings together with the BrdU ELISA suggest that Norrin might act as a mitogenic stimulus on microvascular/capillary ECs of the SRVP (Fig. 3C). This also can explain the delayed outgrowth of the SRVP. A key to understand the complexity of the retinal vascular phenotype in $Ndp^{y/-}$ mice could be the differentiated view of events at the angiogenic front and within the central plexus. Transient peripheral phenomena like local hotspots of proliferation and remodeling, thickening of the vasculature and supernumerary filopodia could be interpreted as inability of vascular sprouts to escape the existing plexus. Hence, filopodia-projecting tip cells could be overrun by stalk cells, cluster and form the observed bulky areas. The supposed explanation for the $Ndp^{y/-}$ superficial plexus phenotype is also supported by *in silico* models of vascular network formation. Travasso *et al*. (36) recently found, utilizing a mathematical model of sprouting angiogenesis, that low tip cell motility leads to a sparsely ramified plexus and increased stalk cell proliferation. Due to the lack of long tip cell protrusions projecting into the avascular space ahead of the vascular front, also characteristic for $Ndp^{y/-}$ mice, stalk cells spend more angiogenic factors which decrease its concentrations and inhibits branching. The same study highlights that low overall EC proliferation also leads to reduced vessel ramification, corroborating our observations.

Veins and capillaries of $Ndp^{y/-}$ retinas possess supernumerary central filopodia

To investigate the properties of ACs and VCs, we stained retinal whole-mounts against endomucin and SMA.

The surface of veins and capillaries in $Ndp^{y/-}$ retinas was laced with endomucin-positive filopodia instead of being smooth and covered with none or very few filopodia as in control mice. The abundance of central filopodia peaks around P9, exactly when deep vascular sprouting in wild-type mice occurs. Interestingly, deep sprouting exclusively originates from venous vessels and capillaries but not from arteries. Therefore, it seems that veins and capillaries of the SRVP from $Ndp^{y/-}$ retinas are able to create misaligned central filopodia. However, these filopodia might not be functional, since $Ndp^{y/-}$ mice lack deep sprouting. It is also unclear which molecular mechanisms lead to those central supernumerary filopodia since published data focuses exclusively on the regulation of tip cell filopodia.

Veins and capillaries of $Ndp^{y/-}$ retinas are excessively covered by MCs

Staining of retinal blood vessels for SMA revealed extensive MC coverage of veins and capillaries from P9 onwards. This coverage persists at least till P21. We previously reported upregulation of *PDGFβ* and *PDGFRβ* within the same timeframe (14). Interaction of all these genes regulates MC recruitment. Here, overexpression of *PDGFβ* and its receptor (*PDGFRβ*) could stimulate MC recruitment and the missing upregulation of *Angl* on MCs might prevent restriction of MC recruitment. Considering this as the likely mechanism of the excessive MC recruitment, we believe that this might be a response to vessel leakiness caused by upregulation of *VEGF-A* and *PLVAP* (14,18) due to hypoxia. Currently, it is unclear if this extensive MC recruitment goes along with a gain of AC in the affected veins and venules. If so, the gain in arterial or loss of VC could explain the disability to form the DRVP out of the SRVP from $Ndp^{y/-}$ retinas, since deep sprouts emerge exclusively from venous vessels and capillaries of the SRVP (37). The fact that we still can morphologically distinguish ACs and VCs and that we detected supernumerary endomucin-positive central filopodia on veins, venules and capillaries, but not on arteries, argues against a complete loss of the VC. However, the formation of uncoordinated central endomucin-positive filopodia at P9 and the excessive MC recruitment of venous vessels may indicate at least a partial loss of venous identity of the respective ECs with the consequence that central tip cells might develop, but being unable to induce proper deep sprouting.

The morphometric analysis together with results from the DAPT injections does not suggest a direct link between Norrin-Wnt and Notch signaling via Jag1. Our results suggest that Norrin is a mitogenic stimulus for IB4-positive ECs of the SRVP which explains its delayed outgrowth in $Ndp^{y/-}$ mice. The A/V crossing occurs unlikely due to a disturbed astrocyte–EC interaction and it is unclear if the altered basal membrane of the SRVP contributes to this effect. We found that Norrin is able to stimulate MAPK signaling and also previously reported that MAPK signaling

might be the primarily altered pathway in Norrin KO retinas. All this together with the A/V crossing phenotype suggests that MAPK signaling might be significantly altered in Norrin KO retinas. We also found excessive MC coverage of veins, venules and capillaries in $Ndp^{y/-}$ retinas which might indicate a partial loss of venous identity but also contribute to the appearance of the altered basal lamina and possibly to the appearance of the thorn-like supernumerary central filopodia. Postnatal stages after P7 in mice mimic developmental stages from patients when hypoxia increases and leads to pathologic alterations of various retinal angiogenic maturation processes. These data are crucial for the investigation of related diseases, like familial exudative vitreoretinopathy or Coats' disease, with a less severe phenotype than Norrie disease, which have a realistic chance for the development of treatment regimens.

MATERIALS AND METHODS

Animals

Generation of the $Ndp^{y/-}$ mouse line has been described elsewhere (4). The research was performed in accordance with the ARVO Statement for the Use of Animals in Ophthalmic and Vision Research and was approved by the Veterinary Office of the State of Zurich (Switzerland).

Immunohistochemical staining

Retinas for whole-mount immunohistochemistry were fixed in 4% paraformaldehyde for 2 h or overnight at 4°C. After fixation, retinas were blocked using 1–10% normal goat or rabbit serum (VectorLabs) in PBST and subsequently incubated overnight with biotinylated IB4 (1:200; VectorLabs). The following primary antibodies were diluted in 1–5% serum in PBST and incubated over night: αSMA-CY3 (1:500; Sigma), ColIV (AbD serotec, 1:200), PDGFRα (R&D Systems, 1:500) and Endomucin (R&D Systems, 1:100). For secondary detection, Alexa Fluor streptavidin conjugates (Molecular Probes, 1:100) or anti-goat/rabbit Alexa Fluor-coupled secondary antibodies (Invitrogen, 1:500) were used. Retinas were washed five times with PBS, flat mounted and analyzed under bright-light illumination with a microscope (Axioplan 2, AxioCam HRc; Carl Zeiss) equipped with ApoTome (Carl Zeiss) or by confocal imaging using the CLSM Leica SP2 inverse microscope (Leica). The protocol from Pitulescu *et al*. (46) was used to stain for proliferating ECs (BrdU staining).

Image processing

Image J 1.44p (NIH) and Photoshop CS5 (Adobe) software were used for image processing. Overall image brightness was adjusted in a linear fashion on whole images if it was necessary to improve picture quality for prints. These adjustments did not influence interpretation and are in concert with suggestions for image processing in reference (38). Results shown were obtained by performing at least two different independent experiments including at least four mutant or control animals per stage.

Morphometric analysis of retinal flatmounts

Each morphometric parameter was determined by averaging over four non-overlapping images per retina (one retina used per animal) with a minimum of four animals per group. Vascular density was determined by measuring the endothelial coverage per 300 × 300 μm field at the vascular front. The number of branch points was determined by counting vessel branch points within 300 × 300 μm fields. The number of filopodia at the vascular front within 68 × 51 μm fields was counted and normalized to 100 μm length of vasculature. BrdU-positive endothelial nuclei were counted in 424 × 317 μm fields at the vascular front and normalized to endothelial coverage within the same field (21).

In vivo Notch inhibition

Notch signaling was inhibited by subcutaneous injection of 0.3 mg/g body weight N-[N-(3,5-Difluorophenacetyl-L-alanyl)]-S-phenylglycine t-butylester (DAPT, Merck) dissolved in 10% ethanol and 90% peanut oil. DAPT solution was injected twice at P5 and P6. Retinas were collected at P7. Control litters were injected with vehicle only. Seven litters were DAPT injected. Quantification of vascular density and number of filopodia in DAPT-treated versus untreated KO and WT mice were performed as described above (23).

Quantification of Norrin-dependent proliferation and MAPK signaling *in vitro*

Stably wild-type or mutant p.C95R Norrin expressing HEK293T cells were used in these assays. Equal expression levels of wild-type and mutant Norrin were determined by western blot analysis (data not shown). To examine the proliferation rate or MAPK signaling activity, 8×10^4 cells/well of a 24-well plate were seeded and incubated at 37°C/5% CO_2 overnight. Cells were transiently co-transfected with pE2F or pSRF firefly luciferase reporter and pRenilla constructs (SABiosciences) using the calcium precipitation method (39,40). Luciferase activity was measured using DualGlo-LuciferaseReporterAssaySystem (Promega). Firefly luciferase activity was normalized to co-transfected *Renilla* luciferase.

Statistical analysis

Statistical analysis was performed in SPSS 18.0 (IBM) using two-tailed unpaired Student's *t*-test.

Quantitative data from DAPT-injection experiments were processed with univariate analysis of variance with two independent variables. Avoiding bias due to unequal sample sizes, the estimated marginal means were calculated instead of arithmetically means. *P*-values below $\alpha = 0.05$ were considered significant.

SUPPLEMENTARY MATERIAL

Supplementary Material is available at *HMG* online.

ACKNOWLEDGEMENTS

We thank Britta Seebauer for contributing the immunostainings against α-SMA at P7. We also would like to thank Rui Benedito, Ralf Adams and Hiroyuki Yamamoto for giving practical advice and discussing this work as well as Wei Chi for donating the pFZD4 construct and He Xi and Bryan McDonalds for providing the pLRP5 construct.

Conflict of Interest statement. None declared.

FUNDING

This work was supported by the Velux Foundation, Zurich, Switzerland and by the Swiss National Science Foundation (Grant number 31003A_122359), Bern, Switzerland.

REFERENCES

1. Berger, W., Meindl, A., van de Pol, T.J., Cremers, F.P., Ropers, H.H., Doerner, C., Monaco, A., Bergen, A.A., Lebo, R. and Warburg, M. (1992) Isolation of a candidate gene for Norrie disease by positional cloning. *Nat. Genet.*, **1**, 199–203.
2. Berger, W., van de Pol, D., Warburg, M., Gal, A., Bleeker-Wagemakers, L., de Silva, H., Meindl, A., Meitinger, T., Cremers, F. and Ropers, H.H. (1992) Mutations in the candidate gene for Norrie disease. *Hum. Mol. Genet.*, **1**, 461–465.
3. Warburg, M. (1966) Norrie's disease. A congenital progressive oculo-acoustico-cerebral degeneration. *Acta Ophthalmol. (Copenh.)*, **85 (suppl.)**, 5–147.
4. Berger, W., van de Pol, D., Bachner, D., Oerlemans, F., Winkens, H., Hameister, H., Wieringa, B., Hendriks, W. and Ropers, H.H. (1996) An animal model for Norrie disease (ND): gene targeting of the mouse ND gene. *Hum. Mol. Genet.*, **5**, 51–59.
5. Chen, Z.Y., Battinelli, E.M., Fielder, A., Bundey, S., Sims, K., Breakefield, X.O. and Craig, I.W. (1993) A mutation in the Norrie disease gene (NDP) associated with X-linked familial exudative vitreoretinopathy. *Nat. Genet.*, **5**, 180–183.
6. Shastry, B.S., Hejtmancik, J.F. and Trese, M.T. (1997) Identification of novel missense mutations in the Norrie disease gene associated with one X-linked and four sporadic cases of familial exudative vitreoretinopathy. *Hum. Mutat.*, **9**, 396–401.
7. Black, G.C., Perveen, R., Bonshek, R., Cahill, M., Clayton-Smith, J., Lloyd, I.C. and McLeod, D. (1999) Coats' disease of the retina (unilateral retinal telangiectasis) caused by somatic mutation in the NDP gene: a role for norrin in retinal angiogenesis. *Hum. Mol. Genet.*, **8**, 2031–2035.
8. Shastry, B.S., Pendergast, S.D., Hartzer, M.K., Liu, X. and Trese, M.T. (1997) Identification of missense mutations in the Norrie disease gene associated with advanced retinopathy of prematurity. *Arch. Ophthalmol.*, **115**, 651–655.
9. Ye, X., Wang, Y. and Nathans, J. (2010) The Norrin/Frizzled4 signaling pathway in retinal vascular development and disease. *Trends Mol. Med.*, **16**, 417–425.
10. Nikopoulos, K., Gilissen, C., Hoischen, A., van Nouhuys, C.E., Boonstra, F.N., Blokland, E.A., Arts, P., Wieskamp, N., Strom, T.M., Ayuso, C. *et al.* (2010) Next-generation sequencing of a 40 Mb linkage interval reveals TSPAN12 mutations in patients with familial exudative vitreoretinopathy. *Am. J. Hum. Genet.*, **86**, 240–247.
11. Poulter, J.A., Ali, M., Gilmour, D.F., Rice, A., Kondo, H., Hayashi, K., Mackey, D.A., Kearns, L.S., Ruddle, J.B., Craig, J.E. *et al.* (2010) Mutations in TSPAN12 cause autosomal-dominant familial exudative vitreoretinopathy. *Am. J. Hum. Genet.*, **86**, 248–253.
12. Xu, Q., Wang, Y., Dabdoub, A., Smallwood, P.M., Williams, J., Woods, C., Kelley, M.W., Jiang, L., Tasman, W., Zhang, K. and Nathans, J. (2004) Vascular development in the retina and inner ear: control by Norrin and Frizzled-4, a high-affinity ligand-receptor pair. *Cell*, **116**, 883–895.
13. Junge, H.J., Yang, S., Burton, J.B., Paes, K., Shu, X., French, D.M., Costa, M., Rice, D.S. and Ye, W. (2009) TSPAN12 regulates retinal vascular development by promoting Norrin- but not Wnt-induced FZD4/beta-catenin signaling. *Cell*, **139**, 299–311.
14. Luhmann, U.F., Lin, J., Acar, N., Lammel, S., Feil, S., Grimm, C., Seeliger, M.W., Hammes, H.P. and Berger, W. (2005) Role of the Norrie disease pseudoglioma gene in sprouting angiogenesis during development of the retinal vasculature. *Invest. Ophthalmol. Vis. Sci.*, **46**, 3372–3382.
15. Richter, M., Gottanka, J., May, C.A., Welge-Lussen, U., Berger, W. and Lutjen-Drecoll, E. (1998) Retinal vasculature changes in Norrie disease mice. *Invest. Ophthalmol. Vis. Sci.*, **39**, 2450–2457.
16. Xia, C.H., Yablonka-Reuveni, Z. and Gong, X. (2010) LRP5 is required for vascular development in deeper layers of the retina. *PLoS ONE*, **5**, e11676.
17. Rehm, H.L., Zhang, D.S., Brown, M.C., Burgess, B., Halpin, C., Berger, W., Morton, C.C., Corey, D.P. and Chen, Z.Y. (2002) Vascular defects and sensorineural deafness in a mouse model of Norrie disease. *J. Neurosci.*, **22**, 4286–4292.
18. Schafer, N.F., Luhmann, U.F., Feil, S. and Berger, W. (2009) Differential gene expression in Ndph-knockout mice in retinal development. *Invest. Ophthalmol. Vis. Sci.*, **50**, 906–916.
19. Liebner, S., Corada, M., Bangsow, T., Babbage, J., Taddei, A., Czupalla, C.J., Reis, M., Felici, A., Wolburg, H., Fruttiger, M. *et al.* (2008) Wnt/beta-catenin signaling controls development of the blood-brain barrier. *J. Cell Biol.*, **183**, 409–417.
20. Gerhardt, H., Golding, M., Fruttiger, M., Ruhrberg, C., Lundkvist, A., Abramsson, A., Jeltsch, M., Mitchell, C., Alitalo, K., Shima, D. and Betsholtz, C. (2003) VEGF guides angiogenic sprouting utilizing endothelial tip cell filopodia. *J. Cell Biol.*, **161**, 1163–1177.
21. Lobov, I.B., Renard, R.A., Papadopoulos, N., Gale, N.W., Thurston, G., Yancopoulos, G.D. and Wiegand, S.J. (2007) Delta-like ligand 4 (Dll4) is induced by VEGF as a negative regulator of angiogenic sprouting. *Proc. Natl Acad. Sci. USA*, **104**, 3219–3224.
22. Benedito, R., Roca, C., Sorensen, I., Adams, S., Gossler, A., Fruttiger, M. and Adams, R.H. (2009) The notch ligands Dll4 and Jagged1 have opposing effects on angiogenesis. *Cell*, **137**, 1124–1135.
23. Hellstrom, M., Phng, L.K., Hofmann, J.J., Wallgard, E., Coultas, L., Lindblom, P., Alva, J., Nilsson, A.K., Karlsson, L., Gaiano, N. *et al.* (2007) Dll4 signalling through Notch1 regulates formation of tip cells during angiogenesis. *Nature*, **445**, 776–780.
24. Fantin, A., Schwarz, Q., Davidson, K., Normando, E.M., Denti, L. and Ruhrberg, C. (2011) The cytoplasmic domain of neuropilin 1 is dispensable for angiogenesis, but promotes the spatial separation of retinal arteries and veins. *Development*, **138**, 4185–4191.
25. Haigh, J.J., Morelli, P.I., Gerhardt, H., Haigh, K., Tsien, J., Damert, A., Miquerol, L., Muhlner, U., Klein, R., Ferrara, N. *et al.* (2003) Cortical and retinal defects caused by dosage-dependent reductions in VEGF-A paracrine signaling. *Dev. Biol.*, **262**, 225–241.
26. Katoh, M. and Katoh, M. (2006) Notch ligand, JAG1, is evolutionarily conserved target of canonical WNT signaling pathway in progenitor cells. *Int. J. Mol. Med.*, **17**, 681–685.
27. Estrach, S., Ambler, C.A., Lo, C.C., Hozumi, K. and Watt, F.M. (2006) Jagged 1 is a beta-catenin target gene required for ectopic hair follicle formation in adult epidermis. *Development*, **133**, 4427–4438.
28. Singh, S., Johnson, J. and Chellappan, S. (2010) Small molecule regulators of Rb-E2F pathway as modulators of transcription. *Biochim. Biophys. Acta*, **1799**, 788–794.
29. Isashiki, Y., Ohba, N., Yanagita, T., Hokita, N., Doi, N., Nakagawa, M., Ozawa, M. and Kuroda, N. (1995) Novel mutation at the initiation codon in the Norrie disease gene in two Japanese families. *Hum. Genet.*, **95**, 105–108.
30. Baluk, P., Morikawa, S., Haskell, A., Mancuso, M. and McDonald, D.M. (2003) Abnormalities of basement membrane on blood vessels and endothelial sprouts in tumors. *Am. J. Pathol.*, **163**, 1801–1815.
31. Baffert, F., Le, T., Sennino, B., Thurston, G., Kuo, C.J., Hu-Lowe, D. and McDonald, D.M. (2006) Cellular changes in normal blood capillaries undergoing regression after inhibition of VEGF signaling. *Am. J. Physiol. Heart Circ. Physiol.*, **290**, H547–H559.
32. Liu, C., Shao, Z.M., Zhang, L., Beatty, P., Sartippour, M., Lane, T., Livingston, E. and Nguyen, M. (2001) Human endomucin is an endothelial marker. *Biochem. Biophys. Res. Commun.*, **288**, 129–136.
33. Samulowitz, U., Kuhn, A., Brachtendorf, G., Nawroth, R., Braun, A., Bankfalvi, A., Bocker, W. and Vestweber, D. (2002) Human endomucin: distribution pattern, expression on high endothelial venules, and decoration with the MECA-79 epitope. *Am. J. Pathol.*, **160**, 1669–1681.

34. Chen, J., Stahl, A., Krah, N.M., Seaward, M.R., Dennison, R.J., Sapieha, P., Hua, J., Hatton, C.J., Juan, A.M., Aderman, C.M. *et al.* (2011) Wnt signaling mediates pathological vascular growth in proliferative retinopathy. *Circulation*, **124**, 1871–1881.
35. Ohlmann, A., Seitz, R., Braunger, B., Seitz, D., Bosl, M.R. and Tamm, E.R. (2010) Norrin promotes vascular regrowth after oxygen-induced retinal vessel loss and suppresses retinopathy in mice. *J. Neurosci.*, **30**, 183–193.
36. Travasso, R.D., Poire, E.C., Castro, M., Rodrguez-Manzaneque, J.C. and Hernandez-Machado, A. (2011) Tumor angiogenesis and vascular patterning: a mathematical model. *PLoS ONE*, **6**, e19989.
37. Fruttiger, M. (2007) Development of the retinal vasculature. *Angiogenesis*, **10**, 77–88.
38. Rossner, M. and Yamada, K.M. (2004) What's in a picture? The temptation of image manipulation. *J. Cell Biol.*, **166**, 11–15.
39. Jordan, M., Schallhorn, A. and Wurm, F.M. (1996) Transfecting mammalian cells: optimization of critical parameters affecting calcium-phosphate precipitate formation. *Nucleic Acids Res.*, **24**, 596–601.
40. Jordan, M. and Wurm, F. (2004) Transfection of adherent and suspended cells by calcium phosphate. *Methods*, **33**, 136–143.
41. Xia, C.H., Liu, H., Cheung, D., Wang, M., Cheng, C., Du, X., Chang, B., Beutler, B. and Gong, X. (2008) A model for familial exudative vitreoretinopathy caused by LPR5 mutations. *Hum. Mol. Genet.*, **17**, 1605–1612.
42. Chen, J., Stahl, A., Krah, N.M., Seaward, M.R., Joyal, J.S., Juan, A.M., Hatton, C.J., Aderman, C.M., Dennison, R.J., Willett, K.L. *et al.* (2012) Retinal expression of wnt-pathway mediated genes in low-density lipoprotein receptor-related protein 5 (lrp5) knockout mice. *PLoS ONE*, **7**, e30203.
43. Phng, L.K., Potente, M., Leslie, J.D., Babbage, J., Nyqvist, D., Lobov, I., Ondr, J.K., Rao, S., Lang, R.A., Thurston, G. and Gerhardt, H. (2009) Nrarp coordinates endothelial Notch and Wnt signaling to control vessel density in angiogenesis. *Dev. Cell*, **16**, 70–82.
44. Gale, N.W., Thurston, G., Hackett, S.F., Renard, R., Wang, Q., McClain, J., Martin, C., Witte, C., Witte, M.H., Jackson, D. *et al.* (2002) Angiopoietin-2 is required for postnatal angiogenesis and lymphatic patterning, and only the latter role is rescued by Angiopoietin-1. *Dev. Cell*, **3**, 411–423.
45. Caprara, C., Thiersch, M., Lange, C., Joly, S., Samardzija, M. and Grimm, C. (2011) HIF1A is essential for the development of the intermediate plexus of the retinal vasculature. *Invest. Ophthalmol. Vis. Sci.*, **52**, 2109–2117.
46. Pitulescu, M.E., Schmidt, I., Benedito, R. and Adams, R.H. (2010) Inducible gene targeting in the neonatal vasculature and analysis of retinal angiogenesis in mice. *Nat. Protoc.*, **5**, 1518–1534.

Appendix E – Contributions

Individual contributions – genetic screening and mutational analyses						
gene	**gene selection**	**primer design**	**genetic screening**	**sequence data analysis**	**construct cloning**	**functional assays**
ATOH7	LM	LM, SF	SF	LM, SF	LM	LM, BS
NEUROD1	LM	LM, SF	SF	LM, SF	-	-
NINJ1	LS, LM, WB	LM, LS	LM, LS	LS	LM, LS	LM, LS
ZNF408	FC, RC	LM, LS	LM, LS	LM, LS	RC	RC
ILK	HY, RA	LM	SF, MW, LM, LS	LM, LS	LM, LS	HY, LM, LS
ITGB3	HY, RA, LM, LS, WB	LM, LS	SF, MW, LM, LS	LM, LS	LM, LS	-
PARVA	HY, RA, LM, LS, WB	LM, LS	LM, LS	LM, LS	-	-
SRF	AN	SF	SF	LM, LS, MF, SF,WB, JZ	BS	LM, BS, JZ
MKL1	AN, LM, WB, JZ	SF	SF, WM	LM, SF, MW	BS	LM, BS, JZ
MKL2	AN, LM, WB, JZ	SF	SF	LM, SF, BS	BS	LM, BS, JZ
NDP	WB	WB	SF	SF, LM	-	-
TSPAN12	LM, NS, WB, JZ	NS	SF	LM, NS, SF	-	-

Abbrivation	**First name**	**Last name**
AN	Alfred	Nordheim
BS	Britta	Seebauer
FC	Frans	Cremers
HY	Hiroyuki	Yamamoto
JZ	Jurian	Zürcher
LM	Lucas	Mohn
LS	Lea	Sollfrank
MF	Martin	Fritsche
MW	Mariana	Wittmer
NS	Nikolaus	Schäfer
RA	Ralf	Adams
RC	Rob	Collin
SF	Silke	Feil
WB	Wolfgang	Berger

Curriculum vitae

Name: **Lucas Raphael Mohn**
Date of birth: **March 26th, 1981**
Place of birth: **Uznach SG, Switzerland**
Citizenship: **Swiss & German**

Academic Education

Dr. sc. nat.	PhD student Institute of Medical Molecular Genetics, University of Zurich, Switzerland	10/2007-12/2012
	International PhD program in Neuroscience Neuroscience Center Zurich (ZNZ), University/ETH Zurich, Switzerland	
	Titel of the PhD thesis: *"The understanding of Norrins role in angiogenesis."*	
M Sc UZH	Master of Science in Humanbiology University of Zurich, Switzerland	07/2006-08/2007
	Master thesis at the Institute of Medical Genetics University of Zurich, Switzerland	
	Titel of the Master thesis: *"Expression of Norrin towards the understanding of its role in retinal angiogenesis"*	
B Sc UZH	Bachelor of Science in Biology University of Zurich, Switzerland	11/2002-06/2006

Basic Education

Matura	Stiftsschule, Matura Typus B, Einsiedeln, Switzerland	08/1994-06/2000
Primary School	Primarschule, Einsiedeln, Switzerland	08/1991-07/1994
Primary School	Primarschule, Schmerikon, Switzerland	08/1988-07/1991

Working Experience

Teaching Assistant, University of Zurich, Zurich, Switzerland	2007-2012
Biology Teacher, Highschool level, Niederhasli, Switzerland	10/2004-08/2005
Administration (Front and Back Office), Bluewin AG, Zurich, Switzerland	03/2002-09/2002
Administration (Front and Back Office), Bluewin AG, Zurich, Switzerland	06/2001-11/2001
Teacher, FlicFlac GmbH, Pfaeffikon SZ, Switzerland	02/2001-10/2001
Military Service, Swiss Army, Frauenfeld, Switzerland	06/2000-09/2000
Step in Hall, Einsiedeln, Switzerland	05/1996-05/1999

Other Information

Studies in Electrical Engineering, ETH Zurich, Switzerland	09/2000-03/2001
Stay abroad (Journey through Australia)	12/2001-03/2002

Publications

Mohn L., Seebauer B., Feil S., Sims K., Berger W. (2012) Pathogenic Mechanism of a Deletion in the Basic Domain of ATOH7 Responsible for Retinal Dysplasia., submitted.

Collin R. W. J., Nikopoulos K., Dona M., Gilissen Ch., Hoischen A., Boonstra F. N., Poulter J. A.., Kondo H., Berger W., Toomes C., Tahira T., **Mohn L. R**., Blokland E. A., Hetterschijt L., Ali M., Groothuismink J., Inglehearn Ch. F., Sollfrank L., Strom T. M., Uchio E., van Nouhuys C. E., Veltman J. A., and Cremers F. P. M. (2012) *ZNF408* is mutated in familial exudative vitreoretinopathy and crucial for the development of zebrafish retinal vasculature., submitted.

Zuercher J., Fritsche M., Feil S., **Mohn L**., Berger W. (2012) Norrin stimulates cell proliferation in the superficial retinal vascular plexus and is pivotal for the recruitment of mural cells. *Hum. Mol. Genet*., **21**, 2619-30.

Conferences / Scientific Meetings

Mohn L., Feil S., Berger W. (2011) „Protein Expression and Functional Characterization of Norrin". Swiss Eye Research Meeting, Biel, Sitzerland, oral presentation

Mohn L., Feil S., Berger W. (2010) „The understanding of Norrin's role in angiogenesis". PhD Retreat of the Center of Neuroscience (ZNZ) Uni/ETH Zurich, Valens, Switzerland, oral presentation

Mohn L., Feil S., Berger W. (2009) „The understanding of Norrin's role in retinal angiogenesis". Swiss Eye Research Meeting, Brunnen, Sitzerland, oral presentation

Mohn L., Feil S., Berger W. (2008) „The understanding of Norrin's role in retinal angiogenesis". ProRetina Research Colloquium, Potsdam, Germany, poster presentation

Reviewer activity

Reviewer for PLoS ONE: Low Dose Rapamycin Exacerbates Autoimmune Experimental Uveitis. (2012)

Languages

German: native
English: very good
French: good
Italian: basic